ISBN 978-82-326-1574-2 (printed version)
ISBN 978-82-326-1575-9 (electronic version)
ISSN 1503-8181

Doctoral theses at NTNU, 2016:118

Snorre Foss Westman

Vapor-liquid equilibrium measurement data for the two binary systems carbon dioxide + nitrogen and carbon dioxide + oxygen

NTNU
Norwegian University of Science and Technology

NTNU
Norwegian University of Science and Technology

Doctoral theses at NTNU, 2016:118

NTNU

NTNU
Norwegian University of Science and Technology
Faculty of Engineering Science and Technology
Department of Energy and Process Engineering

NTNU
Norwegian University of Science and Technology

Snorre Foss Westman

Vapor-liquid equilibrium measurement data for the two binary systems carbon dioxide + nitrogen and carbon dioxide + oxygen

Thesis for the degree of Philosophiae Doctor

Trondheim, January 2016

Norwegian University of Science and Technology
Faculty of Engineering Science and Technology
Department of Energy and Process Engineering

NTNU
Norwegian University of
Science and Technology

NTNU
Norwegian University of Science and Technology

Thesis for the degree of Philosophiae Doctor

Faculty of Engineering Science and Technology
Department of Energy and Process Engineering

ISBN 978-82-326-1574-2 (printed version)
ISBN 978-82-326-1575-9 (electronic version)
ISSN 1503-8181

Doctoral theses at NTNU, 2016:118

Printed by Skipnes Kommunikasjon as

Abstract

This thesis presents new, accurate, isothermal vapor-liquid equilibrium (VLE) measurement data for the two binary systems carbon dioxide and nitrogen (CO_2+N_2) and carbon dioxide and oxygen (CO_2+O_2). These measurements contribute to meeting the demand for thermophysical property data for the CO_2-rich mixtures that will be handled within carbon capture, transport and storage (CCS), the focus in this work being the conditioning and transport processes within the CCS chain.

The thermophysical properties of pure CO_2 are relatively well described by accurate equations of state and models. However, as a trade-off between the cost of capturing CO_2 within CCS and the required purity of the captured CO_2 has to be made, it is expected that different impurities will be present in the captured CO_2 stream. These impurities can significantly affect the thermophysical behavior of the mixture compared to that of pure CO_2, and impact how processes within the CCS chain should be designed and operated. Examples of these changes in behavior are the possibility for an increase in the minimum operating pressure to keep the mixture in dense phase during transport, and an increase in the required compressor work required to bring the mixture up to this pressure. In addition, the behavior of CO_2 with impurities during depressurization of a pipeline, either as a planned operation or in the case of a pipeline rupture, differs from the behavior of pure CO_2 in ways that can influence safety aspects of the operation.

To be able to make safe and economic decisions of how to design and operate these parts of the CCS chain, knowledge about the thermophysical properties of the CO_2-rich mixtures that will be handled is required. Several recent literature studies have revealed large gaps in the thermophysical data for these CO_2-rich mixtures, and modeling efforts have been limited by the lack of data and the dubious accuracy of some of the existing data.

The VLE measurements presented in this thesis contribute to achieving more

knowledge about the thermophysical properties of CO_2-rich mixtures. This can contribute to achieving the goal of the development of a reference equation of state for the mixtures handled within CCS, which has been identified by several authors as one of the hindrances for the development and realization of CCS.

The measurements of the VLE of CO_2+N_2 were carried out to validate the experimental apparatus, as there existed significant amounts of data for this system, some of which were of high quality. Equations of state describing this system were also readily available for comparison. In addition to validating the apparatus, the measurement campaign also resulted in new data for several temperature and pressure states where no data could be found in the open literature.

The VLE measurements of the CO_2+O_2 system cover six temperatures from close to the triple point temperature (216.59 K) to close to the critical temperature of pure CO_2 (304.13 K), and range from the vapor pressure of pure CO_2 to close to the mixture critical point at each temperature. The VLE measurements reconcile the inconsistencies in the literature data for this system, noted in several literature reviews and modeling efforts. The measurements significantly improve the thermodynamic data situation for this system, and form the basis for improving equations of state.

Preface

This thesis is the result of my PhD project carried out at the Department of Energy and Process Engineering at the Norwegian University of Science and Technology (NTNU) in the period from January 2013 to December 2015, with Professor Ivar Ståle Ertesvåg as my main supervisor, and Dr. Hans Georg Jacob Stang as my co-supervisor.

My work has been performed within the "CO_2 Mixture Properties (CO_2Mix)" project, led by SINTEF Energy Research under the research program CLIMIT and the BIGCCS Centre, performed under the Norwegian research program Centres for Environment-friendly Energy Research (FME). The research activity has also received funding from the European Community's Seventh Framework Programme through the IMPACTS project.

First of all, I would like to thank my supervisors, Professor Ivar Ståle Ertesvåg and Dr. Hans Georg Jacob Stang, for their support and thorough guidance during these three years. Their know-how of both the finer points of academic writing and the multitude of electrical and mechanical doodads my days consisted of fixing and repairing was essential. Second, I would like to direct special thank to Dr. Sigurd W. Løvseth, who has been the project leader of the CO_2Mix project, for his scrutiny and keen interest of the myriad of details that had to be sorted out for the project participants to be able to carry out measurements of this high quality.

I would like to give a huge thanks to the other participants in the project I have worked with for their massive help: Dr. Anders Austegard, Ingrid Snustad, Sigmund Ø. Størset, Bjarne Malvik and Håvard Rekstad. Also, I would like to thank Helge Johansen of SINTEF Energy Research for teaching me the intricate details of temperature and pressure calibration, and Reidar Tellebon and the many others of the laboratory staff at NTNU for always being available with ingenious solutions to how to repair all the bits and parts of the laboratory equipment that never failed to break down at the most inconvenient of times.

When I started on my PhD project, a lot of the groundwork had already been done. The very intricate experimental setup had been planned and constructed prior to my arrival, and for this I am very grateful.

Furthermore, a thank is directed to all my colleagues at NTNU and SINTEF Energy Research for their support. In addition, many thanks is given to the summer interns at SINTEF Energy Research, Bjorn Holst Pettersen, Ingeborg Treu Røe, Maximilian Schillings, Petter Vollestad and Asgeir Bjørgan, for their contributions and enthusiasm in the project.

The feedback and discussions with Professor Roland Span of Ruhr-Universität Bochum and Dr. Eric W. Lemmon of NIST were very fruitful, and I thank you both for this.

Finally, the work presented here would not have been completed if it had not been for the massive support I've had from my parents and my friends. Thank you very, very much.

Contents

List of publications

Articles included in thesis

The main part of the thesis is the two journal article manuscripts identified below. The articles are included at the end of the thesis.

Article I [1] **S.F. Westman**, H.G.J. Stang, S.W. Løvseth, A. Austegard, I. Snustad, S.Ø. Størset, I.S. Ertesvåg, Vapor-liquid equilibrium data for the carbon dioxide and nitrogen (CO_2 + N_2) system at the temperatures 223, 270, 298 and 303 K and pressures up to 18 MPa, Fluid Phase Equilib. 409 (2016) 207-241, doi:10.1016/j.fluid.2015.09.034

Article II [2] **S.F. Westman**, H.G.J. Stang, S.W. Løvseth, A. Austegard, I. Snustad, I.S. Ertesvåg, Vapor-liquid equilibrium data for the carbon dioxide and oxygen (CO_2 + O_2) system at the temperatures 218, 233, 253, 273, 288 and 298 K and pressures up to 14 MPa, *submitted to Fluid Phase Equilibria. Revised version accepted for publication can be found at* doi:10.1016/j.fluid.2016.04.002

Author's contributions

The articles included in the thesis were a collaborative effort. The contributions from the author of the thesis and the co-authors of the articles are identified below.

Article I

For the study presented in the article, the author of the thesis performed the following work:

- Most of the refinement of the experimental procedures
- Most of the maintenance, repair and testing of the VLE measurement apparatus
- Participation in planning the VLE measurement campaign
- Calibration of the temperature and pressure measurement system and the development of the methodology of the associated uncertainty analysis
- Approximately 40% of the calibration of the gas chromatograph for the composition analysis, excluding the preparation of the calibration gas mixtures and the development of the methodology of the associated uncertainty analysis
- Approximately 30% of the running of the VLE measurements
- Development of the data reduction methodology and the raw data treatment and analysis
- Analysis and interpretation of the measurements
  - Fitting of the equations of state
- Writing most of the article

For the study presented in the article, the co-authors have performed the following work:

- Design and construction of the experimental apparatus (Løvseth, Stang)
- Initial development of experimental procedures (Løvseth, Stang)
- Participation in the refinement of the experimental procedures (Løvseth, Stang, Austegard, Snustad, Størset)
- Some of the maintenance, repair and testing of the VLE measurement apparatus (Stang and members of the laboratory staff)
- Participation in planning the VLE measurement campaign (Løvseth, Stang, Austegard, Snustad)

- Guidance for the calibration of the temperature (Stang) and pressure (Stang) measurement system and the development of the methodology of the associated uncertainty analysis (Stang, Løvseth)
- Approximately 60% of the calibration of the gas chromatograph for the composition analysis (Austegard, Størset)
- Preparation of the calibration gas mixtures (Snustad)
- Development of the methodology of the composition uncertainty analysis (Løvseth, Størset, Snustad)
- Approximately 70% of the running of the VLE measurements (Snustad, Austegard, Stang)
- Analysis and interpretation of the measurements (All co-authors)
  - Fitting of the equations of state (Austegard)
  - Fitting of the scaling law (Austegard, Løvseth)
- Writing the draft about the uncertainty analysis of the composition (Løvseth)
- Writing the section about the critical point estimation (Løvseth, Austegard)
- Critical review of the article (All co-authors)

Article II

For the study presented in the article, the author of the thesis performed the following work:

- Most of the refinement of the experimental procedures
- Most of the maintenance, repair and testing of the VLE measurement apparatus
- Participation in planning the VLE measurement campaign
- Calibration of the temperature and pressure measurement system and the associated uncertainty analysis
- The calibration of the gas chromatograph for the composition analysis and the associated uncertainty analysis, excluding the preparation of the calibration gas mixtures

- Approximately 60% of the running of the VLE measurements
- Raw data treatment and analysis
- Development of the data reduction methodology and the raw data treatment and analysis
- Analysis and interpretation of the measurements
  - Fitting of the equations of state
  - Fitting the scaling law
- Writing the article

For the study presented in the article, the co-authors have performed the following work:

- Participation in the refinement of the experimental procedures (Løvseth, Stang)
- Some of the maintenance, repair and testing of the VLE measurement apparatus (Stang and members of the laboratory staff)
- Participation in planning the VLE measurement campaign (Løvseth, Stang, Austegard, Snustad)
- Guidance for the calibration of the temperature (Stang) and pressure (Stang) measurement system and the associated uncertainty analysis (Stang, Løvseth)
- Preparation of the calibration gas mixtures (Snustad)
- Approximately 40% of the running of the VLE measurements (Austegard, Snustad)
- Analysis and interpretation of the measurements (All co-authors)
- Critical review of the article (All co-authors)

Additional publications and presentations

Conference papers

[3] **S.F. Westman**, H.G.J. Stang, S.Ø. Størset, H. Rekstad, A. Austegard, S.W. Løvseth, Accurate phase equilibrium measurements of CO_2 mixtures, 7th Trond-

heim Conference on CO_2 capture, Transport and Storage, June 2013, Energy Procedia 51 (2014) 392-401, doi:10.1016/j.egypro.2014.07.046

[4] S.W. Løvseth, H.G.J. Stang, **S.F. Westman**, I. Snustad, A. Austegard, Experimental investigations of impurity impact on CO_2 mixture phase equilibria, 12th International Conference on Greenhouse Gas Control Technologies, GHGT-12, October 2014, Energy Procedia 63 (2014) 2589-2595, doi:10.1016/j.egypro.2014.11.281

[5] S.W. Løvseth, H.G.J. Stang, A. Austegard, **S.F. Westman**, R. Span, R. Wegge, Measurements of CO_2-rich mixture properties: status and CCS needs, The 8th Trondheim Conference on CO_2 Capture, Transport and Storage, June 2015, accepted for publication in Energy Procedia

Presentations

S.F. Westman, H.G.J. Stang, B. Malvik, S.Ø. Størset, H. Rekstad, A. Austegard, S.W. Løvseth, Accurate phase equilibrium measurements of CO_2 mixtures. Presented at the 8th Trondheim Conference on CO_2 Capture, Transport and Storage (TCCS-8), June 4-6, 2013, Trondheim, Norway.

S.F. Westman, H.G.J. Stang, S.W. Løvseth, A. Austegard, I. Snustad, I.S. Ertesvåg, Accurate vapor-liquid phase equilibrium measurements on the binary CO_2-O_2 system. Presented at the 19th Symposium on Thermophysical Properties, June 21-26, 2015, Boulder, CO, USA.

1 Introduction

1.1 Background and motivation

A vast amount of human activities involves processes that generate CO_2 as a by-product, examples being the burning of fossil fuels for energy in power plants and in transportation equipment, the production of concrete for construction purposes, and from other industrial processes. Is has been thoroughly established that the emission of CO_2 and other greenhouse gases into the atmosphere contribute to global warming and climate change, and measures to lower these emissions are being initiated by governments around the world. The most recent result of these efforts is the United Nations Paris Agreement, where 195 of the nations of the world successfully negotiated a plan to decrease climate change [6].

The motivations for the actions to limit climate change are many. According to the latest report by the Intergovernmental Panel on Climate Change (IPCC) [7], the increasing global temperature will have results like increasing ocean levels and increasing occurrences of extreme weather phenomena. Factors such as these are predicted to cause, among other aspects, major economical losses, the extinction of many animal species, a decrease in food and water security, and increase the displacement of humans and other species. Policy instruments such as governmental legislations, emissions trading systems and carbon taxing could prove to be incentives for taking action to lower the emissions of greenhouse gases.

The paths to lowering the emissions are many. One of the methods is to capture CO_2 from the exhaust gases produced in the processes mentioned above before the remaining gases are released into the atmosphere. The capture of the CO_2 can be performed through many processes, one example being the use of amines to separate the CO_2 from the remaining exhaust gases. The captured CO_2 can then be conditioned and transported using, for instance, gas

pipelines or ships to a storage location. Examples of storage locations are underground geological formations such as depleted oil and gas reservoirs, and aquifers. These examples are part of the developing technology known as CO_2 capture, transport and storage (CCS) [8]. To achieve the International Energy Agency's two-degree scenario (2DS), CCS will be an important technology in the portfolio of measures required to reduce the emissions of greenhouse gases [9].

Common for many of the processes within CCS involving capture, transport and storage of CO_2 is the need for knowledge about how the captured CO_2 behaves under different conditions of temperature and pressure, that is, the thermophysical behavior of the fluid. The thermophysical behavior can be divided in the thermodynamic behavior, comprised of aspects such as the pressure-volume-temperature behavior and phase equilibria, and the transport property behavior, comprised of, for example, thermal conductivity and viscosity. The thermodynamic behavior of pure CO_2 is well described by the equation of state (EOS) by Span and Wagner [10], and the transport properties by models such those by Vesovic et al. [11], Fenghour et al. [12].

However, as pointed out by, for example, [8, 13, 14], the cost of CO_2 capture depends on the required level of impurities in the captured CO_2 stream, and higher purity comes at a higher cost. Therefore, it is expected that different impurities will be present together with the captured CO_2. Estimates for the impurity levels are given in Table 1.1. The presence of these impurities can significantly affect the behavior of the fluid, compared to pure CO_2. This change in behavior compared to pure CO_2 influences the design and operation of the processes within CCS, as described by [13–16]. As noted by these authors, the presence of different impurities can increase both the minimum operating pressure required if the CO_2-rich mixture is to be kept in dense phase during transport and the compressor work required to bring the mixture up to this pressure. In addition to these economic and operating factors, the change in behavior caused by the impurities can influence the safety of the operation of the processes. An example of this is the behavior during depressurization in the ordinary operation of a pipeline or depressurization in the event of a pipeline rupture, see e.g. [17].

To be able to make informed decisions regarding the economical and safe design and operation of these systems, and set requirements on the maximum level of impurities, it is therefore of importance to have an accurate description of the thermophysical behavior of the CO_2-rich mixtures which will be handled. Additionally, an accurate description of the density of these mixtures enables accurate calculations of the amounts transported, which can be impor-

tant in transport price determinations [15].

Recently reported overviews of the available models and data for the thermophysical properties of these CO_2-rich mixtures are given in, for instance, [13, 16, 18–20], and the authors point out the large gaps in both the data and the available models. The lack of accurate data limits the accuracy of the descriptions of the mixtures by EOSs and models.

Even with the progress within the field of molecular modeling, empirical equations of state currently have the possibility for the most accurate description of the thermodynamic properties of multi-component mixtures such as the CO_2-rich mixtures within CCS. The accuracy of the representation of experimental data depends on the type of EOS fitted to the data, and as discussed by, for example, [13], depending on the requirements for a given calculation, different EOSs can be utilized to describe CO_2-rich mixtures. Recently, several studies have been performed to develop EOSs with sufficient flexibility in the number of terms and parameters utilized to be able to describe these mixtures with the highest possible accuracy, examples being [18, 19, 21]. One of these, the equation of state called EOS-CG [18, 19], was developed to describe the thermodynamic behavior of combustion gases, humid gases and CO_2-rich mixtures containing carbon dioxide CO_2, nitrogen (N_2), oxygen (O_2), water (H_2O), argon (Ar), and carbon monoxide (CO). This EOS was developed using the highly flexible mathematical framework of the GERG-2008 EOS [22], which has been adopted as a ISO standard for describing natural gas mixtures with high accuracy. However, as was noted by the authors of EOS-CG, the description of many of the binary systems suffered from the lack of high quality data [18, 19].

The project called "CO_2Mix", under which the thesis work has been performed,

Table 1.1
Expected concentrations in captured CO_2 streams [13, 14].

Chemical name	Min. mole-percent	Max. mole-percent
CO_2	75	99
N_2	0.02	10
O_2	0.04	5
Ar	0.005	3.5
SO_2	<0.0001	1.5
H_2S+COS	0.01	1.5
NO_x	0.0002	0.3
CO	0.0001	0.2
H_2	0.06	4
CH_4	0.7	4

aimed to perform accurate vapor-liquid equilibrium (VLE), speed of sound and density measurements of CO_2-rich mixtures at conditions relevant for CO_2 conditioning and transport [15]. Estimated temperature and pressure ranges for the conditioning and transport processes are given in Table 1.2. The new data resulting from this project were intended to fill in some of the knowledge gaps, and form the basis for improving equations of state describing the thermodynamic properties of these mixtures.

The work in this thesis focused on the measurement of the VLE for some of the binary combinations of components in the CO_2-rich mixtures. As described by, for instance, [15, 18], empirical equations of state used to describe multi-component mixtures are often fitted to data for the combinations of binary systems the mixture contains, and multi-component data are used to validate the description of the EOSs. In addition, the experimental data should not only cover the CO_2 mole fraction range indicated in Table 1.1. One of the reasons for this is that the impurities will at some temperature and pressure conditions cause the formation of a vapor phase with an equilibrium CO_2 mole fraction that is much lower than the overall CO_2 mole fraction of the CO_2-rich mixture. An example of this behavior is found in the CO_2+N_2 system at the lower end of the temperature ranges in Table 1.2. The inclusion of experimental data spanning a large range of conditions also help ensure the accuracy and robustness of the models fitted to the data, as stated by [15, 21]. Equations of state accurately describing a wide range of conditions have another significant advantage: For properly formulated EOSs, all thermodynamic properties, such as heat capacities, enthalpies and speed of sound, can be calculated directly through analytical expressions. From the so-called *fundamental* equations of state, formulated in, for example, the Helmholtz energy as function of density, temperature and composition, the thermodynamic properties can be calculated directly through the combinations of analytic derivatives, as discussed by, for example, [10, 19, 23]. Examples of such EOSs include the previously mentioned mixture models EOS-CG [18], GERG-2008 [22] and the EOS for pure CO_2 by Span and Wagner [10].

As stated by Li et al. [13], the development of a reference quality equation of state for the thermodynamic properties for the fluids handled within CCS

Table 1.2
Estimated temperature and pressure ranges of conditioning and transport within CCS [13].

Process	Pressure range (MPa)	Temperature range (K)
CO_2 conditioning	0-11	219.15-423.15
CO_2 transport	0.5-20	218.15-303.15

processes should be a goal, where, according to the designation by Span [23], such a reference EOS should be able to represent the best experimental data for the thermodynamic properties within their estimated uncertainties. This will enable decisions to be made based on the most accurate estimates for the behavior of the systems. The accurate VLE measurements presented in this thesis is a contribution to achieving this goal.

2 Methodology

2.1 Introduction

The experimental apparatus used for the VLE measurements was first described in [24], in [3] and in greater detail in Article I [1]. A summary will be provided here, with focus on the capabilities of the apparatus.

The VLE measurements were performed using an isothermal analytical method employing a variable-volume cell, which is one of the many experimental methods for the measurement of high-pressure fluid phase equilibria described in the review articles by [25–29]. The method used in the present work consists of determining the equilibrium compositions of all phases present at the given temperature and pressure. For the measurements performed in Article I and Article II [2], the equilibrium compositions of two coexisting phases were measured, a vapor phase and a liquid phase. As each of the systems studied contained two components, Gibbs' phase rule states that it is possible to vary two intensive properties freely. In the experiments, the temperature and the pressure were the independent variables. The temperature of the cell and its content was kept constant using a thermostatic bath, and the pressure was controlled by injecting CO_2 and the impurity component in question into the cell. The cell itself consisted of a transparent sapphire cylinder placed between two titanium flanges, the internal volume of the cell being approximately 100 cm^3. A picture of the equilibrium cell is shown in Fig. 2.1, and a overview picture of the experimental apparatus with the ancillary equipment is shown in Fig. 2.2.

A stirrer was used to stir the cell content to stabilization of the temperature and pressure at VLE. When the temperature and pressure had stabilized, the stirrer was turned off to allow the phases to settle according to density. The pressure and temperature were measured at regular intervals. A borescope was used to visually inspect the cell content to determine when the phases had settled. After the phases had settled, samples of the phases were withdrawn using cap-

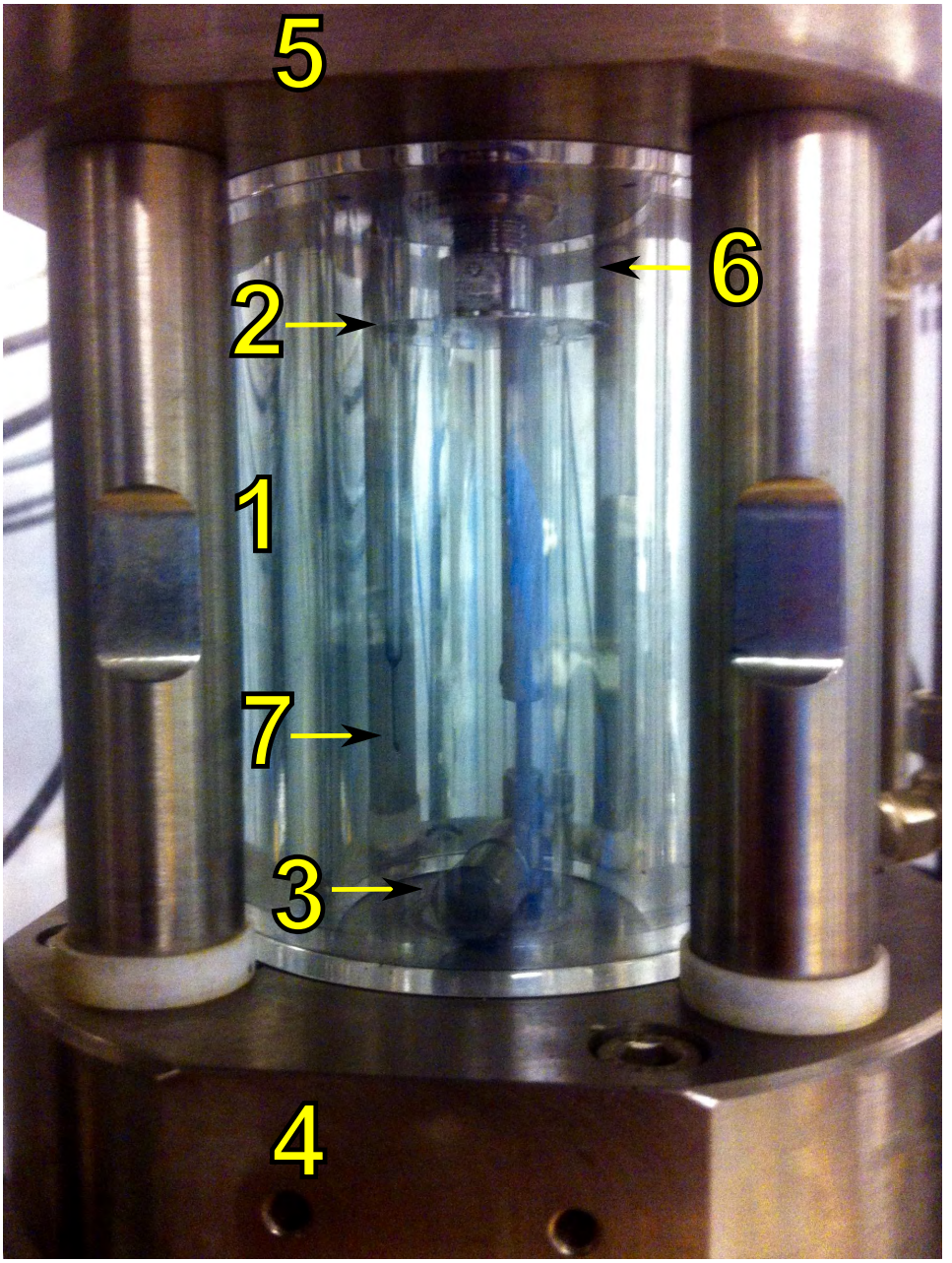

Fig. 2.1. Overview picture of equilibrium cell. Sapphire cell (1), plate bellows (2) with maximum volume expansion $\sim$1 cm^3, stirrer with magnetic coupling (3), bottom flange (4) containing one standard platinum resistance thermometer (SPRT), top flange (5) containing the other SPRT, vapor phase sampler capillary inlet (6, hidden behind bellows), movable liquid phase sampler capillary inlet (7).

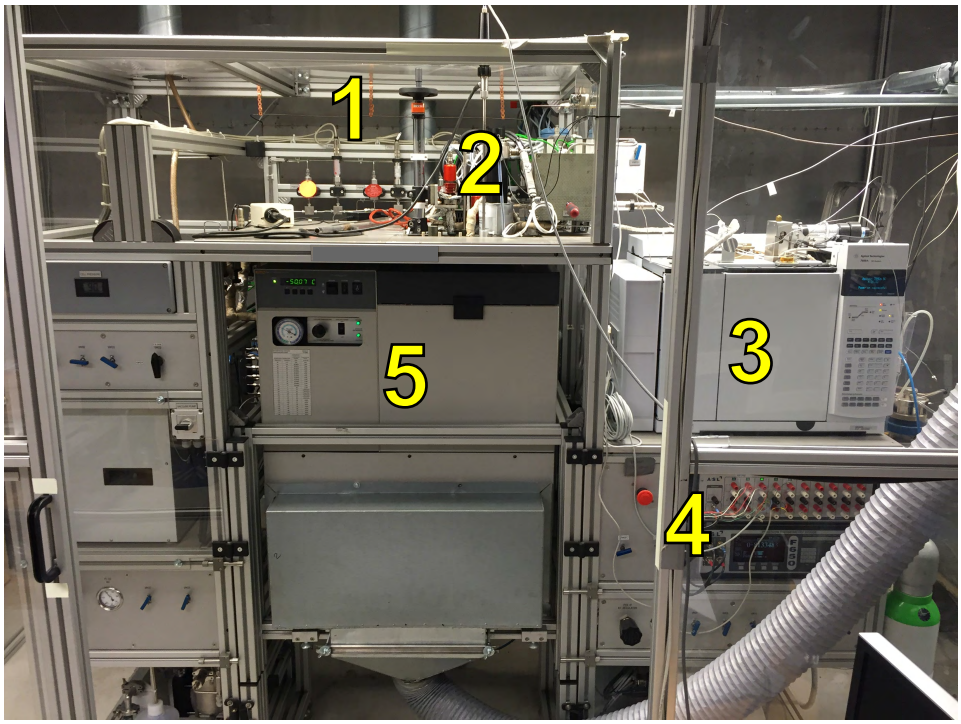

Fig. 2.2. Overview picture of experimental apparatus and ancillary equipment. Pressure sensor array (1), sampling valves (2), gas chromatograph (3), thermometry bridge and switch (4), thermostatic bath (5) placed around the equilibrium cell, which is not visible in the picture.

illary sampling valves. The samples were analyzed using a gas chromatograph. To prevent a decrease in cell pressure when a sample was taken from the cell, which would have disturbed the equilibrium, a plate bellows placed inside the cell was expanded to decrease the cell volume upon sampling.

This setup can be designated as "AnTCapValVisVar" according to the classification by Dohrn et al. [26].

The temperature sensors, one placed in each of the flanges enclosing the cell, were calibrated in-house using fixed-point cells according to the International Temperature Scale of 1990 (ITS-90). The pressure sensors were also calibrated in-house, against a recently calibrated dead weight tester. The calibration references were traceable to accredited calibration laboratories. The gas chromatograph was calibrated against gravimetrically prepared gas mixtures, made in-house from source gases of high purity.

2.2 Capabilities of the VLE apparatus

As described in [24], the VLE apparatus was built for performing measurements in the temperature range from 213 to 423 K, and pressures from 0.4 to 20 MPa. The design of the apparatus and ancillary equipment was performed such that measurements could be carried out on systems containing corrosive, explosive and toxic components, like many of the substances identified in Table 1.1. Examples of this is the use of sapphire and titanium for the cell components exposed to the fluid, sulfinert treated tubing and pumps for the loading of the impurity, and a extensive ventilation and gas sensor system for dealing with the possibility for leakages.

The apparatus is designed to facilitate sampling of more than two phases. The sampler used for liquid phase sampling in VLE measurements can be moved vertically inside the cell. Using the borescope for visual inspection of the cell, this enables accurate placement of the sampler inlet. This opens the possibility for studies involving other types of phase equilibria than VLE, for instance vapor-liquid-liquid equilibria (VLLE).

3 Summary of the articles

In the studies in Articles I and II [1, 2], the VLE of the two binary mixtures CO_2+N_2 and CO_2+O_2 were investigated at temperatures from close to the triple point temperature of CO_2 (216.59 K [10]) to close to the critical temperature of CO_2 (304.13 K [10]) and pressures up to 18.2 MPa. For this temperature range, both of these systems consist of a supercritical component, N_2 or O_2, dissolved in CO_2. As discussed by [19], these two systems are quite similar in terms of the shape of the vapor-liquid phase boundaries. The vapor-liquid region is bounded in terms of the temperature by the critical temperature of CO_2 and the temperature at the melting or sublimation line at the lower end, whose deviation from the the triple point temperature of CO_2 (216.59 K [10]) depends on the pressure and the dissolved component [19]. See for example [30] for measurements of the solid-liquid-vapor phase locus for the systems CO_2+N_2 and CO_2+H_2.

3.1 Article I: Validation of apparatus and new VLE data for CO_2+N_2

In Article I, the primary objectives of the study was to perform a validation of the experimental VLE apparatus, which was installed in the laboratories of SINTEF Energy Research and NTNU in August 2012, to gain experience and improve the experimental procedures developed during initial design and testing, and to acquire measurements in previously uncovered temperature and pressure regions. The validation of the experimental apparatus was performed by conducting VLE measurements on the binary CO_2+N_2 system, for which there existed a significant amount of data in the literature, where much of the data were of high quality. The existing literature data were well described by equations of state such as EOS-CG [18, 19] and the GERG-2008 EOS [22], which employed an almost equivalent model for this particular system. Calibrations

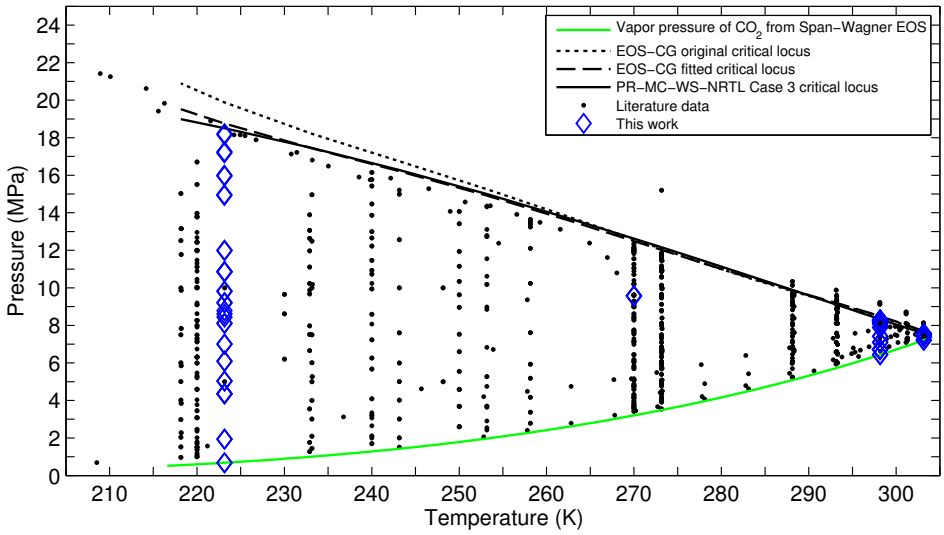

Fig. 3.1. CO_2+N_2 system: Temperature-pressure diagram with available literature data [30–52] and data measured in Article I. Vapor pressure of pure CO_2 calculated from [10]. Critical locus calculated from EOS-CG original model in [18, 19] and fitted EOS-CG model and cubic model in Article I.

of the temperature and pressure sensors were performed in-house. Calibration gas mixtures of CO_2+N_2 spanning the expected compositions of the VLE samples were prepared in-house, and a calibration procedure was developed, followed by the calibration of the gas chromatograph.

In the article, VLE measurements are reported for the CO_2+N_2 system at the temperatures 223, 270, 298 and 303 K. A graphical overview of the reported measurements in the article are given in Fig. 3.1, together with data from the open literature and EOS calculations. This figure was not included in Article I. For all temperatures, except at 270 K, the measurements span from the vapor pressure of pure CO_2 to close to the mixture critical pressure, with the lowest and highest measured pressures being respectively 0.7 and 18.2 MPa. The measured CO_2 mole fractions range from 0.57 to 0.995 in the liquid phase, and from 0.19 to 0.992 in the vapor phase.

A detailed uncertainty analysis of the pressure, temperature and phase composition measurements was carried out, and explained thoroughly in the article. Details concerning the experimental apparatus related to the uncertainty analysis were given.

The measurements in Article I agreed very well with the existing high quality data, and the operation of the apparatus was deemed to be validated for the use over the temperature, pressure and composition ranges the measurements span. In addition, it was shown that the apparatus was able to perform accurate measurements in the critical region, much due to the use of the bellows pressure compensation upon sampling. This is a challenging task, especially at the higher temperatures close to the critical temperature of CO_2, where the two-phase region spans very small ranges of composition and pressure.

The contributions from this in terms of new data were the measurements in the critical region at 223 and 303 K, and the measurements at 298 K. The critical region data at 223 and 298 K were used to fit a scaling law model, resulting in high accuracy estimates for the critical points at these temperatures.

The data of Article I were used to fit the VLE prediction two different equations of state. First, two of the parameters for CO_2+N_2 of EOS-CG [18, 19] were fitted, resulting in a better agreement between the new critical region data at 223 K than with the original EOS-CG model. Second, the Peng-Robinson EOS [53] utilizing the alpha correction by Mathias and Copeman [54], the mixing rules by Wong and Sandler [55], and the NRTL [56] excess Gibbs energy model was fitted to the data in Article I and selected data from the open literature. Expressions for the temperature dependencies of the parameters were developed, enabling VLE calculations at temperatures from 223 to 303 K. The data in Article I were described quite accurately by these two EOSs, the exception being the critical region at the higher temperatures.

The standard uncertainties of the VLE data were estimated to be maximum 6 mK in temperature, maximum 3 kPa in pressure, and maximum 0.0004 in the mole fractions of the phases. As noted in Article I, the estimated uncertainties in the mole fractions were probably underestimated for the data where the match with the fitted EOS-CG model was not satisfactory. As will be seen in the discussion concerning Article II that follows below, these estimates could probably have been improved if the VLE composition derivatives with respect to pressure had been estimated from the scaling law, instead of from the fitted EOS-CG model that was utilized in Article I.

3.2 Article II: New accurate VLE data for CO_2+O_2

The experience gained from the experiments in the study in Article I allowed us to improve the experimental procedures. The experimental procedures were improved significantly based on the experience with the operation and response of the bellows, the necessary length of the settling times at different pressure and temperature states for a system such as CO_2+N_2, and the estimation of the necessary sample sizes.

Following the validation of the apparatus in Article I, the study in Article II focused on performing VLE measurements on the CO_2+O_2 system. Several literature reviews [13, 19] had identified inconsistencies in the VLE data for this binary system. As discussed by the authors of EOS-CG [18, 19], the model for CO_2+O_2 suffered from the lack of high quality data for this system. The study in Article II sought to improve the VLE data situation for this system, and to reconcile the identified inconsistencies.

Similar to in the study in Article I, calibration gas mixtures of CO_2+O_2 were prepared. The calibration procedure was adjusted to the new system, and calibration of the gas chromatograph was performed.

Article II reports VLE measurements at the temperatures 218, 233, 253, 273, 288 and 298 K. A graphical overview of the measurements in Article II is given in Fig. 3.2, together with data from the open literature and EOS calculations. This figure was not included in Article II. For all six temperatures, the data in Article II range from the vapor pressure of pure CO_2 to close to the mixture critical point. The measured CO_2 mole fractions span from approximately 0.45 to 0.987 in the liquid phase, and from 0.15 to 0.956 in the vapor phase.

Estimates for the standard uncertainties in the measured temperatures, pressures and phase compositions were calculated using the methodology developed in Article I, with the necessary modifications for use on the CO_2+O_2 system.

Also in Article II, the Peng-Robinson EOS [53] utilizing the alpha correction by Mathias and Copeman [54], the mixing rules by Wong and Sandler [55], and the NRTL [56] excess Gibbs energy model was fitted to the data from the study. Expressions for the temperature dependencies of the model parameters were developed, enabling model VLE calculations at temperatures from 218 to 298 K, and possibly for extrapolation to the critical temperature of pure CO_2 at 304.13 K. The agreement between the data in Article II and the model was quite good. The shortcomings of the model were the inaccuracies in the de-

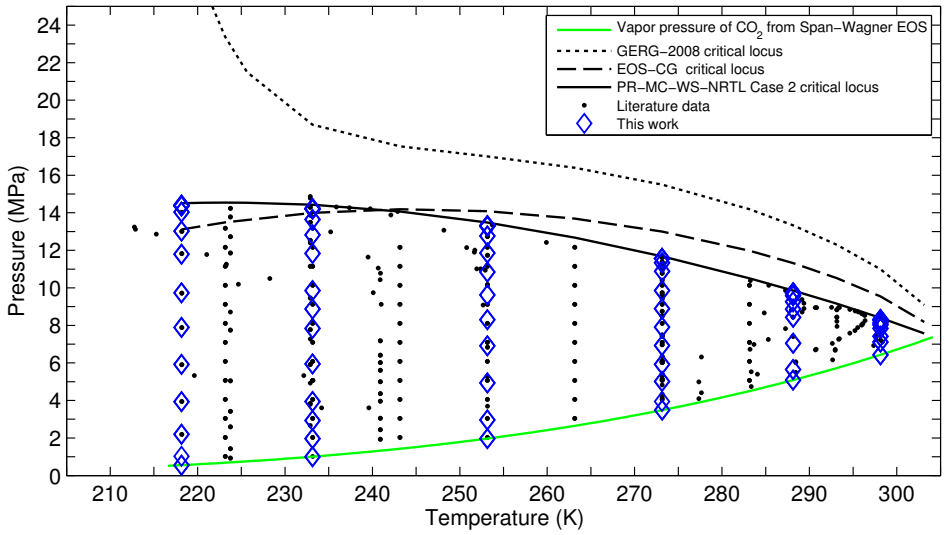

Fig. 3.2. CO_2+O_2 system: Temperature-pressure diagram with available literature data [35, 42, 49, 57–62] and data measured in Article II. Vapor pressure of pure CO_2 calculated from [10]. Critical locus calculated from GERG-2008 [22], EOS-CG model [18, 19] and fitted cubic EOS in Article II.

scription of the vapor phase compositions and the data in the critical region. The model was also compared to data from the open literature, and the agreement was satisfactory, considering the inconsistencies and scatter in the data.

At the temperatures 218, 233, 253 and 273 K, a special procedure was used in the mixture critical region to obtain VLE measurements very close to the mixture critical point. This procedure is described in detail in Article II. To summarize, the cell content was brought from a state close to the mixture critical point in the two-phase region out into the supercritical region by slightly increasing the cell pressure using the bellows. By using the sampling as a method to decrease the cell pressure, at each temperature a pressure-temperature-composition state point in the supercritical region was obtained, followed by VLE measurements at several pressures very close to the mixture critical point.

At each of the six temperatures, a scaling law model was fitted to the VLE measurements closest to the mixture critical points, giving estimates for the mixture critical composition and pressure at each temperature. A sensitivity analysis showed that the estimated critical points did not change significantly as long as the data closest to the mixture critical points were included in data used for the fits. The measured supercritical state points were outside the

VLE phase boundary indicated by the scaling law models, indicative of the consistency of the critical point estimates.

In contrast to in Article I, the standard uncertainties in the measured VLE compositions of the phases in the mixture critical regions were calculated using composition derivatives with respect to pressure calculated from the scaling law model, instead of from the EOS fitted to the all of the data at each temperature. These standard uncertainties were deemed to be more realistic estimates than if the methodology in Article I had been used.

The standard uncertainties of the VLE data measured in Article II were estimated to be maximum 8 mK in temperature, maximum 3 kPa in pressure, and maximum 0.0031 in the mole fractions of the phases in the mixture critical regions, and approximately 0.0005 in the mole fractions outside the mixture critical regions. The data measured in the study in Article II showed significantly less scatter than the data found in the open literature, and include measurements in the mixture critical regions and estimates for the critical points. With this significant improvement in the data situation, there is a very good basis for developing better equations of state for the CO_2+O_2 system. The data can be used together with other thermodynamic property data such as density and speed of sound to improve the system description of multi-parameter EOSs such as EOS-CG.

4 Concluding remarks and recommendations for further work

The study in Article I, although mainly intended for validation of the experimental apparatus, resulted in accurate VLE measurements for the CO_2+N_2 system at temperature and pressure states where no data could be found in the open literature, and also in more accurate data for states where there existed literature data. The new data are a contribution to the knowledge about the behavior of this system, and provide a basis for improving the description of the thermodynamic properties of the system by equations of state such as EOS-CG [18, 19] to a even higher degree of accuracy, if needed.

Article II reports accurate VLE measurements for the CO_2+O_2 system at temperatures from close to the triple point temperature of CO_2 to close to the critical temperature of CO_2. The measurements are a significant contribution to the data base for the thermodynamic properties of this system, and can be used to enhance equations of state such as EOS-CG. The data close to the mixture critical points could aid in achieving an accurate description of the critical locus of the system.

Another possible use for the VLE measurements reported in the articles is validation of molecular modeling efforts.

The studies in Articles I and II demonstrates that the apparatus is able to perform accurate VLE measurements on two different binary systems over a wide range of temperatures, pressures and phase compositions, also in the critical region. This apparatus can be used further in the coming years to investigate different systems where the data situation requires improvements, where many of the binary and ternary combinations of the different components in

Table 1.1 are possible candidates. After the experiments reported in this thesis were concluded, measurement campaigns using the apparatus on different systems were initiated within other projects.

The experimental procedures were significantly improved during the studies in Articles I and II. The detailed procedures are given in the articles, and the knowledge about the VLE behavior of these two systems and the procedures used to perform the measurements can be developed further and adapted for the use in other laboratory setups for similar measurements.

The VLE data in this thesis and the data eventually resulting from experiments carried out using the apparatus could contribute to achieving the goal of a reference quality equation of state for CCS mixtures.

References

[1] S. F. Westman, H. G. J. Stang, S. W. Løvseth, A. Austegard, I. Snustad, S. Ø. Størset, I. S. Ertesvåg, Vapor-liquid equilibrium data for the carbon dioxide and nitrogen (CO_2 + N_2) system at the temperatures 223, 270, 298 and 303 K and pressures up to 18 MPa, Fluid Phase Equilib. 409 (2016) 207–241, URL http://dx.doi.org/10.1016/j.fluid.2015.09.034.

[2] S. F. Westman, H. G. J. Stang, S. W. Løvseth, A. Austegard, I. Snustad, I. S. Ertesvåg, Vapor-liquid equilibrium data for the carbon dioxide and oxygen (CO_2 + O_2) system at the temperatures 218, 233, 253, 273, 288 and 298 K and pressures up to 14 MPa, URL http://dx.doi.org/10.1016/j.fluid.2016.04.002, accepted for publication in Fluid Phase Equilib.

[3] S. F. Westman, H. G. J. Stang, S. Ø. Størset, H. Rekstad, A. Austegard, S. W. Løvseth, Accurate Phase Equilibrium Measurements of CO_2 Mixtures, Energy Procedia 51 (2014) 392–401, URL http://dx.doi.org/10.1016/j.egypro.2014.07.046.

[4] S. W. Løvseth, H. G. J. Stang, S. F. Westman, I. Snustad, A. Austegard, Experimental Investigations of Impurity Impact on CO_2 Mixture Phase Equilibria, Energy Procedia 63 (2014) 2589–2595, URL http://dx.doi.org/10.1016/j.egypro.2014.11.281.

[5] S. W. Løvseth, H. G. J. Stang, A. Austegard, S. F. Westman, R. Span, R. Wegge, Measurements of CO_2-rich mixture properties: status and CCS needs, accepted for publication in Energy Procedia.

[6] Historic Paris Agreement on Climate Change, http://newsroom.unfccc.int/unfccc-newsroom/finale-cop21/, accessed: 2015-12-16, 2015.

[7] IPCC, Climate Change 2014: Synthesis Report. Contribution of Working Groups I, II and III to the Fifth Assessment Report of the Intergovernmental Panel on Climate Change [Core Writing Team, R.K. Pachauri and L.A. Meyer (eds.)], Geneva, Switzerland, 151 pp, 2014.

[8] IPCC, IPCC Special Report on Carbon Dioxide Capture and Storage. Prepared by Working Group III of the Intergovernmental Panel on Climate Change [Metz, B., O. Davidson, H. C. de Coninck, M. Loos, and L. A. Meyer (eds.)], Cambridge University Press, Cambridge, United Kingdom and New York, NY, USA, 442 pp, 2005.

[9] IEA, Energy Technology Perspectives 2012: Pathways to a Clean Energy System, OECD Publishing, Paris, URL http://dx.doi.org/10.1787/energy_tech-2012-en, 2012.

[10] R. Span, W. Wagner, A New Equation of State for Carbon Dioxide Covering the Fluid Region from the Triple-Point Temperature to 1100 K at Pressures up to 800 MPa, J. Phys. Chem. Ref. Data 25 (1996) 1509, URL http://dx.doi.org/10.1063/1.555991.

[11] V. Vesovic, W. A. Wakeham, G. A. Olchowy, J. V. Sengers, J. T. R. Watson, J. Millat, The transport properties of carbon dioxide, J. Phys. Chem. Ref. Data 19 (3) (1990) 763–808, URL http://dx.doi.org/10.1063/1.555875.

[12] A. Fenghour, W. A. Wakeham, V. Vesovic, The viscosity of carbon dioxide, J. Phys. Chem. Ref. Data 27 (1) (1998) 31–44, URL http://dx.doi.org/10.1063/1.556013.

[13] H. Li, J. P. Jakobsen, Ø. Wilhelmsen, J. Yan, PVTxy Properties of CO_2 Mixtures Relevant for CO_2 Capture, Transport and Storage: Review of Available Experimental Data and Theoretical Models, Appl. Energy 88 (11) (2011) 3567–3579, URL http://dx.doi.org/10.1016/j.apenergy.2011.03.052.

[14] E. de Visser, C. Hendriks, M. Barrio, M. J. Mølnvik, G. de Koeijer, S. Liljemark, Y. Le Gallo, Dynamis CO_2 Quality Recommendations, Int. J. Greenhouse Gas Control 2 (4) (2008) 478–484, URL http://dx.doi.org/10.1016/j.ijggc.2008.04.006.

[15] S. W. Løvseth, G. Skaugen, H. G. J. Stang, J. P. Jakobsen, Ø. Wilhelmsen, R. Span, R. Wegge, CO_2 Mix Project: Experimental Determination of Thermo-Physical Properties of CO_2-Rich Mixtures, Energy Procedia 37

(2013) 7841–7849, URL http://dx.doi.org/10.1016/j.egypro.2014.09.001.

[16] H. Li, Ø. Wilhelmsen, Y. Lv, W. Wang, J. Yan, Viscosities, Thermal Conductivities and Diffusion Coefficients of CO_2 Mixtures: Review of Experimental Data and Theoretical Models, Int. J. Greenhouse Gas Control 5 (5) (2011) 1119–1139, URL http://dx.doi.org/10.1016/j.ijggc.2011.07.009.

[17] S. T. Munkejord, M. Hammer, Depressurization of CO_2-rich mixtures in pipes: Two-phase flow modelling and comparison with experiments, Int. J. Greenhouse Gas Control 37 (2015) 398–411, URL http://dx.doi.org/10.1016/j.ijggc.2015.03.029.

[18] J. Gernert, R. Span, EOS-CG: A Helmholtz energy mixture model for humid gases and CCS mixtures, J. Chem. Thermodyn. 93 (2016) 274–293, URL http://dx.doi.org/10.1016/j.jct.2015.05.015.

[19] G. J. Gernert, A New Helmholtz Energy Model for Humid Gases and CCS Mixtures, PhD dissertation, Fakultät für Maschinenbau, Ruhr-Universität Bochum, Bochum, URL http://www-brs.ub.ruhr-uni-bochum.de/netahtml/HSS/Diss/GernertGeorgJohannes/diss.pdf, 2013.

[20] S. T. Munkejord, M. Hammer, S. W. Løvseth, CO_2 transport: Data and models – a review, submitted.

[21] T. A. Demetriades, R. S. Graham, A new equation of state for CCS pipeline transport: Calibration of mixing rules for binary mixtures of CO_2 with N_2, O_2 and H_2, J. Chem. Thermodyn. 93 (2016) 294–304, URL http://dx.doi.org/10.1016/j.jct.2015.07.045.

[22] O. Kunz, W. Wagner, The GERG-2008 Wide-Range Equation of State for Natural Gases and Other Mixtures: An Expansion of GERG-2004, J. Chem. Eng. Data 57 (11) (2012) 3032–3091, URL http://dx.doi.org/10.1021/je300655b.

[23] R. Span, Multiparameter equations of state: an accurate source of thermodynamic property data, Springer, Berlin, 2000.

[24] H. G. J. Stang, S. W. Løvseth, S. Ø. Størset, B. Malvik, H. Rekstad, Accurate Measurements of CO_2 Rich Mixture Phase Equilibria Relevant for CCS Transport and Conditioning, Energy Procedia 37 (2013) 2897–2903, URL http://dx.doi.org/10.1016/j.egypro.2013.06.175.

[25] J. M. S. Fonseca, R. Dohrn, S. Peper, High-pressure fluid-phase equilibria: Experimental methods and systems investigated (2005–2008), Fluid Phase Equilib. 300 (1–2) (2011) 1–69, URL http://dx.doi.org/10.1016/j.fluid.2010.09.017.

[26] R. Dohrn, S. Peper, J. M. S. Fonseca, High-pressure fluid-phase equilibria: Experimental methods and systems investigated (2000–2004), Fluid Phase Equilib. 288 (1–2) (2010) 1–54, URL http://dx.doi.org/10.1016/j.fluid.2009.08.008.

[27] M. Christov, R. Dohrn, High-pressure fluid phase equilibria: Experimental methods and systems investigated (1994–1999), Fluid Phase Equilib. 202 (1) (2002) 153–218, URL http://dx.doi.org/10.1016/S0378-3812(02)00096-1.

[28] R. Dohrn, G. Brunner, High-Pressure Fluid-phase equilibria: Experimental Methods and Systems Investigated (1988–1993), Fluid Phase Equilib. 106 (1-2) (1995) 213–282, URL http://dx.doi.org/10.1016/0378-3812(95)02703-H.

[29] R. E. Fornari, P. Alessi, I. Kikic, High pressure fluid phase equilibria: experimental methods and systems investigated (1978–1987), Fluid Phase Equilib. 57 (1) (1990) 1–33, URL http://dx.doi.org/10.1016/0378-3812(90)80010-9.

[30] O. Fandiño, J. P. M. Trusler, D. Vega-Maza, Phase behavior of (CO_2+H_2) and (CO_2+N_2) at temperatures between (218.15 and 303.15) K at pressures up to 15 MPa, Int. J. Greenhouse Gas Control 36 (2015) 78–92, URL http://dx.doi.org/10.1016/j.ijggc.2015.02.018.

[31] Y. Arai, G.-I. Kaminishi, S. Saito, The experimental determination of the P–V–T–X relations for the carbon dioxide-nitrogen and the carbon dioxide-methane systems, J. Chem. Eng. Jpn. 4 (2) (1971) 113–122, URL http://dx.doi.org/10.1252/jcej.4.113.

[32] T. A. Al-Sahhaf, A. J. Kidnay, E. D. Sloan, Liquid+Vapor Equilibria in the N_2+CO_2+ CH_4 System, Ind. Eng. Chem. Fundam. 22 (4) (1983) 372–380, URL http://dx.doi.org/10.1021/i100012a004.

[33] T. S. Brown, V. G. Niesen, E. D. Sloan, A. J. Kidnay, Vapor-liquid equilibria for the binary systems of nitrogen, carbon dioxide, and n-butane at temperatures from 220 to 344 K., Fluid Phase Equilib. 53 (1989) 7–14, URL http://dx.doi.org/10.1016/0378-3812(89)80067-6.

[34] T. S. Brown, E. D. Sloan, A. J. Kidnay, Vapor-liquid equilibria in the nitrogen+carbon dioxide+ethane system, Fluid Phase Equilib. 51 (1989) 299–313, URL http://dx.doi.org/10.1016/0378-3812(89)80372-3.

[35] G. Kaminishi, T. Toriumi, Vapor-Liquid Phase Equilibrium in the CO_2-H_2, CO_2-N_2 and CO_2-O_2 Systems [in Japanese], Kogyo Kagaku Zasshi 69 (1966) 175–178, URL http://doi.org/10.1246/nikkashi1898.69.2_175.

[36] I. R. Krichevskii, N. E. Khazanova, L. S. Lesnevskaya, L. Y. Sandalova, Equilibrium of Liquid-Gas at High Pressures in the System Nitrogen-Carbon Dioxide [in Russian], Khim. Prom-st. 3 (1962) 169–171.

[37] F. A. Somait, A. J. Kidnay, Liquid-Vapor Equilibria at 270.00 K for Systems Containing Nitrogen, Methane, and Carbon Dioxide, J. Chem. Eng. Data 23 (4) (1978) 301–305, URL http://dx.doi.org/10.1021/je60079a019.

[38] D. S. Tsiklis, Heterogeneous Equilibria in Binary Systems [in Russian], Zh. Fiz. Khim. 20 (1946) 181–188.

[39] N. Xu, J. Dong, Y. Wang, J. Shi, High pressure vapor liquid equilibria at 293 K for systems containing nitrogen, methane and carbon dioxide, Fluid Phase Equilib. 81 (1992) 175–186, URL http://dx.doi.org/10.1016/0378-3812(92)85150-7.

[40] M. Yorizane, S. Yoshimura, H. Masouka, Vapor-Liquid Equilibrium at High Pressure (N_2-CO_2, H_2-CO_2) [in Japanese], J. Chem. Eng. Jpn. 34 (1970) 953–957.

[41] B. Yucelen, A. J. Kidnay, Vapor-Liquid Equilibria in the Nitrogen+Carbon Dioxide+Propane System from 240 to 330 K at Pressures to 15 MPa, J. Chem. Eng. Data 44 (5) (1999) 926–931, URL http://dx.doi.org/10.1021/je980321e.

[42] G. H. Zenner, L. I. Dana, Liquid-vapor equilibrium compositions of carbon dioxide-oxygen-nitrogen mixtures, in: Chem. Eng. Prog., Symp. Ser., vol. 59, 36–41, 1963.

[43] B. Bian, Y. Wang, J. Shi, E. Zhao, B. C.-Y. Lu, Simultaneous determination of vapor-liquid equilibrium and molar volumes for coexisting phases up to the critical temperature with a static method, Fluid Phase Equilib. 90 (1) (1993) 177–187, URL http://dx.doi.org/10.1016/0378-3812(93)85012-B.

[44] M. Yorizane, S. Yoshimura, H. Masuoka, Y. Miyano, Y. Kakimoto, New Procedure for Vapor-Liquid Equilibria. Nitrogen+Carbon Dioxide, Methane+Freon 22, and Methane+Freon 12, J. Chem. Eng. Data 30 (2) (1985) 174–176, URL http://dx.doi.org/10.1021/je00040a012.

[45] G. Trappehl, Experimentelle Untersuchung der Dampf-Flüssigkeits-Phasengleichgewichte und kalorischen Eigenschaften bei tiefen Temperaturen und hohen Drücken an Stoffgemischen bestehend aus N_2, CH_4, C_2H_6, C_3H_8 und CO_2, Ph.D. thesis, Technische Universität Berlin, 1987.

[46] T. A. Al-Sahhaf, Vapor–liquid equilibria for the ternary system N_2+CO_2+CH_4 at 230 and 250 K, Fluid Phase Equilib. 55 (1) (1990) 159–172, URL http://dx.doi.org/10.1016/0378-3812(90)85010-8.

[47] W. Weber, S. Zeck, H. Knapp, Gas solubilities in liquid solvents at high pressures: apparatus and results for binary and ternary systems of N_2, CO_2 and CH_3OH, Fluid Phase Equilib. 18 (3) (1984) 253–278, URL http://dx.doi.org/10.1016/0378-3812(84)85011-6.

[48] Y. A. Abdulayev, The Study of the Equilibrium Systems of Liquid Carbon Dioxide in the Presence of Technical Gases, Zh. Khim. Prom. 16 (1939) 37–40.

[49] N. K. Muirbrook, Experimental and Thermodynamic Study of the High-Pressure Vapor-Liquid Equilibria for the Nitrogen-Oxygen-Carbon Dioxide System, Ph.D. thesis, University of California, Berkeley, 1964.

[50] H. A. Duarte-Garza, J. C. Holste, K. R. Hall, K. N. Marsh, B. E. Gammon, Isochoric pVT and phase equilibrium measurements for carbon dioxide+ nitrogen, J. Chem. Eng. Data 40 (3) (1995) 704–711, URL http://dx.doi.org/10.1021/je00019a038.

[51] G. J. Esper, D. M. Bailey, J. C. Holste, K. R. Hall, Volumetric behavior of near-equimolar mixtures for CO_2+CH_4 and CO_2+N_2, Fluid Phase Equilib. 49 (1989) 35–47, URL http://dx.doi.org/10.1016/0378-3812(89)80004-4.

[52] M.-J. Tenorio, A. J. Parrott, J. A. Calladine, Y. Sanchez-Vicente, A. J. Cresswell, R. S. Graham, T. C. Drage, M. Poliakoff, J. Ke, M. W. George, Measurement of the vapour–liquid equilibrium of binary and ternary mixtures of CO_2, N_2 and H_2, systems which are of relevance to CCS technology, Int. J. Greenhouse Gas Control 41 (2015) 68–81, URL http://dx.doi.org/10.1016/j.ijggc.2015.06.009.

[53] D.-Y. Peng, D. B. Robinson, A New Two-Constant Equation of State, Ind.

Eng. Chem. Fundam. 15 (1) (1976) 59–64, URL http://dx.doi.org/10.1021/i160057a011.

[54] P. M. Mathias, T. W. Copeman, Extension of the Peng-Robinson equation of state to complex mixtures: Evaluation of the various forms of the local composition concept, Fluid Phase Equilib. 13 (1983) 91–108, URL http://dx.doi.org/10.1016/0378-3812(83)80084-3.

[55] D. S. H. Wong, S. I. Sandler, A Theoretically Correct Mixing Rule for Cubic Equations of State, AIChE J. 38 (5) (1992) 671–680, URL http://dx.doi.org/10.1002/aic.690380505.

[56] H. Renon, J. M. Prausnitz, Local compositions in thermodynamic excess functions for liquid mixtures, AIChE J. 14 (1) (1968) 135–144, URL http://dx.doi.org/10.1002/aic.690140124.

[57] A. Fredenslund, G. A. Sather, Gas-liquid equilibrium of the oxygen-carbon dioxide system, J. Chem. Eng. Data 15 (1) (1970) 17–22, URL http://dx.doi.org/10.1021/je60044a024.

[58] A. Fredenslund, J. Mollerup, O. Persson, Gas-liquid equilibrium of oxygen-carbon dioxide system, J. Chem. Eng. Data 17 (4) (1972) 440–443, URL http://dx.doi.org/10.1021/je60055a019.

[59] R. Engberg, D. Köpke, R. Eggers, Die Grenzflächenspannungen von CO_2–O_2–und Rauchgas-Mischungen, Chem. Ing. Tech. 81 (9) (2009) 1439–1443, URL http://dx.doi.org/10.1002/cite.200900052.

[60] W. H. Keesom, Isothermals of mixtures of oxygen and carbon dioxide (with two plates), Commun. Phys. Lab. Univ. Leiden 88 (1903) 1–85.

[61] H. S. Booth, J. M. Carter, The Critical Constants of Carbon Dioxide-Oxygen Mixtures, J. Phys. Chem. 34 (12) (1930) 2801–2825, URL http://dx.doi.org/10.1021/j150318a013.

[62] M. Ahmad, J. Gernert, E. Wilbers, Effect of impurities in captured CO_2 on liquid–vapor equilibrium, Fluid Phase Equilib. 363 (2014) 149–155, URL http://dx.doi.org/10.1016/j.fluid.2013.11.009.

Articles

Article I

Vapor-liquid equilibrium data for the carbon dioxide and nitrogen (CO_2 + N_2) system at the temperatures 223, 270, 298 and 303 K and pressures up to 18 MPa [1]

S.F. Westman, H.G.J. Stang, S.W. Løvseth, A. Austegard, I. Snustad, S.Ø. Størset, I.S. Ertesvåg, Fluid Phase Equilib. 409 (2016) 207-241, doi:10.1016/j.fluid.2015.09.034

Fluid Phase Equilibria 409 (2016) 207–241

Contents lists available at ScienceDirect

Fluid Phase Equilibria

journal homepage: www.elsevier.com/locate/fluid

Vapor–liquid equilibrium data for the carbon dioxide and nitrogen ($CO_2 + N_2$) system at the temperatures 223, 270, 298 and 303 K and pressures up to 18 MPa

Snorre Foss Westman [a, *], H.G. Jacob Stang [b], Sigurd W. Løvseth [b, **], Anders Austegard [b], Ingrid Snustad [b], Sigmund Ø. Størset [b], Ivar S. Ertesvåg [a]

[a] Norwegian University of Science and Technology, Department of Energy and Process Engineering, Kolbjørn Hejes vei 1b, NO-7491 Trondheim, Norway
[b] SINTEF Energy Research, NO-7465 Trondheim, Norway

ARTICLE INFO

Article history:
Received 3 July 2015
Received in revised form
14 September 2015
Accepted 17 September 2015
Available online 25 September 2015

Keywords:
Vapor–liquid equilibrium
Experimental measurements
Carbon dioxide
Nitrogen
CO_2 capture and storage

ABSTRACT

A new setup for the measurement of vapor–liquid phase equilibria of CO_2-rich mixtures relevant for carbon capture and storage (CCS) transport conditions is presented. An isothermal analytical method with a variable volume cell is used. The apparatus is capable of highly accurate measurements in terms of pressure, temperature and composition, also in the critical region. Vapor-liquid equilibrium (VLE) measurements for the binary system $CO_2 + N_2$ are reported at 223, 270, 298 and 303 K, with estimated standard uncertainties of maximum 0.006 K in the temperature, maximum 0.003 MPa in the pressure, and maximum 0.0004 in the mole fractions of the phases. These measurements are verified against existing data. Although some data exists, there is little trustworthy data around critical conditions, and our data indicate a need to revise the parameters of existing models. A fit made against our data of the vapor–liquid equilibrium prediction of GERG-2008/EOS-CG for $CO_2 + N_2$ is presented. At 223 and 298 K, the critical region of the isotherm are fitted using a scaling law, and high accuracy estimates for the critical composition and pressure are found.

1. Introduction

Knowledge about how CO_2-rich mixtures behave under different conditions is important for the development of carbon capture, transport and storage (CCS) processes. For instance, an accurate equation of state (EOS) describing the thermodynamic properties of these mixtures is needed to model and dimension the various processes along the CCS value chain. Moreover, an EOS can be used to set requirements on the amount of impurities present in the CO_2 to be transported. Even with the recent progress of molecular modeling, empirical EOSs still provide the most accurate description of thermodynamic properties of such systems. Unfortunately, even for relatively simple binary mixtures, the data situation is not satisfactory for all relevant mixtures and conditions [1–3]. Hence, new and accurate experimental data are needed in order to improve the thermodynamic property predictions, by developing new EOS models or modifying the parameters and structure of existing ones.

Even small amounts of impurities in CO_2-rich mixtures can significantly affect the behavior of the fluid [3,4]. As an example, the maximum pressure at which a mixture of CO_2 and only 5% N_2 can be in the two-phase region, the cricondenbar, will increase to approximately 8.4 MPa compared to the critical pressure of CO_2, 7.3773 MPa [4–6].

Until recently, the most accurate EOS model describing CO_2-rich mixtures has been the GERG-2008 [7,8]. This EOS [7] covers most of the relevant mixtures expected in CO_2 conditioning and transport found in CCS [8,3,9]. The structure and parameters in this EOS were developed and fitted with focus on natural gas mixtures.

In the works by Gernert and Span [1] and Gernert [2], an equation of state called EOS-CG (Equation Of State for Combustion Gases and combustion gas like mixtures) has been developed specifically for CO_2-rich mixtures. The EOS was based on the structure of GERG-2008, with modifications for the binary CO_2-rich systems found within CCS. The EOS was fitted against a significantly

* Corresponding author.
** Corresponding author.
E-mail addresses: snorre.f.westman@ntnu.no (S.F. Westman), sigurd.w.lovseth@sintef.no (S.W. Løvseth).

http://dx.doi.org/10.1016/j.fluid.2015.09.034
0378-3812/

extended literature data base for CO_2-rich mixtures compared to the GERG-2008 data base [1,2].

However, as Gernert and Span [1] and Gernert [2] pointed out in the review of available literature data, large gaps occur in the experimental data for thermophysical properties of CO_2-rich mixtures [3,10]. Moreover, some of the existing data from different authors are systematically inconsistent with those of other authors within the stated uncertainty estimates. As a consequence, the accuracy of the equations of state fitted to the data could be increased significantly by reconciling the inconsistencies and filling in the gaps in the available data.

The work to be presented here is part of a project called CO_2Mix. As described by Løvseth et al. [5], the CO_2Mix project aims at performing accurate vapor–liquid equilibrium (VLE), speed of sound and density measurements of CO_2-rich mixtures at conditions relevant for transport and conditioning in CCS [3,9]. As part of this project, a setup has been specifically designed and constructed in order to perform highly accurate phase equilibria measurements on CO_2-rich mixtures under relevant conditions for CCS.

The present paper reports the results of VLE measurements on the CO_2 + N_2 binary system, with measurements over the whole VLE pressure region at the temperatures 223, 298 and 303 K, and one VLE data point at 270 K. For some conditions, high quality literature data exist for this system, making it suitable to validate the operation of the experimental setup. Furthermore, several measurements were taken at conditions where no previous data or only data of dubious quality could be found, for instance at pressures close to the critical point of the binary mixture at the measured temperatures. Additionally, measurements were performed at temperatures close to the critical temperature of CO_2. The results are compared to existing EOS models, and new fits are presented.

Special care has been taken by the authors to present the results and analysis in accordance with the IUPAC Guidelines for reporting of phase equilibrium measurements given in the work by Chirico et al. [11]. One of the most important aspects of this is the thorough estimation of the standard uncertainties, as specified in the ISO Guide for the Estimation of Uncertainty in Measurement, commonly referred to as “GUM” [12]. Error-free dissemination of the resulting experimental data with the uncertainty estimates is ensured by supplying the data in a file written in the NIST ThermoML format [13–16].

In the current work, the experimental setup and the operational procedures applied will be described in detail in Section 2. In Section 3, an analysis of the pressure, temperature and composition measurement uncertainty will be presented, with references to further details in the appendix. The measurement results will be provided in Section 4, before an analysis of the data with regards to existing data and models in Section 5. Section 5 will also present fitting of existing models to the new data.

2. Experimental apparatus

2.1. Description of setup

The experimental setup has been described briefly in Ref. [17]. A more detailed description will be given here. Additional details necessary for the uncertainty analysis for the measurement of pressure, temperature, and composition will be given in Sections 3.2, 3.3, and 3.4, respectively.

The vapor–liquid equilibrium measurements were carried out using an isothermal analytical method with a variable-volume cell, as described by Ref. [18]. This method involves determination of the equilibrium composition of both phases at given temperature and pressure. A diagram of the cell and the ancillary apparatus is shown in Fig. 1.

In our experiments with 2 components, CO_2 and N_2, Gibbs' phase rule states that we can vary 2 intensive properties freely when we have 2 coexisting phases present. We controlled the temperature T by means of a thermostatic bath, and the pressure p by the injection of CO_2 and N_2 into the cell. We can then state the equilibrium compositions of the liquid and vapor phases, x_{CO_2} and y_{CO_2}, respectively, as functions of T and p:

$$x_{CO_2} = f(T, p), \tag{1}$$

$$y_{CO_2} = f(T, p). \tag{2}$$

The cell consisted of a transparent sapphire cylinder tube placed between two titanium flanges. The internal volume of the cell was approximately 100 ml. To keep the temperature constant, the cell was placed in a thermostatic bath kept at the desired temperature (Fluke Hart Scientific model 7080 for subambient temperatures, and model 6020 with external cooling water for temperatures above ambient). The following two bath fluids were used: at temperatures below ambient, ethanol, and for temperatures close to the critical temperature of CO_2, distilled water.

The temperature of the cell was monitored by two Fluke model 5686 glass capsule standard platinum resistance thermometers (SPRT) placed inside the top and bottom flanges.

The cell pressure was measured indirectly through a Rosemount 1199 diaphragm connected by an oil-filled circuit to a Rosemount 3051 differential pressure transmitter with an array of four absolute pressure sensors p_i, where i = 1, 2, 3, 4, (Keller model PAA-33X) with full scales of 1, 3, 10 and 20 MPa respectively, on the other side. The absolute pressure sensor circuit was filled with nitrogen and maintained at a pressure such that the differential pressure between this circuit and the cell circuit was close to zero, using syringe pump 5 (TOP Industrie, model PMHP 100–500).

Three different syringe pumps (from TOP Industrie) were used to fill the components into the cell. Pump 2 was dedicated to injecting CO_2 (model PMHP 100–500). Pump 3 was used to inject an impurity, which was N_2 in the case of the present work (model PMHP 200-200). The surface of the parts of the pump and the tubing in contact with the fluid was sulfinert treated to minimize adsorption. Pump 4 could be used to inject fluids in liquid state, such as water, in later work (model PMHP 100–500). All three pumps could be evacuated through a connection to a vacuum pump (Trivac® E 2 from Leybold).

These pumps were connected via tubing to valves that were integrated in the cell flanges. Integrated valves were used to minimize the dead volume inside the cell. An additional integrated valve could be opened to ventilation when the cell pressure needed to be reduced.

The vacuum pump was connected to an integrated valve, enabling evacuation of the cell before the filling took place.

A magnetic stirrer was placed at the bottom of the cell, and could be rotated at up to 800 rpm to reach VLE faster.

A borescope was used to inspect the content of the cell through the transparent sapphire cylinder, to ensure that the liquid level was appropriate.

A custom made National Instruments LabVIEW program was used for data acquisition of the measured pressure and temperature values, which were logged every second.

The resistance of the two SPRTs were measured one at a time using an ASL SB148 switchbox to change between the two SPRTs, which in turn was connected to an ASL F650AC thermometry bridge. A resistance measurement point of one resistor was obtained once every 20 s when the ASL bridge was set to obtain the most accurate ratio value. The ASL bridge measured ratio values

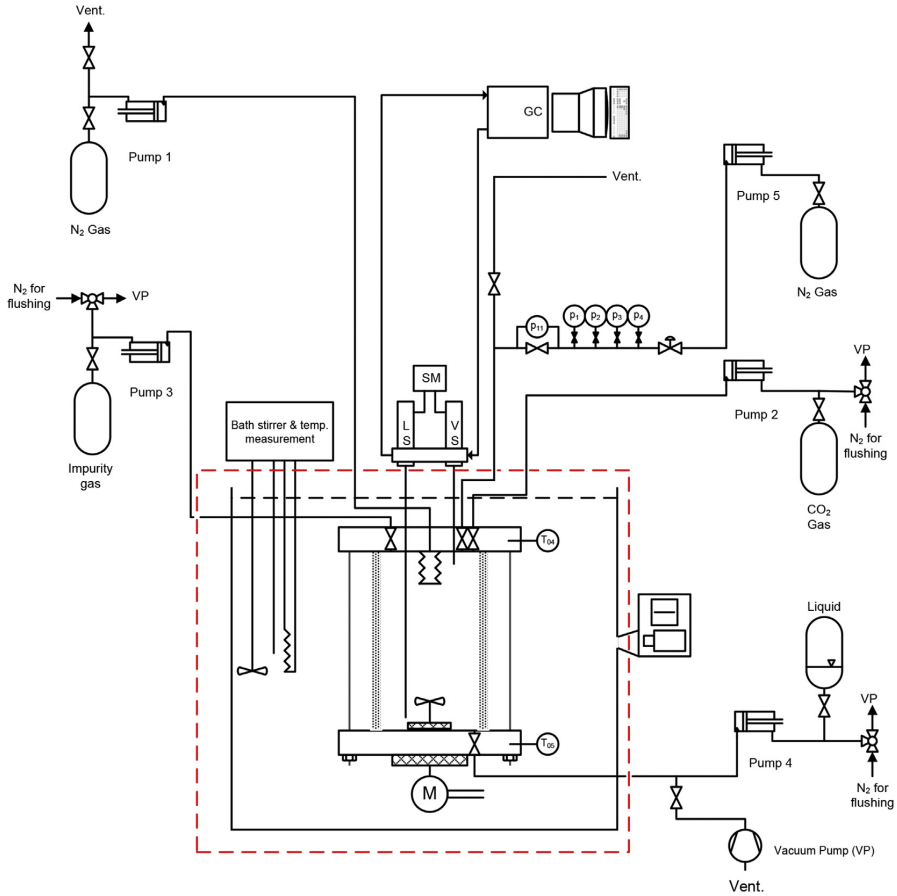

Fig. 1. Principal diagram of cell and ancillary apparatus. LS,VS: Liquid and vapor phase Rolsi™ samplers, respectively. SM: Rolsi™ controller. M: Gear for rotating permanent magnet below cell, which rotates stirrer inside cell. Gear connected to electric motor outside bath. T_{04}: top flange SPRT. T_{05}: bottom flange SPRT.

were obtained by the logging program through an USB connection.

The update rates of the four pressure sensors p_i were 400 Hz, and the dead time of the differential pressure sensor p_{11} was approximately 45 ms. The measured pressure values of p_i were obtained by the logging program using the digital output of the sensors through a RS485 serial connection. The values of p_{11} were obtained using a conversion of the analog 4–20 mA DC current output of the sensor to a digital output read through a RS485 serial connection by the logging program.

The compositions of the vapor and liquid phases were measured by extracting a sample from a phase using Rolsi™ electromagnetic samplers (Armines patent [19]. Pneumatic version of the Rolsi™ sampler described in Ref. [20]). The vapor phase sampling capillary inlet was placed close to the top flange inside the cell, while the liquid phase capillary inlet could be moved vertically inside the cell to be at an appropriate position in the liquid phase. The use of these Rolsi™ samplers for VLE measurements was first described in Ref. [21].

Using the LabVIEW program, the electromagnetically controlled valves of the Rolsi™ samplers were opened for a specified time period to let a sample flow out of the cell. The sample flowed out through the capillaries into a heated gas chromatograph (GC) helium carrier gas circuit at close to atmospheric pressure. The low-pressure side of the Rolsi™ valves and piping between the valves and GC were also heated above the critical temperature of CO_2, ensuring that both the vapor and liquid samples were in gaseous form. The sample was swept by the carrier gas into the GC (Agilent 7890A) equipped with a Supelco Carboxen-1010 PLOT Capillary GC Column (from Sigma–Aldrich, column length 30 m, internal diameter 0.53 mm) where the CO_2 and N_2 were separated. Downstream of the column, a thermal conductivity detector (TCD) measured the difference in voltage needed to keep the gas passing the detector at a constant temperature. The detector response was monitored as a function of time at 5 Hz, resulting in two separate peaks corresponding to N_2 and CO_2. At sampling, the logging of the detector response was started automatically with the Agilent OpenLAB CDS EZChrom GC data acquisition and control software.

When a sample was taken, pump 1 was used to apply an increased N_2 overpressure compared to the cell pressure on a plate bellows inside the cell, to expand the bellows and thereby decreasing the cell volume, preventing a decrease in cell pressure after each sample. Fully expanded, the bellows caused an

approximate volume decrease inside the cell of maximum 1 cm^3.

The internal diameter of the Rolsi™ capillaries were 150 μm, and the length of the liquid and vapor phase capillaries were 0.4 and 0.3 m, respectively. The internal volumes of the liquid and vapor capillaries corresponded to approximately 0.007 and 0.005% of the cell volume, respectively. The upper part of the both the liquid and the vapor capillaries were outside the thermostatic bath, and were heated to 313 K to avoid condensation.

As the liquid in the heated upper part of the liquid capillary would boil off, too small samples would only consist of the boil-off gas with a composition that would not be representative of the liquid phase in the cell. In order to be sure to measure the true liquid composition, the number of moles of each liquid sample should at least be as large as what is found in a volume of the whole liquid capillary with the same density and composition as the liquid phase inside the cell. As some of the volume of the liquid sampler was occupied by a vapor phase with lower density than a liquid phase, the calculated liquid sample size was probably an overestimate, but helped ensure thorough flushing of the liquid capillary for each sample. Because the sample size should be sufficient to flush the capillaries, the expansion of the bellows was necessary to prevent a significant change in the cell pressure. For the vapor samples, the first samples of a series at a pressure/temperature point were of a sufficient size to flush the vapor capillary. Consecutive sample sizes were set large enough to give a good repeatability in the composition measurements. The repeatability as a function of sample size was determined from the calibration of the GC using the calibration gas mixtures.

In practical terms, the sample volumes discussed above were estimated from the GC traces. The liquid phase density and composition were calculated using the GERG-2008 EOS [7] at the cell pressure and temperature. An estimate of the number of moles in a sample as a function of the peak areas of each component in the GC traces was established by injecting each of the components into the GC through a sample loop with a known volume, kept at ambient temperature and slightly higher than atmospheric pressure. The densities of the pure components were calculated using the EOSs by Refs. [6,22].

2.2. Calibration

The two SPRTs used for temperature measurements had been calibrated in-house according to the International Temperature Scale of 1990 (ITS-90) [23], against fix point cells calibrated at accredited calibration laboratories. Details about the calibration of the SPRTs can be found in Section 3.3.

The absolute pressure sensors had been calibrated in-house against a dead weight tester recently calibrated at an accredited calibration laboratory. For details, see Section 3.2.

The GC had been calibrated against gravimetrically prepared calibration gas mixtures made in-house. See Section 3.4 for details.

The manufacturer's specified purity of the CO_2 and N_2 samples used for both the VLE experiments, and for preparing the calibration gas mixtures, are listed in Table 1. We did not perform any additional analysis of the specified purity of the samples by for instance mass spectroscopy. However, as we performed vapor pressure measurements of CO_2 at the different temperatures where VLE measurements were performed, we asserted that the vapor pressures were in agreement with the calculated vapor pressures from the EOS by Span and Wagner [6], within the combined uncertainty in our pressure measurements and in the EOS calculations.

2.3. Experimental procedures

Before starting a VLE experiment, the whole circuit in connection with the VLE cell was evacuated, using the vacuum pump. The evacuation included the gas lines to the cell from the gas cylinders of pure CO_2 and N_2, and all lines transporting the gases into the cell.

The CO_2 pump and N_2 impurity pump and lines were first evacuated once, and then flushed with the respective gases to dilute any remaining impurities in the lines and pumps. This evacuation and flushing were repeated 5 times for each pump. After the final evacuation, the gases were filled onto their respective lines and pumps, and maintained at a pressure of at least 0.5 MPa to prevent contamination of the gases.

After the flushing of the gas lines and pumps, the cell was flushed with CO_2, and evacuated. As with the pumps, the flushing and evacuation were repeated 5 times.

Following the flushing, and with the thermostatic bath kept at the desired temperature, CO_2 was injected until the volume fraction of liquid CO_2 was approximately 50% of the cell.

The stirrer then ran until the pressure and temperature measurements had stabilized. After the stirrer had been turned off, the vapor pressure of CO_2 was measured. If the measured vapor pressure were within the combined uncertainty of the Span-Wagner EOS [6] and our measurements, the purity of the CO_2 in the cell was deemed to be sufficient.

After the CO_2 vapor pressure measurements, N_2 was filled onto the cell to increase the pressure, and the stirrer was run until the temperature and pressure had stabilized. The liquid level in the cell was adjusted to keep a liquid volume fraction of approximately 50%, by either injecting more CO_2 or venting out either some of the vapor or liquid phase. The liquid phase capillary inlet was placed such as to always be more than 10 mm below the liquid level in the cell.

After this, the borescope was removed from the thermostatic bath to prevent heat transfer from the surroundings into the bath fluid. When the cell pressure and temperature had stabilized, the stirrer was turned off, and the vapor and liquid phases were left to settle before sampling started.

From this point on, there were two different procedures employed in this work. The series of experiments started off with VLE measurements at 298 K, and then 303, 223 and 270 K. At the end of the VLE experiments at 303 K, the bellows started leaking N_2 into the cell. To avoid delay in the measurements, it was decided to replace the bellows with a blind plug, and proceed with VLE experiments at the 223 and 270 K without pressure compensation of sampling, and hence using slightly different procedures than for the previous isotherms.

Table 1
Chemical samples used.

Chemical name	CASRN	Source	Initial mole fraction purity	Purification method	Final mole fraction purity	Analysis method
Carbon dioxide	124-38-9	Yara Praxair	0.99999	None	0.99999	None
Nitrogen	7727-37-9	Yara Praxair	0.999999	None	0.999999	None
Helium[a]	7440-59-7	Yara Praxair/AGA	0.999999	None	0.999999	None

[a] GC carrier gas.

For the measurements at 298 and 303 K, with the pressure drop due to sampling compensated by using the bellows, a sample was withdrawn from the cell every 25 min.

For the measurements at 223 and 270 K, the pressure dropped slightly after each sample. Two different methods were used to approach the VLE state of the new pressure value. In the first method, the stirrer was run for 15 min after each sampling, and then turned off to allow the phases to separate for the remaining 10 min before the next sample was taken. In the second method, the stirrer was not used between the samples. Instead, the period between each sample was increased from 25 min to 2–3 h.

3. Uncertainty analysis

3.1. Definitions

The "GUM" [12] terms and definitions will be used in the following analysis. For ease of reading, and, since several of the estimation methods will be used repeatedly, some of the symbols used will be defined here.

The uncertainty components will be evaluated as standard uncertainties, with symbol $u(y)$, where y is the estimate of the measurand Y, that is, the measurement result. Standard uncertainty is the uncertainty of the result of a measurement expressed as an estimated experimental sample standard deviation, with symbol $s(y)$ [12].

Type A evaluation of uncertainty refers to uncertainties evaluated by statistical analysis of a series of observations [12]. Examples include the evaluation of the uncertainty of the mean values of pressure and temperature in the time before a single sample is taken of the composition of the phases in the cell.

Type B evaluation of uncertainty refers to uncertainties evaluated by other means, for example specifications of measurement equipment provided by the manufacturer, or when the uncertainty of a value has to be subjectively evaluated, as in the case of measured physical distances on the laboratory apparatus for the calculation of the hydrostatic pressure. Common for these type of evaluations is that the uncertainties have to be modeled using an applicable probability distribution [12].

The propagation of the standard uncertainties in the input quantities X_i to the standard uncertainty in the final estimate of the measurand is described by the combined standard uncertainty, symbol $u_c(y)$.

For N uncorrelated input quantities, the general expression for $u_c(y)$ is given by Ref. [12] as

$$u_c^2(y) = \sum_{i=1}^{N} \left(\frac{\partial f}{\partial x_i}\right)^2 u^2(x_i), \tag{3}$$

where $Y = f(X_1, X_2, \ldots, X_N)$.

When it is difficult to determine if the input quantities are independent, or if the correlation of the quantities is not possible to determine, the most conservative estimate is assumed, that the maximum errors in each contribution occurs simultaneously:

$$u_c(y) = \sum_{i=1}^{N} \left|\frac{\partial f}{\partial x_i}\right| |u(x_i)|. \tag{4}$$

Some of the standard uncertainty terms $u(x_i)$ in these equations have to be evaluated from other underlying standard uncertainties without knowing the functional form of f. This is the case, for example, for manufacturers' specifications of several sources of uncertainties contributing to the total uncertainty in the measured value. When this is the case, and the contributions are assumed to be independent, the total standard uncertainty is evaluated with Eq. (5a).

When the contributions cannot be assumed to be independent, the most conservative estimate is assumed, similar to Eq. (4), shown in Eq. (5b).

$$u(x_i) = \begin{cases} \sqrt{\Sigma_{k=1}^{N} u^2(x_k)} & \text{if independent,} \quad (5a) \\ \Sigma_{k=1}^{N} \left|u(x_k)\right| & \text{if not independent.} \quad (5b) \end{cases}$$

These maximum estimates are also used in cases where such a maximum estimate does not contribute significantly to the final combined uncertainty in a value. Examples include cases where another source of uncertainty completely dominates the final combined uncertainty.

It is sometimes only possible to assume that a quantity X_i lies within an interval $[a_-, a_+]$ with a probability equal to one. In these cases, the quantity is modeled using either a rectangular or triangular probability distribution. If the expected value of X_i is estimated as $x_i = (a_- + a_+)/2$, and $a = |a_- - a_+|/2$, the standard uncertainty is estimated as $u(x_i) = a/\sqrt{3}$ for the rectangular distribution, and $u(x_i) = a/\sqrt{6}$ for the triangular distribution.

3.2. Pressure

The standard uncertainties connected to the measurement of pressure p at VLE are summarized in Table 2, and the justification for these uncertainties is presented in Appendix A.1.

To illustrate the final estimated uncertainty in the pressure measurements resulting from the analysis in Appendix A.1, Fig. 2 shows the pressure standard uncertainty relative to the measured pressure for the VLE measurements performed in this work.

3.3. Temperature

The standard uncertainties connected to the measurement of temperature T at VLE are summarized in Table 3, and the justification for these uncertainties is presented in Appendix A.2.

The temperature standard uncertainty estimated in Appendix A.2 is illustrated by Fig. 3, which shows the temperature uncertainty for the VLE experiments performed in this work.

3.4. Composition

The results of the calibration of the GC, and the analysis of the estimated uncertainty in the measured compositions of the phases, are given in detail in Appendix A.3. The standard uncertainty in the CO_2 mole fractions of the phases is estimated to be $u(x_{CO_2}) = u(y_{CO_2}) = 2.7 \cdot 10^{-4}$.

3.5. Data reduction

As mentioned in Section 2.3, there is a small pressure drop after each composition sample is withdrawn from the cell. The experiments at 298 and 303 K were carried out using pressure compensation after each composition sample was extracted, while no pressure compensation was done at 223 and 270 K.

For the experiments at 298 and 303 K, the cell pressure returned to its original value around 3–5 min after liquid or vapor sampling, after which the cell pressure was stable for the remaining 20 min until the next composition sample was taken. In these measurements, it was not possible to see a trend in the composition from sample to sample. Therefore, it was assumed that each composition sample represented the equilibrium composition at the pressure and temperature just before the sample was withdrawn from the

Table 2
Summary of standard uncertainty components for pressure measurements.

Symbol	Description and unit	u
Hydrostatic pressure p_{hs}		
$u(\rho_1)$	EOS-CG[b] vapor density of $CO_2 + N_2$ (kg m^{-3})	$3\cdot10^{-3}\cdot\rho_1$
$u(\rho_2)$	Same as $u(\rho_1)$ (kg m^{-3})	$3\cdot10^{-3}\cdot\rho_2$
$u(\rho_{4,1})$	SW[a] density at 313.15 K (kg m^{-3})	$3\cdot10^{-4}\cdot\rho_{4,1}$
$u(\rho_{4,2})$	Same as $u(\rho_1)$ (kg m^{-3})	$3\cdot10^{-3}\cdot\rho_{4,2}$
u(CAD)	(m)	0
$u_c(h_1)$	(m)	0.0048
$u(h_{liq})$	(m)	0.0048
$u(h_{liq},1)$	Borescope h_{liq} (m)	0.0048
$u(h_{liq},2)$	Variation in h_{liq} (m)	0
$u(h_2)$	Bath liquid level variation (m)	0.006
$u_c(h_3)$	(m)	0.006
$u(h_4)$	Same as u(CAD) (m)	0
$u(g_L)$	Local g (m s^{-2})	$2\cdot10^{-7}$
Differential pressure p_{11}		
$u(p_{11},1)$	Ambient temperature (MPa)	0
$u(p_{11},2)$	Line pressure zero (MPa)	0
$u(p_{11},3)$	Line pressure span (MPa)	$4.9\cdot10^{-5}$ MPa$^{-1}\cdot p_i\cdot p_{11}$
$u(p_{11},4)$	Mounting (MPa)	0
$u(p_{11},5)$	Vibration (MPa)	$2.8\cdot10^{-5}$
$u(p_{11},6)$	Power supply (MPa)	0
$u(p_{11},7)$	A/D conversion (MPa)	$2.4\cdot10^{-4}$
Pressure sensors p_i		
$u(p_1)$	1 MPa sensor (MPa)	$2.24\cdot10^{-4}$
$u(p_2)$	3 MPa sensor (MPa)	$2.33\cdot10^{-4}$
$u(p_3)$	10 MPa sensor (MPa)	$7.64\cdot10^{-4}$
$u(p_4)$	20 MPa sensor (MPa)	$1.965\cdot10^{-3}$

[a] Span and Wagner [6].
[b] Gernert and Span [1] and Gernert [2].

cell. With respect to temperature, it has not been possible to see any variations caused by the withdrawal of a composition sample from the cell.

For the experiments at 223 and 270 K, the cell pressure decreased after each composition sample. To reach equilibrium at this new lowered pressure, the stirrer inside the cell was run for 10 min right after the composition sample was extracted, and then turned off to let the contents of the cell settle for the remaining 15 min until the next composition sample. For some of the series, instead of stirring after each sample, we waited for 2 or 3 h to let the cell reach VLE again before a new sample was taken. The changes in composition from sample to sample were consistent with the decrease in pressure, considering the derivatives $\partial x_{CO_2}/\partial p$ and $\partial y_{CO_2}/\partial p$ evaluated numerically from the fitted version of EOS-CG

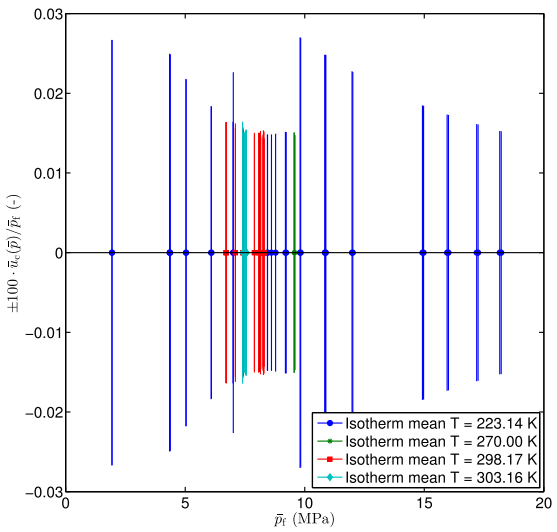

Fig. 2. Pressure standard uncertainty relative to the measured pressure for the VLE measurements performed, expressed as $100\cdot\overline{u}_c(\overline{p})/\overline{p}_f$. Measured pressure $\overline{p}_f$. Standard uncertainty $\overline{u}_c(\overline{p})$.

Table 3
Summary of standard uncertainty components for temperature measurements.

Symbol	Unit	u
$u(W_b)$	(−)	$0.35\cdot10^{-6}$
$u(R_{ref})$	(Ω)	$8.5\cdot10^{-6}$
$u(T_{H_2O})$	(mK)	0.51
$u(T_{Hg})$	(mK)	1.43
$u(T_{Ga})$	(mK)	0.85
For experiments at 298 K and 303 K		
$u(R_{H_2O}(T_{04}))$	(Ω)	$2.06\cdot10^{-5}$
$u(R_{H_2O}(T_{05}))$	(Ω)	$2.41\cdot10^{-5}$
$u(R_{Hg}(T_{04}))$	(Ω)	$2.29\cdot10^{-5}$
$u(R_{Hg}(T_{05}))$	(Ω)	$1.84\cdot10^{-5}$
$u(R_{Ga}(T_{04}))$	(Ω)	$2.19\cdot10^{-5}$
$u(R_{Ga}(T_{05}))$	(Ω)	$2.37\cdot10^{-5}$
$u(W_{Hg}(T_{04}))$	(−)	$6.1\cdot10^{-6}$
$u(W_{Hg}(T_{05}))$	(−)	$6.1\cdot10^{-6}$
$u(W_{Ga}(T_{04}))$	(−)	$4.2\cdot10^{-6}$
$u(W_{Ga}(T_{05}))$	(−)	$4.3\cdot10^{-6}$
For experiments at 223 K and 270 K		
$u(R_{H_2O}(T_{04}))$	(Ω)	$3.94\cdot10^{-5}$
$u(R_{H_2O}(T_{05}))$	(Ω)	$2.57\cdot10^{-5}$
$u(R_{Hg}(T_{04}))$	(Ω)	$2.29\cdot10^{-5}$
$u(R_{Hg}(T_{05}))$	(Ω)	$1.84\cdot10^{-5}$
$u(R_{Ga}(T_{04}))$	(Ω)	$2.69\cdot10^{-5}$
$u(R_{Ga}(T_{05}))$	(Ω)	$2.37\cdot10^{-5}$
$u(W_{Hg}(T_{04}))$	(−)	$6.2\cdot10^{-6}$
$u(W_{Hg}(T_{05}))$	(−)	$6.1\cdot10^{-6}$
$u(W_{Ga}(T_{04}))$	(−)	$4.5\cdot10^{-6}$
$u(W_{Ga}(T_{05}))$	(−)	$4.3\cdot10^{-6}$

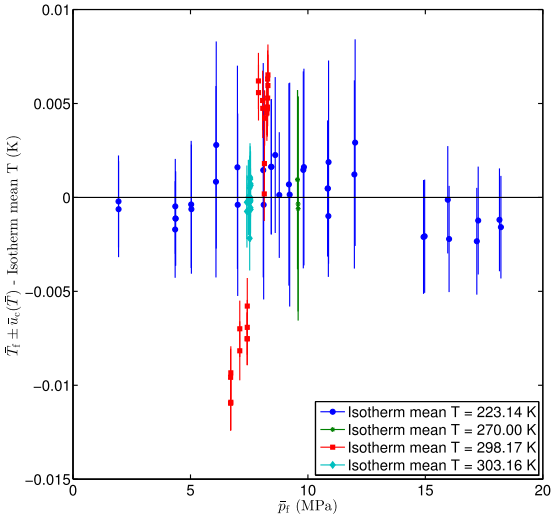

Fig. 3. Temperature deviations for each VLE measurement from isotherm mean temperature, and temperature standard uncertainty, expressed together as $\overline{T}_f \pm \overline{u}_c(\overline{T})$ - isotherm mean temperature, versus VLE experiment pressure $\overline{p}_f$. VLE experiment mean temperature $\overline{T}_f$. Temperature standard uncertainty $\overline{u}_c(\overline{T})$.

(See Section 5.4.2). Hence, the composition of each sample withdrawn was assumed to represent the equilibrium composition at the pressure and temperature just before the composition sample was withdrawn.

For each sample, the equilibrium pressure and temperature were assumed to be represented by the pressure and temperature measurements averaged over a time period equal to 75% of the sampling period ending just before the sample extraction starts, denoted $\overline{p}$ and $\overline{T}$, respectively. During these time periods, no systematic trends in pressure and temperature were seen.

The standard systematic uncertainty of these mean values, $\overline{u}(p)$ and $\overline{u}(T)$, were assumed to be equal to the arithmetic mean values of the standard systematic uncertainties of the p_i and T_i measurements, $u_c(p_i)$ and $u(T_i)$, used to calculate the mean pressure and temperature. $u_c(p_i)$ and $u(T_i)$ were obtained from the analysis presented in Appendix A.1.4 and Appendix A.2.1, in Eqs. (A.8) and (A.16), respectively.

The standard random uncertainties of $\overline{p}$ and $\overline{T}$, $s(\overline{p})$ and $s(\overline{T})$, cannot be evaluated in the form $s/\sqrt{n}$, as the measurements used to calculate the mean values were autocorrelated. Using the approach of Box et al. [24] and Law and Kelton [25], approximate values can be obtained as

$$s(\overline{z}) \approx \frac{s(z)}{\sqrt{n}} \cdot \sqrt{\frac{n-1}{n/a-1}}, \tag{6}$$

where $z = p$ or T, and

$$s(z) = \sqrt{\sum_{i=1}^{n} \frac{(z_i - \overline{z})^2}{n-1}}, \tag{7}$$

$$a = 1 + 2\sum_{k=1}^{n-1} (1 - k/n)\widehat{\rho}_k, \tag{8}$$

$$\widehat{\rho}_k = \frac{\sum_{i=1}^{n-k}(z_i - \overline{z})(z_{i+k} - \overline{z})}{\sum_{i=1}^{n}(z_i - \overline{z})^2}. \tag{9}$$

The combined standard uncertainty of the mean values $\overline{p}$ and $\overline{T}$ are then given as

$$\begin{aligned} u_c(\overline{p}) &= \sqrt{s^2(\overline{p}) + \overline{u}^2(p)}, \\ u_c(\overline{T}) &= \sqrt{s^2(\overline{T}) + \overline{u}^2(T)}. \end{aligned} \tag{10}$$

For each series of pressure, temperature and composition samples, the arithmetic mean values, $\overline{p}_f$, $\overline{T}_f$ and $\overline{x}_{CO_2}$ or $\overline{y}_{CO_2}$, were calculated. The subscript f is used to differentiate between the pressure and temperature values for each composition sample, and the mean values of the pressure and temperature for each series of samples. With $\overline{u}_c(\overline{p})$, $\overline{u}_c(\overline{T})$, $\overline{u}_{tot}(x_{CO_2})$ and $\overline{u}_{tot}(y_{CO_2})$ calculated as the means of $u_c(\overline{p})$, $u_c(\overline{T})$, $u_{tot}(x_{CO_2})$ and $u_{tot}(y_{CO_2})$ in each series, respectively, the propagation of uncertainty is calculated in the following manner:

$$u_c(\overline{p}_f) = \sqrt{s^2(\overline{p}_f) + \overline{u}_c^2(\overline{p})}, \tag{11}$$

$$u_c(\overline{T}_f) = \sqrt{s^2(\overline{T}_f) + \overline{u}_c^2(\overline{T})}, \tag{12}$$

$$u_c(\overline{x}_{CO_2}) = \sqrt{s^2(\overline{x}_{CO_2}) + \overline{u}_{tot}^2(x_{CO_2})}, \tag{13}$$

$$u_c(\overline{y}_{CO_2}) = \sqrt{s^2(\overline{y}_{CO_2}) + \overline{u}_{tot}^2(y_{CO_2})}, \tag{14}$$

with $s(\overline{p}_f)$, $s(\overline{T}_f)$, $s(\overline{x}_{CO_2})$ and $s(\overline{y}_{CO_2})$ calculated according to Eq. (7) divided by $\sqrt{n}$.

4. Results

VLE measurements at 223.14, 270.00, 298.17 and 303.16 K were conducted.

The existence of liquid and vapor phases was confirmed visually before the sampling of the phase compositions. Furthermore, the volumes occupied by the liquid and vapor phases inside the cell were measured visually. This visual inspection also assisted in determining the proximity to the critical point, that is, when the liquid and vapor phases for the $CO_2 + N_2$ system become clouded due to the small density difference of the phases, caused by critical opalescence, see e.g. Ref. [26]. The difference in the appearance of the phases as the VLE pressure was increased at 303.16 K is shown in Fig. 4, where Fig. 4a shows the appearance of the phases at a pressure relatively far from the critical point at 303.16 K, and Fig. 4b at a pressure closer to the critical point.

The pressure $\overline{p}$, temperature $\overline{T}$ and composition x_{CO_2} or y_{CO_2} for each VLE sample are given with the corresponding uncertainties in Tables B.2 and B.3. The mean pressure $\overline{p}_f$, temperature $\overline{T}_f$ and composition $\overline{x}_{CO_2}$ or $\overline{y}_{CO_2}$ and corresponding uncertainties for each series are given in Tables 4 and 5. These averaged measured data and estimated uncertainties are plotted in Figs. 7 to 10 for the temperatures 223.14, 270.00, 298.17 and 303.16 K, respectively. The measured relative volatility for the different temperatures is plotted as a function of pressure in Fig. 11.

At 223 and 270 K, the approach used to calculate the values in Tables 4 and 5 described in Section 3.5 will yield too high estimates for the sample standard deviation of the mean for the measurements, $s(\overline{p}_f)$, $s(\overline{x}_{CO_2})$ and $s(\overline{y}_{CO_2})$. The reason is that the pressure, and thereby the composition, from sample to sample changes to a new

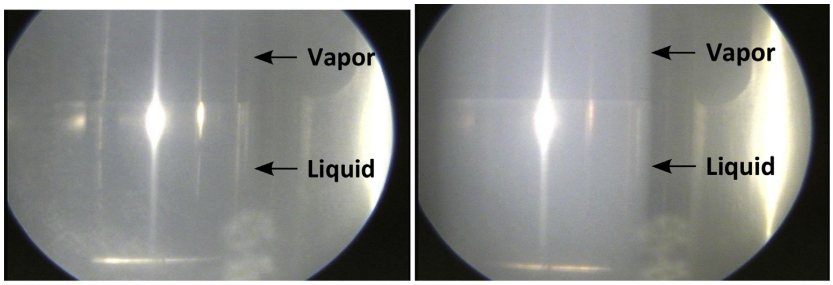

(a) Before sampling liquid point L30 at 7.4035 MPa. Far from critical point.

(b) Before sampling liquid point L34 at 7.5531 MPa. Closer to critical point, more similar density and composition in phases.

Fig. 4. Borescope pictures of liquid and vapor interface at 303.16 K for two different pressures.

equilibrium condition. The data shown in the tables for these two temperatures should only be regarded as a summary of the data, and the more detailed values found in Tables B.2 and B.3 should be considered for further modeling work.

For the measurements at 298.17 and 303.16 K, where the bellows was used to prevent a decrease in cell pressure after sampling, the variation in the compositions of the samples was expected to be minimal. With reference to Tables 4 and 5, the maximum value of the sample standard deviation of the mean of the mole fractions in the liquid phase, $s(\overline{x}_{CO_2})$, was $3.2 \cdot 10^{-5}$, and the corresponding maximum value for the vapor phase was $9.0 \cdot 10^{-5}$. It was not possible to see any significant increasing trend in these sample standard deviations for the measurements in the critical region compared to the measurements at lower pressures.

With reference to Tables B.2 and B.3, it can be seen that the combined standard uncertainty in temperature, $u_c(\overline{T})$, was below 6 mK for all VLE measurements. The standard uncertainty in pressure, $u_c(\overline{p})$, ranged from 0.5 kPa at the lowest measured pressure around 0.68 MPa (0.07%), to 3 kPa at 18 MPa (0.02%). The standard uncertainty in phase mole fractions, $u_{tot}(x_{CO_2})$ and $u_{tot}(y_{CO_2})$, were for most of the samples around $2.8 \cdot 10^{-4}$. For the samples at the highest pressures at 223.14 K, the uncertainty increased to around $3.6 \cdot 10^{-4}$. Due to the proximity to the critical point, the uncertainty in pressure contributed at a greater effect to the total uncertainty in the mole fractions, as described by Eq. (A.33). This same increase in uncertainty in the mole fractions is not seen in Tables B.2 and B.3 for the VLE measurements in the critical region at 298.17 and 303.16 K, which was caused by lack of match between the fitted version of EOS-CG and the measured data in this region. The uncertainty in the mole fractions in this region should therefore be higher than what is given in Tables B.2 and B.3.

5. Analysis and discussion

5.1. Comparison with literature data

Identified literature data around the temperatures 223, 270, 298 and 303 K are plotted together with the measurement data and uncertainties of this work in Figs. 7 to 10.

The only literature data found in the vicinity of 223.14 K were the bubble and dew point measurements at 5 and 10 MPa by Weber et al. [27]. Their measurements at 5 MPa were in very good agreement with our measurements. Their measurements at 10 MPa seemed to be slightly off in composition, compared with our neighboring data points at 9.8 and 10.9 MPa.

There was very good agreement between our measurements at 270.00 K and 9.6 MPa, and the corresponding high quality data points of Brown et al. [28]. The differences were within their stated pressure and composition uncertainties.

At 298.17 K, there were very little high quality literature data. Our liquid and vapor points at 7.41 MPa and our liquid points at 8.15 MPa and the data of Yorizane et al. [29] were in good agreement, given their stated composition and pressure uncertainty. The remaining data of Yorizane et al. [29] were not in agreement with our measurements, and they predicted a higher critical point, compared to our measurements.

At 303.16 K, our data and the recent data by Fandiño et al. [30] seemed to be in good agreement up to their liquid and vapor points at 7.42 MPa. Above this pressure, their bubble point at 7.5 MPa was lower in CO_2 content than the bubble point line predicted by our data. In addition, their data contained a bubble point at 7.5717 MPa, which was 0.014 MPa higher than the maximum pressure of our bubble and dew points. Our data at the highest pressures suggested close proximity to the critical point, lower than what was suggested by the bubble point of Fandiño et al. [30]. At 303.16 K, some instability was seen in the composition of our vapor data. This was probably due to a small leakage in the nitrogen filled bellows into the VLE cell, which were later detected. However, this leakage did not explain the apparent difference in critical pressure between our measurements and those of Fandiño et al. [30]. For comparison, in our apparatus, the transition between the two-phase region into the supercritical region could visually be observed and accurately determined within approximately 0.02 MPa for the VLE measurements at 298.17 K.

There was a possibility that some of our measurements close to the critical point at 303.16 K were affected by incomplete separation of the liquid and vapor phase before sampling took place, causing the measured liquid and vapor compositions to be closer to the total composition in the cell than the actual VLE composition at the actual temperature and pressure.

5.2. Critical point estimation

For binary mixtures the critical point in terms of pressure and temperature is dependent on the composition. For a given temperature, we denote the composition, if any, where the critical point is attained for the critical composition, as $z_{CO_2,c}$. The critical composition and pressure, p_c, are identified as the maximum pressure point in closed isothermal pressure-composition phase envelopes of binary mixtures, as seen in e.g. Figs. 7 to 10. For a long time, thermodynamic behavior around critical points in a range of different systems including VLE has been estimated using scaling laws from statistical mechanics [31–33]. For binary mixtures, the following scaling law can be applied [34,35]:

Table 4
Experimental VLE data for CO_2 (1) + N_2 (2) at mean temperature $\overline{T}_f$, mean pressure $\overline{p}_f$, and mean liquid phase mole fraction $\overline{x}_{CO_2}$.[a]

ID	Data			Temperature			Pressure			Composition			
	$\overline{T}_f$ (K)	$\overline{p}_f$ (MPa)	$\overline{x}_{CO_2}$ (−)	$s(\overline{T}_f)$ (K)	$\overline{u}_c(\overline{T})$ (K)	$u_c(\overline{T}_f)$ (K)	$s(\overline{p}_f)$ (MPa)	$\overline{u}_c(\overline{p})$ (MPa)	$u_c(\overline{p}_f)$ (MPa)	$s(\overline{x}_{CO_2})$ (−)	$\overline{u}_{tot}(x_{CO_2})$ (−)	$u_c(\overline{x}_{CO_2})$ (−)	$x_{CO_2,calc}$ (−)
P1	223.138	0.6829[b]	0.99999	5.3e-5	2.5e-3	2.5e-3	2.5e-6	5.0e-4	5.0e-4				
L1	223.140	1.9354	0.98156	4.5e-5	2.4e-3	2.4e-3	4.4e-5	5.2e-4	5.2e-4	9.3e-6	2.7e-4	2.7e-4	0.98346
L2	223.138	4.3468	0.94422	1.1e-4	2.6e-3	2.6e-3	2.5e-4	1.1e-3	1.1e-3	4.2e-6	2.7e-4	2.7e-4	0.94892
L3	223.139	5.0287	0.93314	1.4e-4	3.4e-3	3.4e-3	6.2e-4	1.1e-3	1.3e-3	8.0e-6	2.7e-4	2.7e-4	0.93846
L4	223.143	6.0976	0.91557	1.7e-4	5.5e-3	5.5e-3	7.8e-4	1.1e-3	1.4e-3	1.0e-5	2.7e-4	2.7e-4	0.92134
L5	223.141	6.9979	0.90041	7.6e-5	5.4e-3	5.4e-3	1.1e-3	1.1e-3	1.6e-3	2.1e-5	2.7e-4	2.7e-4	0.90618
L6	223.139	8.1151	0.88108	1.9e-4	5.0e-3	5.0e-3	1.0e-3	1.2e-3	1.6e-3	1.1e-5	2.7e-4	2.7e-4	0.88632
L7	223.140	8.7815	0.86908	6.5e-5	3.3e-3	3.3e-3	2.1e-3	1.3e-3	2.5e-3	4.4e-5	2.7e-4	2.8e-4	0.87386
L8	223.140	9.2232	0.86112	2.6e-4	6.0e-3	6.0e-3	1.8e-3	1.4e-3	2.2e-3	3.3e-5	2.7e-4	2.8e-4	0.86532
L9	223.141	9.8292	0.85043	6.2e-5	5.2e-3	5.2e-3	3.0e-3	2.7e-3	4.0e-3	1.2e-5	2.8e-4	2.8e-4	0.85322
L10	223.140	10.8430	0.82974	5.8e-5	3.6e-3	3.6e-3	3.3e-3	2.7e-3	4.3e-3	4.6e-5	2.8e-4	2.8e-4	0.83187
L11	223.142	10.8779	0.82920	7.6e-5	5.4e-3	5.4e-3	2.7e-3	2.7e-3	3.8e-3	5.4e-5	2.8e-4	2.8e-4	0.83111
L12	223.143	12.0106	0.80546	8.9e-5	5.5e-3	5.5e-3	4.2e-3	2.7e-3	5.0e-3	8.4e-5	2.8e-4	2.9e-4	0.80527
L13	223.138	14.9228	0.73343	1.8e-4	3.0e-3	3.0e-3	5.8e-3	2.8e-3	6.4e-3	1.6e-4	2.9e-4	3.3e-4	0.72553
L14	223.140	15.9554	0.70046	7.6e-5	2.9e-3	2.9e-3	6.9e-3	2.8e-3	7.5e-3	2.5e-4	2.9e-4	3.8e-4	0.68981
L15	223.137	17.1911	0.64879	1.6e-4	2.8e-3	2.8e-3	8.0e-3	2.8e-3	8.4e-3	4.2e-4	3.1e-4	5.2e-4	0.63665
L16	223.139	18.1560	0.57419	1.1e-4	2.7e-3	2.7e-3	8.4e-3	2.8e-3	8.8e-3	1.2e-3	3.5e-4	1.3e-3	0.57689
L17	269.996	9.5824	0.86046	1.2e-4	5.7e-3	5.7e-3	2.2e-3	1.4e-3	2.6e-3	5.1e-5	2.8e-4	2.8e-4	0.85932
P2	298.174	6.4369[c]	0.99999	1.9e-5	1.6e-3	1.6e-3	8.0e-6	1.2e-3	1.2e-3				
L18	298.158	6.7090	0.99359	2.2e-4	1.5e-3	1.5e-3	1.1e-4	1.1e-3	1.1e-3	2.7e-6	2.7e-4	2.7e-4	0.99371
L19	298.160	6.7192	0.99334	5.5e-5	1.4e-3	1.4e-3	5.0e-5	1.1e-3	1.1e-3	3.7e-6	2.7e-4	2.7e-4	0.99347
L20	298.161	7.1003	0.98384	3.6e-4	1.6e-3	1.6e-3	1.0e-4	1.1e-3	1.1e-3	9.9e-7	2.7e-4	2.7e-4	0.98411
L21	298.162	7.4191	0.97525	1.6e-4	1.5e-3	1.5e-3	1.7e-4	1.2e-3	1.2e-3	3.0e-6	2.7e-4	2.7e-4	0.97557
L22	298.175	7.8946	0.96050	4.3e-4	1.5e-3	1.5e-3	3.0e-4	1.2e-3	1.2e-3	3.7e-6	2.8e-4	2.8e-4	0.96091
L23	298.174	8.0782	0.95344	1.2e-4	1.6e-3	1.6e-3	3.0e-5	1.2e-3	1.2e-3	4.8e-6	2.8e-4	2.8e-4	0.95412
L24	298.171	8.1479	0.95029	1.5e-4	1.4e-3	1.4e-3	2.2e-4	1.2e-3	1.3e-3	1.1e-5	2.8e-4	2.8e-4	0.95126
L25	298.173	8.1544	0.94976	2.5e-4	1.5e-3	1.5e-3	4.0e-4	1.2e-3	1.3e-3	2.3e-6	2.8e-4	2.8e-4	0.95099
L26	298.174	8.2531	0.94359	3.6e-4	1.5e-3	1.5e-3	3.1e-4	1.2e-3	1.2e-3	3.2e-5	2.8e-4	2.8e-4	0.94654
L27	298.174	8.2743	0.94155	4.4e-4	1.5e-3	1.6e-3	1.4e-4	1.3e-3	1.3e-3	1.8e-5	2.8e-4	2.8e-4	0.94551
L28	298.174	8.2862	0.94041	2.8e-4	1.5e-3	1.5e-3	1.5e-5	1.3e-3	1.3e-3	6.4e-6	2.8e-4	2.8e-4	0.94492
L29	298.176	8.2971	0.93797	2.0e-5	1.6e-3	1.6e-3	1.8e-4	1.2e-3	1.2e-3	2.0e-5	2.8e-4	2.8e-4	0.94437
P3	303.158	7.2105[d]	0.99999	9.5e-6	2.0e-3	2.0e-3	3.0e-5	1.1e-3	1.1e-3				
L30	303.156	7.4035	0.99450	5.0e-4	1.9e-3	2.0e-3	3.0e-5	1.1e-3	1.1e-3	1.4e-6	2.7e-4	2.7e-4	0.99457
L31	303.155	7.5216	0.99044	3.0e-4	1.7e-3	1.7e-3	3.2e-5	1.1e-3	1.1e-3	1.2e-6	2.8e-4	2.8e-4	0.99078
L32	303.157	7.5345	0.98985	3.1e-5	1.7e-3	1.7e-3	4.3e-5	1.1e-3	1.1e-3	3.3e-6	2.8e-4	2.8e-4	0.99035
L33	303.157	7.5452	0.98928	8.9e-5	1.7e-3	1.7e-3	2.8e-5	1.2e-3	1.2e-3	5.1e-6	2.8e-4	2.8e-4	0.98997
L34	303.157	7.5531	0.98883	5.8e-5	1.8e-3	1.8e-3	2.5e-5	1.2e-3	1.2e-3	2.0e-6	2.8e-4	2.8e-4	0.98969
L35	303.157	7.5539	0.98894	5.2e-5	1.7e-3	1.7e-3	6.7e-5	1.1e-3	1.1e-3	1.8e-6	2.8e-4	2.8e-4	0.98966
L36	303.157	7.5575	0.98840	1.7e-4	1.7e-3	1.7e-3	4.6e-5	1.1e-3	1.1e-3	5.2e-6	2.8e-4	2.8e-4	0.98954

[a] Sample standard deviation of the mean of the temperatures $s(\overline{T}_f)$, mean of the standard systematic uncertainty of the temperatures $\overline{u}_c(\overline{T})$, total standard uncertainty of the temperature $u_c(\overline{T}_f)$, sample standard deviation of the mean of the pressures $s(\overline{p}_f)$, mean of the standard systematic uncertainty of the pressures $\overline{u}_c(\overline{p})$, total standard uncertainty of the pressure $u_c(\overline{p}_f)$, sample standard deviation of the mean of the mole fractions $s(\overline{x}_{CO_2})$, mean of the total standard uncertainty of the mole fractions $\overline{u}_{tot}(x_{CO_2})$, total standard uncertainty of the mole fraction $u_c(\overline{x}_{CO_2})$, fitted EOS-CG calculated mole fraction $x_{CO_2,calc}(\overline{T}_f, \overline{p}_f)$.
[b] Span–Wagner CO_2 vapor pressure is 0.6820 ± 0.0002 MPa.
[c] Span–Wagner CO_2 vapor pressure is 6.4379 ± 0.0019 MPa.
[d] Span–Wagner CO_2 vapor pressure is 7.2149 ± 0.0021 MPa.

$$z_{CO_2} = z_{CO_2,c} + \left(\lambda_1 + \varepsilon\frac{\lambda_2}{2}\right)(p_c - p) + \varepsilon\frac{\mu}{2}(p_c - p)^{\beta}, \quad \text{where} \quad \varepsilon = \begin{cases} 1 \text{ for bubble points,} \\ -1 \text{ for dew points.} \end{cases} \tag{15}$$

Here, z_{CO_2} is the boiling point ($z_{CO_2} = x_{CO_2}$) or dew point ($z_{CO_2} = y_{CO_2}$) CO_2 mole fraction at pressure p, p_c is the critical pressure, and $z_{CO_2,c}$ is the critical composition. β is an universal scaling exponent, which here was fixed at 0.325 [36]. The other parameters of Eq. (15) are regressed by using data close to the critical point. In this work, the fitting parameters were regressed using data reported in Tables 4 and 5 at 223.14 and 298.17 K. The regression was performed using ordinary least squares method. No weighing of data was performed. Based on the standard error of regression and estimated uncertainty of the measured data, an estimate of the uncertainties of the critical point can be found:

$$u_{z_{CO_2,c}} = \sqrt{S_E^2(\hat{z}_{CO_2,c}) + \left[\frac{1}{n_p}\sum_{i=1}^{n_p} u_c(\overline{x}_{i,CO_2})\right]^2} \tag{16}$$

$$u_{p_c} = \sqrt{S_E^2(\hat{p}_c) + \left[\frac{1}{n_p}\sum_{i=1}^{n_p} u_c\left(\overline{p}_{i,f}\right)\right]^2} \tag{17}$$

Here $\hat{z}_{CO_2,c}$ and $\hat{p}_c$ are the regressed estimates for the critical composition and pressure based on Eq. (15) and the n_p number of data points i used in the regression. S_E are standard errors of regression coefficients, and $u_c(\overline{x}_{i,CO_2})$ and $u_c(\overline{p}_{i,f})$ are the estimated uncertainties of data point i taken from Tables 4 and 5. The uncertainties estimates provided in Eqs. (16) and (17) are conservative in that it was assumed that the measurement errors were systematic, but the uncertainty estimates of the critical points did not fully take into account possible model errors.

The regression parameters and the uncertainties are provided in Table 6, and the fits, critical points and data points used are shown

in Fig. 5. The critical points are also included in Figs. 7 and 9 together with the other data and equations of state to be discussed in the following. The scaling law of Eq. (15) appeared to provide an adequate fit of the data of this work around the critical region. The estimated uncertainties of the critical mole fraction area were around 10^{-3} at 223.14 K and $4\cdot10^{-4}$ at 298.17 K, whereas the corresponding estimated relative uncertainties in pressure were 0.05 and 0.02%, respectively. The pressure measurement uncertainty was a significant contributor to the critical point estimate uncertainty at 223.14 K. As discussed in Section 4, the uncertainty estimates for the data at 223.14 K without pressure compensation were probably exaggerated. In Fig. 5b, also some supercritical data points are included, which were outside the estimated uncertainty bounds of the critical point at 298.17 K. Also the measurement points not used in the regression included in Fig. 5a seemed to confirm that the scaling law was suitable for our measurements.

5.3. Comparison to EOS-CG

In the development of EOS-CG, the parameters and mixture model used by Gernert and Span [1] and Gernert [2] for the description of $CO_2 + N_2$, were the same as in the GERG-2008 EOS [7].

At present, EOS-CG (or GERG-2008) gives the best prediction of the VLE of the $CO_2 + N_2$ system. On this basis, it was of interest to determine how well our data agreed with EOS-CG.

The VLE predictions of EOS-CG using the original parameters [1,2] are shown with the measurement data and uncertainty estimates of the current work in Figs. 7 to 10. The relative volatility of the new data and EOS-CG can be compared in Fig. 11.

At 223.14 K, our data showed very good agreement with EOS-CG up to pressures of 12 MPa. Above this pressure, the estimate for the critical point from Section 5.2 was $\widehat{p}_c = 18.26$ MPa and $\widehat{z}_{CO_2,c} = 0.4880$, while EOS-CG with original parameters indicated $\widehat{p}_c = 19.88$ MPa and $\widehat{z}_{CO_2,c} = 0.479$. Hence, it seemed like EOS-CG overpredicted the critical pressure at this temperature by about 1.6 MPa. The deviations between our data and the model were in this region order of magnitudes larger than the estimated uncertainties of our data and critical point estimate.

According to the literature data review of Gernert and Span [1] and Gernert [2], there were no VLE literature data in the critical region at temperatures below the data provided by Al-Sahhaf et al. [37] at 240 K. There were, however, some phase boundary measurements in the temperature region 208–240 K with CO_2 mole fractions from 0.4 to 0.5, in the works by Esper [38,39], and Duarte-Garza et al. [40]. As Gernert and Span [1] and Gernert [2] noted, these phase boundary measurements indicated that EOS-CG overpredicted the critical pressure at these lower temperatures, which was in accordance with our measurements.

Both at 298.17 and 303.16 K, our data indicated a critical point at lower pressures and higher total CO_2 compositions than EOS-CG.

At 298.17 K, EOS-CG indicated a critical point at approximately $\widehat{p}_c = 8.449$ MPa and $\widehat{z}_{CO_2,c} = 0.9286$, while the estimation of the critical point from Section 5.2 was $\widehat{p}_c = 8.295$ MPa and $\widehat{z}_{CO_2,c} = 0.9342$. Hence, the new data indicated that EOS-CG overpredicts the critical pressure by approximately 0.15 MPa.

At 303.16 K, the critical point indicated by EOS-CG was approximately $\widehat{p}_c = 7.665$ MPa and $\widehat{z}_{CO_2,c} = 0.9834$, while the data of this work indicated $\widehat{p}_c = 7.558$ MPa and $\widehat{z}_{CO_2,c} = 0.9877$. Based on this comparison, EOS-CG overpredicts the critical pressure by approximately 0.11 MPa.

Overall, EOS-CG seems to predict higher critical pressures than indicated by our data.

5.4. Model fitting

5.4.1. Introduction

The parameters of two different equations of state were fitted against the experimental data. First, EOS-CG [1,2] was fitted to obtain the best possible description of the critical region. Second, the Peng-Robinson (PR) cubic EOS [41] with the alpha correction by Mathias and Copeman [42] (MC), the mixing rules by Wong and Sandler [43] (WS) and the NRTL [44] excess Gibbs energy model, were chosen. This combination of EOS, alpha correction, mixing rule and excess Gibbs energy model, designated here as PR-MC-WS-NRTL, has previously been used with some success to fit VLE data of the CO_2-Ar system [45], for instance with regard to the critical region at a certain temperature. This EOS is computationally less time-consuming than EOS-CG.

The phase equilibrium calculations were performed by solving the equation of state using the equilibrium condition, expressed as an equality of the fugacities of each component, $i = CO_2, N_2$, in the liquid and vapor phase [46]:

$$f_{i,L}(T,p,x_i) = f_{i,V}(T,p,y_i). \tag{18}$$

The solution of this equation was performed using an in-house software.

The model fit was performed using orthogonal distance regression (ODR), which in our case consisted of minimizing an objective function with weighting of the error between data and model prediction in both composition x_{CO_2} and y_{CO_2}, and in pressure $\overline{p}$, at a fixed temperature. The Python™ implementation of NIST's ODRPACK [47] was used to perform the regression. With z_{CO_2} equal to x_{CO_2} or y_{CO_2}, the objective function S minimized can be stated as:

$$S^2 = \frac{1}{n-n_p}\sum_i \left(\frac{p_{i,calc} - \overline{p}_i}{u_c(\overline{p}_i)}\right)^2 + \frac{1}{n-n_p}\sum_i \left(\frac{z_{i,CO_2,calc} - z_{i,CO_2}}{u(z_{i,CO_2})}\right)^2, \tag{19}$$

where n is the total number of experimental data points, and n_p is the number of parameters adjusted in the model fit.

It should be noted that by using Eq. (19), the data are only weighted according to their estimated uncertainty. Hence, more weight was put on regions with higher number of data points, which may skew the model since we are using an incomplete set of data. For the present purpose of interpreting the data, this simple approach was deemed sufficient.

In addition to the value of the objective function S, two statistics were used to describe the agreement between model and data, the absolute average deviation (AAD) and the bias (BIAS):

$$AAD = \frac{100}{n}\sum_i \left|z_{i,CO_2} - z_{i,CO_2,calc}\right|, \tag{20}$$

and

$$BIAS = \frac{100}{n}\sum_i \left(z_{i,CO_2} - z_{i,CO_2,calc}\right). \tag{21}$$

The fitted models were compared with a selection of some of the high quality VLE data from the literature. An overview of these data is given in Table 8.

5.4.2. EOS-CG VLE

For EOS-CG [1,2], two parameters in the reducing function for

Table 5
Experimental VLE data for CO_2 (1) + N_2 (2) at mean temperature $\overline{T}_f$, mean pressure $\overline{p}_f$, and mean vapor phase mole fraction $\overline{y}_{CO_2}$.[a]

ID	Data			Temperature			Pressure			Composition			
	$\overline{T}_f$ (K)	$\overline{p}_f$ (MPa)	$\overline{y}_{CO_2}$ (−)	$s(\overline{T}_f)$ (K)	$\overline{u}_c(\overline{T})$ (K)	$u_c(\overline{T}_f)$ (K)	$s(\overline{p}_f)$ (MPa)	$\overline{u}_c(\overline{p})$ (MPa)	$u_c(\overline{p}_f)$ (MPa)	$s(\overline{y}_{CO_2})$ (−)	$\overline{u}_{tot}(y_{CO_2})$ (−)	$u_c(\overline{y}_{CO_2})$ (−)	$y_{CO_2,calc}$ (−)
P1	223.138	0.6829[b]	0.99999	5.3e-5	2.5e-3	2.5e-3	2.5e-6	5.0e-4	5.0e-4				
V1	223.139	1.9383	0.40700	1.1e-4	2.6e-3	2.6e-3	3.6e-4	5.2e-4	6.3e-4	1.2e-4	2.9e-4	3.1e-4	0.41050
V2	223.139	4.3535	0.23253	8.2e-5	2.5e-3	2.5e-3	1.2e-3	1.1e-3	1.6e-3	3.8e-5	2.8e-4	2.8e-4	0.23398
V3	223.139	4.3652	0.23239	1.8e-4	2.5e-3	2.5e-3	1.1e-3	1.1e-3	1.5e-3	6.9e-5	2.8e-4	2.8e-4	0.23364
V4	223.139	5.0378	0.21785	1.2e-4	3.4e-3	3.4e-3	1.0e-3	1.1e-3	1.5e-3	4.8e-5	2.7e-4	2.8e-4	0.21745
V5	223.141	6.0853	0.20174	8.5e-5	5.1e-3	5.1e-3	1.8e-3	1.1e-3	2.1e-3	4.7e-5	2.7e-4	2.8e-4	0.20185
V6	223.139	7.0097	0.19326	1.3e-4	4.9e-3	4.9e-3	1.6e-3	1.6e-3	2.2e-3	9.8e-5	2.7e-4	2.9e-4	0.19449
V7	223.141	8.0989	0.18971	1.2e-4	5.7e-3	5.7e-3	1.5e-3	1.2e-3	2.0e-3	6.6e-5	2.7e-4	2.8e-4	0.19118
V8	223.141	8.4403	0.18981	1.7e-4	3.6e-3	3.6e-3	1.7e-3	1.3e-3	2.1e-3	1.1e-5	2.7e-4	2.7e-4	0.19110
V9	223.142	8.6079	0.18980	4.4e-4	4.2e-3	4.2e-3	1.5e-3	1.3e-3	2.0e-3	5.7e-5	2.7e-4	2.8e-4	0.19122
V10	223.140	9.1920	0.19069	2.8e-4	5.4e-3	5.4e-3	1.3e-3	1.4e-3	1.9e-3	3.8e-5	2.7e-4	2.8e-4	0.19234
V11	223.141	9.8050	0.19283	6.6e-5	5.2e-3	5.2e-3	2.0e-3	2.6e-3	3.3e-3	6.9e-5	2.7e-4	2.8e-4	0.19470
V12	223.139	10.8694	0.19990	2.4e-4	3.2e-3	3.2e-3	1.9e-3	2.7e-3	3.3e-3	1.0e-4	2.7e-4	2.9e-4	0.20150
V13	223.141	11.9787	0.20881	3.5e-4	5.0e-3	5.0e-3	2.5e-3	2.7e-3	3.7e-3	9.6e-5	2.8e-4	2.9e-4	0.21230
V14	223.138	14.9699	0.25683	3.6e-4	3.0e-3	3.0e-3	3.3e-3	2.8e-3	4.3e-3	2.6e-4	2.8e-4	3.8e-4	0.26333
V15	223.138	16.0098	0.28507	1.1e-4	2.8e-3	2.8e-3	3.5e-3	2.8e-3	4.5e-3	1.6e-4	2.9e-4	3.3e-4	0.29132
V16	223.139	17.2510	0.33148	1.6e-4	2.9e-3	2.9e-3	3.3e-3	2.8e-3	4.3e-3	1.6e-4	3.0e-4	3.4e-4	0.33698
V17	223.138	18.2173	0.41480	5.8e-5	2.7e-3	2.7e-3	3.3e-3	2.8e-3	4.3e-3	6.1e-4	3.6e-4	7.1e-4	0.39381
V18	269.997	9.5571	0.58169	7.3e-5	4.8e-3	4.8e-3	4.5e-3	1.4e-3	4.8e-3	2.5e-4	2.8e-4	3.8e-4	0.58466
V19	269.996	9.5839	0.58095	1.1e-4	6.0e-3	6.0e-3	2.6e-3	1.4e-3	2.9e-3	2.3e-4	2.8e-4	3.6e-4	0.58453
P2	298.174	6.4369[c]	0.99999	1.9e-5	1.6e-3	1.6e-3	8.0e-6	1.2e-3	1.2e-3				
V20	298.159	6.7088	0.98174	2.2e-5	1.5e-3	1.5e-3	4.2e-5	1.1e-3	1.1e-3	9.0e-5	2.8e-4	3.0e-4	0.98181
V21	298.158	6.7194	0.98097	8.7e-5	1.5e-3	1.5e-3	1.3e-4	1.1e-3	1.1e-3	6.8e-6	2.8e-4	2.8e-4	0.98113
V22	298.162	7.0988	0.95952	5.3e-6	1.5e-3	1.5e-3	2.4e-5	1.2e-3	1.2e-3	1.5e-5	2.8e-4	2.8e-4	0.95949
V23	298.161	7.4163	0.94435	6.9e-5	1.4e-3	1.4e-3	1.0e-4	1.1e-3	1.1e-3	5.6e-5	2.8e-4	2.8e-4	0.94439
V24	298.163	7.4175	0.94434	1.1e-4	1.5e-3	1.5e-3	2.9e-4	1.1e-3	1.2e-3	3.8e-5	2.8e-4	2.8e-4	0.94435
V25	298.175	7.8935	0.92792	1.5e-5	1.5e-3	1.5e-3	1.5e-4	1.2e-3	1.2e-3	2.3e-5	2.8e-4	2.8e-4	0.92736
V26	298.174	8.0724	0.92467	7.7e-5	1.6e-3	1.6e-3	3.0e-4	1.2e-3	1.2e-3	3.9e-5	2.7e-4	2.8e-4	0.92293
V27	298.169	8.1434	0.92461	3.0e-4	1.4e-3	1.5e-3	8.1e-5	1.2e-3	1.2e-3	5.2e-5	2.7e-4	2.8e-4	0.92153
V28	298.173	8.2526	0.92610	7.3e-5	1.5e-3	1.5e-3	1.4e-4	1.2e-3	1.2e-3	4.2e-5	2.7e-4	2.8e-4	0.92011
V29	298.174	8.2721	0.92694	8.9e-5	1.5e-3	1.5e-3	8.8e-5	1.2e-3	1.2e-3	8.4e-5	2.7e-4	2.9e-4	0.91995
V30	298.175	8.2862	0.92730	1.2e-5	1.5e-3	1.5e-3	1.0e-4	1.3e-3	1.3e-3	4.6e-5	2.7e-4	2.8e-4	0.91988
V31	298.175	8.2972	0.93025	3.6e-4	1.6e-3	1.7e-3	7.6e-5	1.2e-3	1.2e-3	3.4e-5	2.7e-4	2.8e-4	0.91982
P3	303.158	7.2105[d]	0.99999	9.5e-6	2.0e-3	2.0e-3	3.0e-5	1.1e-3	1.1e-3				
V32	303.157	7.4007	0.99154	2.7e-4	2.0e-3	2.0e-3	1.7e-5	1.2e-3	1.2e-3	1.4e-5	2.8e-4	2.8e-4	0.99157
V33	303.157	7.4672	0.98904	2.4e-4	2.0e-3	2.0e-3	5.5e-5	1.1e-3	1.1e-3	2.6e-5	2.8e-4	2.8e-4	0.98888
V34	303.158	7.5217	0.98695	1.8e-5	1.7e-3	1.7e-3	7.9e-5	1.1e-3	1.1e-3	1.5e-5	2.8e-4	2.8e-4	0.98682
V35	303.158	7.5350	0.98699	3.5e-5	1.8e-3	1.8e-3	5.7e-5	1.2e-3	1.2e-3	9.4e-6	2.8e-4	2.8e-4	0.98635
V36	303.158	7.5450	0.98683	2.0e-5	1.7e-3	1.7e-3	2.1e-5	1.2e-3	1.2e-3	2.3e-5	2.8e-4	2.8e-4	0.98600
V37	303.158	7.5532	0.98681	2.4e-4	1.8e-3	1.8e-3	1.1e-4	1.2e-3	1.2e-3	6.6e-5	2.8e-4	2.8e-4	0.98571
V38	303.158	7.5540	0.98662	3.2e-5	1.8e-3	1.8e-3	6.2e-5	1.1e-3	1.1e-3	1.6e-5	2.8e-4	2.8e-4	0.98568
V39	303.157	7.5543	0.98641	1.0e-4	1.7e-3	1.7e-3	1.9e-5	1.1e-3	1.1e-3	1.1e-5	2.8e-4	2.8e-4	0.98571
V40	303.158	7.5574	0.98708	2.3e-5	1.7e-3	1.7e-3	6.2e-5	1.1e-3	1.1e-3	8.2e-6	2.8e-4	2.8e-4	0.98568

[a] Sample standard deviation of the mean of the temperatures $s(\overline{T}_f)$, mean of the standard systematic uncertainty of the temperatures $\overline{u}_c(\overline{T})$, total standard uncertainty of the temperature $u_c(\overline{T}_f)$, sample standard deviation of the mean of the pressures $s(\overline{p}_f)$, mean of the standard systematic uncertainty of the pressures $\overline{u}_c(\overline{p})$, total standard uncertainty of the pressure $u_c(\overline{p}_f)$, sample standard deviation of the mean of the mole fractions $s(\overline{y}_{CO_2})$, mean of the total standard uncertainty of the mole fractions $\overline{u}_{tot}(y_{CO_2})$, total standard uncertainty of the mole fraction $u_c(\overline{y}_{CO_2})$, fitted EOS-CG calculated mole fraction $y_{CO_2,calc}(\overline{T}_f, \overline{p}_f)$.
[b] Span–Wagner CO_2 vapor pressure is 0.6820 ± 0.0002 MPa.
[c] Span–Wagner CO_2 vapor pressure is 6.4379 ± 0.0019 MPa.
[d] Span–Wagner CO_2 vapor pressure is 7.2149 ± 0.0021 MPa.

temperature in EOS-CG for CO_2 (1) + N_2 (2), $\beta_{T,12}$ and $\gamma_{T,12}$, were fitted. These two parameters were chosen for fitting as their main influence is on the shape of the VLE two-phase region, which is what we wanted to adjust to our data. The three remaining parameters in the reducing functions, and the 34 parameters of the departure function, were kept at the values given in Refs. [1,2]. For details about these parameters and the structure of the EOS, see Gernert and Span [1] and Gernert [2].

The binary parameters for the reducing function for temperature in EOS-CG for CO_2 (1) + N_2 (2), $\beta_{T,12}$ and $\gamma_{T,12}$, were fitted against our VLE pressure, temperature and composition data for the temperatures 223.14, 298.17 and 303.16 K in Tables 4 and 5.

The fitted parameters of EOS-CG are shown in Table 7 together with the original parameter set from Refs. [1,2,7]. The values of the objective function S in Eq. (19) are also shown.

The VLE predictions of EOS-CG using the fitted parameters from Table 7 are shown in Figs. 7 to 10 together with relevant data and the uncertainty estimates of this work. The relative volatilities calculated from the fitted EOS-CG and the new data can be compared in Fig. 11.

The objective function value S decreased significantly by fitting the parameters, and it can be seen that the fitted model matched much better with our data in the critical region at 223.14 K than the original model, without causing significantly larger deviations at lower pressures. However, at 298.17 and 303.16 K, the fitted model matched slightly worse with our data in the critical region than the original model. This development can also be seen from the objective function values calculated for each temperature, shown in Table 8. The S value at 223.14 K decreases significantly, at expense of the slight increase in the S values at 298.17 and 303.16 K. This was probably caused by the inadequacy of the weighting of the model deviations in the objective function at the different temperatures, as mentioned in Section 5.4.1.

Fig. 12a shows the deviations between our measured CO_2 mole

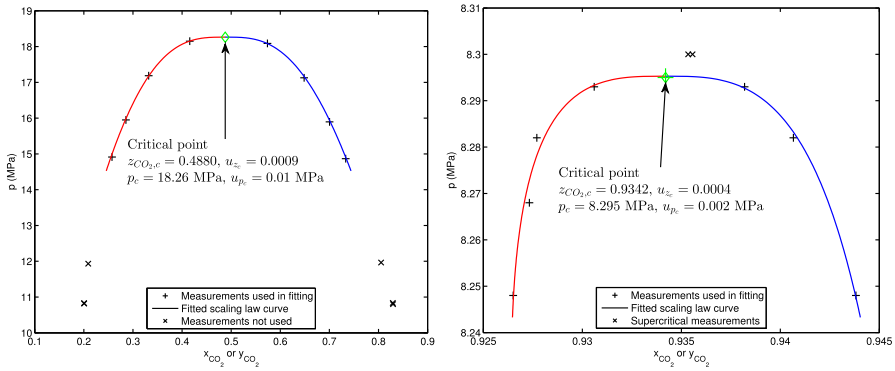

(a) 223.14 K **(b)** 298.17 K

Fig. 5. Estimation of phase behavior around the critical point by regression analysis of scaling law in Eq. (15). Note that the scales are very different in the two graphs.

fractions and those calculated by both the original and fitted version of EOS-CG at the same temperatures and pressures.

Fig. 13 shows the VLE predictions of the original and fitted model at a selection of temperatures different than those measured at in the present work. These temperatures were chosen on the basis of a selection of literature data used in the model fitting in Section 5.4.3, and an overview of the literature data is shown in Table 8.

With reference to these figures, it can be seen that the fitted model lowers the critical pressure significantly at the lower temperatures 218 to approximately 258 K, compared to the original model. At temperatures above this, the critical pressure started to shift from decrease to a slight increase. The critical composition changed very little compared to the original version of EOS-CG.

Fig. 12b shows the deviations between the measured CO_2 mole fractions in the literature data in Table 8 and those calculated by both the original and fitted version of EOS-CG at the same temperatures and pressures.

The figure shows that the fitted version of EOS-CG matched better than the original EOS-CG the data in the critical region at 240.00 K by Al-Sahhaf et al. [37] and at 243.15 K by Fandiño et al. [30]. For the remaining literature data, the fitted version of EOS-CG matches better than the original version of EOS-CG in some temperature regions, and somewhat worse at other temperatures. This is indicated by the AAD, BIAS and S values found in Table 8.

The fitted version of EOS-CG presented here, indicated a possibility to improve the description of the VLE in the critical region by EOS-CG. Only the VLE data measured at 223.15, 298.15 and 303.15 K in the present work was used to perform the fit. Therefore, the model with the fitted parameters cannot be used to calculate other properties for the $CO_2 + N_2$ binary system, such as density, heat capacity and others. For this, a complete new fit of the parameters is necessary, including the data for these properties, as well.

5.4.3. Peng-Robinson EOS

The alpha correction by Mathias and Copeman is given as [42]

$$\alpha_i(T) = \begin{cases} \left(1 + c_{1,i}h(T) + c_{2,i}h^2(T) + c_{3,i}h^3(T)\right)^2 & \text{if } T < T_{c,i}, \\ \left(1 + c_{1,i}h(T)\right)^2 & \text{if } T \geq T_{c,i}, \end{cases}$$
$$h(T) = 1 - \sqrt{T/T_{c,i}}, \tag{22}$$

where $i = CO_2$ or N_2. The values for $c_{1,i}$, $c_{2,i}$, $c_{3,i}$, and the critical temperatures $T_{c,i}$ and pressures $p_{c,i}$, are given in Table 9.

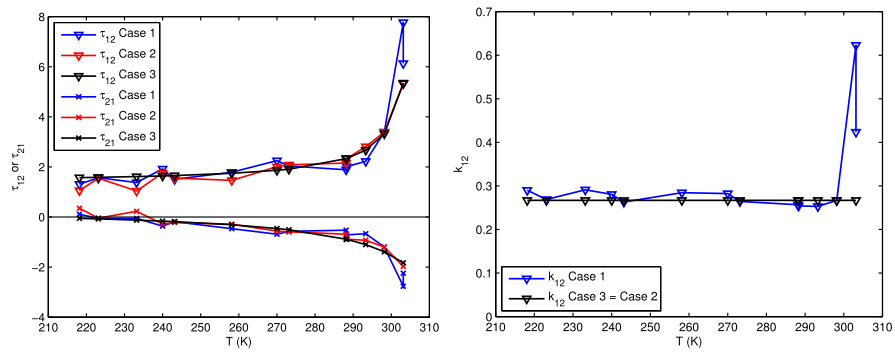

(a) Optimal values for τ_{12} and τ_{21} for the different temperature data sets in Table 8.

(b) Optimal values for k_{12} for the different temperature data sets in Table 8.

Fig. 6. Optimal values for τ_{12}, τ_{21} and k_{12} for the different temperature data sets in Table 8.

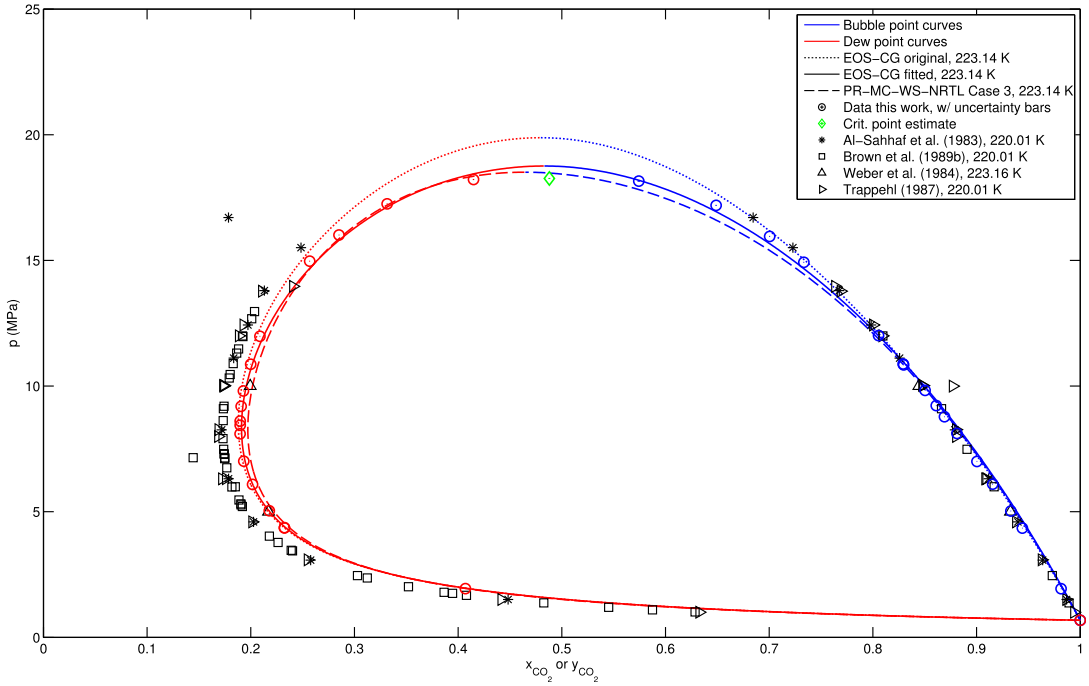

Fig. 7. Isothermal VLE data from literature [37,28,27,52], EOS calculations at mean temperature $T = 223.14$ K, and measurements with estimated uncertainties from present work: $\bar{x}_{CO_2}$, $\bar{y}_{CO_2}$, $\bar{p}_f$, $u_c(\bar{x}_{CO_2})$, $u_c(\bar{y}_{CO_2})$ and $u_c(\bar{p}_f)$ from Tables 4 and 5. Critical point estimation and its uncertainties are from Section 5.2.

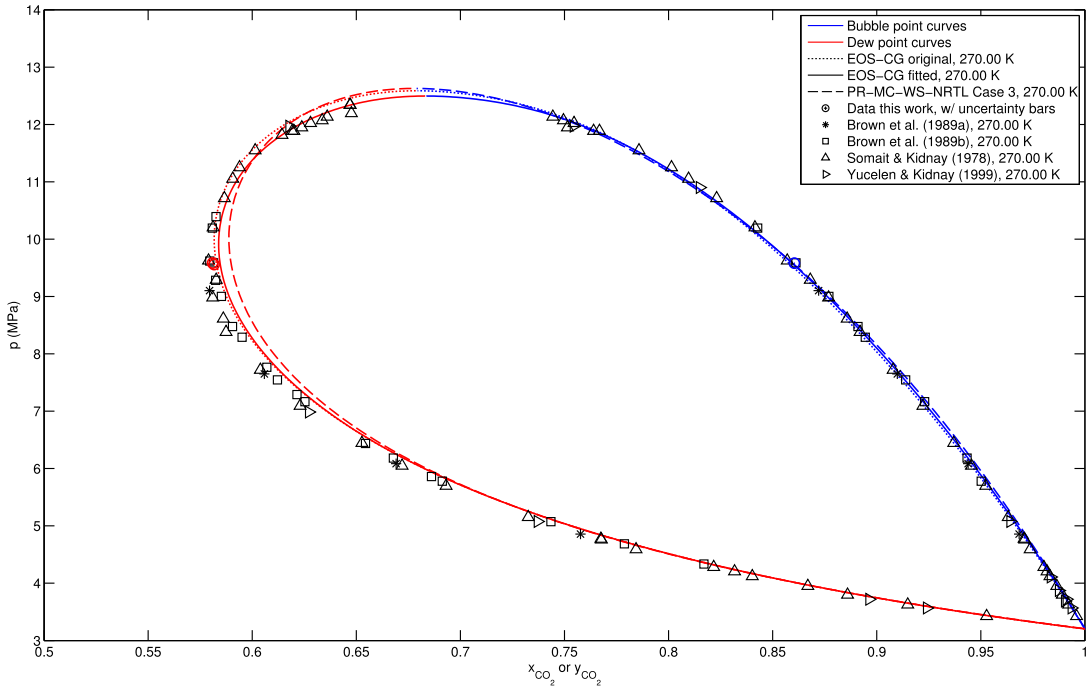

Fig. 8. Isothermal VLE data from literature [49,28,50,48], EOS calculations at mean temperature $T = 270.00$ K, and measurements with estimated uncertainties from present work: $\bar{x}_{CO_2}$, $\bar{y}_{CO_2}$, $\bar{p}_f$, $u_c(\bar{x}_{CO_2})$, $u_c(\bar{y}_{CO_2})$ and $u_c(\bar{p}_f)$ from Tables 4 and 5.

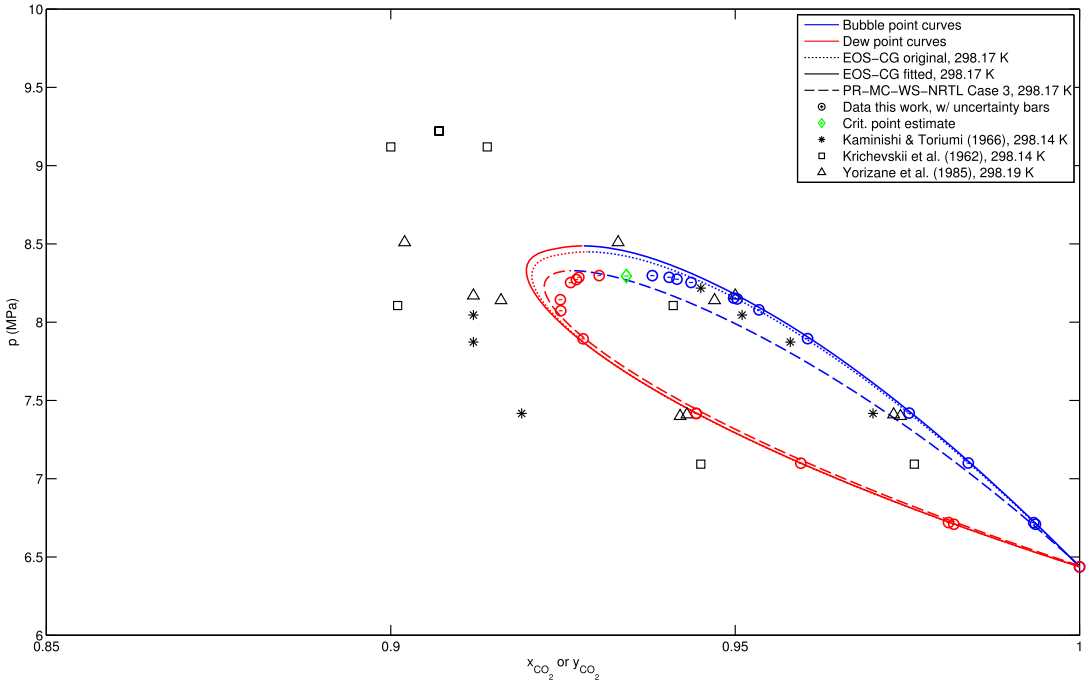

Fig. 9. Isothermal VLE data from literature [53,54,29], EOS calculations at mean temperature $T = 298.17$ K, and measurements with estimated uncertainties from present work: $\bar{x}_{CO_2}$, $\bar{y}_{CO_2}$, $\bar{p}_f$, $u_c(\bar{x}_{CO_2})$, $u_c(\bar{y}_{CO_2})$ and $u_c(\bar{p}_f)$ from Tables 4 and 5. Critical point estimation and its uncertainties are from Section 5.2.

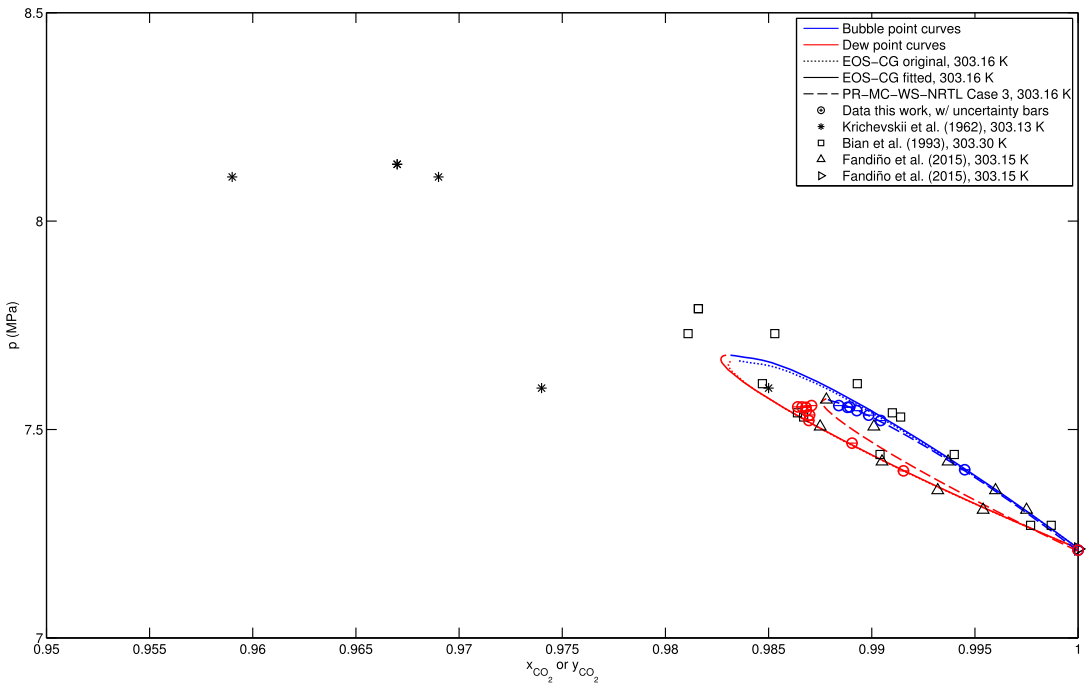

Fig. 10. Isothermal VLE data from literature [54,55,30], EOS calculations at mean temperature $T = 303.16$ K, and measurements with estimated uncertainties from present work: $\bar{x}_{CO_2}$, $\bar{y}_{CO_2}$, $\bar{p}_f$, $u_c(\bar{x}_{CO_2})$, $u_c(\bar{y}_{CO_2})$ and $u_c(\bar{p}_f)$ from Tables 4 and 5.

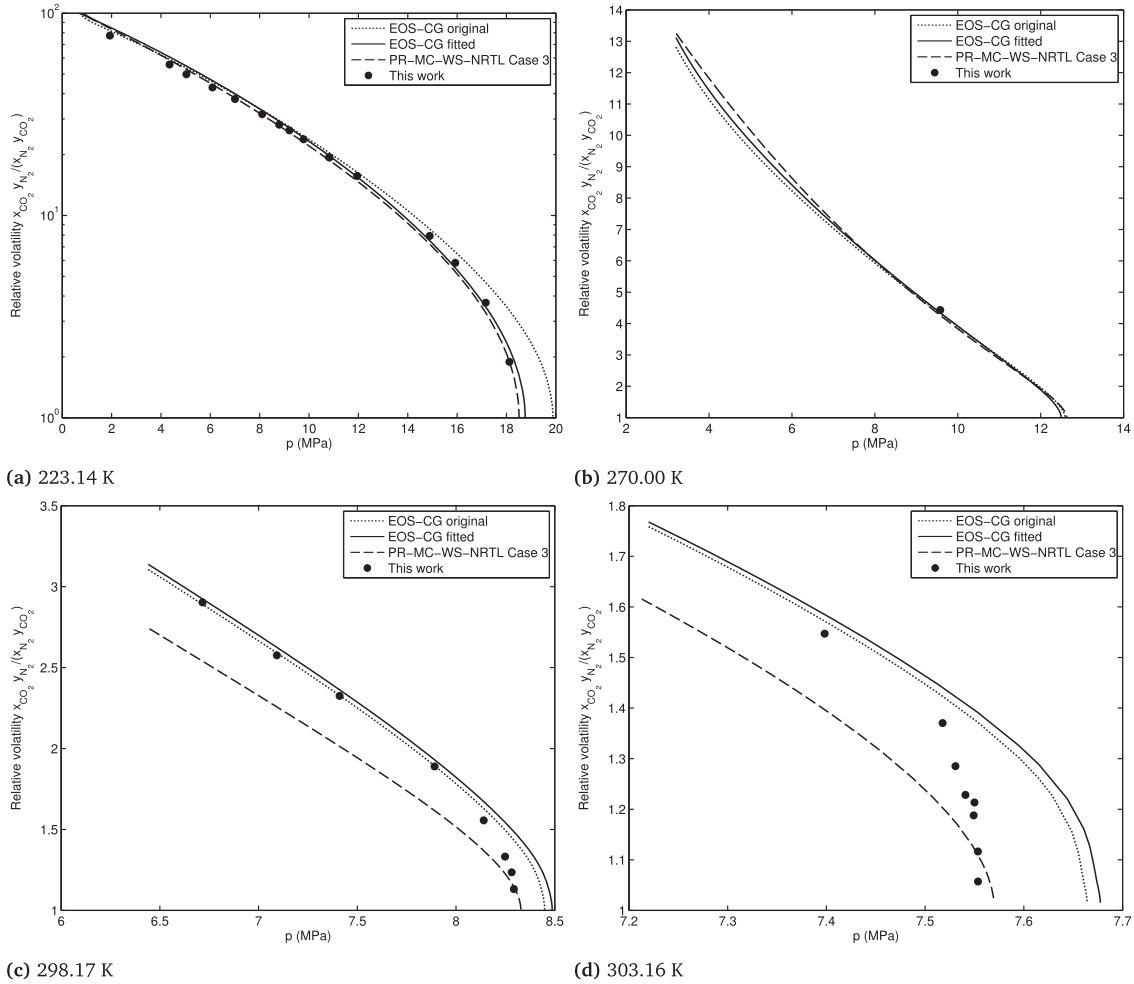

Fig. 11. Measured relative volatilities compared with different models.

The mixing rule by Wong and Sandler (WS) is given as [43]

$$b_m = \frac{\sum_i \sum_j x_i x_j \left(b - \frac{a}{RT}\right)_{ij}}{1 - \frac{A^E_\infty}{CRT} - \sum_i x_i \left(\frac{a_i}{b_i RT}\right)}, \tag{23}$$

$$a_m = b_m RT - RT \sum_i \sum_j x_i x_j \left(b - \frac{a}{RT}\right)_{ij}, \tag{24}$$

where a_m and b_m are the mixture parameters, and a_i and b_i are the pure component parameters, of the Peng-Robinson EOS. The cross second virial coefficient is given by [43]

Table 6
Regressed parameters of scaling law in Eq. (15) in this work and other parameters relevant for fit.

Symbol	Unit	$T = 223.14$ K	$T = 298.17$ K
n_p		8	7
$\hat{\lambda}_1(T)$	(MPa^{-1})	$1.8247 \cdot 10^{-3}$	0.020517
$\hat{\lambda}_2(T)$	(MPa^{-1})	0.012694	−0.075047
$\hat{\mu}(T)$	($MPa^{-\beta}$)	0.29375	0.056131
$\hat{z}_{CO_2,c}(T)$		0.4880	0.9342
$\hat{p}_c(T)$	(MPa)	18.26	8.295
$s_{z_{CO_2,c}}$		0.0008	0.0002
$u_{z_{CO_2,c}}$		0.0009	0.0004
s_{p_c}	(MPa)	0.008	0.001
u_{p_c}	(MPa)	0.01	0.002

Table 7
Original and fitted parameters and objective function S value (Eq. (19)) for VLE calculation for CO_2 (1) + N_2 (2) in EOS-CG, valid for $T \in [223.15, 303.16]$ K.

	Original	Fitted
$\beta_{T,12}$	0.994140013	1.000800075
$\gamma_{T,12}$	1.107654104	1.110649656
$\beta_{v,12}$	1.022709642	
$\gamma_{v,12}$	1.047578256	
F_{12}	1	
S	36	14

Table 8
AAD and BIAS of the different EOSs, for data from the present work and data from literature.

ID	T (K)	EOS-CG original			EOS-CG fitted			PR-MC-WS-NRTL[a]			Data[b]	$n_{x_{CO_2}}$, $n_{y_{CO_2}}$	Source
		AAD	BIAS	S	AAD	BIAS	S	AAD	BIAS	S	p_{min}–p_{max} (MPa)		
1*	218.16	0.21	−0.14	5.73	0.38	−0.28	11.00	0.60	−0.09	15.93	0.97–15.03	11, 11	[30]
2	223.14	0.95	0.11	52.12	0.47	−0.08	16.86	0.78	0.03	25.81	1.94–18.22	16, 17	This work
3*	233.15	0.20	0.04	5.86	0.39	−0.11	11.90	0.64	−0.43	16.86	1.44–14.96	10, 10	[30]
4	240.00	1.03	−0.06	11.25	0.60	−0.25	6.38	1.07	−0.81	7.95	1.70–16.15	25, 21	[37,48]
5	243.15	0.62	−0.15	23.78	0.38	−0.21	10.74	0.81	−0.67	19.86	1.51–15.21	11, 11	[30]
6	258.15	0.66	−0.46	18.49	0.63	−0.60	15.47	0.95	−0.95	23.24	2.79–13.64	13, 13	[30]
7*	270.00	0.22	0.05	11.57	0.24	−0.12	13.70	0.49	−0.40	N/A	9.56–9.58	1, 2	This work
8	270.00	0.39	−0.13	2.57	0.36	−0.26	2.21	0.53	−0.33	3.29	3.43–12.34	54, 63	[49,28,50,48]
9	273.15	0.39	−0.14	11.05	0.38	−0.26	9.39	0.49	−0.13	14.10	3.54–11.79	11, 11	[30]
10	288.15	0.29	−0.27	7.91	0.29	−0.29	7.04	0.41	0.16	10.45	5.24–9.70	7, 7	[30]
11	288.30	0.51	−0.50	4.95	0.56	−0.54	5.20	0.35	−0.02	3.91	6.61–9.70	8, 8	[51]
12	293.30	0.32	0.06	2.81	0.38	0.03	2.92	0.63	0.39	10.03	6.00–9.11	10, 10	[51]
13	298.17	0.23	0.13	13.05	0.28	0.12	14.93	0.38	0.34	17.49	6.71–8.30	12, 12	This work
14	303.15	0.03	−0.02	1.04	0.04	−0.03	1.19	0.05	−0.04	1.41	7.31–7.57	6, 6	[30]
15	303.16	0.06	0.02	2.86	0.07	0.02	3.02	0.06	−0.05	2.83	7.40–7.56	7, 7	This work

*Not used for fitting the coefficients of Eqs. (28) and (29) since no data in the critical region.
[a] PR-MC-WS-NRTL Case 3.
[b] Data pressure range p_{min}–p_{max}, number of liquid points $n_{x_{CO_2}}$ and vapor point $n_{y_{CO_2}}$. ID is a data set identifier. T is the mean temperature of the data set.

$$\left(b-\frac{a}{RT}\right)_{ij}=\frac{\left(b_i-\frac{a_i}{RT}\right)+\left(b_j-\frac{a_j}{RT}\right)}{2}(1-k_{ij}), \tag{25}$$

where k_{ij} is the Wong–Sandler binary interaction parameter.

The molar excess Helmholtz energy, $\underline{A}^{E}_{\infty}$, is modeled in the present work using the NRTL model [43]

$$\frac{\underline{A}^{E}_{\infty}}{RT}=\sum_i x_i\left(\frac{\sum_j x_j\tau_{ji}\exp(-\alpha_{ji}\tau_{ji})}{\sum_k x_k\exp(-\alpha_{ki}\tau_{ki})}\right), \tag{26}$$

where α_{ij} are the non-randomness parameters and τ_{ij} are the binary interaction parameters of the NRTL model.

The following restrictions are put on the parameters:

$$\begin{aligned} &k_{ij}=k_{ji}, \quad k_{ii}=0,\\ &\alpha_{ij}=\alpha_{ji}, \quad \alpha_{ii}=0,\\ &\tau_{ij}\neq\tau_{ji}, \quad \tau_{ii}=0. \end{aligned} \tag{27}$$

As in the work by Coquelet et al. [45], we have assumed a constant value for $\alpha_{12}=\alpha_{21}=0.3$, based on the suggestions by Renon and Prausnitz [44] for a system of two non-polar components. This leaves 3 adjustable parameters in the PR-MC-WS-NRTL model: k_{12}, τ_{12} and τ_{21}. These parameters are assumed to be temperature dependent.

With temperature dependent parameters, it is of interest to fit the parameters to data at different temperatures, and try to determine a model for the temperature dependence of the parameters, enabling the use of the EOS at temperatures over the whole temperature range of the data.

To ensure some form of temperature dependency in the parameters, it was chosen to only perform parameter fitting for temperatures where measurements existed in the whole range from the vapor pressure of CO_2 up to the critical region. Our data contained measurements covering this region for the three temperatures 223, 298 and 303 K. These data were used to fit the three parameters k_{12}, τ_{12} and τ_{21} of the PR-MC-WS-NRTL EOS. In addition, these three parameters were fitted against literature data with measurements spanning the same pressure region for other temperatures. The selected literature data used for fitting the parameters are shown in Table 8.

The resulting parameter values for the different temperatures are shown in Table 10 and Figs. 6a and b, designated as Case 1.

With reference to Fig. 6a, the temperature dependencies of τ_{12} and τ_{21} could be described approximately by functions on the following form:

$$\tau_{12}(T)=a_{\tau_{12}}+b_{\tau_{12}}/(T-c_{\tau_{12}}), \tag{28}$$

$$\tau_{21}(T)=a_{\tau_{21}}+b_{\tau_{21}}/(T-c_{\tau_{21}}). \tag{29}$$

The optimal values of k_{12} seemed to be approximately constant up to 298.17 K. For the two data sets at 303 K, the optimal values were significantly higher. The reason for this seemed to be that the parameters of the EOS cannot be adjusted such as to simultaneously get a good fit of the data in the critical region at these higher temperatures and a good fit of the data below the critical region. The optimal parameters at these two temperatures gave a reasonable description of the data below the critical region, but predicted a significantly higher critical pressure than what was suggested by the data.

Based on this, the values of τ_{12} and τ_{21} were fitted again for these two temperature data sets, keeping k_{12} fixed at a value equal to the k_{12} optimal values at the lower temperature, approximately $k_{12}=0.27$. This gave a significantly better match between the model prediction of the critical pressure and the critical pressure suggested by the data, at expense of the match of the model to the composition of the phases below the critical pressure.

To obtain an approximation to the temperature dependency of τ_{12} and τ_{21}, it was decided to fit τ_{12} and τ_{21} against the data sets in Table 8 using a constant value of $k_{12}=0.266801$. The optimal values of τ_{12} and τ_{21} under this restriction are given in Table 10 as Case 2 and in Figs. 6a and b.

With $c_{\tau_{12}}$ fixed at 308 K, the coefficients $a_{\tau_{12}}$ and $b_{\tau_{12}}$ in Eq. (28) were fitted against the optimal values of τ_{12} for Case 2 for the temperatures where critical region data exist. Please refer to Table 8 for the data sets that were included. With $c_{\tau_{21}}$ fixed at 323 K, the coefficients $a_{\tau_{21}}$ and $b_{\tau_{21}}$ in Eq. (29) were fitted in a similar way. The fit was performed using unweighted least squares.

The fitted coefficients are shown in Table 10 as Case 3, together with the calculated values of τ_{12} and τ_{21} from Eqs. (28) and (29).

The VLE predictions of PR-MC-WS-NRTL EOS model using the Case 3 parameters for the temperatures 223.14, 270.00, 298.17 and 303.16 K are shown in Figs. 7 to 10 with the measurement data, uncertainties, and other models considered in this work. The

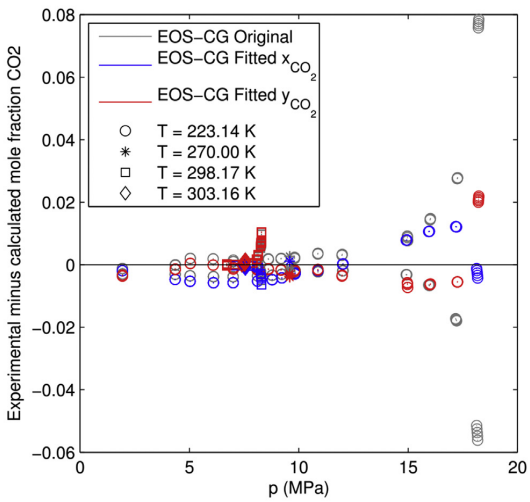

(a) VLE CO_2 mole fraction deviations between data in the present work and EOS-CG.

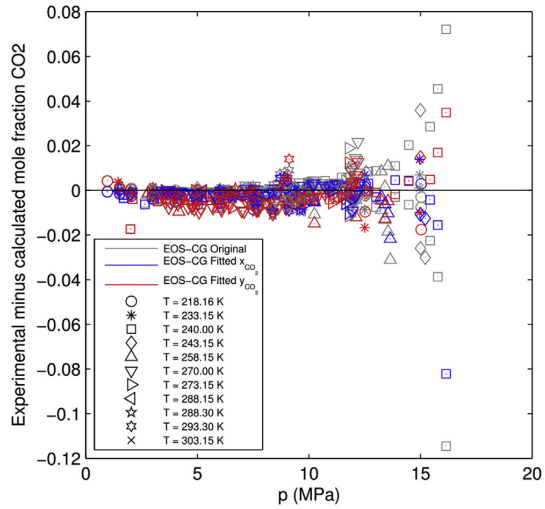

(b) VLE CO_2 mole fraction deviations between literature data and EOS-CG. Data listed in Table 8.

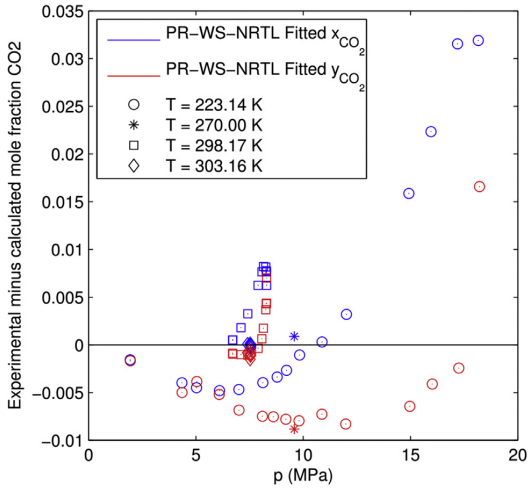

(c) VLE CO_2 mole fraction deviations between data in the present work and the PR-MC-WS-NRTL model.

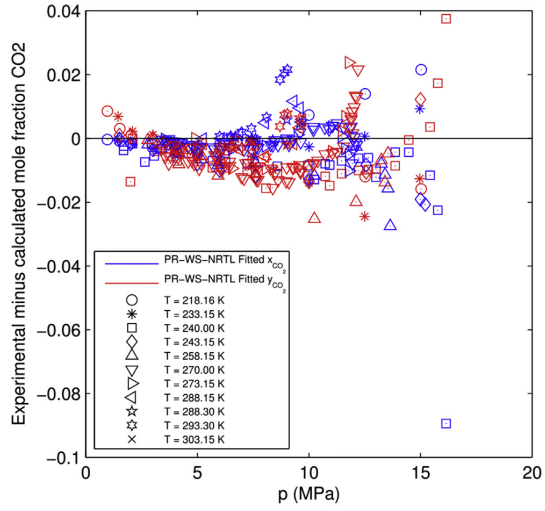

(d) VLE CO_2 mole fraction deviations between literature data and the PR-MC-WS-NRTL model. Data listed in Table 8.

Fig. 12. Mole fraction deviations between data and models.

corresponding relative volatilities are shown in Fig. 11. The PR-MC-WS-NRTL EOS VLE predictions for the temperatures of the literature data in Table 8 are plotted in Fig. 13.

As it can be seen in Figs. 12c and d, the deviation between the model prediction of the composition of the phases and the experimental data was for most of the data points higher than for the fitted version of EOS-CG, shown in Figs. 12a and b. This was also reflected in the increased AAD and S values for the majority of the temperature data sets compared to the fitted version of EOS-CG, which can be found in Table 8. The loss in accuracy is augmented by the simpler formulation of the PR-MC-WS-NRTL model, compared to EOS-CG.

The prediction of the critical point from the PR-MC-WS-NRTL model (Case 3) was comparable with that of the fitted version of EOS-CG for the lower temperature range, except at 218.16 K. At temperatures above approximately 270 K, the critical pressure predicted by the PR-MC-WS-NRTL model agreed better with our experimental data than the fitted version of EOS-CG. However, the fitted version of EOS-CG gave a more accurate description of the composition of the phases below the critical region, as can be seen from Figs. 7 to 10.

The PR-MC-WS-NRTL EOS with $\alpha = 0.3$, $k_{12} = k_{21} = 0.266801$ and τ_{12} and τ_{21} described by Eqs. (28) and (29), respectively, provided an approximate description of the VLE of $CO_2 + N_2$ over the temperature range 223.14–303.16 K. Although the model was less accurate than the fitted version of EOS-CG, it provided a fairly accurate description of the critical pressure at the different temperatures.

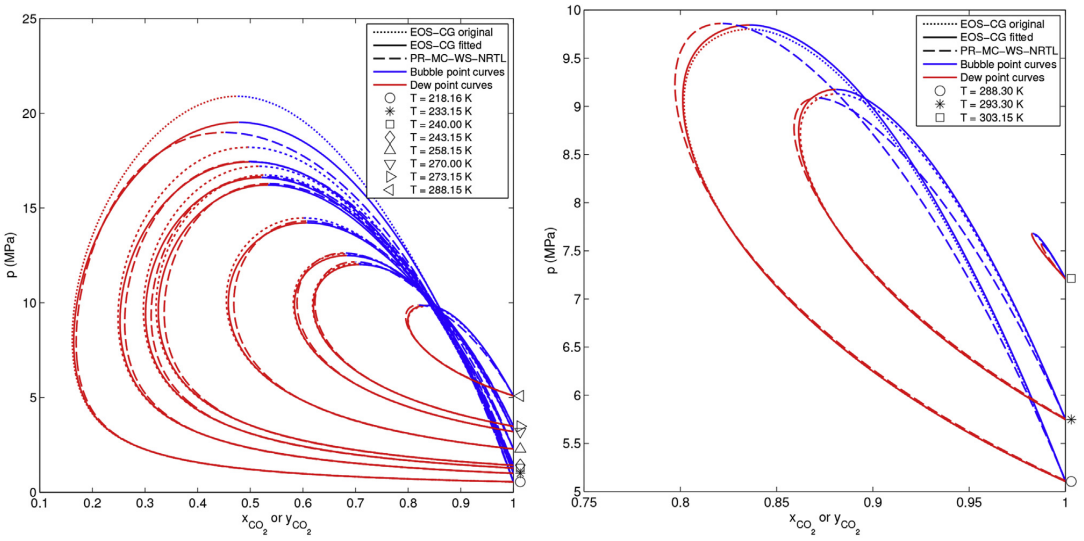

(a) Original and fitted EOS-CG and PR-MC-WS-NRTL EOS Case 3 plotted for the literature data temperatures T ≤ 288.15 K in Table 8. **(b)** Original and fitted EOS-CG and PR-MC-WS-NRTL EOS Case 3 plotted for the literature data temperatures T ≥ 288.30 K in Table 8.

Fig. 13. Original and fitted versions of EOS-CG and PR-MC-WS-NRTL model for the literature data temperatures in Table 8.

Table 9
Critical properties[a] and Mathias–Copeman coefficients[b] used in PR-MC-WS-NRTL EOS for CO_2 and N_2.

i	$T_{c,i}$ (K)	$p_{c,i}$ (MPa)	$c_{1,i}$	$c_{2,i}$	$c_{3,i}$
CO_2	304.2	7.3765	0.704606	−0.314862	1.89083
N_2	126.161	3.3944	0.404606	0.391057	−0.963495

[a] Values used by the in-house software. Slightly different from the values used in Refs. [6,22]: $T_{c,CO_2} = 304.1282$ K, $p_{c,CO_2} = 7.3773$ MPa, $T_{c,N_2} = 126.192$ K, $p_{c,N_2} = 3.3958$ MPa.
[b] Parameters for CO_2 from Ref. [45]. Parameters for N_2 obtained by fitting the N_2 vapor pressure calculated using PR-MC against N_2 vapor pressures calculated by the N_2 reference EOS by Span et al. [22] over the temperature range between the N_2 triple point and the critical point.

6. Conclusions

This work describes a new facility for the measurement of vapor–liquid equilibria (VLE) of CO_2-rich mixtures, and reports the measurements of this setup on mixtures of CO_2 and N_2. More accurate VLE data will be required for a number of relevant mixtures in order to build better predictive models to be used in order to optimize the design and operation of various processes needed within CCS.

Our data covers a large range of VLE liquid and vapor phase CO_2 compositions, spanning from approximately 0.57 to 0.995 in the liquid phase, and from 0.19 to 0.992 in the vapor phase. Our

Table 10
Optimal parameters k_{12}, τ_{12} and τ_{21} for the PR-MC-WS-NRTL model, fitted against data from the present work and literature data.

ID[d]	T (K)	Case 1[a]				Case 2[b]			Case 3[c]		
		k_{12}	τ_{12}	τ_{21}	S	τ_{12}	τ_{21}	S	τ_{12}	τ_{21}	S
1*	218.16	0.2900	1.3089	0.1064	4.6	1.0545	0.3482	6.5	1.5691	−0.0567	15.9
2	223.14	0.2689	1.5661	−0.0569	23.6	1.5478	−0.0432	23.6	1.5817	−0.0773	25.8
3*	233.15	0.2910	1.3736	−0.0553	8.1	1.0386	0.2261	9.9	1.6122	−0.1258	16.9
4	240.00	0.2805	1.9191	−0.3681	4.5	1.7554	−0.2797	4.7	1.6383	−0.1656	7.9
5	243.15	0.2630	1.5047	−0.1917	11.6	1.5545	−0.2235	11.6	1.6521	−0.1862	19.9
6	258.15	0.2844	1.7847	−0.4687	13.3	1.4619	−0.2874	13.7	1.7419	−0.3119	23.2
8	270.00	0.2824	2.2506	−0.6894	3.5	2.0062	−0.5610	3.4	1.8629	−0.4615	3.3
9	273.15	0.2643	2.0383	−0.5748	12.1	2.0802	−0.5959	12.1	1.9090	−0.5133	14.1
10	288.15	0.2567	1.8852	−0.5275	7.5	2.1554	−0.6901	7.5	2.3286	−0.8879	10.5
11	288.30	0.2541	2.0092	−0.7143	3.9	2.3286	−0.8882	3.9	2.3358	−0.8931	3.9
12	293.30	0.2529	2.2199	−0.6667	4.4	2.8110	−0.9317	4.2	2.6696	−1.1035	10.0
13	298.17	0.2669	3.3958	−1.2019	7.5	3.3919	−1.2001	7.5	3.3219	−1.3902	17.5
14	303.15	0.6231	7.7672	−2.7658	0.6	5.3201	−1.9738	1.5	5.3417	−1.8284	1.4
15	303.16	0.4235	6.1298	−2.2467	1.2	5.3199	−1.9738	3.5	5.3493	−1.8294	2.8

*Data set does not contain data in the critical region. Optimal values τ_{12} and τ_{21} for Case 2 not used for fitting coeffiecients of Eqs. (28) and (29).
[a] $k_{12} = k_{21}$ varies freely, $\alpha = 0.3$
[b] $k_{12} = k_{21} = 0.266801$, $\alpha = 0.3$
[c] $k_{12} = k_{21} = 0.266801$, $\alpha = 0.3$. τ_{12} and τ_{21} calculated from Eqs. (28) and (29) respectively using $a_{\tau_{12}} = 1.35373$, $b_{\tau_{12}} = -19.3496$, $c_{\tau_{12}} = 308$ K, and $a_{\tau_{21}} = 0.357156$, $b_{\tau_{21}} = 43.3883$, $c_{\tau_{21}} = 323$ K.
[d] ID number corresponds to ID in Table 8.

measured CO_2 vapor pressures at the temperatures 223.14, 298.17 and 303.16 K are all within the values calculated from the Span-Wagner EOS. The agreement between our VLE data and high quality literature data is very good, the differences being within our and the literature data author's uncertainty estimates. The apparatus have shown that it is able to perform very stable measurements in the critical region, especially at the higher temperatures 298.17 and 303.16 K, where the two-phase region spans over very small pressure and composition ranges. It is reasonable to assume that our apparatus is working properly when it comes to performing VLE measurements of high quality in these temperature, pressure and composition ranges.

The VLE measurements in the critical region at 223.14 and 303.16 K, and the accurate measurements at 298.17 K are new contributions, as no data for these regions with the same accuracy could be found in the literature. These have been used to calculate estimates with low uncertainties for the critical points using a scaling law.

The equation of state (EOS) giving the current best description of the VLE of $CO_2 + N_2$ system, the GERG-2008 EOS [7] (or EOS-CG [1,2]), predicts a higher critical pressure than the measurements in this work suggests. At 223.14 K, this EOS predicts a critical pressure approximately 1.6 MPa higher than indicated by our data. The same behavior occurs at 298.17 and 303.16 K, with a predicted critical pressure 0.15 and 0.11 MPa higher than our data, respectively.

Two different EOSs have been fitted to our data and literature data. Two of the parameters of EOS-CG [1,2] have been fitted. In addition, a fit has been made of the Peng-Robinson EOS [41] utilizing the alpha correction by Mathias and Copeman [42], the mixing rule by Wong and Sandler [43] and the NRTL excess Gibbs energy model [43]. These EOSs are able to describe the data in the present work quite accurately at the lower temperatures, especially in the critical region. However, at the higher temperatures, the description of the critical region is not so accurate. The EOSs also describe literature data quite accurately. Hence, this work illustrate the need to improve current models also with regards to a system which is relatively well known compared with other binary systems relevant for CCS.

Acknowledgments

This publication has been produced with support from the research program CLIMIT and the BIGCCS Centre, performed under the Norwegian research program Centres for Environment-friendly Energy Research (FME). The authors acknowledge the following partners for their contributions: Gassco, Shell, Statoil, TOTAL, ENGIE and the Research Council of Norway (193816/S60 and 200005/S60).

The research leading to these results has also received funding from the European Community's Seventh Framework Programme (*FP7-ENERGY-20121-1-2STAGE*) under *grant agreement* n° 308809 (The IMPACTS project). The authors acknowledge the project partners and the following funding partners for their contributions: Statoil Petroleum AS, Lundin Norway AS, Gas Natural Fenosa, MAN Diesel & Turbo SE and Vattenfall AB.

The authors would like to thank Dr. Morten Hammer, Dr. Geir Skaugen, Øivind Wilhelmsen, Eskil Aursand and Magnus Aashammer Gjennestad at SINTEF Energy Research for the in-house software used for VLE calculations and the model fitting. We would also like to thank Bjarne Malvik and Helge Johansen at SINTEF Energy Research and Håvard Rekstad and Reidar Tellebon of NTNU for their contributions.

Furthermore, the authors would like to thank Professor Roland Span of Ruhr-Universität Bochum and Dr. Eric W. Lemmon of NIST for suggesting parameters for fitting EOS-CG to the VLE data in the present work. Also, the authors would like to thank Dr. Johannes Gernert and Professor Span for the access to their literature data base [1].

Finally, the authors would like to thank the following summer interns at SINTEF Energy Research for their contributions: Asgeir Bjørgan, Petter Vollestad, Maximilian Schillings, Bjørn Holst Pettersen and Ingeborg Treu Røe.

List of symbols

a	half-width used to model uncertainties using a rectangular or triangular probability distribution (−)
a_i	Peng–Robinson pure component i parameter (−)
a_m	Peng–Robinson mixture parameter (−)
A^E_∞	molar excess Helmholtz energy at infinite pressure (J mol^{-1})
b_i	Peng–Robinson pure component i parameter (−)
b_m	Peng–Robinson mixture parameter (−)
C	EOS-dependent constant in WS mixing rule. For PR, $C = \ln(\sqrt{2}-1)/\sqrt{2}$ (−)
$f_{i,L}$	Section 5.4.1: fugacity of component i in the liquid phase (MPa)
$f_{i,V}$	Section 5.4.1: fugacity of component i in the vapor phase (MPa)
F_{12}	EOS-CG weight parameter for $CO_2 + N_2$ (−)
g_L	local acceleration of gravity (m s^{-2})
h_i	i = 1, 2, 3, 4, liq. Distance used in p_{hs} calculation. See Section Appendix A.1 (m)
k_{ij}	WS binary interaction parameter between components i and j in Eq. (25) (−)
M	molar mass (kg mol^{-1})
p	pressure at VLE (MPa)
p_i	absolute pressure of sensor i, where i = 1, 2, 3, 4 (MPa)
p_0	pressure at cell side of p_{11} (MPa)
p_{11}	differential pressure (MPa)
p_c	critical pressure (MPa)
p_{hs}	hydrostatic pressure (MPa)
$\overline{p}$	pressure at VLE: mean pressure before one composition sample in Tables B.2 and B.3 (MPa)
$\overline{p}_f$	pressure at VLE: mean of the pressures $\overline{p}$ for a series of composition samples in Tables 4 and 5 (MPa)
R	resistance of SPRT at a temperature (Ω)
R	universal gas constant = 8.3145 J K^{-1} mol^{-1}
R_{Ga}	resistance of SPRT at T_{Ga} (Ω)
R_{H_2O}	resistance of SPRT at T_{H_2O} (Ω)
R_{Hg}	resistance of SPRT at T_{Hg} (Ω)
R_{ref}	resistance of reference normal (Ω)
$s(z)$	sample standard deviation of variable z (−)
$s(\overline{z})$	sample standard deviation of the mean of variable z (−)
S	model fitting objective function to be minimized (−)
T_{04}	ITS-90 temperature of top flange SPRT (K)
T_{05}	ITS-90 temperature of bottom flange SPRT (K)
T	ITS-90 temperature at VLE (K)
$\overline{T}$	ITS-90 temperature at VLE: mean temperature before one composition sample in Tables B.2 and B.3 (K)
$\overline{T}_f$	ITS-90 temperature at VLE: mean of the temperatures $\overline{T}$ for a series of composition samples in Tables 4 and 5 (K)
T_{Ga}	ITS-90 temperature at gallium melting point (K)
T_{H_2O}	ITS-90 temperature at water triple point (K)
T_{Hg}	ITS-90 temperature at mercury triple point (K)
$u(z)$	standard uncertainty of variable z (−)
$u_c(z)$	combined standard uncertainty of variable z (−)
$u_{tot}(z)$	total standard uncertainty of variable $z = x_{CO_2}$ or y_{CO_2}, from Eq. (A.33) (−)

W ITS-90 ratio R/R_{H_2O} (−)
W_b thermometry bridge ratio R/R_{ref} (−)
W_r ITS-90 reference function (−)
x_{CO_2} liquid phase CO_2 mole fraction at VLE in Table B.2 (−)
$\bar{x}_{CO_2}$ liquid phase CO_2 mole fraction at VLE: mean mole fraction a series of composition samples in Table 4 (−)
$x_{CO_2,calc}$ liquid phase CO_2 mole fraction at VLE, calculated from fitted EOS-CG. See Section 5.4.2 (−)
y_{CO_2} vapor phase CO_2 mole fraction at VLE in Table B.3 (−)
$\bar{y}_{CO_2}$ vapor phase CO_2 mole fraction at VLE: mean mole fraction a series of composition samples in Table 5 (−)
$y_{CO_2,calc}$ vapor phase CO_2 mole fraction at VLE, calculated from fitted EOS-CG. See Section 5.4.2 (−)
z_{CO_2} liquid or vapor phase mole fraction at VLE (−)
$z_{CO_2,c}$ estimated critical composition in terms of CO_2 mole fraction, defined in Section 5.2 (−)

Greek letters

α_{ij} NRTL non-randomness parameter for binary interaction between components i and j in Eq. (26) (−)
β Universal critical exponent of scaling law in Eq. (15)
$\beta_{T,12}$ EOS-CG parameter in temperature reducing function for $CO_2 + N_2$ (−)
$\beta_{v,12}$ EOS-CG parameter in density reducing function for $CO_2 + N_2$ (−)
$\gamma_{T,12}$ EOS-CG parameter in temperature reducing function for $CO_2 + N_2$ (−)
$\gamma_{v,12}$ EOS-CG parameter in density reducing function for $CO_2 + N_2$ (−)
$\lambda_1, \lambda_2, \mu$ parameters of scaling law in Eq. (15)
ρ density (kg m^{-3})
ρ_i density in the four different regions $i = 1, 2, 3, 4$ used for calculation of p_{hs} (kg m^{-3})
$\rho_{4,1}$ density of pure CO_2 in Region 4 used for calculation of p_{hs} (kg m^{-3})
$\rho_{4,2}$ density of fluid in Region 4 used for calculation of p_{hs} (kg m^{-3})
σ standard deviation (−)
τ_{ij} NRTL parameter for binary interaction between components i and j in Eq. (26) (−)

Subscripts

c critical state

Superscripts

$\bar{}$ arithmetic mean

Abbreviations

ABBA weighing cycle of A and B comparisons
CAD computer-aided design
CCS carbon capture, transport and storage
EOS equation of state
EOS-CG equation of state for combustion gases and combustion gas like mixtures
GC gas chromatograph
GUM ISO guide for the estimation of uncertainty in measurement
MC Mathias–Copeman alpha correction
NRTL non-random two-liquid excess Gibbs energy model
OIML Organisation Internationale de Métrologie Légale
PLC programmable logic controller
PR Peng–Robinson EOS
SPRT standard platinum resistance thermometer
SW Span–Wagner EOS for CO_2
TCD thermal conductivity detector in GC
URL upper range limit for p_{11}
VLE vapor–liquid equilibrium
WS Wong–Sandler mixing rule

Appendix A. Detailed uncertainty analysis

Appendix A.1. Uncertainty analysis of pressure

As mentioned in Section 2.1, the equilibrium pressure at the vapor–liquid interface p was measured indirectly. The setup is shown in Fig. A.1. The absolute pressure sensor in use for a given experiment is designated p_i, where the index $i = 1, 2, 3, 4$ corresponds to the sensor in use, with increasing full scale pressure for increasing indices. The differential pressure transducer, designated p_{11}, was placed at the same elevation as the p_i sensors, to avoid a pressure difference due to a hydrostatic pressure. The differential pressure sensor and the tubing going down to the cell was heated to a temperature T_{10} above the cell temperature, to avoid condensation of the vapor phase in the tubing. Using these definitions, the pressure on the cell circuit side of the differential pressure sensor can be stated as $p_0 = p_i + p_{11}$.

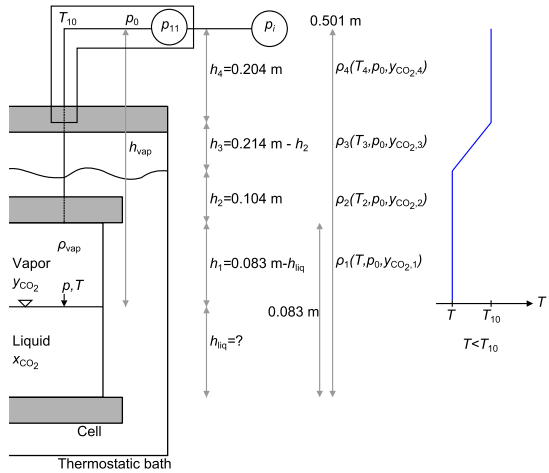

Fig. A.1. Sketch of pressure measurement system.

At thermodynamic equilibrium, the pressure at the vapor–liquid interface p is equal to p_0 plus the hydrostatic pressure of the fluid in the vertical distance between the position where p_0 is measured and the vapor–liquid interface. This hydrostatic pressure is designated p_{hs}. The pressure at the vapor–liquid interface can then be stated as

$$p = p_i + p_{11} + p_{hs}. \tag{A.1}$$

Appendix A.1.1. Hydrostatic pressure p_{hs}

The hydrostatic pressure is in general equal to $\rho g_L h$, that is, density times gravity times vertical height difference. This pressure will in most cases be very small compared to the cell pressure, as the fluid column is less than 0.5 m high, and, as the density of the fluid is approximately proportional to the cell pressure. The density of the fluid column ρ depends on the contents of the cell. The height depends on the liquid level in the cell h_{liq}, and can be measured quite accurately using a borescope to inspect the cell contents

visually. The local gravity used, $g_L = 9.82146\ ms^{-2}$, was based on a measurement by the Geological Survey of Norway (NGU) in the room where the experimental setup is located. The hydrostatic pressure p_{hs} was calculated based on the mean absolute pressure value p_i over the time period of the VLE experiment, to obtain the equilibrium pressure p.

The tubing connecting the point where p_0 was calculated and the bulk contents of the cell was quite small in internal diameter (approximately 0.6 mm), and it was not certain that the contents of this tubing had the same composition and temperature as the bulk vapor phase in the cell, when the bulk contents of the cell had reached VLE. This made it difficult to calculate the density of the fluid very accurately.

In addition, the density of the fluid column will vary in the vertical region between p and p_0. As shown in Fig. A.1, the vertical region was divided into four different subregions, indicated with vertical distances h_i, with corresponding temperatures T_i, CO_2 mole fractions $y_{CO_2,i}$ and densities ρ_i, where $i = 1, 2, 3, 4$.

In Regions $i = 1, 2$ and 4, we could assume that the temperature, and thereby the composition, in the fluid column was approximately constant. Between the vapor–liquid interface and up to the thermostatic bath fluid surface, the temperature was assumed to be equal to T, as the bath fluid should keep a specified temperature given by the set point of the bath. The temperature in Regions 1 and 2 was therefore equal to T. In Region 4 the temperature was kept at T_{10}, and is assumed to be constant. We assumed that the temperature in Region 3, between the thermostatic bath liquid surface at T and the circuit kept at T_{10} was increasing linearly, as shown in Fig. A.1. This was not necessarily correct, as the region between the bath fluid surface and the bottom of the insulating lid was filled with air.

The pressure in these four regions was assumed to be equal to p_0, to be able to perform the calculation of the densities needed to calculate the hydrostatic pressure.

Based on the assumption of the temperature behavior in Region 3, we assumed that the density in Region 3 was decreasing linearly from the density in Regions 2 to 4 as we move up vertically. Assuming a vertical height datum $z = 0$ at the interface between Regions 2 and 3, the densities in this and the other regions could be expressed as

$$\begin{aligned}\rho_1 &= \rho_{vap}\left(T, p_0, y_{CO_2}\right),\\ \rho_2 &= \rho_2\left(T, p_0, y_{CO_2,2}\right),\\ \rho_3 &= \rho_2 + z(\rho_4 - \rho_2)/h_3,\\ \rho_4 &= \rho_4\left(T_{10}, p_0, y_{CO_2,4}\right).\end{aligned} \tag{A.2}$$

Under these assumptions, a general expression for the hydrostatic pressure could be written as

$$\begin{aligned}p_{hs} &= f(\rho_1, \rho_2, \rho_4, h_1, h_2, h_3, h_4, g_L)\\ &= \rho_1 g_L h_1 + \rho_2 g_L h_2 + \int_{z=0}^{h_3} \rho_3(z) g_L \mathrm{d}z + \rho_4 g_L h_4\\ &= \rho_1 g_L h_1 + \rho_2 g_L h_2 + g_L\left(\rho_2 h_3 + \frac{\rho_4 - \rho_2}{2} h_3\right) + \rho_4 g_L h_4.\end{aligned} \tag{A.3}$$

During the experiments, T_{10} was kept at 313 K. At this temperature we were above the critical temperature of both N_2 (126.192 K [22]) and CO_2 (304.1282 K [6]), ensuring that the fluid in Region 4 was supercritical.

When making assumptions about the composition in the four different regions, we had several possibilities. In the current experimental procedure, CO_2 was filled into the cell first, and then the second component N_2. Regions 2–4 will therefore initially consist of pure CO_2, and the mixing of the contents of the cell using the stirrer did not affect the contents of these regions very much. Any mass transport from Region 1 to Regions 2–4 and back again, therefore, mainly relied on diffusion along the thin tubing.

As all our VLE experiments were carried out at temperatures above the critical temperature of N_2 and below the critical temperature of CO_2, vapor and liquid phases at equilibrium could only exist at pressures above the vapor pressure of CO_2. Based on this fact, the only place where pure CO_2 could exist at cell pressure p (above the vapor pressure of CO_2) was where the temperature was above the critical temperature of CO_2. This included Region 4 and the upper part of Region 3. For simplicity we assumed that only Region 4 was included. If we assumed that only the vapor phase of the cell had been in contact with the entrance of the tubing, the two extreme points for the possible total composition in Region 4, $y_{CO_2,4}$, were either pure CO_2 or the composition of the vapor phase with the lowest CO_2 content in the previous and current VLE measurements. Consequently, the difference in the calculated density in Region 4 was the largest during VLE measurements at low temperatures far from T_{10}, where the N_2 content of the vapor phase would increase.

The best solution to this would be to wait for a sufficiently long time after VLE has been reached in the cell, to ensure that the composition in Regions 2–4 is closer to that of the cell vapor phase. It was, however, difficult to determine what sufficient time would be.

Based on this discussion, the following assumptions were made about the contents of the fluid column: The density in Region 2 was assumed to be equal to that in Region 1, $\rho_2 = \rho_1(T, p_0, y_{CO_2})$. The density and corresponding uncertainty in Region 4 were based on the most conservative estimate. It was assumed that the probability that the density in Region 4 is not included in the interval defined by the two density extremes (a_- and a_+) is equal to zero. A rectangular probability distribution was assumed, with the expected value of the density $\rho_4 = (a_+ + a_-)/2$. The standard uncertainty was then $u(\rho_4) = 0.5 \cdot |a_+ - a_-|/\sqrt{3}$. The two density extremes were designated $\rho_{4,1} = \rho_4(T_{10}, p_0, y_{CO_2,4} = 1)$ for pure CO_2, and $\rho_{4,2} = \rho_4(T_{10}, p_0, y_{CO_2,4} = y_{CO_2})$ for CO_2 and N_2 with the composition equal to that of the cell vapor phase y_{CO_2}. The density of supercritical pure CO_2 was calculated using the Span-Wagner EOS [6]. The density of the cell vapor phase was calculated using EOS-CG [1,2]. The standard uncertainties in density for these EOSs at the relevant temperatures and pressures are given in Table 2.

Taking into the account the uncertainties in the densities calculated from the EOSs, the combined standard uncertainty $u_c(\rho_4)$ is given by Eq. (3),

$$\begin{aligned}u_c^2(\rho_4) &= u^2(\rho_4) + \left[u(\rho_{4,1})\left(\partial\rho_4/\partial\rho_{4,1}\right)_{\rho_{4,2}}\right]^2\\ &\quad + \left[u(\rho_{4,2})\left(\partial\rho_4/\partial\rho_{4,2}\right)_{\rho_{4,1}}\right]^2\\ &= u^2(\rho_4) + \left[u(\rho_{4,1})/2\right]^2 + \left[u(\rho_{4,2})/2\right]^2.\end{aligned} \tag{A.4}$$

For specifying the height of the fluid column, there are two types of input variables. The first type are the numbers specified as constants in Fig. A.1 in the expressions for h_1, h_3 and h_4, which were taken from the CAD drawing of the apparatus and verified by manual measurements on the apparatus. The second type are the only two variables in the calculation of the fluid column height, h_{liq} and the distance from the bottom of the top flange to the thermostatic bath liquid surface, h_2.

The uncertainty in the liquid level h_{liq} can be significant, and this has two causes. The first is the uncertainty connected to measuring the level from a borescope picture, $u(h_{liq},1)$. The second source for

uncertainty is that the liquid level might change slightly from sample to sample, $u(h_{liq},2)$. The current procedure is to sample a volume equal to the capillary sampler volume. The liquid sampler capillary had an internal volume of approximately $7.1\cdot10^{-3}$ cm^3, or 0.0071% of the cell internal volume. For the vapor sampler capillary, the internal volume was $5.3\cdot10^{-3}$ cm^3, or 0.0053% of the cell volume. Because of the relatively small volume of the samples withdrawn compared to the cell volume, the change in liquid level was found to be insignificant. The change in liquid level was calculated using an EOS, and checked using the borescope before and after the samples were taken. During the performed experiments, it was not possible to see a change in the liquid level before and after a series of liquid and vapor samples.

The standard uncertainty in the borescope determination of the liquid level was modeled using a rectangular distribution, with maximum bounds a estimated as 10% of the maximum liquid level 0.083 m, $a = 0.0083$ m, yielding a standard uncertainty of $u(h_{liq},1) = a/\sqrt{3} \approx 0.0048$ m. Since it was not possible to see a change in liquid level during the course of one experiment, the uncertainty contribution from this source was considered negligible compared to the borescope determination of the liquid level, and $u(h_{liq},2) \approx 0$ m was assumed. Assuming independence of the two contributions, and using Eq. (5a), the total standard uncertainty was given as $u(h_{liq}) = [u^2(h_{liq},1) + u^2(h_{liq},2)]^{0.5} = 0.0048$ m. The height h_2, determined by the fluid level in the thermostatic bath, was subject to some variations. h_2 was also modeled using a rectangular distribution, with estimated $a = 0.010$ m, yielding $u(h_2) \approx 0.006$ m.

The uncertainty in the lengths obtained from the CAD drawing were assumed to be negligible compared to the uncertainty in h_{liq}. Using Eq. (3), this gave $u_c(h_1) = [1^2\cdot u^2(\mathrm{CAD}) + (-1)^2\cdot u^2(h_{liq})]^{0.5} = 0.0048$ m and $u_c(h_3) = [1^2\cdot u^2(\mathrm{CAD}) + (-1)^2\cdot u^2(h_2)]^{0.5} = 0.006$ m.

The variables of Eq. (A.3) are not independent, and as it is difficult to determine the correlations, the Type B evaluation of Eq. (4) was used for the combined standard uncertainty of p_{hs}:

$$u(p_{hs}) = \sum_{i=1,2}\left|u(\rho_i)\frac{\partial p_{hs}}{\partial \rho_i}\right| + \left|u_c(\rho_4)\frac{\partial p_{hs}}{\partial \rho_4}\right| + \sum_{i=1,3}\left|u_c(h_i)\frac{\partial p_{hs}}{\partial h_i}\right| + \sum_{i=2,4}\left|u(h_i)\frac{\partial p_{hs}}{\partial h_i}\right| + \left|u(g_L)\frac{\partial p_{hs}}{\partial g_L}\right|. \tag{A.5}$$

In the temperature range 223.15–303.15 K, the standard uncertainty $u(p_{hs})$ was less than $10^{-4}\cdot p$. The main contributors were $u(\rho_4)$ and to a lesser extent $u_c(h_{liq})$ and $u(h_2)$.

Appendix A.1.2. Differential pressure p_{11}

The differential pressure was measured using a Rosemount 3051S1CD differential pressure transmitter, in combination with a Rosemount 1199 remote mount seal/diaphragm. The transmitter can measure pressure differences over the diaphragm in the range ±0.0623 MPa. The transmitter was kept at a fairly constant temperature, as the room temperature was kept at around 22 °C by air-conditioning.

According to the specification of the transmitter, the measured value of the differential pressure is influenced by the temperature of the surroundings, the line pressure, the span of the measurements, how the transmitter is mounted, vibrations and changes in the voltage of the power supply. In addition, there is a discretization error due to the AD-conversion. Hence, in total 7 different uncertainty terms have been identified, with uncalibrated values given by:

$$u(p_{11},1) = 0.44\mathrm{Pa/K}\cdot\Delta T, \quad \text{Temperature} \tag{A.6a}$$

$$u(p_{11},2) = 7.6\cdot10^{-7}\cdot p_i, \quad \text{Line pressure} \tag{A.6b}$$

$$u(p_{11},3) = 4.9\cdot10^{-5}\ \mathrm{MPa}^{-1}\cdot p_i\cdot p_{11}, \quad \text{Span} \tag{A.6c}$$

$$u(p_{11},4) = 0.10\ \mathrm{kPa}, \quad \text{Mounting} \tag{A.6d}$$

$$u(p_{11},5) = 28\ \mathrm{Pa}, \quad \text{Vibrations} \tag{A.6e}$$

$$u(p_{11},6) = 2.1\ \mathrm{Pa\,V^{-1}}\cdot\Delta V, \quad \text{Voltage} \tag{A.6f}$$

$$u(p_{11},7) = 0.24\ \mathrm{kPa}. \quad \text{AD converter} \tag{A.6g}$$

In addition to these terms, a long term stability of 42 Pa was guaranteed for a period of 10 years. As the transmitter was bought 3 years ago, the stability should still be within this specification. The uncertainties were specified at $\pm3\sigma$, and are functions of the calibrated URL and span. As nothing else was stated by the manufacturer, it was assumed that a normal probability distribution has been used in the estimation of the uncertainties. Hence, the specified uncertainties U were assumed to be three times the standard uncertainty u, $u = U/3$.

Some of the terms of Eq. (A.6) were reduced to insignificant levels through the design and procedures of the setup. The temperature dependent uncertainty $u(p_{11},1)$ was eliminated by controlling the ambient temperature. The line pressure $u(p_{11},2)$ and mounting dependent $u(p_{11},4)$ zero reading uncertainty were eliminated by physically connecting the two sides of the transmitter at different line pressures. Based on these measurements, an offset function using linear interpolation was constructed at T_{10}. The uncertainty caused by voltage variations, $u(p_{11},6)$, was negligible, leaving only the span error $u(p_{11},3)$, effect of vibrations, $u(p_{11},6)$, and AD-conversion error, $u(p_{11},7)$. The former term was in most measurements reduced, but not always completely eliminated, by controlling the pressure levels such that p_{11} was small. The transmitter was subjected to some small vibrations, especially from the motors powering the compressor in the cold thermostatic bath.

The largest contribution to uncertainty of p_{11} turned out to be the AD conversion. The specified accuracy of the used PLC was 0.3% FS, where the full scale was 20 mA DC. Since nothing else was stated, this was assumed to be at $\pm2\sigma$ calculated using a normal distribution, in accordance with the "GUM" [12]. This error can be reduced by decreasing the span or using an AD converter with higher resolution.

The contributing uncertainties in the differential pressure p_{11} are summarized in Table 2.

As the different contributions were independent we got

$$u(p_{11}) = \sqrt{u^2(p_{11},3) + u^2(p_{11},5) + u^2(p_{11},7)}. \tag{A.7}$$

It should be noted that the dominating source of uncertainty, $u(p_{11},7)$, was independent of line pressure, with a relative contribution of $3–4\cdot10^{-4}$ at the lowest measured line pressures around 0.7 MPa. Hence, for most of our data, the uncertainty contribution from the differential pressure measurements was insignificant.

Appendix A.1.3. Pressure transmitter p_i

The pressure transmitters p_i (Keller model PAA-33X) were delivered with certified "precision" stated as 0.01% of the full scale pressure for the temperature range 10–40 °C, when the RS485 digital readout is used. The sensors had been calibrated in-situ

before and after the VLE measurements were performed, against a dead weight tester that was calibrated by IKM Laboratorium in Norway in 2013 (Desgranges et Huot model 26000 M). It was not possible to see any drift in the response of the sensors from the first to the second calibration. Based on the calibrations, the standard uncertainties of the sensor values were those given as $u(p_i)$ for $i = 1$, 2, 3, 4 in Table 2.

Appendix A.1.4. Total uncertainty in cell pressure p

As the hydrostatic pressure p_{hs} is a function of the absolute pressure p_i, and p_{11} changes when p_i changes, the three terms in Eq. (A.1) could not be assumed to be independent. Therefore, we had to use Eq. (4) to estimate the combined standard uncertainty in the cell pressure:

$$u_c(p) = \left|\frac{\partial p}{\partial p_i}\right| |u(p_i)| + \left|\frac{\partial p}{\partial p_{11}}\right| |u(p_{11})| + \left|\frac{\partial p}{\partial p_{hs}}\right| |u(p_{hs})| = |u(p_i)| + |u(p_{11})| + |u(p_{hs})|. \quad \text{(A.8)}$$

For the higher pressures between 10 and 20 MPa, the total uncertainty was dominated by the uncertainties in sensors p_3 and p_4, while for lower pressures below 10 MPa, the uncertainties in sensors p_1 and p_2 were of the same magnitude as the uncertainty caused by the A/D conversion in sensor p_{11}. For all pressures, the uncertainty in the hydrostatic pressure was small compared to these other sources.

Appendix A.2. Uncertainty analysis of temperature

The sensors T_{04} and T_{05} were standard platinum resistance thermometers (SPRT). The temperature of a SPRT is calculated by measuring the resistance of the SPRT at the unknown temperature and comparing this resistance to the measured resistance at other known temperatures. The framework used for doing this comparison was the International Temperature Scale of 1990 (ITS-90) [23]. As the VLE measurements were carried out in the temperature range 223.14–303.16 K, the ITS-90 calibrations were performed in the subrange defined by the triple point of mercury ($T_{90} \equiv 234.3156$ K), triple point of water ($T_{90} \equiv 273.16$ K) and the melting point of gallium ($T_{90} \equiv 302.9146$ K). The ITS-90 deviation function for this subrange (Section 3.3.3 in Ref. [23]) have been used together with the ITS-90 reference functions W_r (Eqs. (9a) and (10a) in Ref. [23]) to calculate the ITS-90 temperatures T_{90}. The extrapolation of this deviation function to 303.16 K, 0.24 K above the gallium melting point, was assumed to give negligible contribution to the temperature uncertainty. According to Ref. [56], the extrapolation of the deviation function to 223.14 K, 11 K below the mercury triple point is not advised when the utmost accurate temperature measurements are to be taken.

The resistance of the SPRT at a certain temperature was measured using an ASL F650AC Thermometry Bridge, together with a external Tinsley 5685A resistance normal placed inside a Tinsley 5648 temperature-controlled enclosure as reference. The measured input quantity was the bridge ratio:

$$W_b = \frac{R(T_{90})}{R_{ref}}, \quad \text{(A.9)}$$

where $R(T_{90})$ is the resistance of the SPRT at the unknown ITS-90 temperature T_{90}, and R_{ref} is the resistance of the Tinsley resistance normal. The resistance normal was calibrated inside the temperature-controlled enclosure by the Norwegian national metrology service Justervesenet on 2012-04-12. The calibration certificate stated $R_{ref} = 24.998982\ \Omega$ with a standard uncertainty of $u(R_{ref},1) = 6 \cdot 10^{-6}\ \Omega$. Taking into account the temperature stability of the enclosure and its effect on the resistance of the resistance normal, and the long term stability of the resistance, the total standard uncertainty at the time of use was estimated using Eq. (5a) to be $u(R_{ref}) = 8.5 \cdot 10^{-6}\ \Omega$.

The uncertainty $u(T_{90})$ in the calculated temperature T_{90} can be stated as

$$u(T_{90}) = |u(W_r(T_{90})) \cdot [\partial T_{90}/\partial W_r(T_{90})]|, \quad \text{(A.10)}$$

where $W_r(T_{90})$ is the ITS-90 reference function calculated based on the resistance of the SPRT at the calculated temperature and the resistance of the SPRT at the calibration points. Two reference functions were given in the ITS-90, and which one to use depends on the temperature. The derivative was obtained analytically as the inverse of $\partial W_r(T_{90})/\partial T_{90}$. For details, please refer to Ref. [23].

The simplified framework for uncertainty estimation of an ITS-90 temperature prepared by the Measurement Standards Laboratory of New Zealand [57] was used in the present work. To be able to use their simplified analysis, some requirements must be fulfilled.

The measurements on the calibration points should be performed using the same thermometry bridge. The calibrations were performed in-situ with the same bridge as used in the VLE measurements, so this requirement was fulfilled.

The uncertainty in the measurement of the ratio of Eq. (A.9) should be negligible. The ASL thermometry bridge specified accuracy in the ratio measurements was $6 \cdot 10^{-7}$. For the current value of R_{ref}, this corresponded to approximately 0.16 mK. Assuming a rectangular distribution gave $u(W_b) = 0.6 \cdot 10^{-6}/\sqrt{3} \approx 0.35 \cdot 10^{-6}$. The resolution of the ratio measurements was $1 \cdot 10^{-7}$, or approximately 0.025 mK, so the last digit should not be considered significant during the measurements. When uncertainties in the resistance measurements below 0.16 mK were considered to be negligible, this requirement was also satisfied.

The uncertainties in the ratio measurements at the triple point of water should be negligible. That is, the measured ratio of the SPRT when placed in the fixed point cell for the triple point of water was not significantly different from what it should have been if the SPRT was at the exact triple point temperature of water, defined in the ITS-90 to be 273.16 K. This offset can be caused by a number of reasons, which will be discussed here.

According to the calibration certificate of the water triple point cell, the standard uncertainty caused by the difference between the temperature of the water triple point cell and a reference cell at the National Physical Laboratory in England was 0.05 mK.

According to the specification of the cell, the temperature at the point where the SPRT is placed was approximately 0.2 mK lower than the true triple point temperature (273.16 K) due to the hydrostatic pressure effect.

The self-heating effect of the two SPRTs was checked at the triple point of water comparing the resistance at a measuring current of 1 mA and $1 \cdot \sqrt{2}$ mA according to the method of Veltcheva et al. [58], and the temperature at zero current was found to be approximately 0.6 mA lower than at the utilized measuring current 1 mA.

To ensure good heat transfer between the SPRT and the water triple point cell, the part of the cell well where the SPRT is placed was filled with distilled water during calibration.

Also, the temperature of the SPRT can be higher than the triple point temperature in the cell if heat is transferred from the surroundings down into the thermometer well. The triple point cell

was placed inside an insulated dewar during calibration to minimize this effect.

The effect of both hydrostatic pressure and self-heating can be minimized by correcting the measured resistance. However, these effects were quite small, so the uncorrected resistances were used, and a rectangular distribution was assumed for these effects. The total standard uncertainty of the measurement of the water triple point temperature was estimated using Eq. (5b) as $u(T_{H_2O}) \approx 0.51$ mK.

The assumptions can be said to be fulfilled, and the standard uncertainty in the ITS-90 ratio $W(T_{90}) = R(T_{90})/R_{H_2O}$ at an unknown temperature T_{90} could be expressed as [57]

$$\begin{aligned} u^2(W) &= f\left(u(R), u(R_{H_2O}), u(T,\mathrm{diff}), u(T_{H_2O})\right) \\ &= \left(\frac{\partial W}{\partial R}\Big|_{T_{90}} u(R)\right)^2 + \left(\frac{\partial W}{\partial R_{H_2O}}\Big|_{T_{90}} u(R_{H_2O})\right)^2 \\ &\quad + \left(\frac{\partial W}{\partial T_{90}}\Big|_{T_{90}} u(T,\mathrm{diff})\right)^2 + \left(\frac{\partial W}{\partial T_{H_2O}}\Big|_{T_{90}} u(T_{H_2O})\right)^2 \\ &\approx \left(\frac{1}{R_{H_2O}} u(R)\right)^2 + \left(\frac{W}{R_{H_2O}} u(R_{H_2O})\right)^2 \\ &\quad + \left(\frac{\partial W_r}{\partial T_{90}}\Big|_{T_{90}} u(T,\mathrm{diff})\right)^2 + \left(W\frac{\partial W_r}{\partial T_{90}}\Big|_{T_{90}} u(T_{H_2O})\right)^2, \end{aligned} \tag{A.11}$$

where $u(R)$ and $u(R_{H_2O})$ are the standard uncertainty in the resistance measurement at the unknown temperature and at the triple point of water. They were calculated as $u_R = \left|R_{ref} \cdot u(W_b)\right| + \left|W_b \cdot u(R_{ref})\right|$.

$u(T,\mathrm{diff})$ is the uncertainty caused by the SPRT being at a temperature other than the one we want to measure, and this is usually the largest contribution to the total uncertainty in a temperature measurement. For the mercury triple point and the gallium melting point calibration points, this is equal to $u(T_{Hg})$ and $u(T_{Ga})$, and they were evaluated in the same way as for $u(T_{H_2O})$. At an unknown temperature during the VLE experiments, this uncertainty was assumed to be equal to the difference between the measured temperatures of the two SPRTs and was modeled using a rectangular distribution: $u(T,\mathrm{diff}) = |T_{04} - T_{05}|/\sqrt{3}$.

The drift in the resistance can be controlled by performing regular calibration of the SPRT at the fixed points. The effect on the SPRT not being at the temperature we are trying to measure can only be controlled by ensuring the best possible heat transfer between the cell contents, which has the temperature we want to measure, and the SPRT. This can be ensured by, for example, avoiding having stagnant air surrounding the SPRT in the pocket in which it is placed. In the experimental setup, we had two SPRTs, one placed in the top flange and one in the bottom flange. Aluminum oxide powder was placed around the SPRTs in the pockets in which they were placed, to ensure good heat transfer to the titanium in the cell flanges. By having two sensors at these locations, we could be more certain that the temperatures measured by the SPRTs represented the temperature of the fluid inside the cell.

The standard uncertainty of the calculated reference function value is expressed as [57]

$$u^2(W_r(T_{90})) = u^2(W) + u^2(W_{Hg},\mathrm{tot}) + u^2(W_{Ga},\mathrm{tot}). \tag{A.12}$$

Here,

$$u^2(W_{Hg},\mathrm{tot}) = \left[\frac{(W-1)\cdot(W-W_{Ga})}{(W_{Hg}-1)\cdot(W_{Hg}-W_{Ga})}\right]^2 \cdot u^2(W_{Hg}), \tag{A.13}$$

and

$$u^2(W_{Ga},\mathrm{tot}) = \left[\frac{(W-1)\cdot(W-W_{Hg})}{(W_{Ga}-1)\cdot(W_{Ga}-W_{Hg})}\right]^2 \cdot u^2(W_{Ga}), \tag{A.14}$$

where $u(W_{Hg})$ and $u(W_{Ga})$ were evaluated using Eq. (A.11).

Appendix A.2.1. Total uncertainty in cell temperature T

The discussion in the previous section concerns the uncertainty analysis of one of the two SPRTs used to measure the temperature, T_{04} and T_{05}. When the contents of the cell is at VLE, the temperature at the vapor/liquid interface, designated T, should be somewhere between the temperatures in the top flange, T_{04}, and in the bottom flange, T_{05}. This will be a reasonable assumption if the temperature of the thermostatic bath fluid is sufficiently uniform and stable in the heat transfer regions between the cell and the bath fluid. The uniformity and stability can be investigated by measuring the temperature around the perimeter of the cell seen from above and at different vertical positions ranging from the position of the top flange to the bottom flange.

Given that the uniformity and stability in these regions are sufficient, the VLE temperature can be approximated using the arithmetic mean of the two measured temperatures

$$T = \frac{T_{04} + T_{05}}{2}. \tag{A.15}$$

T_{04} and T_{05} cannot be assumed to be independent, so the uncertainty in T must be expressed as

$$\begin{aligned} u(T) &= \left|u(T_{04})\frac{\partial T}{\partial T_{04}}\right| + \left|u(T_{05})\frac{\partial T}{\partial T_{05}}\right| \\ &= |u(T_{04})/2| + |u(T_{05})/2|. \end{aligned} \tag{A.16}$$

Appendix A.3. Uncertainty analysis of composition

The VLE composition analysis was performed using a GC, which was calibrated using gas mixtures with composition known to high accuracy. These mixtures were gravimetrically prepared using a custom-built rig in our laboratories at NTNU and SINTEF Energy Research [17], with adherence to the ISO standard [59]. The uncertainty of the VLE composition analysis has contributions from a range of sources, including the impurities of the gases used to prepare the calibration mixtures, the uncertainty in the molar masses, inaccuracies in the weighed masses, adsorption, repeatability/uncertainties of the sampling and GC analysis, and finally the consistency between the GC calibration function and data.

Appendix A.3.1. Composition calibration procedure

Each calibration gas was filled into the cell using the impurity pump shown in Fig. 1. The cell, pump and lines leading to the cell were kept at 313 K, to ensure that the calibration gas was in single phase. Using the same procedure as described in Section 2.3, the

impurity pump and lines were first evacuated once, then flushed with the calibration gas to dilute any remaining impurities in the lines and pumps. This evacuation and flushing was repeated 5 times. After the final evacuation, the calibration gas was filled onto the impurity pump and connected lines, and maintained at a pressure of at least 0.5 MPa to prevent contamination of the gas.

The next step was to flush the cell with the calibration gas from the impurity pump and then evacuate. As with the pump, this process was repeated 5 times to remove most of the remaining impurities in the cell. After the final evacuation of the cell, the cell was flushed with the calibration gas once more, to minimize the effects of surface adsorption of the components in the calibration gas. The cell was then filled to different pressures in the range of 5–10 MPa.

Samples of varying sizes were withdrawn from the cell at various pressures. These samples formed the basis for the calibration of the composition analysis, giving a relation between the CO_2 mole fractions of the calibration gas mixtures and the GC detector response.

Appendix A.3.2. Source gas composition and molar mass

When preparing a calibration mixture gravimetrically, the composition and its uncertainty are affected by both the molar mass and purity of the source gases. According to Refs. [60,61], the molar masses of monoatomic carbon C, monoatomic oxygen O in commercial tank gas CO_2 and monoatomic nitrogen N in commercial tank gas N_2 generally lie within ranges of width 0.6, 0.15, and 0.05 mg mol^{-1}, respectively. The arithmetic mean values of these ranges were used as the molar masses of the atomic elements, and, as a conservative estimate, the half width of the ranges used as standard uncertainties in the atomic element molar masses. The standard uncertainty in the molecular molar masses of CO_2 and N_2 were calculated using Eq. (3). The molar masses M_{CO_2}, M_{N_2} and uncertainties are summarized in Table A.1. As can be seen, the relative uncertainties of M_{CO_2} and M_{N_2} were of the order of 10 and 1 ppm, respectively. The minimum certified purities of the CO_2 and N_2 gas sources used to prepare the calibration gas mixtures are provided in Table 1. Moreover, the maximum content of certain impurities were specified by the providers of the CO_2 and N_2 gas. Due to impurities, the molar masses of these gases were not exactly equal to the molar masses of CO_2 and N_2, respectively. For the CO_2 gas, the maximum specified impurity content by volume was less than 2 ppm H_2O, 1 ppm O_2, 5 ppm N_2, 1 ppm hydrocarbons C_nH_m and 1 ppm H_2. For the N_2 gas, less than 0.5 ppm H_2O, 0.1 ppm O_2, 0.1 ppm hydrocarbons C_nH_m and 0.5 ppm CO_2 and CO have been specified.

Table A.1
Molar masses of atomic elements and compounds. Data from Refs. [60,61].

Component i	M_i	$u(M_i)$	Unit
C	0.0120108	0.0000003	kg mol^{-1}
O	0.01599938	0.00000007	kg mol^{-1}
N	0.01400673	0.00000002	kg mol^{-1}
CO_2	0.0440096	0.0000003	kg mol^{-1}
N_2	0.02801345	0.00000005	kg mol^{-1}
CO_2 + imp	0.0440094		kg mol^{-1}
N_2 + imp	0.02801345		kg mol^{-1}

Since the composition of the CO_2 and N_2 source gases was not known, but only their minimum purities and maximum concentrations of some impurities, it was assumed that completely pure gases and maximum impurity were equally probable. More specifically, it was assumed that the standard uncertainty of the purity of the source gases equaled half the maximum certified impurity fraction and estimated that the actual purity level was the minimum purity plus this standard uncertainty. Furthermore, it was assumed that the concentration of each impurity component was proportional to its maximum fraction provided in the gas specifications. With the mole fractions of the different components set, the molar mass of the sample of component $i = CO_2$ or N_2 could be estimated as

$$M_{i+\mathrm{imp}} = y_{i,\mathrm{in\ sample}} \cdot M_i + \sum_{j=\mathrm{impurities}} y_{j,\mathrm{in\ sample}} \cdot M_j. \tag{A.17}$$

The molar mass M_j of each impurity j was calculated using data from Wieser et al. [61], assuming methane CH_4 for the hydrocarbon impurity specification, and the mean value of the molar mass of CO_2 and CO for the impurity specification was used where these two components were combined. The calculated molar masses $M_{CO_2+\mathrm{imp}}$ and $M_{N_2+\mathrm{imp}}$ of the gas samples are shown in Table A.1. The effective molar mass of each component $i = CO_2$ or N_2 could be written as

$$M_{i,\mathrm{eff}} = \frac{M_{i+\mathrm{imp}}}{y_{i,\mathrm{in\ sample}}} = M_i + \frac{\left(1 - y_{i,\mathrm{in\ sample}}\right) M_{\mathrm{imp}}}{y_{i,\mathrm{in\ sample}}}, \tag{A.18}$$

where

$$M_{\mathrm{imp}} = \frac{\sum_{j=\mathrm{impurities}} y_{j,\mathrm{in\ sample}} \cdot M_j}{1 - y_{i,\mathrm{in\ sample}}}. \tag{A.19}$$

Appendix A.3.3. Gravimetric preparation

As described in Ref. [17], the calibration gas mixtures were prepared by injecting CO_2 and N_2 consecutively into the calibration gas cylinder and weighing the cylinder accurately using a comparator with certified weights before and after each gas injection. Based on the discussion in Appendix A.3.2 above, the resulting masses of each component, $i = CO_2$ and N_2, with impurities were converted into moles, excluding impurities, using Eq. (A.18):

$$n_i = m_{i+\mathrm{imp}} \big/ M_{i,\mathrm{eff}}. \tag{A.20}$$

Both the numerator and denominator in Eq. (A.20) contribute to uncertainty. The uncertainty in mass $m_{i+\mathrm{imp}}$ was a function of a range of factors, including the repeatability of the ABBA mass comparisons, the uncertainty in the buoyancy correction, the uncertainty in the OIML masses, where the repeatability was the dominating contributor. Using the fact that $y_{CO_2\ \mathrm{in\ sample}}$ was close to unity, it can be shown that the uncertainty term from the effective molar mass, $M_{i,\mathrm{eff}}$, to the first order can be estimated by

$$u\left(n_i, \mathrm{M_{eff}}\right) = n_i \cdot \frac{\sqrt{4u^2\left(y_{i,\mathrm{in\ sample}}\right) M_{\mathrm{imp}}^2 + u^2(M_i)}}{M_i}, \tag{A.21}$$

where

$$u\left(y_{i,\mathrm{in\ sample}}\right) = 1 - y_{i,\mathrm{in\ sample}}. \tag{A.22}$$

Note that the definition in Eq. (A.22) is a formalization of the assumptions made with regards to source gas purity uncertainty discussed in Appendix A.3.2.

Appendix A.3.4. Sampling and estimated composition uncertainty. As discussed in Appendix A.3.1, each of the calibration gas mixtures was filled onto the cell to calibrate the GC. The cell was kept at 313.15 K to ensure that the contents of the cell were in a uniform supercritical state. Samples were taken from the VLE cell using both the liquid and vapor Rolsi™ samplers with different opening times to get samples which spanned the expected sample size during VLE experiments. 7 samples were taken for each selected combination of calibration gas mixture, sampler, and sampler opening time. The first 2 samples were discarded as flushing samples, leaving 5 valid samples. The uncertainty of the calibration mixture uncertainty reaching the GC could be estimated as

$$u_c\left(y_{CO_2,cal}\right) = \sqrt{u^2\left(y_{CO_2,cal}, m\right) + u^2\left(y_{CO_2,cal}, M_{eff}\right) + u^2\left(y_{CO_2,cal}, \text{ads.}\right)}, \tag{A.23}$$

where

$$u(y_{CO_2,cal}, m) = \frac{u(n_{CO_2}, m)\cdot n_{CO_2} + u(n_{N_2}, m)\cdot n_{N_2}}{\left(n_{CO_2} + n_{N_2}\right)^2}, \tag{A.24}$$

$$u\left(y_{CO_2,cal}, M_{eff}\right) = \frac{\sqrt{u^2\left(n_{CO_2}, M_{eff}\right)\cdot n_{CO_2}^2 + u^2\left(n_{N_2}, M_{eff}\right)\cdot n_{N_2}^2}}{\left(n_{CO_2} + n_{N_2}\right)^2}. \tag{A.25}$$

Note that due to the measurement procedure, where the value readings of the scale between the two gas component fillings are used both to calculate the mass of N_2 and CO_2, the deviations in the measured masses of the two components can be negatively correlated, leading to a positive correlation with respect to the impact mole fractions. With reference to Section 3.1, Eq. (A.24) provides a conservative estimate.

The third term in Eq. (A.23), $u(y_{CO_2,cal}, \text{ads.})$, was the contribution to uncertainty from adsorption. It is expected that CO_2 should be adsorbed by metallic surfaces to a small degree, but higher than N_2, but little work has been dedicated to quantify this effect. Leuenberger et al. [62] performed experiments with mixtures including CO_2 on commercial steel and aluminum gas cylinders. No polishing was performed in the experiments. Their measurements indicated that CO_2 formed at most a molecular monolayer on steel bottles using a model ignoring surface roughness. In our case, the pump and most of the piping were sulfinert treated and were expected to have minimum adsorption. Also the cell was expected to have little adsorption. Nevertheless, it was assumed monolayer adsorption in both the cylinders where the calibration mixtures were prepared and in the cell, and the maximum estimated adsorption of CO_2 in the gas cylinder and cell became:

$$\Delta n_{CO_2,max.ads.,cyl.} = \frac{A_{cyl.}}{A_{CO_2}\cdot N_A}, \tag{A.26}$$

$$\Delta n_{CO_2,max.ads.,cell} = \frac{A_{cell}}{A_{CO_2}\cdot N_A}. \tag{A.27}$$

Here, $A_{CO_2}\cdot N_A$ is the surface area of a monolayer of one mole of CO_2. $A_{cyl.}$ and A_{cell} are the inner surface areas of the gas cylinder and VLE cell, respectively. The adsorption will vary depending on unknown experimental conditions, in particular the unknown surface roughness of the gas cylinder. For simplicity, the uncertainty was here estimated based on the adsorption level provided by Eqs. (A.26) and (A.27):

$$u\left(y_{CO_2,cal}, \text{ads.}\right) = \frac{\Delta n_{CO_2,max.ads.,cyl.}\cdot n_{CO_2,cyl.}}{\left(n_{CO_2,cyl.} + n_{N_2,cyl.}\right)^2} + \frac{\Delta n_{CO_2,max.ads.,cell}\cdot n_{CO_2,cell}}{\left(n_{CO_2,cell} + n_{N_2,cell}\right)^2}, \tag{A.28}$$

where $n_{i,j}$ is the number of mole of component i in vessel j. The mole values in the cell were calculated using the GERG-2008 at 0.5 MPa pressure. As seen in Table A.2, this estimate for adsorption uncertainty contribution was of the same order as the other uncertainties for the calibration gas, and, as will be seen later, the adsorption would have to be order of magnitudes larger than assumed in order to be of significance for the final VLE data.

Appendix A.3.5. GC integration and calibration function. The areas under the CO_2 and N_2 peaks in the GC response curve, designated A_{CO_2} and A_{N_2}, were obtained for each sample by careful numerical integration. If the detector response were ideal, the area of each component should be proportional to the number of moles of each component having passed through the detector. However, because of nonlinearities in the detector response, the following model consisting of a linear and a nonlinear term was found to give an adequate description of the relation between moles of each component in the sample to the area of each component:

$$\hat{n}_{CO_2}\cdot k = A_{CO_2} + c_2\cdot\left(A_{CO_2}\right)^{c_4}, \tag{A.29}$$

$$\hat{n}_{N_2}\cdot k = c_1\cdot A_{N_2} + c_3\cdot\left(A_{N_2}\right)^{c_5}, \tag{A.30}$$

$$\hat{y}_{CO_2,cal} = \frac{\hat{n}_{CO_2}}{\hat{n}_{CO_2} + \hat{n}_{N_2}}. \tag{A.31}$$

where the $\hat{y}_{CO_2,cal}$ is the estimator of the CO_2 mole fraction for a calibration gas mixture given the areas for the current sample, and c_i for $i = 1$ through 5 are the parameters of the model. k is an unknown factor relating the areas to the number of moles. However, this factor was not of interest, as only the mole fraction was of interest. For each series of 5 valid samples, the mean value and sample standard deviation of the estimator, $\overline{\hat{y}}_{CO_2,cal}$ and $s(\overline{\hat{y}}_{CO_2,cal})$, were calculated.

The parameters c_i were fitted by performing the following weighted least squares minimization of the objective function S:

$$\min_{c_i} S(c_i) = \sum_{\text{series}} \left(\frac{y_{CO_2,cal} - \bar{\bar{y}}_{CO_2,cal}}{\sqrt{u_c^2\left(y_{CO_2,cal}\right) + s^2\left(\bar{\bar{y}}_{CO_2,cal}\right)}} \right)^2 . \quad \text{(A.32)}$$

The model was fitted against a total of $n = 47$ series (each series consisting of 5 samples), giving the parameter estimates found in Table A.3. As shown in Fig. A.2, the errors between the calibration gas CO_2 mole fractions and the model predictions, $e = y_{CO_2,cal} - \bar{\bar{y}}_{CO_2,cal}$, were randomly scattered around zero over the composition range $y_{CO_2,cal}$, which indicated an appropriate model structure. The sample standard deviation of the errors, $s(e)$, are also given in Table A.3. This model was used to convert the areas resulting from the analysis of a composition sample taken during a VLE experiment into a CO_2 mole fraction.

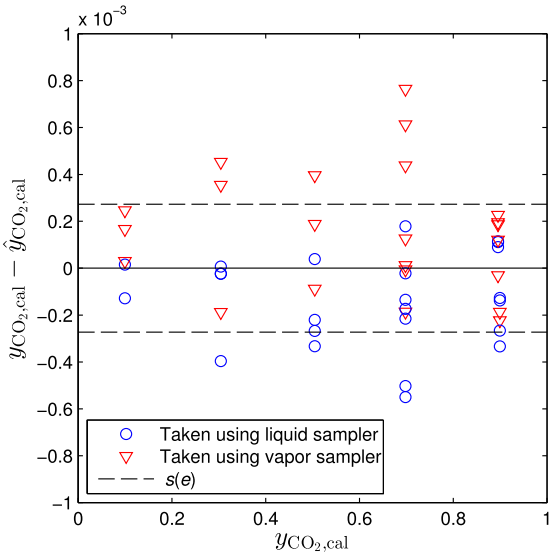

Fig. A.2. Composition calibration: Error between actual compositions in Table A.2 and composition model in Eq. (A.31), given as $y_{CO_2,cal} - \bar{\bar{y}}_{CO_2,cal}$ versus $y_{CO_2,cal}$. Composition analysis uncertainty $u(x_{CO_2}) = u(y_{CO_2}) = s(e)$ from Table A.3.

Since $s(e)$ was about 20–40 times larger than the standard uncertainties of the CO_2 mole fractions of the calibration gases, given in Table A.2, it was assumed that $s(e)$ gave an estimate of the standard uncertainty of the CO_2 mole fraction arising from the composition analysis, $u(x_{CO_2}) = u(y_{CO_2})$. To be precise, $u(x_{CO_2}) = u(y_{CO_2})$ was the standard uncertainty of the CO_2 mole fraction of a composition sample taken from the cell, caused by the *analysis alone*, excluding all uncertainties caused by factors such as that the sample taken had a composition different from the VLE composition of the phase sampled at the current temperature and pressure. Factors such as these, and their influence, could in most cases not be known exactly, and could only be minimized by measures such as sufficient stirring of the cell contents until equilibrium had been reached, sufficient time for the phases to settle after stirring was completed, waiting for some time to let pressure and temperature gradients even out, taking dummy samples to flush the contents of the Rolsi™ samplers before samples were assumed to represent the composition of the bulk of the phase sampled inside the cell, and the other measures described in Section 2.3.

Table A.2
$CO_2 + N_2$ calibration gas mixtures.

$y_{CO_2,cal}$	$u(y_{CO_2,cal}, m)$	$u(y_{CO_2,cal}, M_{eff})$	$u(y_{CO_2,cal}, \text{ads.})$	$u_c(y_{CO_2,cal})$
0.099737	$3.3 \cdot 10^{-6}$	$6.7 \cdot 10^{-6}$	$1.1 \cdot 10^{-6}$	$7.6 \cdot 10^{-6}$
0.304099	$4.8 \cdot 10^{-6}$	$4.1 \cdot 10^{-6}$	$3.4 \cdot 10^{-6}$	$7.2 \cdot 10^{-6}$
0.504479	$6.9 \cdot 10^{-6}$	$3.1 \cdot 10^{-6}$	$5.7 \cdot 10^{-6}$	$9.5 \cdot 10^{-6}$
0.698094	$6.9 \cdot 10^{-6}$	$4.5 \cdot 10^{-6}$	$7.8 \cdot 10^{-6}$	$11.4 \cdot 10^{-6}$
0.899263	$7.2 \cdot 10^{-6}$	$7.4 \cdot 10^{-6}$	$9.8 \cdot 10^{-6}$	$14.3 \cdot 10^{-6}$
0.895405	$4.4 \cdot 10^{-6}$	$7.4 \cdot 10^{-6}$	$9.8 \cdot 10^{-6}$	$13.0 \cdot 10^{-6}$

Table A.3
Fitted parameters of the $\bar{\bar{y}}_{CO_2,cal}$ model and standard uncertainty of composition analysis $u(x_{CO_2}) = u(y_{CO_2})$.

Variable	Value
c_1	1.138315
c_2	$6.799039 \cdot 10^{-5}$
c_3	$5.775209 \cdot 10^{-3}$
c_4	1.830740
c_5	1.398399
$u(x_{CO_2}) = u(y_{CO_2}) = s(e)$	$2.7269 \cdot 10^{-4}$
n	47

Appendix A.3.6. Total uncertainty in liquid and vapor phase mole fractions x_{CO_2} and y_{CO_2}. As described in Section 2.1, the composition of the phases at VLE was a function of T and p. Therefore, for a given set of measured T, p, x_{CO_2} and y_{CO_2} at VLE, the uncertainty of T and p contributed to additional uncertainty in the compositions, giving the following total standard uncertainty of the composition:

$$u_{tot}(z_{CO_2}) = \sqrt{u^2(z_{CO_2}) + \left(u_c(\overline{T}) \cdot \frac{\partial z_{CO_2}}{\partial T}\right)^2 + \left(u_c(\overline{p}) \cdot \frac{\partial z_{CO_2}}{\partial p}\right)^2}, \quad \text{(A.33)}$$

where z_{CO_2} was equal to either x_{CO_2} or y_{CO_2}, and $u_c(\overline{T})$ and $u_c(\overline{p})$ were the experimental standard deviations of the mean of the temperature and pressure measurements taken before the composition sample was taken. The derivatives in Eq. (A.33) were calculated numerically from EOS-CG fitted to our data. Details about this is explained in Section 5.4.2.

Appendix B. Detailed experimental data

Detailed VLE data for the liquid phase samples are given in Table B.2, and for the vapor phase samples in Table B.3. Each row in the tables corresponds to one composition sample. A series of samples taken at the same VLE experiment is identified by the same ID.

For ease of reading, a summary of the symbols used in the tables will be given in Table B.1. The descriptions can also be found in the list of symbols.

Table B.1
Summary of symbols used in Tables B.2 and B.3.

Symbol	Description
ID	Identifier for a series of samples. L, V and P corresponds to liquid, vapor and CO_2 vapor pressure series, respectively.
$\overline{T}$	Mean temperature before the sample is withdrawn from the cell. See Section 3.5.
$\overline{p}$	Mean pressure before the sample is withdrawn from the cell. See Section 3.5.
x_{CO_2}	Liquid phase CO_2 mole fraction of the sample.
y_{CO_2}	Vapor phase CO_2 mole fraction of the sample.
$s(T)$	Sample standard deviation of the measured temperatures used to calculate $\overline{T}$. See Eq. (7).
$s(\overline{T})$	Standard random uncertainty of $\overline{T}$. See Eq. (6).
$\overline{u}(T)$	Standard systematic uncertainty of $\overline{T}$. See Section 3.5.
$u_c(\overline{T})$	Combined standard uncertainty of $\overline{T}$. See Eq. (10).
$s(p)$	Sample standard deviation of the measured pressures used to calculate $\overline{p}$. See Eq. (7).
$s(\overline{p})$	Standard random uncertainty of $\overline{p}$. See Eq. (6).
$\overline{u}(p)$	Standard systematic uncertainty of $\overline{p}$. See Section 3.5.
$u_c(\overline{p})$	Combined standard uncertainty of $\overline{p}$. See Eq. (10).
$u(z_{CO_2})$[a]	Standard uncertainty of a sample from composition analysis alone. See Sections 3.4 and Appendix A.3.
$u_{tot}(z_{CO_2})$[a]	Total standard uncertainty of a sample, caused by additional contribution from the uncertainty in temperature and pressure. See Eq. (A.33).
$z_{CO_2,calc}$[a]	VLE CO_2 mole fraction at ($\overline{T}$, $\overline{p}$), calculated using the fitted version of EOS-CG. See Section 5.4.2.
$\partial z_{CO_2}/\partial T$[a]	Partial derivative of phase composition at VLE with respect to temperature. Used in Eq. (A.33).
$\partial z_{CO_2}/\partial p$[a]	Partial derivative of phase composition at VLE with respect to pressure. Used in Eq. (A.33).

[a] z_{CO_2} equal to either x_{CO_2} or y_{CO_2}.

Table B.2
Liquid phase: Experimental VLE data for $CO_2 + N_2$ at mean temperature $\overline{T}$, mean pressure $\overline{p}$, and sample liquid phase mole fraction x_{CO_2}.

ID	Data			Temperature				Pressure				Composition			Composition derivatives	
	$\overline{T}$	$\overline{p}$	x_{CO_2}	$s(T)$	$s(\overline{T})$	$\overline{u}(T)$	$u_c(\overline{T})$	$s(p)$	$s(\overline{p})$	$\overline{u}(p)$	$u_c(\overline{p})$	$u(x_{CO_2})$	$u_{tot}(x_{CO_2})$	$x_{CO_2,calc}$	$\partial x_{CO_2}/\partial T$	$\partial x_{CO_2}/\partial p$
	(K)	(MPa)	(−)	(K)	(K)	(K)	(K)	(MPa)	(MPa)	(MPa)	(MPa)	(−)	(−)	(−)	(K^{-1})	(MPa^{-1})
P1	223.138	0.6829	0.99999	5.8e-4	5.3e-5	2.5e-3	2.5e-3	1.5e-5	2.5e-6	5.0e-4	5.0e-4					
L1	223.140	1.9355	0.98155	1.1e-3	7.6e-5	2.4e-3	2.4e-3	4.3e-5	3.9e-6	5.2e-4	5.2e-4	2.7e-4	2.7e-4	0.98346	0.00025	−0.01359
	223.139	1.9354	0.98158	9.2e-4	9.6e-5	2.4e-3	2.4e-3	3.6e-5	5.5e-6	5.2e-4	5.2e-4	2.7e-4	2.7e-4	0.98347	0.00025	−0.01359
	223.140	1.9353	0.98156	5.3e-4	3.7e-5	2.5e-3	2.5e-3	2.4e-5	1.9e-6	5.2e-4	5.2e-4	2.7e-4	2.7e-4	0.98347	0.00025	−0.01359
L2	223.138	4.3474	0.94421	6.9e-4	9.6e-5	2.6e-3	2.6e-3	6.8e-5	2.0e-5	1.1e-3	1.1e-3	2.7e-4	2.7e-4	0.94894	0.00000	−0.01510
	223.138	4.3470	0.94421	8.0e-4	8.4e-5	2.6e-3	2.6e-3	7.7e-5	1.9e-5	1.1e-3	1.1e-3	2.7e-4	2.7e-4	0.94895	0.00000	−0.01510
	223.138	4.3466	0.94423	7.7e-4	9.6e-5	2.6e-3	2.6e-3	8.1e-5	2.7e-5	1.1e-3	1.1e-3	2.7e-4	2.7e-4	0.94895	0.00000	−0.01510
	223.138	4.3462	0.94422	1.4e-3	2.5e-4	2.6e-3	2.6e-3	6.6e-5	1.4e-5	1.1e-3	1.1e-3	2.7e-4	2.7e-4	0.94896	0.00000	−0.01510
L3	223.139	5.0305	0.93311	6.3e-4	7.0e-5	3.4e-3	3.4e-3	7.0e-5	1.4e-5	1.1e-3	1.1e-3	2.7e-4	2.7e-4	0.93846	−0.00008	−0.01560
	223.139	5.0296	0.93313	5.2e-4	3.9e-5	3.3e-3	3.3e-3	5.4e-5	4.7e-6	1.1e-3	1.1e-3	2.7e-4	2.7e-4	0.93847	−0.00008	−0.01559
	223.140	5.0287	0.93314	4.7e-4	6.2e-5	3.5e-3	3.5e-3	7.4e-5	2.0e-5	1.1e-3	1.1e-3	2.7e-4	2.7e-4	0.93849	−0.00008	−0.01559
	223.140	5.0278	0.93315	4.4e-4	1.9e-5	3.2e-3	3.2e-3	9.2e-5	3.4e-5	1.1e-3	1.1e-3	2.7e-4	2.7e-4	0.93850	−0.00008	−0.01559
	223.139	5.0270	0.93316	4.3e-4	2.3e-5	3.5e-3	3.5e-3	7.5e-5	2.3e-5	1.1e-3	1.1e-3	2.7e-4	2.7e-4	0.93851	−0.00008	−0.01559
L4	223.143	6.0998	0.91555	4.7e-4	2.8e-5	5.4e-3	5.4e-3	1.0e-4	1.7e-5	1.1e-3	1.1e-3	2.7e-4	2.7e-4	0.92134	−0.00022	−0.01644
	223.143	6.0987	0.91555	5.4e-4	1.3e-4	5.5e-3	5.5e-3	1.1e-4	3.6e-5	1.1e-3	1.1e-3	2.7e-4	2.7e-4	0.92135	−0.00022	−0.01644
	223.142	6.0976	0.91557	4.4e-4	1.1e-4	5.6e-3	5.6e-3	9.2e-5	1.9e-5	1.1e-3	1.1e-3	2.7e-4	2.7e-4	0.92137	−0.00022	−0.01645
	223.142	6.0965	0.91560	4.0e-4	2.8e-5	5.4e-3	5.4e-3	1.1e-4	2.5e-5	1.1e-3	1.1e-3	2.7e-4	2.7e-4	0.92139	−0.00022	−0.01644
	223.142	6.0954	0.91558	4.8e-4	6.7e-5	5.6e-3	5.6e-3	9.2e-5	1.7e-5	1.1e-3	1.1e-3	2.7e-4	2.7e-4	0.92141	−0.00022	−0.01646
L5	223.141	7.0010	0.90034	5.3e-4	5.2e-5	5.4e-3	5.4e-3	1.1e-4	2.5e-5	1.1e-3	1.1e-3	2.7e-4	2.7e-4	0.90617	−0.00035	−0.01723
	223.142	6.9995	0.90037	5.2e-4	5.1e-5	5.6e-3	5.6e-3	1.3e-4	4.0e-5	1.1e-3	1.1e-3	2.7e-4	2.7e-4	0.90619	−0.00035	−0.01723
	223.141	6.9979	0.90042	4.8e-4	3.9e-5	5.4e-3	5.4e-3	1.2e-4	2.8e-5	1.1e-3	1.1e-3	2.7e-4	2.7e-4	0.90622	−0.00035	−0.01723
	223.141	6.9963	0.90045	4.6e-4	4.1e-5	5.3e-3	5.3e-3	1.8e-4	6.9e-5	1.1e-3	1.2e-3	2.7e-4	2.7e-4	0.90625	−0.00035	−0.01723
	223.141	6.9949	0.90046	6.8e-4	1.2e-4	5.3e-3	5.3e-3	1.3e-4	4.1e-5	1.1e-3	1.1e-3	2.7e-4	2.7e-4	0.90627	−0.00035	−0.01723
L6	223.139	8.1168	0.88107	9.3e-4	6.4e-5	4.6e-3	4.6e-3	1.6e-4	5.5e-5	1.2e-3	1.2e-3	2.7e-4	2.7e-4	0.88634	−0.00053	−0.01833
	223.139	8.1152	0.88108	1.3e-3	4.0e-4	5.1e-3	5.1e-3	1.4e-4	2.9e-5	1.2e-3	1.2e-3	2.7e-4	2.7e-4	0.88637	−0.00053	−0.01833
	223.140	8.1132	0.88110	8.2e-4	2.1e-4	5.5e-3	5.5e-3	1.9e-4	6.8e-5	1.2e-3	1.2e-3	2.7e-4	2.7e-4	0.88641	−0.00053	−0.01833
L7	223.140	8.7875	0.86896	1.2e-3	1.0e-4	3.4e-3	3.4e-3	1.9e-4	6.5e-5	1.3e-3	1.3e-3	2.7e-4	2.7e-4	0.87380	−0.00065	−0.01903
	223.140	8.7845	0.86901	9.9e-4	1.2e-4	3.3e-3	3.3e-3	1.4e-4	1.9e-5	1.3e-3	1.3e-3	2.7e-4	2.7e-4	0.87386	−0.00065	−0.01906
	223.140	8.7814	0.86907	8.8e-4	2.5e-4	3.3e-3	3.3e-3	1.6e-4	3.2e-5	1.3e-3	1.3e-3	2.7e-4	2.7e-4	0.87392	−0.00065	−0.01906
	223.140	8.7784	0.86913	5.6e-4	7.7e-5	3.3e-3	3.3e-3	1.2e-4	1.6e-5	1.3e-3	1.3e-3	2.7e-4	2.7e-4	0.87397	−0.00065	−0.01906
	223.140	8.7756	0.86920	5.4e-4	6.5e-5	3.3e-3	3.3e-3	1.4e-4	3.3e-5	1.3e-3	1.3e-3	2.7e-4	2.7e-4	0.87403	−0.00065	−0.01905
L8	223.139	9.2282	0.86102	1.0e-3	4.1e-4	6.2e-3	6.2e-3	2.0e-4	8.3e-5	1.4e-3	1.4e-3	2.7e-4	2.7e-4	0.86529	−0.00074	−0.01959
	223.140	9.2257	0.86108	6.3e-4	1.3e-4	6.0e-3	6.0e-3	2.3e-4	9.7e-5	1.4e-3	1.4e-3	2.7e-4	2.7e-4	0.86533	−0.00074	−0.01958
	223.140	9.2232	0.86113	7.4e-4	1.2e-4	5.9e-3	5.9e-3	2.1e-4	8.7e-5	1.4e-3	1.4e-3	2.7e-4	2.7e-4	0.86538	−0.00074	−0.01958
	223.140	9.2208	0.86118	1.1e-3	1.5e-4	5.9e-3	5.9e-3	1.9e-4	4.9e-5	1.4e-3	1.4e-3	2.7e-4	2.7e-4	0.86543	−0.00074	−0.01958
	223.140	9.2182	0.86120	5.9e-4	9.9e-5	5.8e-3	5.8e-3	2.3e-4	9.9e-5	1.4e-3	1.4e-3	2.7e-4	2.7e-4	0.86548	−0.00074	−0.01957
L9	223.141	9.8378	0.85046	6.2e-4	9.4e-5	5.1e-3	5.1e-3	1.4e-4	1.2e-5	2.7e-3	2.7e-3	2.7e-4	2.8e-4	0.85311	−0.00087	−0.02036
	223.141	9.8334	0.85046	6.0e-4	9.7e-5	5.2e-3	5.2e-3	1.5e-4	1.5e-5	2.7e-3	2.7e-3	2.7e-4	2.8e-4	0.85320	−0.00087	−0.02035
	223.141	9.8290	0.85043	4.1e-4	6.8e-5	5.3e-3	5.3e-3	1.2e-4	1.7e-5	2.7e-3	2.7e-3	2.7e-4	2.8e-4	0.85329	−0.00087	−0.02035
	223.142	9.8249	0.85042	4.9e-4	7.9e-5	5.3e-3	5.3e-3	1.1e-4	1.0e-5	2.7e-3	2.7e-3	2.7e-4	2.8e-4	0.85338	−0.00087	−0.02034
	223.141	9.8207	0.85040	6.3e-4	7.1e-5	5.3e-3	5.3e-3	1.4e-4	1.5e-5	2.7e-3	2.7e-3	2.7e-4	2.8e-4	0.85346	−0.00087	−0.02034
L10	223.140	10.8526	0.82961	5.0e-4	7.4e-5	3.6e-3	3.6e-3	1.6e-4	3.3e-5	2.7e-3	2.7e-3	2.7e-4	2.8e-4	0.83173	−0.00112	−0.02181
	223.140	10.8476	0.82965	5.5e-4	3.4e-5	3.7e-3	3.7e-3	1.4e-4	4.3e-5	2.7e-3	2.7e-3	2.7e-4	2.8e-4	0.83184	−0.00112	−0.02181
	223.140	10.8429	0.82978	5.0e-4	4.1e-5	3.6e-3	3.6e-3	1.8e-4	6.2e-5	2.7e-3	2.7e-3	2.7e-4	2.8e-4	0.83194	−0.00112	−0.02180
	223.140	10.8383	0.82979	6.2e-4	6.8e-5	3.6e-3	3.6e-3	1.4e-4	3.6e-5	2.7e-3	2.7e-3	2.7e-4	2.8e-4	0.83205	−0.00112	−0.02179

(*continued on next page*)

Table B.2 (*continued*)

ID	Data			Temperature				Pressure				Composition			Composition derivatives	
	$\overline{T}$	$\overline{p}$	x_{CO_2}	$s(T)$	$s(\overline{T})$	$\overline{u}(T)$	$u_c(\overline{T})$	$s(p)$	$s(\overline{p})$	$\overline{u}(p)$	$u_c(\overline{p})$	$u(x_{CO_2})$	$u_{tot}(x_{CO_2})$	$x_{CO_2,calc}$	$\partial x_{CO_2}/\partial T$	$\partial x_{CO_2}/\partial p$
	(K)	(MPa)	(−)	(K)	(K)	(K)	(K)	(MPa)	(MPa)	(MPa)	(MPa)	(−)	(−)	(−)	(K^{-1})	(MPa^{-1})
	223.140	10.8337	0.82986	6.1e-4	8.5e-5	3.6e-3	3.6e-3	1.3e-4	3.1e-5	2.7e-3	2.7e-3	2.7e-4	2.8e-4	0.83215	−0.00111	−0.02178
L11	223.142	10.8855	0.82906	5.0e-4	1.2e-4	5.5e-3	5.5e-3	3.4e-4	1.5e-4	2.7e-3	2.7e-3	2.7e-4	2.8e-4	0.83101	−0.00113	−0.02187
	223.142	10.8817	0.82913	5.3e-4	4.8e-5	5.3e-3	5.3e-3	4.0e-4	1.8e-4	2.7e-3	2.7e-3	2.7e-4	2.8e-4	0.83110	−0.00113	−0.02186
	223.142	10.8778	0.82920	4.9e-4	7.4e-5	5.5e-3	5.5e-3	3.3e-4	1.5e-4	2.7e-3	2.7e-3	2.7e-4	2.8e-4	0.83118	−0.00113	−0.02185
	223.142	10.8740	0.82927	7.0e-4	1.7e-4	5.3e-3	5.3e-3	3.6e-4	1.6e-4	2.7e-3	2.7e-3	2.7e-4	2.8e-4	0.83127	−0.00113	−0.02185
	223.142	10.8703	0.82937	5.3e-4	2.4e-5	5.5e-3	5.5e-3	4.3e-4	2.1e-4	2.7e-3	2.7e-3	2.7e-4	2.8e-4	0.83135	−0.00112	−0.02184
L12	223.142	12.0229	0.80523	4.8e-4	6.8e-5	5.6e-3	5.6e-3	2.6e-4	1.0e-4	2.7e-3	2.7e-3	2.7e-4	2.8e-4	0.80506	−0.00147	−0.02384
	223.143	12.0164	0.80533	6.2e-4	1.7e-4	5.6e-3	5.6e-3	1.9e-4	2.1e-5	2.7e-3	2.7e-3	2.7e-4	2.8e-4	0.80522	−0.00146	−0.02380
	223.143	12.0104	0.80544	4.9e-4	3.3e-5	5.4e-3	5.4e-3	1.8e-4	3.6e-5	2.7e-3	2.7e-3	2.7e-4	2.8e-4	0.80536	−0.00146	−0.02381
	223.143	12.0046	0.80558	4.7e-4	3.2e-5	5.5e-3	5.5e-3	2.0e-4	3.9e-5	2.7e-3	2.7e-3	2.7e-4	2.8e-4	0.80550	−0.00146	−0.02380
	223.143	11.9989	0.80570	9.0e-4	2.2e-4	5.4e-3	5.4e-3	2.2e-4	7.5e-5	2.7e-3	2.7e-3	2.7e-4	2.8e-4	0.80563	−0.00146	−0.02375
L13	223.137	14.9391	0.73298	1.2e-3	2.7e-4	3.2e-3	3.2e-3	1.4e-4	2.3e-5	2.8e-3	2.8e-3	2.7e-4	2.9e-4	0.72512	−0.00286	−0.03207
	223.138	14.9309	0.73320	1.3e-3	3.6e-4	3.1e-3	3.1e-3	1.4e-4	1.7e-5	2.8e-3	2.8e-3	2.7e-4	2.9e-4	0.72538	−0.00286	−0.03206
	223.138	14.9227	0.73343	8.0e-4	2.7e-4	2.9e-3	3.0e-3	1.8e-4	2.6e-5	2.8e-3	2.8e-3	2.7e-4	2.9e-4	0.72564	−0.00285	−0.03203
	223.137	14.9146	0.73365	1.3e-3	3.3e-4	2.9e-3	2.9e-3	1.5e-4	1.9e-5	2.8e-3	2.8e-3	2.7e-4	2.9e-4	0.72590	−0.00285	−0.03198
	223.138	14.9066	0.73389	1.1e-3	2.0e-4	2.9e-3	2.9e-3	1.8e-4	2.8e-5	2.8e-3	2.8e-3	2.7e-4	2.9e-4	0.72616	−0.00284	−0.03195
L14	223.140	15.9750	0.69976	4.9e-4	6.6e-5	2.9e-3	2.9e-3	1.6e-4	2.6e-5	2.8e-3	2.8e-3	2.7e-4	2.9e-4	0.68920	−0.00377	−0.03772
	223.140	15.9653	0.70011	5.1e-4	3.9e-5	2.9e-3	2.9e-3	1.5e-4	1.4e-5	2.8e-3	2.8e-3	2.7e-4	2.9e-4	0.68957	−0.00376	−0.03764
	223.140	15.9554	0.70043	7.2e-4	2.7e-5	2.8e-3	2.8e-3	1.9e-4	3.2e-5	2.8e-3	2.8e-3	2.7e-4	2.9e-4	0.68994	−0.00375	−0.03753
	223.140	15.9457	0.70082	4.7e-4	3.8e-5	2.9e-3	2.9e-3	2.1e-4	5.8e-5	2.8e-3	2.8e-3	2.7e-4	2.9e-4	0.69031	−0.00374	−0.03748
	223.140	15.9358	0.70117	4.6e-4	4.4e-5	2.8e-3	2.8e-3	1.9e-4	2.3e-5	2.8e-3	2.8e-3	2.7e-4	2.9e-4	0.69067	−0.00373	−0.03741
L15	223.137	17.2137	0.64760	9.5e-4	1.6e-4	2.9e-3	2.9e-3	3.1e-4	7.1e-5	2.8e-3	2.8e-3	2.7e-4	3.1e-4	0.63566	−0.00577	−0.05066
	223.138	17.2024	0.64820	1.2e-3	3.9e-4	2.9e-3	2.9e-3	3.1e-4	7.0e-5	2.8e-3	2.8e-3	2.7e-4	3.1e-4	0.63623	−0.00574	−0.05048
	223.137	17.1910	0.64881	1.5e-3	3.4e-4	2.8e-3	2.8e-3	1.7e-4	3.6e-5	2.8e-3	2.8e-3	2.7e-4	3.1e-4	0.63681	−0.00571	−0.05029
	223.137	17.1799	0.64938	1.4e-3	3.0e-4	2.8e-3	2.8e-3	2.9e-4	1.1e-4	2.8e-3	2.8e-3	2.7e-4	3.1e-4	0.63737	−0.00569	−0.05012
	223.138	17.1687	0.64996	1.2e-3	4.8e-4	2.7e-3	2.7e-3	2.8e-4	1.1e-4	2.8e-3	2.8e-3	2.7e-4	3.1e-4	0.63793	−0.00566	−0.04991
L16	223.138	18.1797	0.57071	7.6e-4	1.3e-4	2.7e-3	2.8e-3	2.4e-4	6.0e-5	2.8e-3	2.8e-3	2.7e-4	3.6e-4	0.57516	−0.01029	−0.08178
	223.139	18.1679	0.57251	5.3e-4	1.3e-4	2.6e-3	2.6e-3	2.2e-4	7.8e-5	2.8e-3	2.8e-3	2.7e-4	3.5e-4	0.57612	−0.01018	−0.08100
	223.139	18.1560	0.57425	6.5e-4	9.5e-5	2.7e-3	2.7e-3	1.9e-4	5.6e-5	2.8e-3	2.8e-3	2.7e-4	3.5e-4	0.57708	−0.01007	−0.08023
	223.139	18.1442	0.57594	7.2e-4	1.1e-4	2.9e-3	2.9e-3	2.1e-4	4.9e-5	2.8e-3	2.8e-3	2.7e-4	3.5e-4	0.57802	−0.00996	−0.07949
	223.138	18.1323	0.57755	8.1e-4	1.6e-4	2.6e-3	2.6e-3	2.7e-4	6.7e-5	2.8e-3	2.8e-3	2.7e-4	3.5e-4	0.57897	−0.00985	−0.07876
L17	269.996	9.5887	0.86031	1.1e-3	6.0e-5	6.1e-3	6.1e-3	3.7e-4	1.7e-4	1.4e-3	1.4e-3	2.7e-4	2.8e-4	0.85917	0.00078	−0.03037
	269.996	9.5855	0.86039	1.0e-3	1.0e-4	5.6e-3	5.6e-3	3.1e-4	1.3e-4	1.4e-3	1.4e-3	2.7e-4	2.8e-4	0.85927	0.00078	−0.03036
	269.996	9.5824	0.86047	1.0e-3	1.4e-4	5.7e-3	5.7e-3	2.3e-4	9.7e-5	1.4e-3	1.4e-3	2.7e-4	2.8e-4	0.85936	0.00078	−0.03034
	269.996	9.5793	0.86050	1.2e-3	1.1e-4	5.8e-3	5.8e-3	3.6e-4	1.6e-4	1.4e-3	1.4e-3	2.7e-4	2.8e-4	0.85946	0.00079	−0.03033
	269.996	9.5761	0.86061	1.3e-3	9.4e-5	5.5e-3	5.5e-3	3.7e-4	1.8e-4	1.4e-3	1.4e-3	2.7e-4	2.8e-4	0.85955	0.00079	−0.03031
P2	298.174	6.4369	0.99999	2.1e-4	1.9e-5	1.6e-3	1.6e-3	8.5e-5	8.0e-6	1.2e-3	1.2e-3					
L18	298.157	6.7092	0.99359	5.2e-4	7.9e-5	1.4e-3	1.4e-3	1.0e-4	2.9e-5	1.1e-3	1.1e-3	2.7e-4	2.7e-4	0.99370	0.00333	−0.02357
	298.158	6.7091	0.99358	7.6e-4	1.8e-4	1.4e-3	1.4e-3	1.0e-4	9.9e-6	1.1e-3	1.1e-3	2.7e-4	2.7e-4	0.99371	0.00333	−0.02357
	298.158	6.7089	0.99359	6.7e-4	2.6e-4	1.5e-3	1.5e-3	1.1e-4	2.1e-5	1.1e-3	1.1e-3	2.7e-4	2.7e-4	0.99372	0.00333	−0.02357
	298.158	6.7087	0.99359	5.7e-4	2.2e-4	1.5e-3	1.5e-3	1.1e-4	1.3e-5	1.1e-3	1.1e-3	2.7e-4	2.7e-4	0.99372	0.00333	−0.02357
L19	298.160	6.7192	0.99334	3.8e-4	3.1e-5	1.4e-3	1.4e-3	1.3e-4	2.2e-5	1.1e-3	1.1e-3	2.7e-4	2.7e-4	0.99348	0.00333	−0.02362
	298.160	6.7193	0.99334	3.4e-4	2.9e-5	1.4e-3	1.4e-3	8.6e-4	1.5e-4	1.1e-3	1.1e-3	2.7e-4	2.7e-4	0.99347	0.00333	−0.02362
L20	298.160	7.1004	0.98384	3.7e-4	5.2e-5	1.6e-3	1.6e-3	1.1e-4	1.7e-5	1.1e-3	1.1e-3	2.7e-4	2.7e-4	0.98411	0.00331	−0.02566
	298.160	7.1001	0.98385	4.8e-4	4.9e-5	1.6e-3	1.6e-3	1.8e-4	2.7e-5	1.1e-3	1.1e-3	2.7e-4	2.7e-4	0.98411	0.00331	−0.02566
	298.161	7.1005	0.98385	5.9e-4	1.5e-4	1.5e-3	1.5e-3	6.9e-4	1.0e-4	1.1e-3	1.1e-3	2.7e-4	2.7e-4	0.98410	0.00331	−0.02566
	298.161	7.1000	0.98384	5.2e-4	1.2e-4	1.6e-3	1.6e-3	1.6e-4	1.3e-5	1.1e-3	1.1e-3	2.7e-4	2.7e-4	0.98412	0.00331	−0.02566
	298.162	7.1005	0.98384	3.4e-4	5.2e-5	1.6e-3	1.6e-3	3.6e-4	4.7e-5	1.1e-3	1.1e-3	2.7e-4	2.7e-4	0.98411	0.00331	−0.02566
L21	298.162	7.4190	0.97525	3.0e-4	1.1e-4	1.5e-3	1.5e-3	1.9e-4	4.0e-5	1.2e-3	1.2e-3	2.7e-4	2.7e-4	0.97557	0.00325	−0.02807
	298.162	7.4186	0.97526	3.1e-4	1.1e-4	1.4e-3	1.4e-3	1.9e-4	2.1e-5	1.1e-3	1.1e-3	2.7e-4	2.7e-4	0.97558	0.00325	−0.02807
	298.162	7.4197	0.97524	3.1e-4	9.8e-5	1.4e-3	1.4e-3	1.0e-3	1.1e-4	1.2e-3	1.2e-3	2.7e-4	2.7e-4	0.97555	0.00325	−0.02808
	298.162	7.4193	0.97524	2.4e-4	2.4e-5	1.4e-3	1.4e-3	4.0e-4	6.7e-5	1.2e-3	1.2e-3	2.7e-4	2.7e-4	0.97557	0.00325	−0.02808
	298.163	7.4191	0.97525	3.8e-4	4.9e-5	1.5e-3	1.5e-3	2.5e-4	3.3e-5	1.2e-3	1.2e-3	2.7e-4	2.7e-4	0.97557	0.00325	−0.02808
	298.162	7.4187	0.97525	5.7e-4	8.7e-5	1.6e-3	1.6e-3	2.1e-4	2.7e-5	1.2e-3	1.2e-3	2.7e-4	2.7e-4	0.97558	0.00325	−0.02807
L22	298.173	7.8939	0.96051	3.6e-4	3.9e-5	1.4e-3	1.4e-3	1.4e-4	3.1e-5	1.2e-3	1.2e-3	2.7e-4	2.8e-4	0.96094	0.00288	−0.03463
	298.174	7.8953	0.96050	8.9e-4	3.6e-4	1.5e-3	1.5e-3	5.0e-4	6.8e-5	1.2e-3	1.2e-3	2.7e-4	2.8e-4	0.96089	0.00288	−0.03467
	298.175	7.8947	0.96050	3.6e-4	2.8e-5	1.5e-3	1.5e-3	1.4e-4	1.6e-5	1.2e-3	1.2e-3	2.7e-4	2.8e-4	0.96092	0.00288	−0.03465
	298.175	7.8945	0.96050	3.6e-4	1.7e-5	1.5e-3	1.5e-3	1.3e-4	1.1e-5	1.2e-3	1.2e-3	2.7e-4	2.8e-4	0.96092	0.00288	−0.03465
L23	298.174	8.0782	0.95343	2.5e-4	1.7e-5	1.6e-3	1.6e-3	2.5e-4	4.2e-5	1.2e-3	1.2e-3	2.7e-4	2.8e-4	0.95414	0.00248	−0.03964
	298.174	8.0783	0.95345	2.6e-4	8.8e-5	1.6e-3	1.6e-3	2.4e-4	7.7e-5	1.2e-3	1.2e-3	2.7e-4	2.8e-4	0.95413	0.00248	−0.03965
	298.174	8.0782	0.95344	3.1e-4	5.5e-5	1.5e-3	1.5e-3	3.5e-4	5.2e-5	1.2e-3	1.2e-3	2.7e-4	2.8e-4	0.95413	0.00248	−0.03964
	298.173	8.0783	0.95344	2.5e-4	2.9e-5	1.6e-3	1.6e-3	2.9e-4	8.7e-5	1.2e-3	1.2e-3	2.7e-4	2.8e-4	0.95413	0.00248	−0.03965
L24	298.171	8.1485	0.95025	3.8e-4	9.3e-5	1.3e-3	1.3e-3	1.5e-4	1.6e-5	1.2e-3	1.2e-3	2.7e-4	2.8e-4	0.95125	0.00224	−0.04233
	298.171	8.1479	0.95028	2.9e-4	7.1e-5	1.5e-3	1.5e-3	1.7e-4	2.9e-5	1.2e-3	1.2e-3	2.7e-4	2.8e-4	0.95127	0.00224	−0.04231
	298.171	8.1471	0.95031	5.6e-4	2.1e-4	1.4e-3	1.4e-3	1.6e-4	4.2e-5	1.3e-3	1.3e-3	2.7e-4	2.8e-4	0.95131	0.00224	−0.04228
	298.171	8.1480	0.95031	4.9e-4	3.3e-5	1.4e-3	1.4e-3	1.4e-3	2.4e-4	1.2e-3	1.3e-3	2.7e-4	2.8e-4	0.95127	0.00224	−0.04232
	298.171	8.1480	0.95029	3.8e-4	4.6e-5	1.4e-3	1.4e-3	3.6e-4	4.7e-5	1.2e-3	1.2e-3	2.7e-4	2.8e-4	0.95127	0.00224	−0.04231
L25	298.173	8.1552	0.94976	4.5e-4	1.0e-4	1.4e-3	1.4e-3	1.5e-4	1.6e-5	1.2e-3	1.2e-3	2.7e-4	2.8e-4	0.95097	0.00221	−0.04263
	298.174	8.1543	0.94977	6.6e-4	1.1e-4	1.5e-3	1.5e-3	2.4e-4	3.3e-5	1.2e-3	1.2e-3	2.7e-4	2.8e-4	0.95101	0.00221	−0.04260
	298.173	8.1538	0.94976	2.5e-4	4.6e-5	1.5e-3	1.5e-3	1.9e-4	3.5e-5	1.2e-3	1.2e-3	2.7e-4	2.8e-4	0.95103	0.00222	−0.04257
L26	298.175	8.2543	0.94368	2.8e-4	5.7e-5	1.5e-3	1.5e-3	1.0e-3	2.5e-4	1.2e-3	1.2e-3	2.7e-4	2.8e-4	0.94650	0.00169	−0.04793
	298.175	8.2532	0.94366	2.2e-4	2.3e-5	1.5e-3	1.5e-3	1.8e-4	4.0e-5	1.2e-3	1.2e-3	2.7e-4	2.8e-4	0.94656	0.00170	−0.04786

(*continued on next page*)

Table B.2 (*continued*)

ID	Data			Temperature				Pressure				Composition			Composition derivatives	
	$\overline{T}$	$\overline{p}$	x_{CO_2}	$s(T)$	$s(\overline{T})$	$\overline{u}(T)$	$u_c(\overline{T})$	$s(p)$	$s(\overline{p})$	$\overline{u}(p)$	$u_c(\overline{p})$	$u(x_{CO_2})$	$u_{tot}(x_{CO_2})$	$x_{CO_2,calc}$	$\partial x_{CO_2}/\partial T$	$\partial x_{CO_2}/\partial p$
	(K)	(MPa)	(−)	(K)	(K)	(K)	(K)	(MPa)	(MPa)	(MPa)	(MPa)	(−)	(−)	(−)	(K^{-1})	(MPa^{-1})
	298.173	8.2540	0.94344	6.3e-4	1.7e-4	1.4e-3	1.5e-3	2.2e-4	4.4e-5	1.2e-3	1.2e-3	2.7e-4	2.8e-4	0.94651	0.00169	−0.04790
	298.173	8.2532	0.94353	6.0e-4	2.1e-4	1.5e-3	1.5e-3	2.1e-4	3.6e-5	1.2e-3	1.2e-3	2.7e-4	2.8e-4	0.94655	0.00170	−0.04785
	298.173	8.2526	0.94358	5.8e-4	5.7e-5	1.5e-3	1.5e-3	2.4e-4	6.3e-5	1.2e-3	1.2e-3	2.7e-4	2.8e-4	0.94658	0.00170	−0.04781
	298.174	8.2523	0.94362	4.6e-4	9.7e-5	1.5e-3	1.5e-3	1.8e-4	4.0e-5	1.2e-3	1.2e-3	2.7e-4	2.8e-4	0.94660	0.00171	−0.04779
	298.174	8.2521	0.94364	2.4e-4	1.3e-5	1.5e-3	1.5e-3	1.7e-4	3.3e-5	1.2e-3	1.2e-3	2.7e-4	2.8e-4	0.94660	0.00171	−0.04778
L27	298.173	8.2748	0.94151	4.0e-4	1.2e-4	1.4e-3	1.4e-3	2.2e-3	2.5e-4	1.3e-3	1.3e-3	2.7e-4	2.8e-4	0.94550	0.00154	−0.04938
	298.173	8.2743	0.94153	2.4e-4	7.3e-5	1.5e-3	1.5e-3	1.2e-4	2.5e-5	1.3e-3	1.3e-3	2.7e-4	2.8e-4	0.94553	0.00154	−0.04933
	298.173	8.2742	0.94155	2.1e-4	1.6e-5	1.5e-3	1.5e-3	4.8e-4	1.2e-4	1.3e-3	1.3e-3	2.7e-4	2.8e-4	0.94553	0.00154	−0.04933
	298.174	8.2743	0.94162	9.8e-4	4.3e-4	1.5e-3	1.5e-3	1.4e-4	1.8e-5	1.3e-3	1.3e-3	2.7e-4	2.8e-4	0.94553	0.00154	−0.04934
	298.175	8.2740	0.94154	9.8e-5	1.5e-5	1.5e-3	1.5e-3	2.4e-4	5.0e-5	1.2e-3	1.3e-3	2.7e-4	2.8e-4	0.94555	0.00154	−0.04932
L28	298.174	8.2862	0.94039	4.7e-4	4.0e-5	1.5e-3	1.5e-3	1.9e-4	3.0e-5	1.3e-3	1.3e-3	2.7e-4	2.8e-4	0.94494	0.00144	−0.05027
	298.174	8.2863	0.94041	1.9e-4	2.3e-5	1.5e-3	1.5e-3	1.7e-4	3.4e-5	1.3e-3	1.3e-3	2.7e-4	2.8e-4	0.94493	0.00144	−0.05027
	298.174	8.2863	0.94042	2.2e-4	2.1e-5	1.5e-3	1.5e-3	1.2e-4	1.1e-5	1.3e-3	1.3e-3	2.7e-4	2.8e-4	0.94493	0.00144	−0.05027
	298.174	8.2862	0.94042	1.8e-4	2.2e-5	1.5e-3	1.5e-3	1.1e-4	1.5e-5	1.3e-3	1.3e-3	2.7e-4	2.8e-4	0.94494	0.00144	−0.05027
	298.175	8.2863	0.94042	1.5e-4	1.5e-5	1.5e-3	1.5e-3	1.5e-4	3.9e-5	1.3e-3	1.3e-3	2.7e-4	2.8e-4	0.94493	0.00144	−0.05028
L29	298.175	8.2975	0.93795	2.6e-4	3.0e-5	1.6e-3	1.6e-3	1.9e-4	4.1e-5	1.2e-3	1.2e-3	2.7e-4	2.8e-4	0.94437	0.00134	−0.05124
	298.175	8.2972	0.93794	1.6e-4	1.1e-5	1.6e-3	1.6e-3	1.0e-4	2.7e-5	1.2e-3	1.2e-3	2.7e-4	2.8e-4	0.94438	0.00134	−0.05121
	298.175	8.2969	0.93795	1.7e-4	1.3e-5	1.6e-3	1.6e-3	1.5e-4	4.3e-5	1.2e-3	1.2e-3	2.7e-4	2.8e-4	0.94439	0.00134	−0.05119
	298.176	8.2967	0.93802	2.0e-4	1.5e-5	1.6e-3	1.6e-3	1.6e-4	1.7e-5	1.2e-3	1.2e-3	2.7e-4	2.8e-4	0.94441	0.00134	−0.05117
P3	303.158	7.2105	0.99999	3.2e-4	9.5e-6	2.0e-3	2.0e-3	1.4e-4	3.0e-5	1.1e-3	1.1e-3					
L30	303.156	7.4036	0.99451	2.6e-4	5.8e-5	1.9e-3	1.9e-3	2.1e-4	4.4e-5	1.1e-3	1.1e-3	2.7e-4	2.7e-4	0.99457	0.00440	−0.03049
	303.155	7.4035	0.99450	3.4e-4	8.4e-5	1.9e-3	1.9e-3	2.1e-4	3.6e-5	1.1e-3	1.1e-3	2.7e-4	2.7e-4	0.99457	0.00440	−0.03048
	303.156	7.4034	0.99450	2.7e-4	2.8e-5	1.9e-3	1.9e-3	1.2e-4	1.8e-5	1.1e-3	1.1e-3	2.7e-4	2.7e-4	0.99457	0.00440	−0.03048
	303.158	7.4035	0.99450	3.0e-4	4.1e-5	2.0e-3	2.0e-3	1.7e-4	2.6e-5	1.1e-3	1.1e-3	2.7e-4	2.7e-4	0.99458	0.00440	−0.03049
	303.158	7.4036	0.99451	2.1e-4	1.5e-5	2.0e-3	2.0e-3	1.0e-4	1.5e-5	1.1e-3	1.1e-3	2.7e-4	2.7e-4	0.99458	0.00440	−0.03049
L31	303.156	7.5215	0.99044	6.1e-4	1.4e-4	1.7e-3	1.7e-3	1.7e-4	3.5e-5	1.1e-3	1.1e-3	2.7e-4	2.8e-4	0.99079	0.00417	−0.03400
	303.155	7.5217	0.99043	4.6e-4	1.1e-4	1.7e-3	1.7e-3	1.8e-4	3.3e-5	1.1e-3	1.1e-3	2.7e-4	2.8e-4	0.99078	0.00417	−0.03401
	303.155	7.5216	0.99044	3.9e-4	2.1e-5	1.7e-3	1.7e-3	1.8e-4	2.9e-5	1.1e-3	1.1e-3	2.7e-4	2.8e-4	0.99078	0.00417	−0.03400
	303.154	7.5217	0.99044	2.5e-4	2.1e-5	1.7e-3	1.7e-3	1.7e-4	2.8e-5	1.1e-3	1.1e-3	2.7e-4	2.8e-4	0.99078	0.00417	−0.03401
L32	303.157	7.5344	0.98985	3.4e-4	2.2e-5	1.7e-3	1.7e-3	1.0e-4	1.2e-5	1.1e-3	1.1e-3	2.7e-4	2.8e-4	0.99035	0.00412	−0.03456
	303.157	7.5345	0.98986	3.8e-4	2.6e-5	1.7e-3	1.7e-3	1.3e-4	1.2e-5	1.1e-3	1.1e-3	2.7e-4	2.8e-4	0.99035	0.00412	−0.03456
	303.157	7.5345	0.98985	2.3e-4	1.5e-5	1.7e-3	1.7e-3	9.5e-5	7.3e-6	1.1e-3	1.1e-3	2.7e-4	2.8e-4	0.99035	0.00412	−0.03456
	303.157	7.5346	0.98984	5.0e-4	9.6e-5	1.7e-3	1.7e-3	1.3e-4	2.5e-5	1.1e-3	1.1e-3	2.7e-4	2.8e-4	0.99034	0.00412	−0.03457
L33	303.157	7.5452	0.98928	6.5e-4	5.2e-5	1.7e-3	1.7e-3	1.3e-4	2.5e-5	1.2e-3	1.2e-3	2.7e-4	2.8e-4	0.98997	0.00407	−0.03508
	303.157	7.5451	0.98928	5.0e-4	1.8e-5	1.7e-3	1.7e-3	1.4e-4	2.6e-5	1.2e-3	1.2e-3	2.7e-4	2.8e-4	0.98998	0.00407	−0.03507
	303.157	7.5452	0.98928	3.3e-4	2.9e-5	1.7e-3	1.7e-3	1.2e-4	2.2e-5	1.2e-3	1.2e-3	2.7e-4	2.8e-4	0.98998	0.00407	−0.03507
	303.157	7.5451	0.98926	4.1e-4	4.0e-5	1.7e-3	1.7e-3	1.3e-4	1.6e-5	1.2e-3	1.2e-3	2.7e-4	2.8e-4	0.98998	0.00407	−0.03507
L34	303.157	7.5531	0.98883	2.2e-4	2.2e-5	1.8e-3	1.8e-3	1.1e-4	6.7e-6	1.2e-3	1.2e-3	2.7e-4	2.8e-4	0.98970	0.00403	−0.03548
	303.157	7.5531	0.98883	4.1e-4	1.9e-5	1.8e-3	1.8e-3	1.1e-4	1.6e-5	1.2e-3	1.2e-3	2.7e-4	2.8e-4	0.98970	0.00403	−0.03548
	303.157	7.5531	0.98882	3.4e-4	3.6e-5	1.8e-3	1.8e-3	1.2e-4	1.7e-5	1.2e-3	1.2e-3	2.7e-4	2.8e-4	0.98970	0.00403	−0.03548
	303.157	7.5531	0.98883	4.3e-4	3.4e-5	1.8e-3	1.8e-3	1.2e-4	4.2e-5	1.2e-3	1.2e-3	2.7e-4	2.8e-4	0.98970	0.00403	−0.03549
	303.157	7.5532	0.98883	2.2e-4	1.9e-5	1.8e-3	1.8e-3	1.6e-4	2.2e-5	1.2e-3	1.2e-3	2.7e-4	2.8e-4	0.98969	0.00403	−0.03549
L35	303.156	7.5538	0.98893	6.5e-4	1.5e-4	1.7e-3	1.8e-3	1.2e-4	1.1e-5	1.1e-3	1.1e-3	2.7e-4	2.8e-4	0.98967	0.00403	−0.03552
	303.157	7.5539	0.98894	5.3e-4	6.4e-5	1.7e-3	1.7e-3	1.2e-4	1.3e-5	1.1e-3	1.1e-3	2.7e-4	2.8e-4	0.98967	0.00403	−0.03552
	303.157	7.5540	0.98894	4.0e-4	4.7e-5	1.7e-3	1.7e-3	1.1e-4	1.9e-5	1.1e-3	1.1e-3	2.7e-4	2.8e-4	0.98966	0.00403	−0.03553
	303.157	7.5541	0.98894	4.3e-4	3.0e-5	1.7e-3	1.7e-3	1.4e-4	1.1e-5	1.1e-3	1.1e-3	2.7e-4	2.8e-4	0.98966	0.00403	−0.03554
L36	303.157	7.5573	0.98839	4.2e-4	2.5e-5	1.7e-3	1.7e-3	9.8e-5	9.5e-6	1.1e-3	1.1e-3	2.7e-4	2.8e-4	0.98954	0.00401	−0.03572
	303.157	7.5574	0.98840	9.7e-5	1.2e-5	1.7e-3	1.7e-3	1.4e-4	2.5e-5	1.1e-3	1.1e-3	2.7e-4	2.8e-4	0.98954	0.00401	−0.03573
	303.157	7.5575	0.98841	2.0e-4	2.2e-5	1.8e-3	1.8e-3	1.1e-4	7.4e-6	1.1e-3	1.1e-3	2.7e-4	2.8e-4	0.98954	0.00401	−0.03573
	303.157	7.5576	0.98840	4.6e-4	8.0e-5	1.7e-3	1.7e-3	1.1e-4	1.0e-5	1.1e-3	1.1e-3	2.7e-4	2.8e-4	0.98954	0.00401	−0.03573
	303.158	7.5576	0.98842	4.3e-4	8.4e-5	1.8e-3	1.8e-3	1.4e-4	1.7e-5	1.1e-3	1.1e-3	2.7e-4	2.8e-4	0.98954	0.00401	−0.03574

Table B.3
Vapor phase: Experimental VLE data for $CO_2 + N_2$ at mean temperature $\overline{T}$, mean pressure $\overline{p}$, and sample liquid phase mole fraction y_{CO_2}.

ID	Data			Temperature				Pressure				Composition			Composition derivatives	
	$\overline{T}$	$\overline{p}$	y_{CO_2}	$s(T)$	$s(\overline{T})$	$\overline{u}(T)$	$u_c(\overline{T})$	$s(p)$	$s(\overline{p})$	$\overline{u}(p)$	$u_c(\overline{p})$	$u(y_{CO_2})$	$u_{tot}(y_{CO_2})$	$y_{CO_2,calc}$	$\partial y_{CO_2}/\partial T$	$\partial y_{CO_2}/\partial p$
	(K)	(MPa)	(−)	(K)	(K)	(K)	(K)	(MPa)	(MPa)	(MPa)	(MPa)	(−)	(−)	(−)	(K^{-1})	(MPa^{-1})
P1	223.138	0.6829	0.99999	5.8e-4	5.3e-5	2.5e-3	2.5e-3	1.5e-5	2.5e-6	5.0e-4	5.0e-4					
V1	223.139	1.9390	0.40681	6.1e-4	4.4e-5	2.6e-3	2.6e-3	4.3e-5	1.7e-5	5.2e-4	5.2e-4	2.7e-4	2.9e-4	0.41039	0.01519	−0.16961
	223.139	1.9383	0.40723	5.3e-4	6.6e-5	2.5e-3	2.5e-3	3.8e-5	1.5e-5	5.2e-4	5.2e-4	2.7e-4	2.9e-4	0.41050	0.01519	−0.16972
	223.139	1.9377	0.40697	6.9e-4	1.1e-4	2.5e-3	2.5e-3	3.0e-5	1.0e-5	5.2e-4	5.2e-4	2.7e-4	2.9e-4	0.41060	0.01520	−0.16983
V2	223.139	4.3569	0.23252	4.0e-4	2.1e-5	2.5e-3	2.5e-3	6.6e-5	9.1e-6	1.1e-3	1.1e-3	2.7e-4	2.8e-4	0.23389	0.00808	−0.02909
	223.139	4.3551	0.23239	4.8e-4	3.1e-5	2.6e-3	2.6e-3	5.8e-5	4.9e-6	1.1e-3	1.1e-3	2.7e-4	2.8e-4	0.23394	0.00808	−0.02912
	223.139	4.3534	0.23260	4.8e-4	5.2e-5	2.6e-3	2.6e-3	7.4e-5	1.7e-5	1.1e-3	1.1e-3	2.7e-4	2.8e-4	0.23399	0.00808	−0.02915
	223.139	4.3518	0.23256	4.3e-4	2.1e-5	2.5e-3	2.5e-3	6.4e-5	7.8e-6	1.1e-3	1.1e-3	2.7e-4	2.8e-4	0.23404	0.00809	−0.02918
	223.139	4.3502	0.23258	5.5e-4	6.3e-5	2.5e-3	2.5e-3	7.2e-5	1.8e-5	1.1e-3	1.1e-3	2.7e-4	2.8e-4	0.23408	0.00809	−0.02920
V3	223.138	4.3683	0.23235	8.3e-4	5.9e-5	2.6e-3	2.6e-3	7.5e-5	9.6e-6	1.1e-3	1.1e-3	2.7e-4	2.8e-4	0.23355	0.00806	−0.02890

(*continued on next page*)

Table B.3 (*continued*)

ID	Data			Temperature				Pressure				Composition			Composition derivatives	
	$\overline{T}$	$\overline{p}$	y_{CO_2}	$s(T)$	$s(\overline{T})$	$\overline{u}(T)$	$u_c(\overline{T})$	$s(p)$	$s(\overline{p})$	$\overline{u}(p)$	$u_c(\overline{p})$	$u(y_{CO_2})$	$u_{tot}(y_{CO_2})$	$y_{CO_2,calc}$	$\partial y_{CO_2}/\partial T$	$\partial y_{CO_2}/\partial p$
	(K)	(MPa)	(−)	(K)	(K)	(K)	(K)	(MPa)	(MPa)	(MPa)	(MPa)	(−)	(−)	(−)	(K^{-1})	(MPa^{-1})
	223.139	4.3668	0.23262	7.7e-4	2.5e-4	2.5e-3	2.6e-3	6.8e-5	1.6e-5	1.1e-3	1.1e-3	2.7e-4	2.8e-4	0.23360	0.00807	−0.02892
	223.139	4.3652	0.23248	5.6e-4	1.9e-4	2.4e-3	2.5e-3	7.7e-5	2.5e-5	1.1e-3	1.1e-3	2.7e-4	2.8e-4	0.23365	0.00807	−0.02895
	223.138	4.3637	0.23228	5.9e-4	3.2e-5	2.5e-3	2.5e-3	8.7e-5	2.2e-5	1.1e-3	1.1e-3	2.7e-4	2.8e-4	0.23368	0.00807	−0.02898
	223.139	4.3622	0.23224	5.7e-4	1.3e-4	2.5e-3	2.5e-3	7.3e-5	1.1e-5	1.1e-3	1.1e-3	2.7e-4	2.8e-4	0.23373	0.00807	−0.02900
V4	223.139	5.0396	0.21776	4.3e-4	3.5e-5	3.4e-3	3.4e-3	7.6e-5	2.0e-5	1.1e-3	1.1e-3	2.7e-4	2.7e-4	0.21741	0.00732	−0.01979
	223.139	5.0378	0.21786	4.1e-4	4.2e-5	3.4e-3	3.4e-3	7.3e-5	1.6e-5	1.1e-3	1.1e-3	2.7e-4	2.7e-4	0.21745	0.00732	−0.01981
	223.139	5.0360	0.21793	4.2e-4	4.6e-5	3.5e-3	3.5e-3	8.5e-5	2.8e-5	1.1e-3	1.1e-3	2.7e-4	2.7e-4	0.21749	0.00733	−0.01983
V5	223.141	6.0871	0.20170	8.9e-4	2.5e-4	5.3e-3	5.3e-3	1.3e-4	4.5e-5	1.1e-3	1.1e-3	2.7e-4	2.8e-4	0.20183	0.00652	−0.01073
	223.141	6.0835	0.20179	9.4e-4	2.6e-4	4.9e-3	4.9e-3	1.6e-4	6.6e-5	1.1e-3	1.1e-3	2.7e-4	2.7e-4	0.20187	0.00652	−0.01075
V6	223.140	7.0153	0.19315	1.2e-3	3.5e-4	4.8e-3	4.8e-3	1.9e-4	7.9e-5	1.1e-3	1.2e-3	2.7e-4	2.7e-4	0.19446	0.00604	−0.00543
	223.139	7.0072	0.19323	1.8e-3	3.6e-4	4.9e-3	4.9e-3	2.0e-1	3.1e-3	1.1e-3	3.3e-3	2.7e-4	2.7e-4	0.19450	0.00604	−0.00547
	223.139	7.0108	0.19318	1.8e-3	3.2e-4	5.0e-3	5.0e-3	1.5e-4	5.6e-5	1.1e-3	1.1e-3	2.7e-4	2.7e-4	0.19448	0.00604	−0.00545
	223.140	7.0087	0.19365	1.3e-3	4.7e-4	4.7e-3	4.7e-3	1.9e-4	8.0e-5	1.1e-3	1.2e-3	2.7e-4	2.7e-4	0.19450	0.00604	−0.00546
	223.139	7.0065	0.19311	1.6e-3	3.7e-4	4.9e-3	4.9e-3	1.3e-4	4.4e-5	1.1e-3	1.1e-3	2.7e-4	2.7e-4	0.19451	0.00605	−0.00547
V7	223.141	8.1033	0.18991	6.3e-4	3.1e-5	5.6e-3	5.6e-3	1.3e-4	1.1e-5	1.2e-3	1.2e-3	2.7e-4	2.7e-4	0.19118	0.00565	−0.00083
	223.141	8.1011	0.18977	7.7e-4	5.3e-5	5.8e-3	5.8e-3	1.4e-4	3.3e-5	1.2e-3	1.2e-3	2.7e-4	2.7e-4	0.19118	0.00565	−0.00084
	223.141	8.0989	0.18972	6.3e-4	8.1e-5	5.7e-3	5.7e-3	1.5e-4	3.6e-5	1.2e-3	1.2e-3	2.7e-4	2.7e-4	0.19118	0.00565	−0.00085
	223.141	8.0967	0.18957	1.0e-3	1.2e-4	5.8e-3	5.8e-3	1.5e-4	2.6e-5	1.2e-3	1.2e-3	2.7e-4	2.7e-4	0.19118	0.00566	−0.00086
	223.141	8.0947	0.18956	1.0e-3	1.0e-4	5.8e-3	5.8e-3	1.5e-4	3.2e-5	1.2e-3	1.2e-3	2.7e-4	2.7e-4	0.19118	0.00566	−0.00086
V8	223.141	8.4451	0.18984	4.3e-4	1.7e-5	3.6e-3	3.6e-3	1.2e-4	9.8e-6	1.3e-3	1.3e-3	2.7e-4	2.7e-4	0.19110	0.00556	0.00040
	223.141	8.4427	0.18977	5.5e-4	1.1e-4	3.6e-3	3.6e-3	1.4e-4	1.3e-5	1.3e-3	1.3e-3	2.7e-4	2.7e-4	0.19110	0.00556	0.00039
	223.141	8.4402	0.18983	5.6e-4	4.3e-5	3.6e-3	3.6e-3	1.3e-4	2.9e-5	1.3e-3	1.3e-3	2.7e-4	2.7e-4	0.19110	0.00556	0.00038
	223.142	8.4378	0.18980	5.3e-4	5.5e-5	3.6e-3	3.6e-3	1.0e-4	1.6e-5	1.3e-3	1.3e-3	2.7e-4	2.7e-4	0.19111	0.00556	0.00037
	223.142	8.4354	0.18981	4.9e-4	3.7e-5	3.6e-3	3.6e-3	1.1e-4	1.5e-5	1.3e-3	1.3e-3	2.7e-4	2.7e-4	0.19111	0.00556	0.00036
V9	223.143	8.6114	0.18970	1.4e-3	3.7e-4	4.2e-3	4.2e-3	1.8e-4	4.1e-5	1.3e-3	1.3e-3	2.7e-4	2.7e-4	0.19123	0.00552	0.00097
	223.142	8.6090	0.18970	1.2e-3	4.8e-4	4.1e-3	4.1e-3	1.5e-4	5.3e-5	1.3e-3	1.3e-3	2.7e-4	2.7e-4	0.19122	0.00552	0.00097
	223.142	8.6068	0.18989	9.8e-4	2.0e-4	4.1e-3	4.1e-3	1.2e-4	2.9e-5	1.3e-3	1.3e-3	2.7e-4	2.7e-4	0.19122	0.00552	0.00096
	223.141	8.6045	0.18990	1.6e-3	2.0e-4	4.2e-3	4.2e-3	1.2e-4	1.4e-5	1.3e-3	1.3e-3	2.7e-4	2.7e-4	0.19121	0.00552	0.00095
V10	223.140	9.1958	0.19076	8.5e-4	1.0e-4	5.4e-3	5.4e-3	2.6e-4	9.4e-5	1.4e-3	1.4e-3	2.7e-4	2.7e-4	0.19235	0.00540	0.00290
	223.140	9.1939	0.19077	8.9e-4	2.0e-4	5.6e-3	5.6e-3	2.2e-4	8.5e-5	1.4e-3	1.4e-3	2.7e-4	2.7e-4	0.19234	0.00540	0.00289
	223.140	9.1920	0.19071	1.3e-3	2.4e-4	5.3e-3	5.3e-3	3.0e-4	1.3e-4	1.4e-3	1.4e-3	2.7e-4	2.7e-4	0.19234	0.00540	0.00289
	223.141	9.1902	0.19061	1.0e-3	1.9e-4	5.4e-3	5.4e-3	2.6e-4	1.1e-4	1.4e-3	1.4e-3	2.7e-4	2.7e-4	0.19234	0.00540	0.00288
	223.141	9.1883	0.19059	6.0e-4	5.0e-5	5.3e-3	5.3e-3	2.3e-4	8.8e-5	1.4e-3	1.4e-3	2.7e-4	2.7e-4	0.19233	0.00540	0.00287
V11	223.141	9.8106	0.19262	6.0e-4	1.1e-4	5.4e-3	5.4e-3	1.0e-4	2.8e-5	2.6e-3	2.6e-3	2.7e-4	2.7e-4	0.19473	0.00530	0.00481
	223.141	9.8078	0.19301	6.1e-4	7.1e-5	5.3e-3	5.3e-3	1.4e-4	3.3e-5	2.6e-3	2.6e-3	2.7e-4	2.7e-4	0.19472	0.00530	0.00480
	223.141	9.8050	0.19280	4.2e-4	3.3e-5	5.1e-3	5.1e-3	1.4e-4	4.0e-5	2.6e-3	2.6e-3	2.7e-4	2.7e-4	0.19471	0.00530	0.00479
	223.141	9.8022	0.19276	7.1e-4	5.7e-5	5.1e-3	5.1e-3	1.2e-4	2.3e-5	2.6e-3	2.6e-3	2.7e-4	2.7e-4	0.19469	0.00530	0.00479
	223.141	9.7995	0.19294	5.9e-4	6.2e-5	5.3e-3	5.3e-3	1.4e-4	4.4e-5	2.6e-3	2.6e-3	2.7e-4	2.7e-4	0.19468	0.00530	0.00478
V12	223.139	10.8727	0.20008	7.2e-4	1.8e-4	3.2e-3	3.2e-3	1.4e-4	2.5e-5	2.7e-3	2.7e-3	2.7e-4	2.7e-4	0.20154	0.00519	0.00802
	223.139	10.8693	0.19989	1.0e-3	2.7e-4	3.2e-3	3.2e-3	1.3e-4	3.7e-5	2.7e-3	2.7e-3	2.7e-4	2.7e-4	0.20151	0.00519	0.00801
	223.138	10.8661	0.19973	1.1e-3	1.4e-4	3.2e-3	3.2e-3	1.6e-4	3.1e-5	2.7e-3	2.7e-3	2.7e-4	2.7e-4	0.20148	0.00519	0.00800
V13	223.142	11.9841	0.20903	8.7e-4	2.1e-4	4.7e-3	4.7e-3	3.7e-4	1.3e-4	2.7e-3	2.7e-3	2.7e-4	2.8e-4	0.21237	0.00516	0.01149
	223.141	11.9814	0.20890	1.1e-3	1.7e-4	5.0e-3	5.0e-3	3.5e-4	1.4e-4	2.7e-3	2.7e-3	2.7e-4	2.8e-4	0.21234	0.00516	0.01148
	223.140	11.9761	0.20861	1.5e-3	2.9e-4	5.3e-3	5.3e-3	4.1e-4	1.4e-4	2.7e-3	2.7e-3	2.7e-4	2.8e-4	0.21228	0.00516	0.01147
	223.140	11.9733	0.20870	1.2e-3	2.5e-4	5.1e-3	5.1e-3	4.0e-4	1.6e-4	2.7e-3	2.7e-3	2.7e-4	2.8e-4	0.21224	0.00516	0.01146
V14	223.136	14.9794	0.25628	1.6e-3	3.4e-4	3.2e-3	3.2e-3	1.2e-4	9.3e-6	2.8e-3	2.8e-3	2.7e-4	2.8e-4	0.26355	0.00568	0.02379
	223.138	14.9746	0.25617	8.8e-4	2.1e-4	3.0e-3	3.0e-3	1.3e-4	2.4e-5	2.8e-3	2.8e-3	2.7e-4	2.8e-4	0.26345	0.00568	0.02376
	223.138	14.9699	0.25704	1.1e-3	2.4e-4	2.9e-3	2.9e-3	1.7e-4	3.4e-5	2.8e-3	2.8e-3	2.7e-4	2.8e-4	0.26334	0.00568	0.02373
	223.138	14.9652	0.25728	9.4e-4	1.7e-4	2.9e-3	2.9e-3	1.4e-4	2.0e-5	2.8e-3	2.8e-3	2.7e-4	2.8e-4	0.26323	0.00568	0.02371
	223.138	14.9605	0.25740	1.3e-3	2.4e-4	3.0e-3	3.0e-3	1.2e-4	1.2e-5	2.8e-3	2.8e-3	2.7e-4	2.8e-4	0.26311	0.00567	0.02368
V15	223.137	16.0198	0.28550	9.7e-4	2.5e-4	2.8e-3	2.8e-3	1.7e-4	2.2e-5	2.8e-3	2.8e-3	2.7e-4	2.9e-4	0.29163	0.00629	0.03059
	223.138	16.0148	0.28524	7.5e-4	1.2e-4	2.8e-3	2.8e-3	2.1e-4	4.5e-5	2.8e-3	2.8e-3	2.7e-4	2.9e-4	0.29148	0.00628	0.03056
	223.137	16.0098	0.28512	1.0e-3	3.1e-4	2.7e-3	2.7e-3	2.0e-4	5.6e-5	2.8e-3	2.8e-3	2.7e-4	2.9e-4	0.29133	0.00628	0.03051
	223.138	16.0048	0.28489	1.0e-3	3.2e-4	2.8e-3	2.8e-3	1.8e-4	2.9e-5	2.8e-3	2.8e-3	2.7e-4	2.9e-4	0.29118	0.00627	0.03048
	223.138	16.0000	0.28458	8.9e-4	2.0e-4	3.0e-3	3.0e-3	1.9e-4	6.8e-5	2.8e-3	2.8e-3	2.7e-4	2.9e-4	0.29103	0.00627	0.03044
V16	223.139	17.2601	0.33191	1.1e-3	2.8e-4	3.0e-3	3.0e-3	4.0e-4	1.4e-4	2.8e-3	2.8e-3	2.7e-4	3.0e-4	0.33739	0.00794	0.04523
	223.138	17.2552	0.33174	1.5e-3	3.4e-4	2.8e-3	2.8e-3	4.9e-4	2.0e-4	2.8e-3	2.8e-3	2.7e-4	3.0e-4	0.33717	0.00793	0.04514
	223.138	17.2520	0.33148	1.2e-3	3.1e-4	2.8e-3	2.9e-3	2.3e-4	6.8e-5	2.8e-3	2.8e-3	2.7e-4	3.0e-4	0.33702	0.00792	0.04508
	223.139	17.2465	0.33121	1.2e-3	3.2e-4	2.8e-3	2.8e-3	1.5e-4	1.7e-5	2.8e-3	2.8e-3	2.7e-4	3.0e-4	0.33678	0.00791	0.04498
	223.139	17.2414	0.33105	8.2e-4	8.2e-5	2.8e-3	2.8e-3	2.6e-4	5.1e-5	2.8e-3	2.8e-3	2.7e-4	3.0e-4	0.33655	0.00790	0.04488
V17	223.138	18.2267	0.41654	1.0e-3	2.6e-4	2.8e-3	2.8e-3	3.0e-4	5.9e-5	2.8e-3	2.8e-3	2.7e-4	3.6e-4	0.39455	0.01284	0.08223
	223.138	18.2220	0.41566	1.1e-3	2.0e-4	2.6e-3	2.6e-3	2.7e-4	1.2e-4	2.8e-3	2.8e-3	2.7e-4	3.6e-4	0.39416	0.01279	0.08185
	223.138	18.2172	0.41477	1.3e-3	3.1e-4	2.7e-3	2.7e-3	2.3e-4	4.5e-5	2.8e-3	2.8e-3	2.7e-4	3.6e-4	0.39377	0.01273	0.08146
	223.138	18.2126	0.41396	9.5e-4	2.0e-4	2.8e-3	2.8e-3	2.0e-4	6.3e-5	2.8e-3	2.8e-3	2.7e-4	3.6e-4	0.39340	0.01268	0.08108
	223.138	18.2080	0.41307	1.1e-3	1.7e-4	2.8e-3	2.8e-3	2.2e-4	3.2e-5	2.8e-3	2.8e-3	2.7e-4	3.5e-4	0.39302	0.01263	0.08065
V18	269.997	9.5760	0.58157	1.2e-3	8.0e-5	5.0e-3	5.0e-3	6.6e-4	3.2e-4	1.4e-3	1.4e-3	2.7e-4	2.8e-4	0.58456	0.01120	−0.00414
	269.997	9.5703	0.58194	8.8e-4	3.4e-5	4.8e-3	4.8e-3	8.6e-4	4.3e-4	1.4e-3	1.5e-3	2.7e-4	2.8e-4	0.58459	0.01120	−0.00421
	269.997	9.5647	0.58216	1.0e-3	1.0e-4	4.6e-3	4.6e-3	6.6e-4	3.1e-4	1.4e-3	1.4e-3	2.7e-4	2.8e-4	0.58462	0.01120	−0.00428
	269.997	9.5595	0.58144	9.8e-4	9.4e-5	4.7e-3	4.7e-3	7.0e-4	3.4e-4	1.4e-3	1.4e-3	2.7e-4	2.8e-4	0.58464	0.01120	−0.00434
	269.997	9.5541	0.58112	8.9e-4	3.8e-5	4.8e-3	4.8e-3	6.8e-4	3.3e-4	1.4e-3	1.4e-3	2.7e-4	2.8e-4	0.58466	0.01120	−0.00440
	269.997	9.5491	0.58109	9.7e-4	8.1e-5	4.7e-3	4.7e-3	5.9e-4	2.8e-4	1.4e-3	1.4e-3	2.7e-4	2.8e-4	0.58468	0.01120	−0.00446

(*continued on next page*)

Table B.3 (*continued*)

ID	Data			Temperature				Pressure				Composition			Composition derivatives	
	$\overline{T}$	$\overline{p}$	y_{CO_2}	$s(T)$	$s(\overline{T})$	$\overline{u}(T)$	$u_c(\overline{T})$	$s(p)$	$s(\overline{p})$	$\overline{u}(p)$	$u_c(\overline{p})$	$u(y_{CO_2})$	$u_{tot}(y_{CO_2})$	$y_{CO_2,calc}$	$\partial y_{CO_2}/\partial T$	$\partial y_{CO_2}/\partial p$
	(K)	(MPa)	(−)	(K)	(K)	(K)	(K)	(MPa)	(MPa)	(MPa)	(MPa)	(−)	(−)	(−)	(K^{-1})	(MPa^{-1})
	269.997	9.5440	0.58106	1.0e-3	8.7e-5	4.8e-3	4.8e-3	6.1e-4	3.0e-4	1.4e-3	1.4e-3	2.7e-4	2.8e-4	0.58470	0.01120	−0.00453
	269.997	9.5393	0.58315	8.9e-4	7.6e-5	4.7e-3	4.7e-3	6.0e-4	2.8e-4	1.4e-3	1.4e-3	2.7e-4	2.8e-4	0.58473	0.01120	−0.00458
V19	269.995	9.5912	0.58057	1.4e-3	7.1e-5	6.1e-3	6.1e-3	2.5e-4	9.8e-5	1.4e-3	1.4e-3	2.7e-4	2.8e-4	0.58449	0.01121	−0.00396
	269.996	9.5876	0.58046	1.2e-3	9.9e-5	5.7e-3	5.7e-3	2.8e-4	1.1e-4	1.4e-3	1.4e-3	2.7e-4	2.8e-4	0.58451	0.01120	−0.00400
	269.996	9.5840	0.58169	1.3e-3	6.1e-5	6.3e-3	6.3e-3	3.7e-4	1.7e-4	1.4e-3	1.4e-3	2.7e-4	2.8e-4	0.58452	0.01120	−0.00404
	269.995	9.5802	0.58124	9.5e-4	7.8e-5	6.0e-3	6.0e-3	3.6e-4	1.7e-4	1.4e-3	1.4e-3	2.7e-4	2.8e-4	0.58453	0.01120	−0.00409
	269.996	9.5766	0.58080	1.0e-3	1.1e-4	5.7e-3	5.7e-3	2.9e-4	1.3e-4	1.4e-3	1.4e-3	2.7e-4	2.8e-4	0.58455	0.01120	−0.00413
P2	298.174	6.4369	0.99999	2.1e-4	1.9e-5	1.6e-3	1.6e-3	8.5e-5	8.0e-6	1.2e-3	1.2e-3					
V20	298.159	6.7086	0.98156	2.0e-4	1.9e-5	1.5e-3	1.5e-3	1.1e-4	2.1e-5	1.1e-3	1.1e-3	2.7e-4	2.8e-4	0.98182	0.01031	−0.06269
	298.159	6.7089	0.98206	4.4e-4	4.0e-5	1.5e-3	1.5e-3	1.1e-4	3.1e-5	1.1e-3	1.1e-3	2.7e-4	2.8e-4	0.98180	0.01031	−0.06269
	298.159	6.7088	0.98205	6.8e-4	4.1e-5	1.5e-3	1.5e-3	1.3e-4	3.6e-5	1.1e-3	1.1e-3	2.7e-4	2.8e-4	0.98181	0.01031	−0.06269
	298.159	6.7090	0.98161	4.3e-4	2.4e-5	1.5e-3	1.5e-3	1.4e-4	2.8e-5	1.1e-3	1.1e-3	2.7e-4	2.8e-4	0.98180	0.01031	−0.06268
	298.159	6.7090	0.98197	3.2e-4	4.8e-5	1.5e-3	1.5e-3	1.1e-4	1.8e-5	1.1e-3	1.1e-3	2.7e-4	2.8e-4	0.98180	0.01031	−0.06268
	298.159	6.7088	0.98153	3.5e-4	1.7e-5	1.5e-3	1.5e-3	1.1e-4	1.6e-5	1.1e-3	1.1e-3	2.7e-4	2.8e-4	0.98181	0.01031	−0.06269
	298.159	6.7088	0.98142	3.1e-4	4.0e-5	1.5e-3	1.5e-3	1.1e-4	2.4e-5	1.1e-3	1.1e-3	2.7e-4	2.8e-4	0.98181	0.01031	−0.06269
	298.159	6.7087	0.98170	1.9e-4	1.5e-5	1.5e-3	1.5e-3	1.1e-4	2.6e-5	1.1e-3	1.1e-3	2.7e-4	2.8e-4	0.98182	0.01031	−0.06269
V21	298.158	6.7192	0.98099	3.4e-4	6.7e-5	1.5e-3	1.5e-3	2.1e-4	8.6e-5	1.1e-3	1.1e-3	2.7e-4	2.8e-4	0.98114	0.01030	−0.06240
	298.158	6.7190	0.98096	3.7e-4	5.0e-5	1.5e-3	1.5e-3	2.4e-4	1.0e-4	1.1e-3	1.1e-3	2.7e-4	2.8e-4	0.98116	0.01030	−0.06240
	298.158	6.7196	0.98098	4.0e-4	8.2e-5	1.4e-3	1.4e-3	1.2e-4	4.9e-5	1.1e-3	1.1e-3	2.7e-4	2.8e-4	0.98112	0.01030	−0.06238
	298.158	6.7197	0.98095	2.3e-4	2.7e-5	1.5e-3	1.5e-3	8.4e-5	7.4e-6	1.1e-3	1.1e-3	2.7e-4	2.8e-4	0.98112	0.01030	−0.06238
	298.158	6.7195	0.98097	1.8e-4	3.6e-5	1.5e-3	1.5e-3	7.9e-5	6.4e-6	1.1e-3	1.1e-3	2.7e-4	2.8e-4	0.98113	0.01030	−0.06239
V22	298.162	7.0988	0.95950	3.9e-4	5.4e-5	1.6e-3	1.6e-3	2.3e-4	8.3e-5	1.2e-3	1.2e-3	2.7e-4	2.8e-4	0.95950	0.01014	−0.05193
	298.162	7.0989	0.95953	4.3e-4	4.1e-5	1.4e-3	1.4e-3	1.1e-4	1.3e-5	1.1e-3	1.1e-3	2.7e-4	2.8e-4	0.95949	0.01014	−0.05193
V23	298.162	7.4165	0.94445	3.8e-4	2.7e-5	1.4e-3	1.4e-3	2.2e-4	6.1e-5	1.1e-3	1.1e-3	2.7e-4	2.8e-4	0.94438	0.01006	−0.04314
	298.161	7.4163	0.94444	3.8e-4	4.8e-5	1.3e-3	1.3e-3	1.7e-4	1.2e-5	1.1e-3	1.1e-3	2.7e-4	2.8e-4	0.94438	0.01006	−0.04315
	298.161	7.4161	0.94432	3.9e-4	2.2e-5	1.5e-3	1.5e-3	1.9e-4	1.5e-5	1.1e-3	1.1e-3	2.7e-4	2.8e-4	0.94440	0.01006	−0.04315
	298.162	7.4160	0.94421	1.7e-4	3.1e-5	1.5e-3	1.5e-3	1.9e-4	2.6e-5	1.1e-3	1.1e-3	2.7e-4	2.8e-4	0.94440	0.01006	−0.04316
V24	298.162	7.4185	0.94444	4.7e-4	9.0e-5	1.4e-3	1.4e-3	2.9e-4	2.5e-5	1.1e-3	1.1e-3	2.7e-4	2.8e-4	0.94430	0.01006	−0.04308
	298.163	7.4179	0.94414	3.1e-4	3.2e-5	1.6e-3	1.6e-3	2.1e-4	5.2e-5	1.1e-3	1.1e-3	2.7e-4	2.8e-4	0.94434	0.01006	−0.04310
	298.163	7.4182	0.94441	3.0e-4	1.3e-5	1.4e-3	1.4e-3	6.4e-4	1.4e-4	1.1e-3	1.1e-3	2.7e-4	2.8e-4	0.94433	0.01006	−0.04310
	298.163	7.4183	0.94437	3.4e-4	5.8e-5	1.5e-3	1.5e-3	6.4e-4	1.2e-4	1.1e-3	1.1e-3	2.7e-4	2.8e-4	0.94432	0.01006	−0.04309
	298.163	7.4175	0.94443	1.1e-4	1.4e-5	1.5e-3	1.5e-3	2.3e-4	7.0e-5	1.1e-3	1.1e-3	2.7e-4	2.8e-4	0.94435	0.01006	−0.04311
	298.163	7.4169	0.94439	1.5e-4	1.9e-5	1.5e-3	1.5e-3	1.7e-4	2.3e-5	1.1e-3	1.1e-3	2.7e-4	2.8e-4	0.94438	0.01006	−0.04313
	298.163	7.4165	0.94429	3.4e-4	3.0e-5	1.5e-3	1.5e-3	1.9e-4	5.3e-5	1.1e-3	1.2e-3	2.7e-4	2.8e-4	0.94440	0.01006	−0.04314
	298.163	7.4163	0.94423	2.4e-4	1.3e-5	1.5e-3	1.5e-3	1.6e-4	3.6e-5	1.2e-3	1.2e-3	2.7e-4	2.8e-4	0.94441	0.01006	−0.04315
V25	298.175	7.8941	0.92785	3.3e-4	4.1e-5	1.5e-3	1.5e-3	1.8e-4	3.3e-5	1.2e-3	1.2e-3	2.7e-4	2.8e-4	0.92734	0.01019	−0.02817
	298.175	7.8939	0.92790	2.7e-4	2.8e-5	1.4e-3	1.4e-3	1.3e-4	2.1e-5	1.2e-3	1.2e-3	2.7e-4	2.8e-4	0.92735	0.01019	−0.02818
	298.175	7.8937	0.92788	3.8e-4	3.0e-5	1.5e-3	1.5e-3	1.5e-4	2.3e-5	1.2e-3	1.2e-3	2.7e-4	2.8e-4	0.92735	0.01019	−0.02819
	298.175	7.8935	0.92785	2.5e-4	1.9e-5	1.5e-3	1.5e-3	1.3e-4	2.1e-5	1.2e-3	1.2e-3	2.7e-4	2.8e-4	0.92736	0.01019	−0.02820
	298.175	7.8934	0.92797	3.4e-4	3.7e-5	1.5e-3	1.5e-3	1.4e-4	3.1e-5	1.2e-3	1.2e-3	2.7e-4	2.8e-4	0.92736	0.01019	−0.02821
	298.175	7.8932	0.92798	2.1e-4	3.5e-5	1.5e-3	1.5e-3	1.3e-4	2.1e-5	1.2e-3	1.2e-3	2.7e-4	2.8e-4	0.92736	0.01019	−0.02821
	298.175	7.8930	0.92803	1.9e-4	4.0e-5	1.5e-3	1.5e-3	1.7e-4	2.9e-5	1.2e-3	1.2e-3	2.7e-4	2.8e-4	0.92737	0.01019	−0.02821
	298.175	7.8928	0.92790	1.8e-4	1.2e-5	1.5e-3	1.5e-3	1.5e-4	4.8e-5	1.2e-3	1.2e-3	2.7e-4	2.8e-4	0.92738	0.01019	−0.02822
V26	298.174	8.0737	0.92445	2.7e-4	9.9e-5	1.6e-3	1.6e-3	1.7e-4	4.1e-5	1.2e-3	1.2e-3	2.7e-4	2.7e-4	0.92290	0.01046	−0.02074
	298.174	8.0731	0.92481	2.5e-4	1.6e-5	1.6e-3	1.6e-3	1.4e-4	5.0e-5	1.2e-3	1.2e-3	2.7e-4	2.7e-4	0.92292	0.01046	−0.02077
	298.174	8.0728	0.92463	2.0e-4	2.4e-5	1.6e-3	1.6e-3	1.6e-4	2.4e-5	1.2e-3	1.2e-3	2.7e-4	2.7e-4	0.92292	0.01046	−0.02079
	298.174	8.0726	0.92468	1.6e-4	1.5e-5	1.6e-3	1.6e-3	1.7e-4	4.6e-5	1.2e-3	1.2e-3	2.7e-4	2.7e-4	0.92293	0.01046	−0.02080
	298.174	8.0722	0.92466	1.8e-4	4.8e-5	1.6e-3	1.6e-3	1.6e-4	2.9e-5	1.2e-3	1.2e-3	2.7e-4	2.7e-4	0.92294	0.01046	−0.02082
	298.174	8.0718	0.92466	1.7e-4	4.9e-5	1.6e-3	1.6e-3	1.3e-4	2.6e-5	1.2e-3	1.2e-3	2.7e-4	2.7e-4	0.92294	0.01045	−0.02084
	298.174	8.0715	0.92473	1.7e-4	1.5e-5	1.6e-3	1.6e-3	1.9e-4	6.2e-5	1.2e-3	1.2e-3	2.7e-4	2.7e-4	0.92295	0.01045	−0.02085
	298.174	8.0712	0.92477	2.5e-4	7.7e-5	1.6e-3	1.6e-3	1.7e-4	2.1e-5	1.3e-3	1.3e-3	2.7e-4	2.7e-4	0.92295	0.01045	−0.02087
V27	298.168	8.1437	0.92479	2.5e-4	2.3e-5	1.4e-3	1.4e-3	2.3e-4	4.5e-5	1.2e-3	1.2e-3	2.7e-4	2.7e-4	0.92152	0.01065	−0.01708
	298.168	8.1436	0.92480	1.9e-4	5.1e-5	1.4e-3	1.4e-3	2.1e-4	3.0e-5	1.2e-3	1.2e-3	2.7e-4	2.7e-4	0.92152	0.01065	−0.01709
	298.168	8.1435	0.92459	2.7e-4	2.4e-5	1.4e-3	1.4e-3	2.2e-4	4.6e-5	1.2e-3	1.2e-3	2.7e-4	2.7e-4	0.92152	0.01065	−0.01709
	298.168	8.1434	0.92462	2.0e-4	7.0e-5	1.5e-3	1.5e-3	1.5e-4	5.9e-6	1.2e-3	1.2e-3	2.7e-4	2.7e-4	0.92152	0.01065	−0.01710
	298.170	8.1433	0.92433	6.2e-4	1.5e-4	1.6e-3	1.6e-3	1.7e-4	1.9e-5	1.2e-3	1.2e-3	2.7e-4	2.7e-4	0.92154	0.01065	−0.01710
	298.170	8.1432	0.92459	2.5e-4	2.2e-5	1.4e-3	1.4e-3	1.9e-4	2.7e-5	1.2e-3	1.2e-3	2.7e-4	2.7e-4	0.92154	0.01065	−0.01711
	298.170	8.1432	0.92458	2.1e-4	3.9e-5	1.5e-3	1.5e-3	1.8e-4	1.8e-5	1.2e-3	1.2e-3	2.7e-4	2.7e-4	0.92154	0.01065	−0.01711
	298.170	8.1431	0.92462	1.9e-4	2.2e-5	1.5e-3	1.5e-3	1.6e-4	1.3e-5	1.2e-3	1.2e-3	2.7e-4	2.7e-4	0.92154	0.01065	−0.01711
V28	298.174	8.2531	0.92624	3.3e-4	1.3e-4	1.5e-3	1.5e-3	1.1e-4	2.3e-5	1.2e-3	1.2e-3	2.7e-4	2.7e-4	0.92010	0.01121	−0.00920
	298.173	8.2530	0.92622	2.7e-4	3.1e-5	1.4e-3	1.4e-3	1.1e-4	1.3e-5	1.2e-3	1.2e-3	2.7e-4	2.7e-4	0.92010	0.01121	−0.00918
	298.173	8.2527	0.92606	2.8e-4	7.4e-5	1.5e-3	1.5e-3	1.3e-4	2.0e-5	1.2e-3	1.2e-3	2.7e-4	2.7e-4	0.92010	0.01121	−0.00922
	298.173	8.2526	0.92617	1.8e-4	2.2e-5	1.5e-3	1.5e-3	1.6e-4	2.1e-5	1.2e-3	1.2e-3	2.7e-4	2.7e-4	0.92011	0.01121	−0.00923
	298.173	8.2524	0.92608	2.9e-4	5.8e-5	1.5e-3	1.5e-3	2.0e-4	5.6e-5	1.2e-3	1.2e-3	2.7e-4	2.7e-4	0.92011	0.01121	−0.00925
	298.174	8.2522	0.92598	2.2e-4	7.2e-5	1.5e-3	1.5e-3	1.8e-4	2.6e-5	1.2e-3	1.2e-3	2.7e-4	2.7e-4	0.92011	0.01120	−0.00924
	298.174	8.2521	0.92596	2.1e-4	5.1e-5	1.5e-3	1.5e-3	2.0e-4	3.2e-5	1.2e-3	1.2e-3	2.7e-4	2.7e-4	0.92011	0.01120	−0.00929
V29	298.174	8.2725	0.92711	2.7e-4	1.7e-5	1.5e-3	1.5e-3	2.2e-4	4.0e-5	1.2e-3	1.2e-3	2.7e-4	2.7e-4	0.91994	0.01137	−0.00730
	298.174	8.2722	0.92672	2.8e-4	2.1e-5	1.5e-3	1.5e-3	2.1e-4	3.1e-5	1.2e-3	1.2e-3	2.7e-4	2.7e-4	0.91994	0.01137	−0.00732
	298.174	8.2722	0.92707	3.7e-4	2.9e-5	1.5e-3	1.5e-3	2.1e-4	6.1e-5	1.2e-3	1.2e-3	2.7e-4	2.7e-4	0.91995	0.01137	−0.00737
	298.174	8.2721	0.92706	3.2e-4	4.2e-5	1.4e-3	1.4e-3	1.6e-4	2.6e-5	1.2e-3	1.2e-3	2.7e-4	2.7e-4	0.91995	0.01137	−0.00734
	298.174	8.2719	0.92663	3.0e-4	4.5e-5	1.5e-3	1.5e-3	2.0e-4	2.6e-5	1.2e-3	1.2e-3	2.7e-4	2.7e-4	0.91995	0.01137	−0.00734
	298.174	8.2719	0.92704	6.2e-4	2.4e-4	1.5e-3	1.5e-3	1.5e-4	1.8e-5	1.2e-3	1.2e-3	2.7e-4	2.7e-4	0.91995	0.01137	−0.00733
V30	298.175	8.2865	0.92749	1.4e-4	1.5e-5	1.5e-3	1.5e-3	2.0e-4	4.3e-5	1.3e-3	1.3e-3	2.7e-4	2.7e-4	0.91987	0.01151	−0.00574

(*continued on next page*)

Table B.3 (*continued*)

ID	Data			Temperature				Pressure				Composition			Composition derivatives	
	$\overline{T}$	$\overline{p}$	y_{CO_2}	$s(T)$	$s(\overline{T})$	$\overline{u}(T)$	$u_c(\overline{T})$	$s(p)$	$s(\overline{p})$	$\overline{u}(p)$	$u_c(\overline{p})$	$u(y_{CO_2})$	$u_{tot}(y_{CO_2})$	$y_{CO_2,calc}$	$\partial y_{CO_2}/\partial T$	$\partial y_{CO_2}/\partial p$
	(K)	(MPa)	(−)	(K)	(K)	(K)	(K)	(MPa)	(MPa)	(MPa)	(MPa)	(−)	(−)	(−)	(K^{-1})	(MPa^{-1})
	298.175	8.2865	0.92742	1.8e-4	3.6e-5	1.5e-3	1.5e-3	1.7e-4	1.7e-5	1.3e-3	1.3e-3	2.7e-4	2.7e-4	0.91987	0.01151	−0.00573
	298.175	8.2864	0.92734	1.8e-4	1.8e-5	1.5e-3	1.5e-3	1.9e-4	3.9e-5	1.3e-3	1.3e-3	2.7e-4	2.7e-4	0.91987	0.01151	−0.00577
	298.175	8.2863	0.92735	1.9e-4	2.0e-5	1.5e-3	1.5e-3	1.3e-4	2.0e-5	1.3e-3	1.3e-3	2.7e-4	2.7e-4	0.91987	0.01151	−0.00576
	298.175	8.2861	0.92728	1.2e-4	1.0e-5	1.5e-3	1.5e-3	1.7e-4	2.4e-5	1.3e-3	1.3e-3	2.7e-4	2.7e-4	0.91987	0.01151	−0.00601
	298.175	8.2860	0.92719	8.7e-5	1.4e-5	1.5e-3	1.5e-3	1.4e-4	2.1e-5	1.2e-3	1.2e-3	2.7e-4	2.7e-4	0.91987	0.01151	−0.00581
	298.175	8.2858	0.92718	2.4e-4	2.2e-5	1.5e-3	1.5e-3	1.3e-4	2.3e-5	1.2e-3	1.2e-3	2.7e-4	2.7e-4	0.91987	0.01150	−0.00581
	298.175	8.2858	0.92712	1.1e-4	8.8e-6	1.6e-3	1.6e-3	1.4e-4	2.5e-5	1.2e-3	1.2e-3	2.7e-4	2.7e-4	0.91988	0.01150	−0.00582
V31	298.174	8.2969	0.93016	2.9e-4	3.2e-5	1.6e-3	1.6e-3	1.3e-4	2.7e-5	1.2e-3	1.2e-3	2.7e-4	2.7e-4	0.91980	0.01162	−0.00451
	298.174	8.2971	0.93013	2.9e-4	5.1e-5	1.6e-3	1.6e-3	1.4e-4	1.7e-5	1.2e-3	1.2e-3	2.7e-4	2.7e-4	0.91980	0.01163	−0.00449
	298.175	8.2973	0.93033	3.5e-4	1.3e-4	1.7e-3	1.7e-3	1.1e-4	2.1e-5	1.2e-3	1.2e-3	2.7e-4	2.7e-4	0.91982	0.01163	−0.00445
	298.176	8.2971	0.93029	2.2e-4	2.1e-5	1.7e-3	1.7e-3	1.4e-4	2.6e-5	1.2e-3	1.2e-3	2.7e-4	2.7e-4	0.91982	0.01163	−0.00446
	298.176	8.2973	0.93030	2.2e-4	1.9e-5	1.7e-3	1.7e-3	1.1e-4	1.5e-5	1.2e-3	1.2e-3	2.7e-4	2.7e-4	0.91982	0.01163	−0.00444
	298.176	8.2974	0.93027	2.3e-4	1.9e-5	1.6e-3	1.6e-3	1.3e-4	1.7e-5	1.2e-3	1.2e-3	2.7e-4	2.7e-4	0.91982	0.01163	−0.00443
P3	303.158	7.2105	0.99999	3.2e-4	9.5e-6	2.0e-3	2.0e-3	1.4e-4	3.0e-5	1.1e-3	1.1e-3					
V32	303.156	7.4006	0.99148	8.1e-4	4.1e-5	1.8e-3	1.8e-3	9.4e-5	6.6e-6	1.2e-3	1.2e-3	2.7e-4	2.8e-4	0.99157	0.00822	−0.04198
	303.156	7.4007	0.99149	3.6e-4	2.0e-5	1.9e-3	1.9e-3	1.4e-4	1.8e-5	1.2e-3	1.2e-3	2.7e-4	2.8e-4	0.99157	0.00822	−0.04198
	303.156	7.4007	0.99159	2.2e-4	3.5e-5	1.9e-3	1.9e-3	1.2e-4	2.1e-5	1.2e-3	1.2e-3	2.7e-4	2.8e-4	0.99157	0.00822	−0.04198
	303.157	7.4007	0.99157	2.5e-4	2.1e-5	1.9e-3	1.9e-3	1.2e-4	2.5e-5	1.2e-3	1.2e-3	2.7e-4	2.8e-4	0.99157	0.00822	−0.04198
	303.158	7.4007	0.99156	1.4e-4	6.6e-6	2.0e-3	2.0e-3	1.0e-4	2.1e-5	1.2e-3	1.2e-3	2.7e-4	2.8e-4	0.99158	0.00822	−0.04197
	303.158	7.4007	0.99156	3.6e-4	1.8e-5	2.0e-3	2.0e-3	1.2e-4	2.6e-5	1.2e-3	1.2e-3	2.7e-4	2.8e-4	0.99158	0.00822	−0.04198
	303.158	7.4007	0.99153	1.5e-4	1.6e-5	2.0e-3	2.0e-3	1.0e-4	9.1e-6	1.2e-3	1.2e-3	2.7e-4	2.8e-4	0.99158	0.00822	−0.04197
	303.158	7.4008	0.99152	1.4e-4	1.3e-5	2.0e-3	2.0e-3	9.3e-5	8.7e-6	1.2e-3	1.2e-3	2.7e-4	2.8e-4	0.99158	0.00822	−0.04197
V33	303.156	7.4670	0.98914	7.0e-4	6.4e-5	2.0e-3	2.0e-3	1.6e-4	5.6e-5	1.1e-3	1.1e-3	2.7e-4	2.8e-4	0.98888	0.00835	−0.03915
	303.156	7.4672	0.98906	4.5e-4	7.8e-5	1.9e-3	1.9e-3	1.2e-4	1.1e-5	1.1e-3	1.1e-3	2.7e-4	2.8e-4	0.98887	0.00835	−0.03914
	303.157	7.4672	0.98895	4.0e-4	2.1e-5	2.0e-3	2.0e-3	1.0e-4	8.1e-6	1.1e-3	1.1e-3	2.7e-4	2.8e-4	0.98888	0.00835	−0.03913
	303.158	7.4672	0.98908	1.3e-4	2.1e-5	2.0e-3	2.0e-3	1.2e-4	1.4e-5	1.1e-3	1.1e-3	2.7e-4	2.8e-4	0.98888	0.00835	−0.03913
	303.158	7.4673	0.98898	3.4e-4	1.4e-5	2.0e-3	2.0e-3	1.1e-4	1.9e-5	1.1e-3	1.1e-3	2.7e-4	2.8e-4	0.98888	0.00835	−0.03913
	303.158	7.4674	0.98910	1.9e-4	3.3e-5	2.0e-3	2.0e-3	1.6e-4	2.2e-5	1.1e-3	1.1e-3	2.7e-4	2.8e-4	0.98888	0.00835	−0.03912
	303.158	7.4674	0.98899	3.7e-4	3.4e-5	2.1e-3	2.1e-3	1.3e-4	1.4e-5	1.1e-3	1.1e-3	2.7e-4	2.8e-4	0.98887	0.00835	−0.03912
V34	303.158	7.5219	0.98691	3.2e-4	3.3e-5	1.7e-3	1.7e-3	1.2e-4	1.4e-5	1.2e-3	1.2e-3	2.7e-4	2.8e-4	0.98682	0.00851	−0.03633
	303.158	7.5219	0.98698	3.6e-4	1.6e-5	1.7e-3	1.7e-3	1.2e-4	1.8e-5	1.2e-3	1.2e-3	2.7e-4	2.8e-4	0.98682	0.00851	−0.03633
	303.158	7.5219	0.98700	1.5e-4	9.6e-6	1.7e-3	1.7e-3	1.2e-4	2.5e-5	1.2e-3	1.2e-3	2.7e-4	2.8e-4	0.98682	0.00851	−0.03633
	303.158	7.5218	0.98698	4.1e-4	4.3e-5	1.7e-3	1.7e-3	1.4e-4	3.2e-5	1.1e-3	1.1e-3	2.7e-4	2.8e-4	0.98682	0.00851	−0.03634
	303.158	7.5217	0.98700	3.4e-4	3.1e-5	1.7e-3	1.7e-3	1.1e-4	1.1e-5	1.1e-3	1.1e-3	2.7e-4	2.8e-4	0.98682	0.00851	−0.03634
	303.158	7.5215	0.98692	3.0e-4	2.5e-5	1.7e-3	1.7e-3	1.5e-4	1.4e-5	1.1e-3	1.1e-3	2.7e-4	2.8e-4	0.98683	0.00851	−0.03635
	303.158	7.5215	0.98693	3.9e-4	3.0e-5	1.7e-3	1.7e-3	1.6e-4	4.1e-5	1.1e-3	1.1e-3	2.7e-4	2.8e-4	0.98683	0.00851	−0.03636
	303.158	7.5213	0.98689	2.4e-4	3.0e-5	1.7e-3	1.7e-3	1.0e-4	1.1e-5	1.1e-3	1.1e-3	2.7e-4	2.8e-4	0.98684	0.00851	−0.03637
V35	303.158	7.5349	0.98700	3.4e-4	1.6e-5	1.8e-3	1.8e-3	1.6e-4	2.8e-5	1.2e-3	1.2e-3	2.7e-4	2.8e-4	0.98635	0.00856	−0.03556
	303.158	7.5351	0.98700	3.6e-4	5.9e-5	1.8e-3	1.8e-3	1.1e-4	8.8e-6	1.2e-3	1.2e-3	2.7e-4	2.8e-4	0.98635	0.00856	−0.03554
	303.158	7.5350	0.98698	4.0e-4	4.7e-5	1.8e-3	1.8e-3	1.8e-4	3.0e-5	1.2e-3	1.2e-3	2.7e-4	2.8e-4	0.98635	0.00856	−0.03555
	303.158	7.5349	0.98697	1.9e-4	2.7e-5	1.8e-3	1.8e-3	1.1e-4	1.0e-5	1.2e-3	1.2e-3	2.7e-4	2.8e-4	0.98636	0.00856	−0.03556
V36	303.158	7.5449	0.98689	2.4e-4	3.6e-5	1.7e-3	1.7e-3	1.1e-4	2.1e-5	1.1e-3	1.1e-3	2.7e-4	2.8e-4	0.98600	0.00861	−0.03491
	303.158	7.5450	0.98685	4.7e-4	4.3e-5	1.8e-3	1.8e-3	1.5e-4	2.4e-5	1.2e-3	1.2e-3	2.7e-4	2.8e-4	0.98600	0.00861	−0.03489
	303.158	7.5450	0.98677	2.1e-4	9.7e-6	1.8e-3	1.8e-3	1.2e-4	1.5e-5	1.2e-3	1.2e-3	2.7e-4	2.8e-4	0.98600	0.00861	−0.03491
	303.158	7.5450	0.98688	2.9e-4	2.5e-5	1.7e-3	1.7e-3	1.4e-4	3.3e-5	1.2e-3	1.2e-3	2.7e-4	2.8e-4	0.98600	0.00861	−0.03491
	303.158	7.5450	0.98677	2.1e-4	1.3e-5	1.8e-3	1.8e-3	1.0e-4	1.4e-5	1.2e-3	1.2e-3	2.7e-4	2.8e-4	0.98600	0.00861	−0.03491
	303.158	7.5449	0.98680	3.4e-4	1.8e-5	1.8e-3	1.8e-3	1.2e-4	2.3e-5	1.1e-3	1.1e-3	2.7e-4	2.8e-4	0.98600	0.00861	−0.03492
V37	303.157	7.5532	0.98692	8.3e-4	1.4e-4	1.8e-3	1.8e-3	1.8e-4	2.5e-5	1.2e-3	1.2e-3	2.7e-4	2.8e-4	0.98570	0.00865	−0.03435
	303.158	7.5533	0.98692	2.0e-4	1.1e-5	1.8e-3	1.8e-3	1.3e-4	2.2e-5	1.2e-3	1.2e-3	2.7e-4	2.8e-4	0.98571	0.00865	−0.03434
	303.158	7.5535	0.98669	4.8e-4	8.3e-5	1.8e-3	1.8e-3	1.3e-4	1.1e-5	1.2e-3	1.2e-3	2.7e-4	2.8e-4	0.98570	0.00865	−0.03433
	303.158	7.5529	0.98669	3.6e-4	4.6e-5	1.7e-3	1.7e-3	1.1e-4	1.2e-5	1.1e-3	1.1e-3	2.7e-4	2.8e-4	0.98572	0.00865	−0.03437
V38	303.158	7.5542	0.98670	1.5e-4	1.4e-5	1.8e-3	1.8e-3	1.4e-4	3.2e-5	1.1e-3	1.1e-3	2.7e-4	2.8e-4	0.98568	0.00866	−0.03428
	303.158	7.5542	0.98667	1.8e-4	2.5e-5	1.8e-3	1.8e-3	1.9e-4	3.5e-5	1.1e-3	1.1e-3	2.7e-4	2.8e-4	0.98568	0.00866	−0.03428
	303.158	7.5541	0.98662	6.5e-4	4.8e-5	1.8e-3	1.8e-3	1.2e-4	2.1e-5	1.1e-3	1.1e-3	2.7e-4	2.8e-4	0.98568	0.00866	−0.03429
	303.158	7.5540	0.98660	1.9e-4	1.2e-5	1.7e-3	1.7e-3	1.2e-4	1.8e-5	1.1e-3	1.1e-3	2.7e-4	2.8e-4	0.98568	0.00866	−0.03429
	303.158	7.5539	0.98662	3.2e-4	2.7e-5	1.8e-3	1.8e-3	1.1e-4	2.2e-5	1.1e-3	1.1e-3	2.7e-4	2.8e-4	0.98568	0.00866	−0.03430
	303.158	7.5538	0.98659	4.9e-4	1.1e-4	1.7e-3	1.8e-3	1.1e-4	1.7e-5	1.1e-3	1.1e-3	2.7e-4	2.8e-4	0.98569	0.00866	−0.03431
	303.158	7.5538	0.98661	1.9e-4	2.2e-5	1.7e-3	1.7e-3	1.0e-4	2.0e-5	1.1e-3	1.1e-3	2.7e-4	2.8e-4	0.98569	0.00866	−0.03431
	303.158	7.5537	0.98656	1.0e-4	2.6e-5	1.8e-3	1.8e-3	1.1e-4	2.9e-5	1.1e-3	1.1e-3	2.7e-4	2.8e-4	0.98569	0.00866	−0.03431
V39	303.156	7.5542	0.98643	3.7e-4	1.4e-5	1.7e-3	1.7e-3	1.0e-4	9.4e-6	1.1e-3	1.1e-3	2.7e-4	2.8e-4	0.98566	0.00866	−0.03428
	303.157	7.5543	0.98638	4.6e-4	4.7e-5	1.7e-3	1.7e-3	9.2e-5	1.0e-5	1.1e-3	1.1e-3	2.7e-4	2.8e-4	0.98566	0.00866	−0.03428
	303.157	7.5543	0.98641	5.1e-4	1.1e-4	1.7e-3	1.7e-3	1.2e-4	1.9e-5	1.1e-3	1.1e-3	2.7e-4	2.8e-4	0.98566	0.00866	−0.03427
	303.156	7.5543	0.98644	4.0e-4	2.9e-5	1.7e-3	1.7e-3	1.6e-4	1.7e-5	1.1e-3	1.1e-3	2.7e-4	2.8e-4	0.98566	0.00866	−0.03428
	303.156	7.5542	0.98641	3.7e-4	3.6e-5	1.7e-3	1.7e-3	1.5e-4	2.1e-5	1.1e-3	1.1e-3	2.7e-4	2.8e-4	0.98566	0.00866	−0.03428
V40	303.158	7.5577	0.98708	1.2e-4	3.1e-5	1.7e-3	1.7e-3	1.4e-4	2.1e-5	1.1e-3	1.1e-3	2.7e-4	2.8e-4	0.98555	0.00868	−0.03402
	303.158	7.5576	0.98705	4.2e-4	3.5e-5	1.8e-3	1.8e-3	1.6e-4	2.2e-5	1.1e-3	1.1e-3	2.7e-4	2.8e-4	0.98556	0.00868	−0.03403
	303.158	7.5575	0.98705	2.2e-4	1.9e-5	1.8e-3	1.8e-3	1.2e-4	1.3e-5	1.1e-3	1.1e-3	2.7e-4	2.8e-4	0.98556	0.00868	−0.03404
	303.158	7.5575	0.98709	2.7e-4	2.4e-5	1.7e-3	1.7e-3	1.6e-4	3.0e-5	1.1e-3	1.1e-3	2.7e-4	2.8e-4	0.98556	0.00868	−0.03404
	303.158	7.5574	0.98707	1.8e-4	1.3e-5	1.7e-3	1.7e-3	1.0e-4	1.6e-5	1.1e-3	1.1e-3	2.7e-4	2.8e-4	0.98557	0.00868	−0.03405
	303.158	7.5574	0.98710	3.5e-4	3.3e-5	1.7e-3	1.7e-3	1.2e-4	1.4e-5	1.1e-3	1.1e-3	2.7e-4	2.8e-4	0.98557	0.00868	−0.03405
	303.158	7.5572	0.98710	5.0e-4	2.9e-5	1.7e-3	1.7e-3	1.1e-4	2.0e-5	1.1e-3	1.1e-3	2.7e-4	2.8e-4	0.98557	0.00868	−0.03406
	303.158	7.5572	0.98711	3.3e-4	2.9e-5	1.7e-3	1.7e-3	1.2e-4	2.4e-5	1.1e-3	1.1e-3	2.7e-4	2.8e-4	0.98557	0.00868	−0.03406

References

[1] J. Gernert, R. Span, EOS-CG: a Helmholtz Energy Mixture Model for Humid Gases and CCS Mixtures, 2015 in press, http://dx.doi.org/10.1016/j.jct.2015.05.015.

[2] G.J. Gernert, A New Helmholtz Energy Model for Humid Gases and CCS Mixtures, PhD dissertation, Fakultät für Maschinenbau, Ruhr-Universität Bochum, Bochum, 2013. URL: http://www-brs.ub.ruhr-uni-bochum.de/netahtml/HSS/Diss/GernertGeorgJohannes/diss.pdf.

[3] H. Li, J.P. Jakobsen, Ø. Wilhelmsen, J. Yan, PVTxy properties of CO_2 mixtures relevant for CO_2 capture, transport and storage: review of available experimental data and theoretical models, Appl. Energy 88 (11) (2011a) 3567–3579. URL: http://dx.doi.org/10.1016/j.apenergy.2011.03.052.

[4] S.W. Løvseth, G. Skaugen, H.G.J. Stang, J.P. Jakobsen, Ø. Wilhelmsen, R. Span, R. Wegge, CO_2 mix project: experimental determination of thermo-physical properties of CO_2-rich mixtures, Energy Procedia 37 (2013) 7841–7849. URL: http://dx.doi.org/10.1016/j.egypro.2014.09.001.

[5] S.W. Løvseth, H.G.J. Stang, S.F. Westman, I. Snustad, A. Austegard, Experimental investigations of impurity impact on CO_2 mixture phase equilibria, Energy Procedia 63 (2014) 2589–2595. URL: http://dx.doi.org/10.1016/j.egypro.2014.11.281.

[6] R. Span, W. Wagner, A new equation of state for carbon dioxide covering the fluid region from the triple-point temperature to 1100 K at pressures up to 800 MPa, J. Phys. Chem. Ref. Data 25 (1996) 1509. URL: http://dx.doi.org/10.1063/1.555991.

[7] O. Kunz, W. Wagner, The GERG-2008 wide-range equation of state for natural gases and other mixtures: an expansion of GERG-2004, J. Chem. Eng. Data 57 (11) (2012) 3032–3091. URL: http://dx.doi.org/10.1021/je300655b.

[8] R. Span, J. Gernert, A. Jäger, Accurate thermodynamic-property models for CO_2-rich mixtures, Energy Procedia 37 (2013) 2914–2922. URL, http://dx.doi.org/10.1016/j.egypro.2013.06.177.

[9] E. De Visser, C. Hendriks, M. Barrio, M.J. Mølnvik, G. de Koeijer, S. Liljemark, Y. Le Gallo, Dynamis CO_2 quality recommendations, Int. J. Greenhouse Gas Control 2 (4) (2008) 478–484. URL: http://dx.doi.org/10.1016/j.ijggc.2008.04.006.

[10] H. Li, Ø. Wilhelmsen, Y. Lv, W. Wang, J. Yan, Viscosities, thermal conductivities and diffusion coefficients of CO_2 mixtures: review of experimental data and theoretical models, Int. J. Greenhouse Gas Control 5 (5) (2011b) 1119–1139. URL: http://dx.doi.org/10.1016/j.ijggc.2011.07.009.

[11] R.D. Chirico, T.W. de Loos, J. Gmehling, A.R.H. Goodwin, S. Gupta, W.M. Haynes, K.N. Marsh, V. Rives, J.D. Olson, C. Spencer, J.F. Brennecke, J.P.M. Trusler, Guidelines for reporting of phase equilibrium measurements (IUPAC recommendations 2012), Pure Appl. Chem. 84 (8) (2012) 1785–1813. URL: http://dx.doi.org/10.1351/PAC-REC-11-05-02.

[12] BIPM, IEC, IFCC, ILAC, IUPAC, IUPAP, ISO, OIML, Evaluation of measurement data – guide for the expression of uncertainty in measurement, JCGM 100 (2008) 2008.

[13] M. Frenkel, R.D. Chirico, V.V. Diky, Q. Dong, S. Frenkel, P.R. Franchois, D.L. Embry, T.L. Teague, K.N. Marsh, R.C. Wilhoit, ThermoML – an XML-based approach for storage and exchange of experimental and critically evaluated thermophysical and thermochemical property data. 1. Experimental data, J. Chem. Eng. Data 48 (1) (2003) 2–13. URL, http://dx.doi.org/10.1021/je025645o.

[14] R.D. Chirico, M. Frenkel, V.V. Diky, K.N. Marsh, R.C. Wilhoit, ThermoML: an XML-based approach for storage and exchange of experimental and critically evaluated thermophysical and thermochemical property data. 2. Uncertainties, J. Chem. Eng. Data 48 (5) (2003) 1344–1359. URL: http://dx.doi.org/10.1021/je034088i.

[15] M. Frenkel, R.D. Chirico, V.V. Diky, K.N. Marsh, J.H. Dymond, W.A. Wakeham, ThermoML: an XML-based approach for storage and exchange of experimental and critically evaluated thermophysical and thermochemical property data. 3. Critically evaluated data, predicted data, and equation representation, J. Chem. Eng. Data 49 (3) (2004) 381–393. URL: http://dx.doi.org/10.1021/je049890e.

[16] R.D. Chirico, M. Frenkel, V. Diky, R.N. Goldberg, H. Heerklotz, J.E. Ladbury, D.P. Remeta, J.H. Dymond, A.R. Goodwin, K.N. Marsh, et al., ThermoML: an XML-based approach for storage and exchange of experimental and critically evaluated thermophysical and thermochemical property data. 4. Biomaterials, J. Chem. Eng. Data 55 (4) (2010) 1564–1572. URL: http://dx.doi.org/10.1021/je900685d.

[17] S.F. Westman, H.G.J. Stang, S.Ø. Størset, H. Rekstad, A. Austegard, S.W. Løvseth, Accurate phase equilibrium measurements of CO_2 mixtures, Energy Procedia 51 (2014) 392–401. URL: http://dx.doi.org/10.1016/j.egypro.2014.07.046.

[18] J.M.S. Fonseca, R. Dohrn, S. Peper, High-pressure fluid-phase equilibria: experimental methods and systems investigated (2005–2008), Fluid Phase Equilib. 300 (1–2) (2011) 1–69. URL: http://dx.doi.org/10.1016/j.fluid.2010.09.017.

[19] ARMINES, Patent n° FR 2 853 414, Procédé et dispositif pour prélever des micro-échantillons d'un fluide sous pression contenu dans un container, 2003.

[20] P. Guilbot, A. Valtz, H. Legendre, D. Richon, Rapid on-line sampler-injector: a reliable tool for HT-HP sampling and on-line GC analysis, Analysis 28 (5) (2000) 426–431. URL, http://dx.doi.org/10.1051/analusis:2000128.

[21] S. Laugier, D. Richon, New apparatus to perform fast determinations of mixture vapor–liquid equilibria up to 10 MPa and 423 K, Rev. Sci. Instrum. 57 (3) (1986) 469–472. URL: http://dx.doi.org/10.1063/1.1138909.

[22] R. Span, E.W. Lemmon, R.T. Jacobsen, W. Wagner, A. Yokozeki, A Reference Equation of State for the Thermodynamic Properties of Nitrogen for Temperatures from 63.151 to 1000 K and Pressures to 2200 MPa, J. Phys. Chem. Ref. Data 29 (6) (2000) 1361–1433. URL, http://dx.doi.org/10.1063/1.1349047.

[23] H. Preston-Thomas, The International Temperature Scale of 1990 (ITS-90), Metrologia 27 (1) (1990) 3–10. URL, http://dx.doi.org/10.1088/0026-1394/27/1/002.

[24] G.E.P. Box, G.M. Jenkins, G.C. Reinsel, Time Series Analysis : Forecasting and Control, Wiley, 2008, ISBN 9780470272848. URL, http://dx.doi.org/10.1002/9781118619193.oth3.

[25] A.M. Law, W.D. Kelton, Simulation Modeling and Analysis, McGraw-Hill, 1991, ISBN 0071008039.

[26] H.B. Callen, Thermodynamics and an Introduction to Thermostatistics, 2 edn, Wiley, 1985, ISBN 0471862568.

[27] W. Weber, S. Zeck, H. Knapp, Gas solubilities in liquid solvents at high pressures: apparatus and results for binary and ternary systems of N_2, CO_2 and CH_3 OH, Fluid Phase Equilib. 18 (3) (1984) 253–278. URL, http://dx.doi.org/10.1016/0378-3812(84)85011-6.

[28] T.S. Brown, E.D. Sloan, A.J. Kidnay, Vapor-liquid equilibria in the nitrogen+carbon dioxide+ethane system, Fluid Phase Equilib. 51 (1989a) 299–313. URL, http://dx.doi.org/10.1016/0378-3812(89)80372-3.

[29] M. Yorizane, S. Yoshimura, H. Masuoka, Y. Miyano, Y. Kakimoto, New procedure for vapor–liquid equilibria. Nitrogen + carbon dioxide, methane + freon 22, and methane + freon 12, J. Chem. Eng. Data 30 (2) (1985) 174–176. URL, http://dx.doi.org/10.1021/je00040a012.

[30] O. Fandiño, J.P.M. Trusler, D. Vega-Maza, Phase behavior of (CO_2+H_2) and (CO_2+N_2) at temperatures between (218.15 and 303.15) K at pressures up to 15 MPa, Int. J. Greenhouse Gas Control 36 (2015) 78–92. URL, http://dx.doi.org/10.1016/j.ijggc.2015.02.018.

[31] M.S. Green, M. Vicentini-Missoni, J.M.H. Levelt Sengers, Scaling-Law Equation of State for Gases in the Critical Region, Phys. Rev. Lett. 18 (1967) 1113–1117. URL, http://dx.doi.org/10.1103/PhysRevLett.18.1113.

[32] L.P. Kadanoff, W. Götze, D. Hamblen, R. Hecht, E.A.S. Lewis, V.V. Palciauskas, M. Rayl, J. Swift, D. Aspnes, J. Kane, Static Phenomena Near Critical Points: Theory and Experiment, Rev. Mod. Phys. 39 (1967) 395–431. URL, http://dx.doi.org/10.1103/RevModPhys.39.395.

[33] M.E. Fisher, The theory of equilibrium critical phenomena, Rep, Prog. Phys. 30 (2) (1967) 615. URL, http://dx.doi.org/10.1088/0034-4885/30/2/306.

[34] P. Ungerer, B. Tavitian, A. Boutin, Applications of Molecular Simulation in the Oil and Gas Industry. Monte Carlo Methods, Chap. 2, Editions, note: Equation 2.100 is lacking the critical composition term, Technip, Paris, France, 2005.

[35] V. Lachet, T. de Bruin, P. Ungerer, C. Coquelet, A. Valtz, V. Hasanov, F. Lockwood, D. Richon, Thermodynamic behavior of the CO_2 + SO_2 mixture: experimental and Monte Carlo simulation studies, Energy Procedia 1 (1) (2009) 1641–1647, http://dx.doi.org/10.1016/j.egypro.2009.01.215.

[36] J. Sengers, J. Levelt Sengers, A universal representation of the thermodynamic properties of fluids in the critical region, Int. J. Thermophys. 5 (2) (1984) 195–208. ISSN 0195-928X, URL: http://dx.doi.org/10.1007/BF00505500.

[37] T.A. Al-Sahhaf, A.J. Kidnay, E.D. Sloan, Liquid+Vapor Equilibria in the N_2+CO_2+ CH_4 System, Ind. Eng. Chem. Fundam. 22 (4) (1983) 372–380. URL, http://dx.doi.org/10.1021/i100012a004.

[38] G.J. Esper, Direkte und indirekte pvT-Messungen an Fluiden, VDI-Verlag, 1987.

[39] G.J. Esper, D.M. Bailey, J.C. Holste, K.R. Hall, Volumetric behavior of near-equimolar mixtures for CO_2 + CH_4 and CO_2 + N_2, Fluid Phase Equilib. 49 (1989) 35–47. URL: http://dx.doi.org/10.1016/0378-3812(89)80004-4.

[40] H.A. Duarte-Garza, J.C. Holste, K.R. Hall, K.N. Marsh, B.E. Gammon, Isochoric pVT and phase equilibrium measurements for carbon dioxide+ nitrogen, J. Chem. Eng. Data 40 (3) (1995) 704–711. URL: http://dx.doi.org/10.1021/je00019a038.

[41] D.-Y. Peng, D.B. Robinson, A new two-constant equation of state, Ind. Eng. Chem. Fundam. 15 (1) (1976) 59–64. URL: http://dx.doi.org/10.1021/i160057a011.

[42] P.M. Mathias, T.W. Copeman, Extension of the Peng–Robinson equation of state to complex mixtures: evaluation of the various forms of the local composition concept, Fluid Phase Equilib. 13 (1983) 91–108. URL: http://dx.doi.org/10.1016/0378-3812(83)80084-3.

[43] D.S.H. Wong, S.I. Sandler, A theoretically correct mixing rule for cubic equations of state, AIChE J. 38 (5) (1992) 671–680. URL: http://dx.doi.org/10.1002/aic.690380505.

[44] H. Renon, J.M. Prausnitz, Local compositions in thermodynamic excess functions for liquid mixtures, AIChE J. 14 (1) (1968) 135–144. URL: http://dx.doi.org/10.1002/aic.690140124.

[45] C. Coquelet, A. Valtz, F. Dieu, D. Richon, P. Arpentinier, F. Lockwood, Isothermal P, x, y data for the argon + carbon dioxide system at six temperatures from 233.32 to 299.21 K and pressures up to 14 MPa, Fluid Phase Equilib. 273 (1–2) (2008) 38–43. URL: http://dx.doi.org/10.1016/j.fluid.2008.08.010.

[46] B.E. Poling, J.M. Prausnitz, J.P. O'Connell, The Properties of Gases and Liquids, vol. 5, McGraw-Hill, New York, 2001, ISBN 0070116822.

[47] P.T. Boggs, R.H. Byrd, J.E. Rogers, R.B. Schnabel, User's Reference Guide for ODRPACK Version 2.01 Software for Weighted Orthogonal Distance Regression, 1992. URL: http://docs.scipy.org/doc/external/odrpack_guide.pdf.

[48] B. Yucelen, A.J. Kidnay, Vapor–liquid equilibria in the nitrogen + carbon dioxide + propane system from 240 to 330 K at pressures to 15 MPa, J. Chem.

Eng. Data 44 (5) (1999) 926–931. URL: http://dx.doi.org/10.1021/je980321e.
[49] T.S. Brown, V.G. Niesen, E.D. Sloan, A.J. Kidnay, Vapor–liquid equilibria for the binary systems of nitrogen, carbon dioxide, and n-butane at temperatures from 220 to 344 K. Fluid Phase Equilib. 53 (1989) 7–14. URL: http://dx.doi.org/10.1016/0378-3812(89)80067-6.
[50] F.A. Somait, A.J. Kidnay, Liquid–vapor equilibria at 270.00 K for systems containing nitrogen, methane, and carbon dioxide, J. Chem. Eng. Data 23 (4) (1978) 301–305. URL: http://dx.doi.org/10.1021/je60079a019.
[51] N. Xu, J. Dong, Y. Wang, J. Shi, High pressure vapor liquid equilibria at 293 K for systems containing nitrogen, methane and carbon dioxide, Fluid Phase Equilib. 81 (1992) 175–186. URL: http://dx.doi.org/10.1016/0378-3812(92)85150-7.
[52] G. Trappehl, Experimentelle Untersuchung der Dampf-Flüssigkeits-Phasengleichgewichte und kalorischen Eigenschaften bei tiefen Temperaturen und hohen Drücken an Stoffgemischen bestehend aus N_2, CH_4, C_2 H_6, C_3 H_8 und CO_2, Ph.D. thesis, Technische Universität, Berlin, 1987.
[53] G. Kaminishi, T. Toriumi, Vapor–liquid phase equilibrium in the CO_2–H_2, CO_2–N_2 and CO_2–O_2 systems [in Japanese], Kogyo Kagaku Zasshi 69 (1966) 175–178. URL: http://doi.org/10.1246/nikkashi1898.69.2_175.
[54] I.R. Krichevskii, N.E. Khazanova, L.S. Lesnevskaya, L.Y. Sandalova, Equilibrium of liquid–gas at high pressures in the system nitrogen-carbon dioxide [in Russian], Khim. Prom-st. 3 (1962) 169–171.
[55] B. Bian, Y. Wang, J. Shi, E. Zhao, B.C.-Y. Lu, Simultaneous determination of vapor-liquid equilibrium and molar volumes for coexisting phases up to the critical temperature with a static method, Fluid Phase Equilib. 90 (1) (1993) 177–187. URL: http://dx.doi.org/10.1016/0378-3812(93)85012-B.
[56] B. Mangum, G. Furukawa, Guidelines for Realizing the International Temperature Scale of 1990 (ITS-90), 1990. URL, http://www.nist.gov/manuscript-publication-search.cfm?pub_id=905199. NIST Tech. Note 1265.
[57] M. S. L. of New Zealand, MSL Technical Guide 21 Using SPRT Calibration Certificates, 2008. URL: https://www.msl.irl.cri.nz/training-and-resources/technical-guides. retrieved 2015-05-20.
[58] R.I. Veltcheva, J.V. Pearce, R. da Silva, G. Machin, R.L. Rusby, Strategies for minimising the uncertainty of the SPRT self-heating correction, in: AIP Conf. Proc., vol. 1552, 2013, p. 433. URL: http://dx.doi.org/10.1063/1.4821390.
[59] ISO, Gas analysis - Preparation of Calibration Gas Mixtures – Gravimetric Method, ISO 6142:2001, International Organization for Standardization, Geneva, Switzerland, 2001.
[60] M.E. Wieser, T.B. Coplen, Atomic weights of the elements 2009 (IUPAC technical report), Pure Appl. Chem. 83 (2) (2010) 359–396. URL: http://dx.doi.org/10.1351/PAC-REP-10-09-14.
[61] M.E. Wieser, N. Holden, T.B. Coplen, J.K. Böhlke, M. Berglund, W.A. Brand, P. De Bièvre, M. Gröning, R.D. Loss, J. Meija, T. Hirata, T. Prohaska, R. Schoenberg, G. O'Connor, T. Walczyk, S. Yoneda, X.-K. Zhu, Atomic weights of the elements 2011 (IUPAC technical report), Pure Appl. Chem. 85 (5) (2013) 1047–1078. URL: http://dx.doi.org/10.1351/PAC-REP-13-03-02.
[62] M.C. Leuenberger, M.F. Schibig, P. Nyfeler, Gas adsorption and desorption effects on cylinders and their importance for long-term gas records, Atmos. Chem. Phys. Discuss. 14 (13) (2014) 19293–19314. URL: http://dx.doi.org/10.5194/acpd-14-19293-2014.

Article II

Vapor-liquid equilibrium data for the carbon dioxide and oxygen ($CO_2 + O_2$) system at the temperatures 218, 233, 253, 273, 288 and 298 K and pressures up to 14 MPa [2]

S.F. Westman, H.G.J. Stang, S.W. Løvseth, A. Austegard, I. Snustad, I.S. Ertesvåg, *submitted to Fluid Phase Equilibria. Revised version accepted for publication can be found at* doi:10.1016/j.fluid.2016.04.002

Vapor-liquid equilibrium data for the carbon dioxide and oxygen (CO_2 + O_2) system at the temperatures 218, 233, 253, 273, 288 and 298 K and pressures up to 14 MPa

Snorre Foss Westman[a,*], H. G. Jacob Stang[b], Sigurd W. Løvseth[b,**], Anders Austegard[b], Ingrid Snustad[b], Ivar S. Ertesvåg[a]

[a]*Norwegian University of Science and Technology, Department of Energy and Process Engineering, Kolbjørn Hejes vei 1b, NO-7491 Trondheim, Norway*
[b]*SINTEF Energy Research, NO-7465 Trondheim, Norway*

Abstract

Accurate thermophysical data for the CO_2-rich mixtures relevant for carbon capture, transport and storage (CCS) are essential for the development of the accurate equations of state (EOS) and models needed for the design and operation of the processes within CCS. Vapor-liquid equilibrium measurements for the binary system CO_2+O_2 are reported at 218, 233, 253, 273, 288 and 298 K, with estimated standard uncertainties of maximum 8 mK in temperature, maximum 3 kPa in pressure, and maximum 0.0031 in the mole fractions of the phases in the mixture critical regions, and 0.0005 in the mole fractions outside the critical regions. These measurements are compared with existing data. Although some data exists, there are little trustworthy literature data around critical conditions, and the measurements in the present work indicate a need to revise the parameters of existing models. The data in the present work has significantly less scatter than most of the literature data, and range from the vapor pressure of pure CO_2 to close to the mixture critical point pressure at all six temperatures. With the measurements in the present work, the data situation for the CO_2+O_2 system is significantly improved, forming the basis to develop better equations of state for the system. A scaling law model is fitted to the critical region data of each isotherm, and high accuracy estimates for the critical composition and pressure are found. The Peng-Robinson EOS with the alpha correction by Mathias and Copeman, the mixing rules by Wong and Sandler, and the NRTL excess Gibbs energy model is fitted to the data in the present work, with a maximum absolute average deviation of 0.01 in mole fraction.

Keywords:
vapor-liquid equilibrium, experimental measurements, carbon dioxide, oxygen, CO_2 capture and storage

1. Introduction

In the present study, vapor-liquid equilibrium (VLE) measurements for the CO_2+O_2 system are presented. It follows Westman et al. [1], which investigated the VLE of the CO_2+N_2 system. The need for new data for these systems and the other mixtures relevant for carbon capture, transport and storage (CCS) has been discussed for instance in the recently reported comprehensive literature studies by [2, 3, 4, 5]. Calculations using existing equations of state (EOS) [3, 6] show that even small amounts of impurities in CO_2-rich mixtures can significantly affect the behavior of the fluid [5, 7]. As an example, the maximum pressure at which a mixture of CO_2 and 5% O_2 can be in the two-phase region, the cricondenbar, will increase to approximately 8.4 MPa compared to the critical pressure of CO_2, 7.3773 MPa. Even with the recent progress of molecular modeling, empirical equations of state still provide the most accurate description of thermodynamic properties of such systems. Accurate data are required in order to develop such accurate models needed for the design and operation of various processes within CCS. In the development and fitting of the highly flexible and potentially accurate multi-parameter equation of state EOS-CG for CCS mixtures, the development of the model for the CO_2+O_2 system suffered from the lack of high quality data [3, 4]. For instance, some of the seemingly most accurate available vapor-liquid equilibrium data for the CO_2+O_2 system were not consistent with the vapor pressure of pure CO_2 [3, 4], indicating an error in the measured pressure, temperature or composition of these data. The objective of the measurements in the present work was to reconcile the inconsistencies and cover gaps in the available literature data, including states close to critical conditions and temperatures above 273.15 K, where little data of sufficient quality existed.

The work presented here was part of a project called CO_2Mix. As described by Løvseth et al. [7], the CO_2Mix project aimed at performing accurate vapor-liquid equilibrium, speed of sound and density measurements of CO_2-rich mixtures at conditions relevant for transport and conditioning in CCS [5, 8]. As part of this project, a setup has been specifically designed and constructed in order to perform highly accurate phase equilibria measurements on CO_2-rich mixtures under relevant conditions for CCS. This setup has been described in detail in [9, 1]. The experimental appara-

*Corresponding author.
**Corresponding author.
Email addresses: snorre.f.westman@ntnu.no (Snorre Foss Westman), sigurd.w.lovseth@sintef.no (Sigurd W. Løvseth)

tus was validated by the VLE measurements on the CO_2+N_2 system performed by Westman et al. [1], as data of high quality were available for this system.

In the present paper, VLE measurements for the CO_2+O_2 system are reported for six isotherms at 218.15, 233.14, 253.15, 273.15, 288.14 and 298.14 K, spanning the region from close to the triple point temperature to close to the critical temperature of pure CO_2. The pressure ranges from 0.56 to 14.4 MPa. Comparison with existing data and EOSs are provided. Furthermore, an EOS is fitted to the data, with the possibility for use over the whole temperature range of the experimental data.

Special care has been taken to present the results and analysis in accordance with the IUPAC Guidelines for reporting of phase equilibrium measurements given in the work by Chirico et al. [10]. In particular, a thorough estimation of the standard uncertainties, as specified in the ISO Guide for the Estimation of Uncertainty in Measurement, commonly referred to as "GUM" [11], has been performed.

In the following the experimental setup and procedures are described in Section 2, the uncertainty analysis in Section 3. Results will be presented, discussed and analyzed in Sections 4 and 5, including fitting of EOS parameters before conclusions are drawn in Section 6. The detailed experimental data for liquid, vapor and supercritical states are tabulated in Appendix A.

2. Experimental apparatus

2.1. Description of setup

The apparatus used for the VLE measurements in the present work was described in [1]. Therefore, only a short summary of the experimental setup will be given here. A diagram of the cell and apparatus is shown in Fig. 1.

As described in [1], the measurements were performed using an isothermal analytical method with a variable-volume cell. This type of methodology has been described in, for example, [12].

According to Gibbs' phase rule, for a system of two components with two coexisting phases, only two intensive variables can be varied freely. In the experiments in the present work, the temperature and pressure were the independent variables. The equilibrium cell, kept at constant temperature using a thermostatic bath, was filled with both CO_2 and O_2 until both liquid and vapor phases were present. A stirrer was used to mix the content to a stabilization of the temperature and pressure at their equilibrium values. The liquid and vapor phase CO_2 mole fractions at VLE were then the dependent variables. The temperature and pressure were measured. After stopping the stirrer, and waiting for the phases to settle according to density, samples of both the liquid and vapor phases were withdrawn from the cell to determine the VLE phase compositions. The samples were withdrawn using Rolsi^{TM} electromagnetic samplers (Armines patent [13]. Pneumatic version of the Rolsi^{TM} sampler described in [14]), one with the capillary inlet placed in the top of the vapor phase, and one placed in the liquid phase. Several samples were taken of both phases. The samples were analyzed using a gas chromatograph (GC) with helium as the carrier gas, calibrated against gravimetrically prepared calibration gas mixtures. To prevent a decrease in the cell pressure due to the removal of mass from the cell, a plate bellows placed inside the cell was expanded to decrease the cell volume when samples were withdrawn. The bellows could be expanded approximately 1 cm^3. The equilibrium cell consisted of a transparent sapphire cylinder placed between two titanium flanges, the internal cell volume being approximately 100 cm^3.

2.2. Calibration

The calibration of the temperature and pressure sensors performed in [1] was used in the present work. The calibration was performed in-house. The temperature sensors were calibrated against fixed point cells according to the International Temperature Scale of 1990 (ITS-90). The pressure sensors were calibrated against a recently calibrated dead weight tester. Details concerning the estimated temperature and pressure measurement uncertainties are given in Section 3.2 below, and discussed in detail in [1].

The GC was calibrated against calibration gas mixtures prepared in-house using our custom built apparatus for gravimetric preparation of mixtures. Details about the calibration gas mixtures and the calibration can be found in Section 3.3 below. The manufacturer's specification of the purities of these samples are given in Table 1. No additional analysis of the specified purities was performed.

2.3. Experimental procedures

2.3.1. General

The experimental procedures were quite similar to those of [1]. The complete procedure will be given here:

Before starting a VLE experiment, the whole circuit in connection with the VLE cell was evacuated, using the vacuum pump. The evacuation included the gas lines to the cell from the gas cylinders of pure CO_2 and O_2, and all lines transporting the gases into the cell.

The CO_2 pump and O_2 impurity pump and lines were first evacuated once, and then flushed with the respective gases to dilute any remaining impurities in the lines and pumps. This evacuation and flushing were repeated 5 times for each pump. After the final evacuation, the gases were filled onto their respective lines and pumps, and maintained at a pressure of at least 0.5 MPa to prevent contamination of the gases. After the flushing of the gas lines and pumps, the cell was flushed with CO_2, and evacuated. As with the pumps, the flushing and evacuation were repeated 5 times.

Following the flushing, and with the thermostatic bath kept at the desired temperature, CO_2 was injected until the volume fraction of liquid CO_2 was approximately 25% of the cell. The stirrer then ran until the measured pressure and temperature had stabilized. After the stirrer had been turned

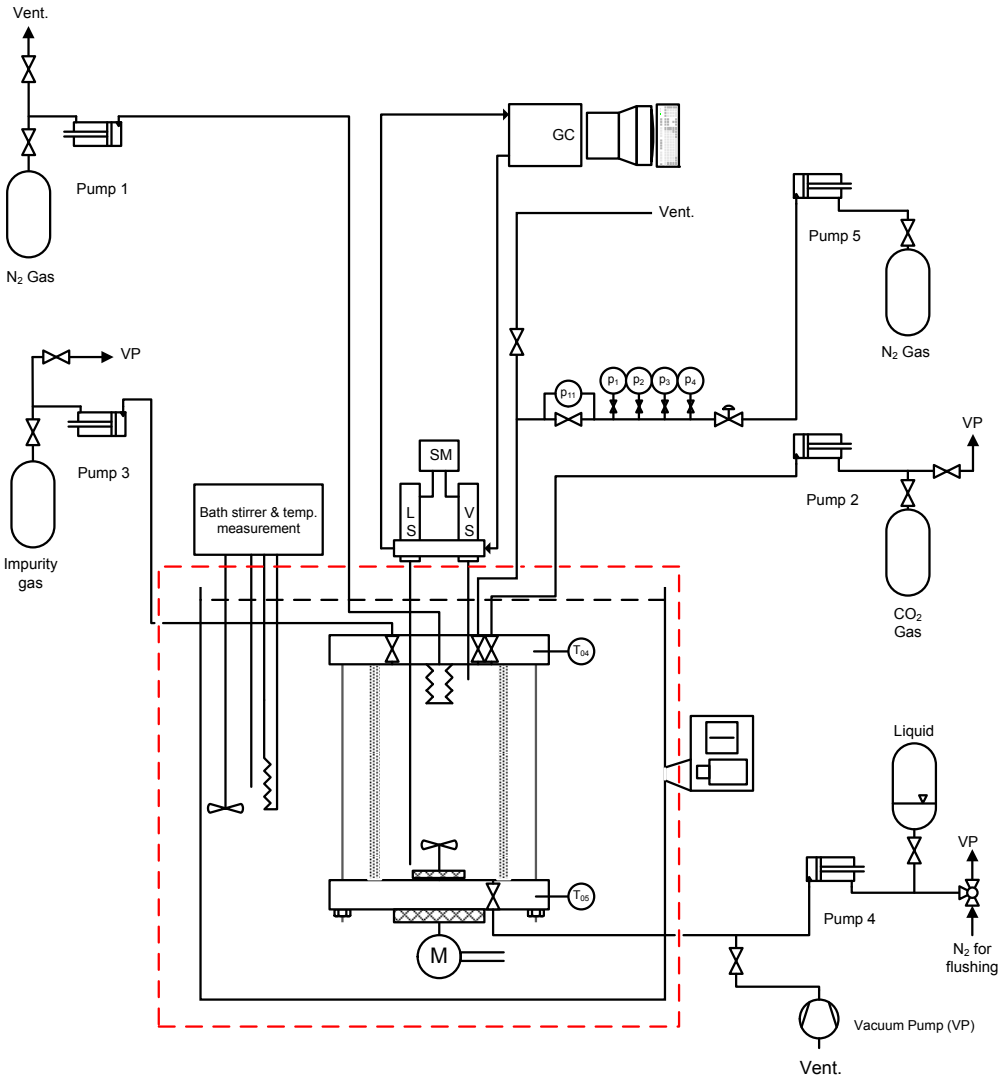

Fig. 1. Figure modified from [1]: Principal diagram of cell and ancillary apparatus. LS,VS: Liquid and vapor phase Rolsi^{TM} samplers, respectively. SM: Rolsi^{TM} controller. M: Gear for rotating permanent magnet below cell, which rotates stirrer inside cell. Gear connected to electric motor outside bath. T_{04}: Top flange SPRT. T_{05}: Bottom flange SPRT.

off, the vapor pressure of CO_2 was measured. If the measured vapor pressure were within the combined uncertainty of the Span-Wagner EOS [6] and our measurements, the purity of the CO_2 in the cell, and the accuracy of the current temperature and pressure measurements, were deemed to be sufficient.

After the CO_2 vapor pressure measurements, the stirrer was started and O_2 was filled onto the cell to increase the pressure. As part of the process of adjusting the pressure to the desired level, the volume fraction of liquid phase in the cell was adjusted to allow for as large as possible vapor samples, either by injecting more CO_2 or venting out some of the vapor or liquid phase. Based on VLE calculations using EOS-CG [3] for the CO_2+O_2 mixture, at constant temperature, as the pressure increased from the vapor pressure of CO_2 up to the critical pressure of the mixture, the difference between the densities of the liquid and vapor phases decreased: the density of the liquid phase decreased and that of the vapor phase increased, and ultimately approached the same value at the critical point. Taking this behavior into account, and considering the limitations of the stirrer size on the minimum liquid level, the liquid volume fraction was adjusted to around 25% for the VLE measurements at the lowest pressures at each temperature, and was gradually increased to around 50% for the measurements in the critical region.

When the pressure and temperature measurements had been stable for at least 20 min, the stirrer was turned off, and the vapor and liquid phases were left to settle before sampling started. The time allowed for settlement of the phases ranged from 30 min to 3 hours, depending on the proximity to the mixture critical pressure. At pressures between the CO_2 vapor pressure and the turning point in the vapor phase composition, the difference in densities of the liquid and vapor phase was quite large, and for these measurements we waited around 30 min for the phases to settle before sampling started. At pressures above the turning point in vapor phase composition, the settling time was increased to 1 hour.

When the pressure was increased to the point where it was observed that running the stirrer caused the phase boundary to disappear, the settling time was increased to 3 hours. At these pressures approaching the critical point, the small density difference of the phases necessitated these longer settling times. During the settling time, the borescope was used to take a picture of the cell content every 30 min. Immediately after the stirrer was turned off, both phases were cloudy white. After 2 hours, the phases were less cloudy, and it was not possible to see a difference in the opacity during the last of these three hours.

During the settling period, the borescope was withdrawn from the thermostatic bath immediately after use to prevent unintended heat transfer from the surroundings into the bath fluid. At the end of the settling period, the borescope was put in for a very short time to confirm the existence of a liquid and vapor phase, and a visual measurement of the volume occupied by the phases was performed.

After the settling period, first the liquid and then the vapor phase was sampled. Nominally, 7 samples were taken from each phase. Upon sampling, the bellows was expanded to compensate for the pressure drop. A sample was withdrawn from the cell every 25 min. For some of the series of liquid and vapor samples at a certain temperature and pressure, we were not able to take as much as 7 samples, as we reached the maximum expansion limit of the bellows.

The same methodology as in [1] was applied to determine the sample size necessary to flush the Rolsi^{TM} capillaries. The first sample from each phase was discarded as a flushing sample.

The pressure sensor readings were logged every second, and ratios of the temperature sensors were logged approximately every 20 seconds. The temperature and pressure measurements in the stable period before the first sample and until the last sample formed the data set for a VLE point measurement series. The treatment of these data sets is described in Section 3.4.

2.3.2. Critical region

At the temperatures 218.15, 233.14, 253.15 and 273.15 K, a special procedure was employed to perform measurements close to the critical point of the mixture at each temperature. In each of these measurement series at constant temperature and pressure, the removal of mass from the cell through the sampling lowered the equilibrium pressure for the following measurement series. This allowed for very small pressure steps compared to the general procedure described earlier, where CO_2 or O_2 was filled onto or removed from the cell using the pumps or the venting valve.

The procedure was as follows: The cell pressure was first increased to as close to the critical pressure as possible, while keeping the liquid volume fraction close to 50%. As mentioned earlier, the close proximity to the critical point was established by observing at which pressure the phases became indistinguishable when the stirrer was running. In addition, at this point the injection of very small amounts of either CO_2 or O_2 caused very large changes to the liquid phase volume

Table 1
Chemical samples used.

Chemical name	CASRN	Source	Initial mole fraction purity	Purification method	Final mole fraction purity	Analysis method
Carbon dioxide[a]	124-38-9	Yara Praxair/AGA	0.99999	None	0.99999	None
Oxygen[b]	7782-44-7	Yara Praxair	0.999999	None	0.999999	None
Helium[c]	7440-59-7	AGA	0.999999	None	0.999999	None

[a] Maximum specified impurity content by volume was less than 2 ppm H_2O, 1 ppm O_2, 5 ppm N_2, 1 ppm hydrocarbons C_nH_m and 1 ppm H_2.
[b] Maximum specified impurity content by volume was less than 0.5 ppm H_2O, 1 ppm N_2, 0.5 ppm Ar, 0.02 ppm methane CH_4, 0.1 ppm CO_2 and 0.2 ppm CO. Manufacturer's specification states that total impurity level was not above 1 ppm. [c] GC carrier gas.

fraction, as could be expected when the cell content was very close to the mixture critical point, but still in the two-phase region.

With the cell content in this state, at a pressure slightly below the critical pressure and with a liquid volume fraction of approximately 50%, the bellows was expanded slightly to increase the cell pressure. If the cell content was sufficiently close to the critical pressure before this pressure increase, the cell content would move out of the two-phase region into the supercritical region. With the stirrer running, this transition out of the two-phase region seemed to be discernible by the disappearance of a swirling motion of the cell content. At this state, it was not possible to observe any qualitative difference in the appearance of the cell content when the stirrer was running, compared to when it was stopped.

The bellows was then used to keep the cell pressure stable, and the stirrer was run for between 30 min and 2 hours, and then stopped. Given the possibility that the cell content could still be in the two-phase region, without any liquid-vapor phase boundary visible using the borescope, the cell content was allowed to settle for 2-3 hours.

Then, samples were withdrawn from the liquid and vapor phase, following the sampling procedure described earlier. After the sampling was finished, the stirrer was started, and the bellows was compressed by lowering the pressure on the bellows circuit. For the critical region measurements for the four temperatures mentioned earlier, the decrease in pressure brought the cell content back into the two-phase region, visible by the swirling motion of the cell content, and the separation of the content into a liquid and vapor phase when the stirrer was stopped.

With the bellows keeping the cell pressure constant at this new lowered pressure, the process of stirring and settling was repeated, and samples were withdrawn from both phases.

This procedure of starting at a pressure slightly into the supercritical region, and using the bellows to keep the pressure stable while samples were taken, and then repeating this at a lowered pressure using the bellows, allowed us to perform several VLE measurements very close to the critical point of the mixture. For each of the temperatures 218.15, 233.14, 253.15 and 273.15 K, this resulted in 2-3 VLE measurements very close to the critical point, and 1 pressure-temperature-composition state point in the supercritical region. Details concerning these measurements are presented in Sections 4 and 5.

3. Uncertainty analysis

3.1. Definitions

The terms and definitions in the "GUM" [11] is used in the uncertainty analysis. The uncertainties are evaluated as standard uncertainties, with symbol $u(y)$, where y is the estimate of the measurand Y. The propagation of the standard uncertainties in input quantities X_i into a final calculated value Y is described by the combined standard uncertainty, with symbol $u_c(y)$.

3.2. Pressure and temperature

A thorough analysis of the uncertainty of the pressure and temperature measurements was performed in [1], where VLE measurements of the CO_2+N_2 system were performed. The same methodology was used for the measurements in the present work, the only difference being that the density used in the hydrostatic pressure calculations was calculated using EOS-CG for CO_2+O_2 instead of CO_2+N_2. Only the resulting uncertainty estimates are given here. The details of the uncertainty analysis methodology can be found in [1].

The uncertainty components contributing to the standard uncertainty for the measured pressure p at VLE are summarized in Table 2, and the resulting standard uncertainties in the pressure measurements are shown in Fig. 2. Similarly, Table 3 and Fig. 3 show the contributors to and the resulting standard uncertainty in the measured temperatures T.

As seen from Fig. 2, the standard uncertainty in the pressure was estimated to be below 0.05% of the measured pressure except at the lowest pressure. Similarly, as seen from Tables 7 and 8 and Fig. 3, the standard uncertainty in the temperature was estimated to be below 8 mK, and the variation in temperature had been less than 5 mK.

Table 2
Summary of standard uncertainty components for pressure measurements, cf. Westman et al. [1].

Symbol	Description and unit	u
Hydrostatic pressure p_{hs}		
$u(\rho_1)$	EOS-CG[a] vapor density of CO_2+O_2 ($\mathrm{kg\,m^{-3}}$)	$1\cdot10^{-2}\cdot\rho_1$
$u(\rho_2)$	Same as $u(\rho_1)$ ($\mathrm{kg\,m^{-3}}$)	$1\cdot10^{-2}\cdot\rho_2$
$u(\rho_{4,1})$	SW[b] density at 313.15 K ($\mathrm{kg\,m^{-3}}$)	$3\cdot10^{-4}\cdot\rho_{4,1}$
$u(\rho_{4,2})$	Same as $u(\rho_1)$ ($\mathrm{kg\,m^{-3}}$)	$1\cdot10^{-2}\cdot\rho_{4,2}$
u(CAD)	(m)	0
$u_{\mathrm{c}}(h_1)$	(m)	0.0048
$u(h_{\mathrm{liq}})$	(m)	0.0048
$u(h_{\mathrm{liq}},1)$	Borescope h_{liq} (m)	0.0048
$u(h_{\mathrm{liq}},2)$	Variation in h_{liq} (m)	0
$u(h_2)$	Bath liquid level variation (m)	0.006
$u_{\mathrm{c}}(h_3)$	(m)	0.006
$u(h_4)$	Same as u(CAD) (m)	0
$u(g_{\mathrm{L}})$	Local g ($\mathrm{m\,s^{-2}}$)	$2\cdot10^{-7}$
Differential pressure p_{11}		
$u(p_{11},1)$	Ambient temperature (MPa)	0
$u(p_{11},2)$	Line pressure zero (MPa)	0
$u(p_{11},3)$	Line pressure span (MPa)	$4.9\cdot10^{-5}\,\mathrm{MPa^{-1}}\cdot p_i\cdot p_{11}$
$u(p_{11},4)$	Mounting (MPa)	0
$u(p_{11},5)$	Vibration (MPa)	$2.8\cdot10^{-5}$
$u(p_{11},6)$	Power supply (MPa)	0
$u(p_{11},7)$	A/D conversion (MPa)	$2.4\cdot10^{-4}$
Pressure sensors p_i		
$u(p_1)$	1 MPa sensor (MPa)	$2.24\cdot10^{-4}$
$u(p_2)$	3 MPa sensor (MPa)	$2.33\cdot10^{-4}$
$u(p_3)$	10 MPa sensor (MPa)	$7.64\cdot10^{-4}$
$u(p_4)$	20 MPa sensor (MPa)	$1.965\cdot10^{-3}$

[a] Gernert and Span [3] and Gernert [4] [b] Span and Wagner [6]

Table 3
Summary of standard uncertainty components for temperature measurements, cf. Westman et al. [1].

Symbol	Unit	u
$u(W_{\mathrm{b}})$	(-)	$0.35\cdot10^{-6}$
$u(R_{\mathrm{ref}})$	(Ω)	$8.5\cdot10^{-6}$
$u(T_{\mathrm{H_2O}})$	(mK)	0.51
$u(T_{\mathrm{Hg}})$	(mK)	1.43
$u(T_{\mathrm{Ga}})$	(mK)	0.85
$u(R_{\mathrm{H_2O}}(T_{04}))$	(Ω)	$3.94\cdot10^{-5}$
$u(R_{\mathrm{H_2O}}(T_{05}))$	(Ω)	$2.57\cdot10^{-5}$
$u(R_{\mathrm{Hg}}(T_{04}))$	(Ω)	$2.29\cdot10^{-5}$
$u(R_{\mathrm{Hg}}(T_{05}))$	(Ω)	$1.84\cdot10^{-5}$
$u(R_{\mathrm{Ga}}(T_{04}))$	(Ω)	$2.69\cdot10^{-5}$
$u(R_{\mathrm{Ga}}(T_{05}))$	(Ω)	$2.37\cdot10^{-5}$
$u(W_{\mathrm{Hg}}(T_{04}))$	(-)	$6.2\cdot10^{-6}$
$u(W_{\mathrm{Hg}}(T_{05}))$	(-)	$6.1\cdot10^{-6}$
$u(W_{\mathrm{Ga}}(T_{04}))$	(-)	$4.5\cdot10^{-6}$
$u(W_{\mathrm{Ga}}(T_{05}))$	(-)	$4.3\cdot10^{-6}$

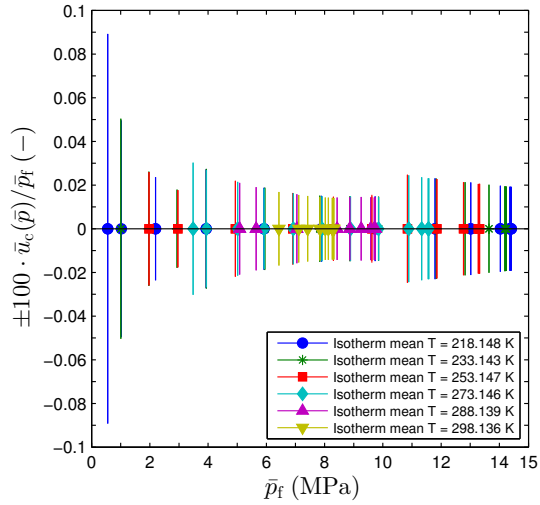

Fig. 2. Pressure standard uncertainty relative to the measured pressure for the VLE measurements performed, expressed as $100\cdot\bar{u}_{\mathrm{c}}(\bar{p})/\bar{p}_{\mathrm{f}}$. Measured pressure $\bar{p}_{\mathrm{f}}$. Standard uncertainty $\bar{u}_{\mathrm{c}}(\bar{p})$.

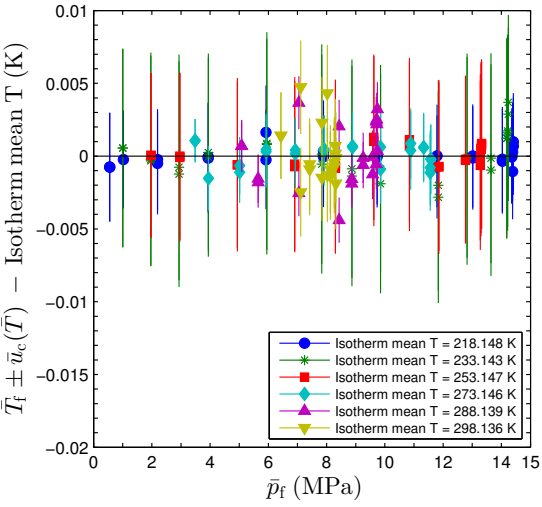

Fig. 3. Temperature deviations for each VLE measurement from isotherm mean temperature, and temperature standard uncertainty, expressed together as $\bar{T}_{\mathrm{f}}\pm\bar{u}_{\mathrm{c}}(\bar{T})$ - isotherm mean temperature, versus VLE experiment pressure $\bar{p}_{\mathrm{f}}$. VLE experiment mean temperature $\bar{T}_{\mathrm{f}}$. Temperature standard uncertainty $\bar{u}_{\mathrm{c}}(\bar{T})$.

Table 4
Molar masses of atomic elements and compounds with uncertainties [16, 17].

Component i	M_i	$u(M_i)$	Unit
C[a]	0.0120108	0.0000003	kg mol^{-1}
O[a]	0.01599938	0.00000007	kg mol^{-1}
O[b]	0.01599940	0.00000035	kg mol^{-1}
CO_2	0.0440096	0.0000003	kg mol^{-1}
O_2	0.03199880	0.00000070	kg mol^{-1}
CO_2+imp	0.0440094		kg mol^{-1}
O_2+imp	0.03199880		kg mol^{-1}
CO_2,eff	0.0440097		kg mol^{-1}
O_2,eff	0.03199881		kg mol^{-1}

[a] In CO_2 molecule [b] In O_2 molecule

3.3. Composition

The VLE phase composition analysis and uncertainty estimation were performed in the same manner as in [1], with the methodology applied to CO_2+O_2 samples instead of CO_2 +N_2. A summary will be provided here, with reference to [1] for further details.

The composition analysis was performed using the same GC as in [1], with its calibration performed using gravimetrically prepared gas mixtures using a custom-built rig in our laboratories [15].

For the measurement method utilized in the present work, it could be stated that the composition uncertainty stemmed from a range of sources, including the impurities of the gases used to prepare the calibration mixtures, the uncertainty in the molar masses, inaccuracies in the weighed masses, adsorption, repeatability / uncertainties of the sampling and GC analysis, and finally the consistency between the GC calibration function and data. The analysis of these contributing factors are given below.

3.3.1. Source gas composition and molar mass

The composition and the corresponding uncertainty of a gravimetrically prepared gas mixture are results of both the purity and the molar mass of the source gases used for the mixture. According to [16, 17], the molar masses of monoatomic carbon C, monoatomic oxygen O in commercial tank gas CO_2 and monoatomic oxygen O in commercial tank gas O_2 generally lie within ranges of width 0.6, 0.15, and 0.7 mg mol^{-1}, respectively. Based on this, the molar masses of CO_2 and O_2, M_{CO_2} and M_{O_2} respectively, were calculated with the corresponding uncertainty estimates shown in Table 4.

The minimum certified purities of the CO_2 and O_2 source gases used to prepare the calibration gas mixtures are given in Table 1, together with the manufacturers' specifications of the maximum content of certain impurities. Since the source gases were not entirely pure, estimates for the molar masses of the source gases, M_{CO_2+imp} and M_{O_2+imp}, should account for the impurities present, following the procedure used in [1].

M_{CO_2+imp} and M_{O_2+imp} were calculated based on the impurity specifications stated in Table 1. The molar mass of each impurity was calculated using data from Wieser et al. [17], assuming methane CH_4 for the hydrocarbon impurity fraction. The molar masses of the source gases, M_{CO_2+imp} and M_{O_2+imp}, together with the effective molar masses of the source gases excluding the impurities, $M_{CO_2,eff}$ and $M_{O_2,eff}$, are shown in Table 4.

3.3.2. Gravimetric preparation

The methodology of gravimetric preparation of the calibration gas mixtures and the uncertainty estimation given in [1, 15] was used in the present work. To summarize the determination of the final composition of the gas mixtures, the mass of each source gas including impurities in the gravimetrically prepared gas mixture, m_{i+imp}, was converted into moles of the primary components CO_2 and O_2 excluding impurities, n_i, as

$$n_i = m_{i+imp}/M_{i,eff}\,, \tag{1}$$

with the mole fraction of CO_2 in the gravimetrically prepared gas mixture expressed as

$$y_{CO_2,cal} = \frac{n_{CO_2}}{n_{CO_2} + n_{O_2}}\,. \tag{2}$$

Six CO_2+O_2 calibration gas mixtures were made, spanning in CO_2 mole fractions $y_{CO_2,cal}$ from 0.13 to 0.95. An overview of the mixtures is given in Table 5.

3.3.3. Composition calibration procedure and estimated composition uncertainty

The calibration of the GC was performed as described in Appendix A.3.1 in [1], with the measures described to prevent adsorption of the gas onto the contact surfaces. In short, each calibration gas was filled onto the VLE cell after thorough evacuation and flushing with the calibration gas at 0.5 MPa, keeping the impurity pump, gas lines and cell at 313 K to ensure that the calibration gas was kept in a uniform supercritical state. Samples of varying sizes were withdrawn from the cell at different pressures between 5 and 10 MPa. These samples formed the calibration basis for the composition analysis, establishing a relation between the CO_2 mole fractions of the calibration gas mixtures and the GC detector response.

The uncertainty contribution from the calibration mixture uncertainty reaching the GC could be estimated as

$$u_c(y_{CO_2,cal}) = \sqrt{u^2(y_{CO_2,cal}, m) + u^2(y_{CO_2,cal}, M_{eff}) + u^2(y_{CO_2,cal}, \text{ads.})}\,, \tag{3}$$

Table 5
CO_2+O_2 calibration gas mixtures: CO_2 mole fractions and corresponding standard uncertainties.

$y_{CO_2,cal}$	$u(y_{CO_2,cal}, m)$	$u(y_{CO_2,cal}, M_{eff})$	$u(y_{CO_2,cal}, \text{ads.})$	$u_c(y_{CO_2,cal})$
0.131144	$2.7 \cdot 10^{-6}$	$17.4 \cdot 10^{-6}$	$1.4 \cdot 10^{-6}$	$17.6 \cdot 10^{-6}$
0.303027	$2.1 \cdot 10^{-6}$	$11.2 \cdot 10^{-6}$	$3.3 \cdot 10^{-6}$	$11.9 \cdot 10^{-6}$
0.549780	$2.6 \cdot 10^{-6}$	$5.4 \cdot 10^{-6}$	$5.9 \cdot 10^{-6}$	$8.4 \cdot 10^{-6}$
0.686269	$1.4 \cdot 10^{-6}$	$4.9 \cdot 10^{-6}$	$7.3 \cdot 10^{-6}$	$8.9 \cdot 10^{-6}$
0.898418	$5.1 \cdot 10^{-6}$	$7.4 \cdot 10^{-6}$	$9.7 \cdot 10^{-6}$	$13.2 \cdot 10^{-6}$
0.945826	$2.4 \cdot 10^{-6}$	$8.2 \cdot 10^{-6}$	$10.1 \cdot 10^{-6}$	$13.3 \cdot 10^{-6}$

where $u(y_{CO_2,cal}, m)$ and $u(y_{CO_2,cal}, M_{eff})$ are the contributing uncertainties stemming from the uncertainties in the masses of CO_2 and O_2 in the gas mixture and the uncertainties in the effective molar masses, respectively. These terms are described in detail in Appendix A.3 of [1]. The last term in Eq. (3), $u(y_{CO_2,cal}, ads.)$, is the contributing uncertainty from adsorption, and was estimated assuming that CO_2 is adsorbed at a higher degree than O_2, in the same way as in [1]. The uncertainty estimates used in Eq. (3) are given in Table 5.

As seen in Table 5, the uncertainty contribution from the molar mass of O_2 caused $u(y_{CO_2,cal}, M_{eff})$ to dominate the combined standard uncertainty of the CO_2 mole fraction $u_c(y_{CO_2,cal})$ for the gas mixtures with the highest O_2-content. For the mixtures with the highest CO_2-content, the uncertainty contribution from the adsorption of CO_2 was the dominating factor. The uncertainty contribution from the adsorption was for all the mixtures of the same order as the two other contributing factors, and as in [1], the uncertainty of the CO_2 mole fractions of the calibration gases, $u_c(y_{CO_2,cal})$, would have to be orders of magnitude larger to be of significance for the final uncertainty in the VLE composition data. As the discussion in the following section will show, the reason for this was that the main contributor to this final uncertainty was the calibration function error.

3.3.4. GC integration and calibration function

The GC column, method and detector used for CO_2+N_2 samples in [1] were utilized on CO_2+O_2 samples in the present work, with helium as the GC carrier gas. This setup gave just as good separation of the CO_2 and O_2 peaks in the GC chromatogram as in [1] for CO_2 and N_2. The areas under the CO_2 and O_2 peaks in the chromatogram, denoted A_{CO_2} and A_{O_2}, were obtained for each sample by numerical integration. The GC thermal conductivity detector (TCD) response was nonlinear with respect to the number of moles of CO_2 and O_2 passing through the detector. The following model, consisting of both linear and nonlinear terms, described adequately the relation between moles of each component in the sample to the area of each component:

$$\hat{n}_{CO_2} \cdot k = A_{CO_2} + (A_{CO_2})^{c_1} + (A_{CO_2})^{c_2} , \quad (4)$$

$$\hat{n}_{O_2} \cdot k = c_3 \cdot \left(A_{O_2} + (A_{O_2})^{c_4} + (A_{O_2})^{c_5}\right) , \quad (5)$$

$$\hat{y}_{CO_2,cal} = \frac{\hat{n}_{CO_2}}{\hat{n}_{CO_2} + \hat{n}_{O_2}} , \quad (6)$$

where $\hat{y}_{CO_2,cal}$ is the estimator of the CO_2 mole fraction of a calibration gas mixture sample given the areas for that sample, and k is an unknown factor relating the areas to the number of moles.

The parameters c_i for $i = 1$ through 5 were fitted by performing a weighted least squares minimization of the objective function S described by Eq. (A.32) in [1]. The mean values of the estimator, $\bar{\hat{y}}_{CO_2,cal}$, calculated for each of the $n = 62$ series, with each series consisting of 6-9 valid samples, were fitted against the calibration mixture mole fractions, $y_{CO_2,cal}$, which resulted in the parameter estimates found in Table 6. As shown in Fig. 4, the errors between the calibration gas CO_2 mole fractions and the model predictions, $e = y_{CO_2,cal} - \bar{\hat{y}}_{CO_2,cal}$, were randomly scattered around zero over the composition range $y_{CO_2,cal}$, which indicated an appropriate model structure. The sample standard deviation of the errors, $s(e)$, are also given in Table 6. This model was used to convert the areas resulting from the analysis of a composition sample taken during a VLE experiment into a CO_2 mole fraction.

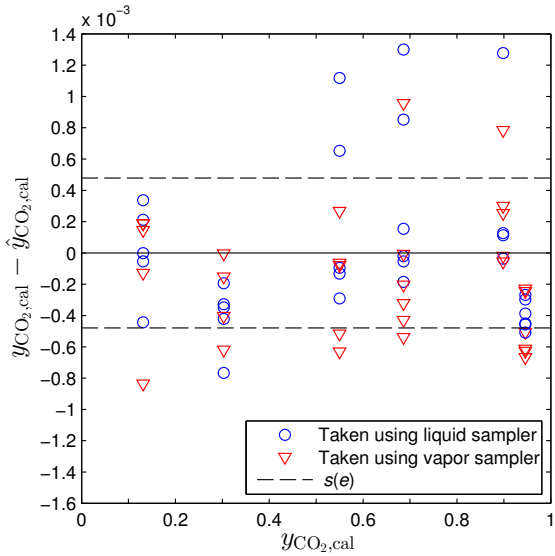

Fig. 4. Composition calibration: Error between actual compositions in Table 5 and composition model in Eq. (6), given as $y_{CO_2,cal} - \hat{y}_{CO_2,cal}$ versus $y_{CO_2,cal}$. Composition analysis uncertainty $u(x_{CO_2}) = u(y_{CO_2}) = s(e)$ from Table 6.

For the same reasons as described in [1], it was assumed that the standard uncertainty of the CO_2 mole fraction of samples taken during VLE measurements, $u(x_{CO_2}) = u(y_{CO_2})$, was estimated by $s(e)$, which was 25-60 times larger than the standard uncertainties in the mole fractions of the calibration mixtures, $y_{CO_2,cal}$. It must be emphasized that this estimate only accounts for the uncertainty caused by the composition analysis of the samples. All other reasons that could cause the sample to not represent the actual VLE composition are not accounted for in this estimate, and these contributors could only be minimized by the measures described in Section 2.3 and in [1].

3.3.5. Total uncertainty in liquid and vapor phase mole fractions x_{CO_2} and y_{CO_2}

For a given VLE measurement, the uncertainty of T and p contributed to additional uncertainty in the composition, giving the following total standard uncertainty of the com-

position:

$$u_{\mathrm{tot}}(z_{\mathrm{CO_2}}) = \sqrt{u^2(z_{\mathrm{CO_2}}) + \left(u_{\mathrm{c}}(\bar{T}) \cdot \frac{\partial z_{\mathrm{CO_2}}}{\partial T}\right)^2 + \left(u_{\mathrm{c}}(\bar{p}) \cdot \frac{\partial z_{\mathrm{CO_2}}}{\partial p}\right)^2} \quad (7)$$

where $z_{\mathrm{CO_2}}$ was equal to either $x_{\mathrm{CO_2}}$ or $y_{\mathrm{CO_2}}$, and the temperature and pressure uncertainties $u_{\mathrm{c}}(\bar{T})$ and $u_{\mathrm{c}}(\bar{p})$ are described in Section 3.4 and in [1]. Similar to [1], the derivatives in Eq. (7) were, in general, calculated numerically from the PR-MC-WS-NRTL Case 2 EOS fitted to our data. Details about this EOS are explained in Section 5.4.2. For the VLE measurements in the critical region used to fit the scaling law in Section 5.3, the derivatives with respect to pressure, $\partial z_{\mathrm{CO_2}}/\partial p$, were calculated analytically from the fitted scaling law in Eq. (13), as this gave better estimates for the derivatives than the PR-MC-WS-NRTL Case 2 EOS in this region. Details concerning the scaling law are given in Section 5.3.

3.4. Data reduction

As described in Section 2.3, the drop in cell pressure after each composition sample was compensated using the bellows to decrease the cell volume. For the VLE measurements in this work, the cell pressure was in most cases back at its original value after around 1-3 min, and for a few of the measurements after around 5 min. After the cell pressure was back to its stable value, it remained stable for the remaining 20-24 min until the next sample was withdrawn.

In each series of either consecutive liquid or vapor phase composition samples, $x_{\mathrm{CO_2}}$ or $y_{\mathrm{CO_2}}$, at a nominal temperature and pressure, it was assumed that each composition sample represented the equilibrium composition at the temperature and pressure just before the sample was withdrawn from the cell. These temperature and pressure values, denoted $\bar{T}$ and $\bar{p}$, respectively, were assumed to be represented by the temperature and pressure measurements averaged over the last 75% of the time period between the previous and the current composition sample. As in [1], the bellows was able to stabilize the cell pressure sufficiently fast after each sample withdrawal, and it was not possible to see any systematic trends in the temperature or pressure during these time periods. It was also not possible to see any temperature variations caused by the removal of mass from the cell in the composition sampling.

Table 6
Fitted parameters of the $\tilde{y}_{\mathrm{CO_2,cal}}$ model and standard uncertainty of composition analysis $u(x_{\mathrm{CO_2}}) = u(y_{\mathrm{CO_2}})$.

Variable	Value
c_1	0.899 902
c_2	1.154 287
c_3	1.270 181
c_4	1.155 333
c_5	0.914 593
$u(x_{\mathrm{CO_2}}) = u(y_{\mathrm{CO_2}}) = s(e)$	$4.7894 \cdot 10^{-4}$
n	62

For each of these series of samples, the arithmetic mean values of the temperature, pressure, liquid and vapor phase compositions were calculated, denoted as $\bar{T}_{\mathrm{f}}$, $\bar{p}_{\mathrm{f}}$, $\bar{x}_{\mathrm{CO_2}}$ and $\bar{y}_{\mathrm{CO_2}}$, respectively. The subscript f is used to differentiate between the temperature and pressure values associated with each composition sample $x_{\mathrm{CO_2}}$ or $y_{\mathrm{CO_2}}$, and of those associated with the average compositions $\bar{x}_{\mathrm{CO_2}}$ or $\bar{y}_{\mathrm{CO_2}}$.

Details about the methodology for describing and calculating the propagation of the uncertainty in the measured variables T, p, $x_{\mathrm{CO_2}}$ and $y_{\mathrm{CO_2}}$ into resulting estimates associated with each composition sample are given in [1], and the symbols used are summarized in Table A.1 together with the data for the individual composition samples.

The propagation of uncertainty from the data of an individual sample, $\bar{T}$, $\bar{p}$, $x_{\mathrm{CO_2}}$ or $y_{\mathrm{CO_2}}$, into the mean values for a series of samples, $\bar{T}_{\mathrm{f}}$, $\bar{p}_{\mathrm{f}}$, $\bar{x}_{\mathrm{CO_2}}$ or $\bar{y}_{\mathrm{CO_2}}$, is defined by:

$$u_{\mathrm{c}}(\bar{T}_{\mathrm{f}}) = \sqrt{s^2(\bar{T}_{\mathrm{f}}) + \bar{u}_{\mathrm{c}}(\bar{T})^2}\,, \quad (8)$$

$$u_{\mathrm{c}}(\bar{p}_{\mathrm{f}}) = \sqrt{s^2(\bar{p}_{\mathrm{f}}) + \bar{u}_{\mathrm{c}}(\bar{p})^2}\,, \quad (9)$$

$$u_{\mathrm{c}}(\bar{x}_{\mathrm{CO_2}}) = \sqrt{s^2(\bar{x}_{\mathrm{CO_2}}) + \bar{u}_{\mathrm{tot}}(x_{\mathrm{CO_2}})^2}\,, \quad (10)$$

$$u_{\mathrm{c}}(\bar{y}_{\mathrm{CO_2}}) = \sqrt{s^2(\bar{y}_{\mathrm{CO_2}}) + \bar{u}_{\mathrm{tot}}(y_{\mathrm{CO_2}})^2}\,, \quad (11)$$

where $\bar{u}_{\mathrm{c}}(\bar{T})$, $\bar{u}_{\mathrm{c}}(\bar{p})$, $\bar{u}_{\mathrm{tot}}(x_{\mathrm{CO_2}})$ and $\bar{u}_{\mathrm{tot}}(y_{\mathrm{CO_2}})$ are calculated as the means of $u_{\mathrm{c}}(\bar{T})$, $u_{\mathrm{c}}(\bar{p})$, $u_{\mathrm{tot}}(x_{\mathrm{CO_2}})$ and $u_{\mathrm{tot}}(y_{\mathrm{CO_2}})$ in each series, respectively. The sample standard deviations of the mean $s(\bar{z})$ were calculated according to the standard formula:

$$s(\bar{z}) = \frac{1}{\sqrt{n}} \sqrt{\sum_{i=1}^{n} \frac{(z_i - \bar{z})^2}{n-1}}\,, \quad (12)$$

where $\bar{z} = \bar{T}_{\mathrm{f}}$, $\bar{p}_{\mathrm{f}}$, $\bar{x}_{\mathrm{CO_2}}$ or $\bar{y}_{\mathrm{CO_2}}$.

4. Results

VLE measurements at the average temperatures 218.15, 233.14, 253.15, 273.15, 288.14 and 298.14 K were conducted, spanning from close to the triple point temperature (216.59 K) to close to the critical temperature of CO_2 (304.13 K), and covered pressures from the vapor pressure of CO_2 up to close to the critical point at each temperature.

The temperature $\bar{T}$, pressure $\bar{p}$ and mole fractions for the liquid phase $x_{\mathrm{CO_2}}$ and the vapor phase $y_{\mathrm{CO_2}}$ for each individual sample are given in Tables A.2 and A.3, together

with their uncertainty estimates. The composition derivatives with respect to pressure, $\partial x_{CO_2}/\partial p$ and $\partial y_{CO_2}/\partial p$, and the total standard uncertainties in the composition of the samples, $u_{tot}(x_{CO_2})$ and $u_{tot}(y_{CO_2})$, which were calculated using the scaling law in Section 5.3, are identified in Tables A.2 and A.3 using the marker symbol $^+$.

The data for each series of samples are given at mean temperature $\bar{T}_f$, mean pressure $\bar{p}_f$ and mean mole fractions for the liquid phase $\bar{x}_{CO_2}$ and the vapor phase $\bar{y}_{CO_2}$ in Tables 7 and 8. These averaged data are plotted with the uncertainties in composition and pressure in Figs. 5a to 5f. The relative volatilities based on the measured data are plotted in Figs. B.1a to B.1f. The means of the total standard uncertainties of the mole fractions, $\bar{u}_{tot}(x_{CO_2})$ and $\bar{u}_{tot}(y_{CO_2})$, and the final standard uncertainties of the mole fractions, $u_c(\bar{x}_{CO_2})$ and $u_c(\bar{y}_{CO_2})$, which were calculated using the scaling law in Section 5.3, are identified in Tables 7 and 8 using the marker symbol $^+$.

As discussed in Section 2.3.2, a special procedure was used to obtain VLE measurements close to the critical point at the temperatures 218.15, 233.14, 253.15 and 273.15 K. Four pressure-temperature-composition state points in the supercritical region were obtained, consisting of 4 pairs of composition sample series taken using both the liquid and vapor phase samplers. The individual sample data are given in Table A.4, and the average values for each series can be found in Table 9. The VLE points obtained using this procedure are identified in Tables A.2, A.3, 7 and 8. These VLE and supercritical measurements will be discussed in detail in Section 5.3.

5. Analysis and discussion

5.1. Summary and analysis of uncertainty estimates

With reference to Table 7, the maximum and average sample standard deviation of the liquid phase mole fractions, $s(\bar{x}_{CO_2})$, were $1.3 \cdot 10^{-4}$ and $1.2 \cdot 10^{-5}$, respectively. Similarly, for the vapor phase mole fractions in Table 8, the maximum and average $s(\bar{y}_{CO_2})$ were respectively $1.2 \cdot 10^{-4}$ and $2.5 \cdot 10^{-5}$. Some of the vapor phase points at the lowest pressures at each temperature showed increase in these standard deviations, as could be expected by the high VLE composition sensitivity to pressure changes. Also, there seemed to be a slight increase in the standard deviations for some of the VLE points at the highest pressures. Inspecting the composition sample data for these points in Tables A.2 and A.3, the liquid and vapor phase mole fractions were respectively increasing and decreasing slightly throughout the series. This could imply that VLE had not been achieved completely or more likely, that the separation of the phases was incomplete, even though the settling times had been increased significantly for these measurements at close proximity to the critical point, as described in Section 2.3. It can be noted that the observed variations did not exceed the estimated uncertainty of the composition analysis, $4.8 \cdot 10^{-4}$ from Table 6. However, if the cause for the variations was incomplete settling, there is a possibility that the actual VLE compositions are outside the values covered by the composition analysis uncertainty.

The mean standard uncertainty in the phase mole fractions caused by the composition analysis and the temperature and pressure uncertainties described in Section 3.3.5, $\bar{u}_{tot}(z_{CO_2})$ where $z_{CO_2} = x_{CO_2}$ or y_{CO_2}, increased as a function of pressure at each temperature. At pressures close to the critical points, where the scaling law was used to estimate the VLE composition sensitivity to pressure, $\partial z_{CO_2}/\partial p$, $\bar{u}_{tot}(z_{CO_2})$ was $3.1 \cdot 10^{-3}$ at its maximum. For the series outside the critical region, $\bar{u}_{tot}(z_{CO_2})$ was close to the composition analysis uncertainty, $4.8 \cdot 10^{-4}$, as the uncertainties in pressure and temperature did not contribute significantly.

The final standard uncertainty of the mole fractions, $u_c(\bar{z}_{CO_2})$, combining $s(\bar{z}_{CO_2})$ and $\bar{u}_{tot}(z_{CO_2})$ described above, was maximum $3.1 \cdot 10^{-3}$ for the series in the critical region, and approximately $5 \cdot 10^{-4}$ for the series outside the critical region.

As can be seen in Tables A.2 and A.3, the combined standard uncertainty of the measured temperatures, $u_c(\bar{T})$, was below 8 mK for all samples, and around 4 mK on average. The combined standard uncertainty of the measured pressures, $u_c(\bar{p})$, ranged from 0.5 kPa at the lowest measured pressure 0.56 MPa (0.09%) to 3 kPa at the highest measured pressure 14.4 MPa (0.02%).

5.2. Comparison with literature data

The literature data reviews in [2, 3, 4, 5] provided in total five works reporting isothermal analytic VLE measurements [18, 20, 19, 25, 26] and two works reporting synthetic VLE measurements [21, 22]. The work by [26] from 2009 contained isothermal VLE measurements at 240.9 K, and apart from this the other works were from 1972 or earlier. In addition, two works reporting synthetic VLE measurements were found, one from 1903 [23] and the other from 2014 [24]. A summary of these literature data is given in Table 10.

Literature data at temperatures comparable to our measurements [18, 20, 19, 22, 23, 21, 24] are plotted together with our data in Figs. 5a to 5f.

At 218.15 K, the bubble point data by Zenner and Dana [18] were in very good agreement with our measurements, while their dew point data showed increasing deviations with our data as the pressure increased. Our three dew and bubble point pairs at the highest pressures close to the critical point cover a region previously not measured.

The data by Zenner and Dana [18] at 232.88 K were at a slightly lower temperature than our data at 233.14 K, but the data should be comparable as the temperature sensitivity of the VLE compositions are relatively low at these temperatures (cf. Tables A.2 and A.3). Like at 218.15 K, the bubble points by Zenner and Dana [18] were in good agreement with our data. However, their dew point data showed much more scatter than our data, and only about half of their data points agreed well with our data. Our three VLE data

Table 7
Liquid phase: Experimental VLE data for CO_2 (1) + O_2 (2) at mean temperature $\bar{T}_f$, mean pressure $\bar{p}_f$, and mean liquid phase mole fraction $\bar{x}_{CO_2}$[a].

	Data			Temperature			Pressure			Composition			
ID	$\bar{T}_f$ (K)	$\bar{p}_f$ (MPa)	$\bar{x}_{CO_2}$ (-)	$s(\bar{T}_f)$ (K)	$\bar{u}_c(\bar{T})$ (K)	$u_c(\bar{T}_f)$ (K)	$s(\bar{p}_f)$ (MPa)	$\bar{u}_c(\bar{p})$ (MPa)	$u_c(\bar{p}_f)$ (MPa)	$s(\bar{x}_{CO_2})$ (-)	$\bar{u}_{tot}(x_{CO_2})$ (-)	$u_c(\bar{x}_{CO_2})$ (-)	$x_{CO_2,calc}$ (-)
P1	218.147	0.5546[b]	0.99999	7.3e-5	3.7e-3	3.7e-3	1.1e-6	4.9e-4	4.9e-4				
L1	218.148	2.1957	0.96687	2.0e-4	3.5e-3	3.5e-3	9.5e-6	5.2e-4	5.2e-4	4.8e-6	4.8e-4	4.8e-4	0.96887
L2	218.148	3.9362	0.92958	7.8e-5	3.7e-3	3.7e-3	1.9e-5	1.1e-3	1.1e-3	3.8e-6	4.8e-4	4.8e-4	0.93250
L3	218.148	5.9189	0.88226	4.3e-4	3.4e-3	3.4e-3	6.8e-6	1.1e-3	1.1e-3	3.5e-6	4.8e-4	4.8e-4	0.88563
L4	218.149	7.8935	0.82832	1.7e-4	3.5e-3	3.5e-3	5.0e-6	1.2e-3	1.2e-3	4.8e-6	4.8e-4	4.8e-4	0.83104
L5	218.148	9.7335	0.76941	9.8e-5	3.4e-3	3.4e-3	5.5e-6	1.4e-3	1.4e-3	3.0e-6	4.8e-4	4.8e-4	0.76955
L6	218.148	11.7910	0.68723	1.3e-4	3.5e-3	3.5e-3	1.0e-5	2.7e-3	2.7e-3	5.3e-6	5.0e-4	5.0e-4	0.67972
L7	218.148	13.0212	0.61994	1.4e-4	3.5e-3	3.5e-3	1.3e-5	2.8e-3	2.8e-3	7.2e-6	5.2e-4	5.2e-4	0.60470
L8	218.148	14.0358	0.53329	1.6e-4	3.6e-3	3.6e-3	2.0e-5	2.8e-3	2.8e-3	2.5e-5	6.0e-4[+]	6.0e-4[+]	0.51002
L9[*]	218.148	14.3563	0.47535	1.2e-4	3.3e-3	3.3e-3	1.3e-5	2.8e-3	2.8e-3	5.0e-6	9.8e-4[+]	9.8e-4[+]	0.45826
L10[*]	218.148	14.3873	0.46440	1.2e-4	3.4e-3	3.4e-3	1.7e-5	2.8e-3	2.8e-3	5.4e-6	1.3e-3[+]	1.3e-3[+]	0.45116
L11[*]	218.149	14.4111	0.45232	2.1e-4	3.3e-3	3.3e-3	1.6e-5	2.8e-3	2.8e-3	2.4e-5	1.9e-3[+]	1.9e-3[+]	0.44512
P2	233.143	1.0048[c]	0.99999	7.4e-5	6.8e-3	6.8e-3	1.1e-5	5.1e-4	5.1e-4				
L13	233.142	1.9677	0.98023	1.1e-4	7.2e-3	7.2e-3	8.4e-6	5.1e-4	5.1e-4	8.9e-5	4.8e-4	4.9e-4	0.98262
L14	233.141	2.9345	0.96020	5.5e-5	7.8e-3	7.8e-3	2.3e-5	5.3e-4	5.3e-4	4.4e-6	4.8e-4	4.8e-4	0.96410
L15	233.143	3.9408	0.93829	2.3e-4	6.8e-3	6.8e-3	4.4e-5	1.1e-3	1.1e-3	4.6e-6	4.8e-4	4.8e-4	0.94358
L16	233.143	5.9477	0.89067	2.6e-4	7.3e-3	7.3e-3	7.2e-6	1.1e-3	1.1e-3	3.0e-6	4.8e-4	4.8e-4	0.89803
L17	233.143	7.8334	0.84017	2.0e-4	7.5e-3	7.5e-3	9.7e-6	1.2e-3	1.2e-3	3.5e-6	4.8e-4	4.8e-4	0.84775
L18	233.142	8.8724	0.80939	6.0e-4	7.5e-3	7.5e-3	9.4e-6	1.3e-3	1.3e-3	1.8e-5	4.8e-4	4.8e-4	0.81577
L19	233.142	9.8514	0.77736	3.3e-4	7.1e-3	7.1e-3	1.1e-5	1.4e-3	1.4e-3	8.9e-6	4.8e-4	4.8e-4	0.78187
L20	233.140	11.8341	0.69897	1.5e-4	7.3e-3	7.3e-3	8.8e-6	2.7e-3	2.7e-3	4.8e-6	5.0e-4	5.0e-4	0.69628
L21	233.142	12.8248	0.64711	1.2e-4	6.9e-3	6.9e-3	8.7e-6	2.7e-3	2.7e-3	7.7e-6	5.1e-4	5.1e-4	0.63897
L22	233.142	13.6445	0.58762	5.2e-4	7.2e-3	7.2e-3	9.3e-6	2.8e-3	2.8e-3	7.4e-6	5.4e-4[+]	5.4e-4[+]	0.57569
L23[*]	233.144	14.1868	0.51081	7.8e-5	6.9e-3	6.9e-3	1.0e-5	2.8e-3	2.8e-3	3.2e-6	9.7e-4[+]	9.7e-4[+]	0.51244
L24[*]	233.144	14.2158	0.50044	9.6e-5	6.7e-3	6.7e-3	1.7e-5	2.8e-3	2.8e-3	4.4e-6	1.3e-3[+]	1.3e-3[+]	0.50771
L25[*]	233.146	14.2407	0.48640	2.5e-4	6.0e-3	6.0e-3	1.1e-5	2.8e-3	2.8e-3	4.3e-6	2.4e-3[+]	2.4e-3[+]	0.50339
P3	253.147	1.9699[d]	0.99999	1.5e-5	5.7e-3	5.7e-3	5.5e-6	5.1e-4	5.1e-4				
L27	253.146	2.9632	0.97899	1.3e-4	5.8e-3	5.8e-3	2.9e-5	5.2e-4	5.2e-4	1.3e-5	4.8e-4	4.8e-4	0.98167
L28	253.146	4.9365	0.93518	1.2e-4	6.0e-3	6.0e-3	9.4e-5	1.1e-3	1.1e-3	2.6e-6	4.8e-4	4.8e-4	0.94105
L29	253.146	6.9081	0.88640	1.9e-4	6.0e-3	6.0e-3	4.4e-5	1.1e-3	1.1e-3	9.5e-6	4.8e-4	4.8e-4	0.89327
L30	253.146	8.3058	0.84783	1.4e-4	5.9e-3	5.9e-3	1.3e-5	1.2e-3	1.2e-3	5.2e-6	4.8e-4	4.8e-4	0.85331
L31	253.148	9.6226	0.80640	1.3e-4	5.7e-3	5.7e-3	3.9e-4	1.5e-3	1.5e-3	8.4e-6	4.8e-4	4.8e-4	0.80906
L32	253.147	10.8463	0.76222	1.4e-4	5.8e-3	5.8e-3	4.3e-5	2.7e-3	2.7e-3	7.7e-6	4.9e-4	4.9e-4	0.75948
L33	253.146	11.8557	0.71747	9.3e-5	6.0e-3	6.0e-3	2.5e-5	2.7e-3	2.7e-3	8.3e-6	5.0e-4	5.0e-4	0.70866
L34	253.146	12.7678	0.66173	8.9e-5	5.7e-3	5.7e-3	3.6e-5	2.7e-3	2.7e-3	6.6e-6	5.2e-4[+]	5.2e-4[+]	0.64728
L35[*]	253.146	13.2762	0.59988	1.2e-4	5.7e-3	5.7e-3	1.7e-5	2.7e-3	2.7e-3	8.6e-6	8.8e-4[+]	8.8e-4[+]	0.59446
L36[*]	253.147	13.3024	0.59165	1.1e-4	5.8e-3	5.8e-3	1.8e-5	2.7e-3	2.7e-3	1.7e-5	1.1e-3[+]	1.1e-3[+]	0.59060
L37[*]	253.147	13.3201	0.58371	1.2e-4	5.8e-3	5.8e-3	5.7e-5	2.7e-3	2.7e-3	1.6e-5	1.6e-3[+]	1.6e-3[+]	0.58784
P4	273.147	3.4848[e]	0.99999	2.4e-5	1.5e-3	1.5e-3	9.9e-7	1.1e-3	1.1e-3				
L39	273.145	5.0161	0.96558	8.5e-5	2.0e-3	2.0e-3	2.2e-5	1.1e-3	1.1e-3	3.0e-6	4.8e-4	4.8e-4	0.96828
L40	273.146	5.9255	0.94385	1.6e-4	2.5e-3	2.5e-3	2.7e-5	1.1e-3	1.1e-3	3.1e-6	4.8e-4	4.8e-4	0.94709
L41	273.146	6.9258	0.91829	6.8e-5	2.4e-3	2.4e-3	3.7e-5	1.1e-3	1.1e-3	2.7e-6	4.8e-4	4.8e-4	0.92127
L42	273.146	7.9107	0.89110	1.2e-4	2.4e-3	2.4e-3	2.9e-5	1.2e-3	1.2e-3	6.6e-6	4.8e-4	4.8e-4	0.89260
L43	273.146	8.8894	0.86113	9.3e-5	2.4e-3	2.4e-3	6.1e-5	1.3e-3	1.3e-3	1.4e-5	4.8e-4	4.8e-4	0.85979
L44	273.145	9.8537	0.82710	1.8e-4	2.4e-3	2.4e-3	1.5e-4	1.4e-3	1.4e-3	6.3e-6	4.8e-4	4.8e-4	0.82128
L45	273.147	10.8864	0.78003	6.0e-5	2.4e-3	2.4e-3	1.6e-5	2.7e-3	2.7e-3	6.8e-5	5.1e-4	5.1e-4	0.76737
L46	273.146	11.3314	0.74899	8.2e-5	2.3e-3	2.3e-3	1.2e-4	2.7e-3	2.7e-3	2.8e-5	5.4e-4[+]	5.4e-4[+]	0.73428
L47[*]	273.145	11.5579	0.71514	2.5e-4	2.6e-3	2.6e-3	1.5e-5	2.7e-3	2.7e-3	1.6e-5	1.1e-3[+]	1.1e-3[+]	0.70945
L48[*]	273.146	11.5779	0.70363	1.7e-4	2.3e-3	2.3e-3	6.6e-6	2.7e-3	2.7e-3	1.3e-4	3.0e-3[+]	3.0e-3[+]	0.70648
P5	288.139	5.0859[f]	0.99999	2.8e-4	1.8e-3	1.8e-3	2.9e-6	1.1e-3	1.1e-3				
L50	288.137	5.6498	0.98649	9.1e-4	1.7e-3	2.0e-3	1.3e-5	1.1e-3	1.1e-3	2.0e-5	4.8e-4	4.8e-4	0.98744
L51	288.136	7.0494	0.95060	4.2e-4	1.6e-3	1.6e-3	7.5e-6	1.1e-3	1.1e-3	1.3e-6	4.8e-4	4.8e-4	0.95110
L52	288.134	8.4289	0.90854	6.8e-4	1.6e-3	1.7e-3	9.2e-6	1.2e-3	1.2e-3	1.8e-6	4.8e-4	4.8e-4	0.90541
L53	288.137	8.8666	0.89230	9.0e-4	1.7e-3	1.9e-3	1.7e-6	1.3e-3	1.3e-3	4.4e-6	4.8e-4	4.8e-4	0.88720
L54	288.138	9.2573	0.87508	1.7e-4	1.6e-3	1.6e-3	1.1e-5	1.3e-3	1.3e-3	6.1e-6	4.8e-4	4.8e-4	0.86795
L55	288.139	9.5784	0.85590	9.8e-4	1.8e-3	2.1e-3	1.0e-5	1.4e-3	1.4e-3	5.2e-6	4.9e-4[+]	4.9e-4[+]	0.84786
L56	288.138	9.7066	0.84282	1.2e-3	1.7e-3	2.1e-3	2.6e-5	1.4e-3	1.4e-3	5.2e-6	5.2e-4[+]	5.2e-4[+]	0.83726
L57	288.141	9.7231	0.84006	4.2e-5	1.8e-3	1.8e-3	1.3e-5	1.4e-3	1.4e-3	3.5e-6	5.5e-4[+]	5.5e-4[+]	0.83565
L58	288.139	9.7447	0.83495	1.5e-3	1.9e-3	2.4e-3	8.7e-6	1.4e-3	1.4e-3	2.6e-5	6.6e-4[+]	6.6e-4[+]	0.83343
P6	298.137	6.4328[g]	0.99999	1.1e-4	3.0e-3	3.0e-3	8.6e-6	1.1e-3	1.1e-3				
L59	298.133	7.1110	0.98137	6.6e-4	3.0e-3	3.1e-3	6.5e-6	1.1e-3	1.1e-3	1.1e-6	4.8e-4	4.8e-4	0.98158
L60	298.135	7.4191	0.97218	5.0e-4	3.1e-3	3.2e-3	5.0e-6	1.1e-3	1.1e-3	7.0e-7	4.8e-4	4.8e-4	0.97195
L61	298.134	7.8403	0.95809	1.0e-3	3.0e-3	3.1e-3	1.1e-4	1.1e-3	1.2e-3	2.3e-6	4.8e-4	4.8e-4	0.95692
L62	298.135	8.0258	0.95087	1.4e-3	3.2e-3	3.5e-3	7.7e-6	1.1e-3	1.1e-3	2.7e-6	4.8e-4	4.8e-4	0.94920
L63	298.135	8.1284	0.94625	2.6e-4	3.0e-3	3.0e-3	9.6e-6	1.2e-3	1.2e-3	1.0e-6	4.8e-4	4.8e-4	0.94443
L64	298.135	8.2648	0.93815	2.3e-4	3.2e-3	3.2e-3	9.7e-6	1.2e-3	1.2e-3	1.5e-6	4.9e-4[+]	4.9e-4[+]	0.93709
L65	298.136	8.3019	0.93439	5.1e-4	3.3e-3	3.3e-3	1.0e-5	1.2e-3	1.2e-3	5.2e-6	5.1e-4[+]	5.1e-4[+]	0.93474
L66	298.134	8.3180	0.93085	4.1e-4	3.1e-3	3.2e-3	4.5e-6	1.2e-3	1.2e-3	2.8e-5	7.2e-4[+]	7.2e-4[+]	0.93363

[a] Sample standard deviation of the mean of the temperatures $s(\bar{T}_f)$, mean of the standard systematic uncertainty of the temperatures $\bar{u}_c(\bar{T})$, total standard uncertainty of the temperature $u_c(\bar{T}_f)$, sample standard deviation of the mean of the pressures $s(\bar{p}_f)$, mean of the standard systematic uncertainty of the pressures $\bar{u}_c(\bar{p})$, total standard uncertainty of the pressure $u_c(\bar{p}_f)$, sample standard deviation of the mean of the mole fractions $s(\bar{x}_{CO_2})$, mean of the total standard uncertainty of the mole fractions $\bar{u}_{tot}(x_{CO_2})$, final standard uncertainty of the mole fraction $u_c(\bar{x}_{CO_2})$, PR-MC-WS-NRTL Case 2 EOS calculated mole fraction $x_{CO_2,calc}(\bar{T}_f, \bar{p}_f)$ [b] Span-Wagner CO_2 vapor pressure is 0.5539 ± 0.0002 MPa. [c] Span-Wagner CO_2 vapor pressure is 1.0042 ± 0.0003 MPa. [d] Span-Wagner CO_2 vapor pressure is 1.9694 ± 0.0006 MPa. [e] Span-Wagner CO_2 vapor pressure is 3.4849 ± 0.0010 MPa. [f] Span-Wagner CO_2 vapor pressure is 5.0859 ± 0.0015 MPa. [g] Span-Wagner CO_2 vapor pressure is 6.4324 ± 0.0019 MPa. [*] Measured together with the supercritical data in Table 9 using the procedure in Section 2.3.2. [+] The derivatives $\partial x_{CO_2}/\partial p$ used in Eq. (7) to obtain $\bar{u}_{tot}(x_{CO_2})$ were calculated using the scaling law in Eq. (13) with the parameters in Table 11 instead of the PR-MC-WS-NRTL Case 2 fitted EOS. See Table A.2 for the values of the derivatives, and Section 5.3 for details.

Table 8
Vapor phase: Experimental VLE data for CO_2 (1) + O_2 (2) at mean temperature $\bar{T}_f$, mean pressure $\bar{p}_f$, and mean vapor phase mole fraction $\bar{y}_{CO_2}$ [a].

	Data			Temperature			Pressure			Composition			
ID	$\bar{T}_f$ (K)	$\bar{p}_f$ (MPa)	$\bar{y}_{CO_2}$ (-)	$s(\bar{T}_f)$ (K)	$\bar{u}_c(\bar{T})$ (K)	$u_c(\bar{T}_f)$ (K)	$s(\bar{p}_f)$ (MPa)	$\bar{u}_c(\bar{p})$ (MPa)	$u_c(\bar{p}_f)$ (MPa)	$s(\bar{y}_{CO_2})$ (-)	$\bar{u}_{tot}(y_{CO_2})$ (-)	$u_c(\bar{y}_{CO_2})$ (-)	$y_{CO_2,calc}$ (-)
P1	218.147	0.5546[b]	0.99999	7.3e-5	3.7e-3	3.7e-3	1.1e-6	4.9e-4	4.9e-4				
V1	218.148	1.0237	0.57354	6.1e-5	3.4e-3	3.4e-3	3.6e-5	5.1e-4	5.1e-4	1.0e-4	5.5e-4	5.6e-4	0.57416
V2	218.148	2.1957	0.29849	2.0e-4	3.5e-3	3.5e-3	1.6e-5	5.2e-4	5.2e-4	5.0e-5	4.8e-4	4.9e-4	0.30252
V3	218.148	3.9362	0.19663	4.8e-5	3.8e-3	3.8e-3	1.1e-5	1.1e-3	1.1e-3	4.2e-5	4.8e-4	4.8e-4	0.20251
V4	218.150	5.9189	0.16093	7.3e-5	3.2e-3	3.2e-3	4.7e-6	1.1e-3	1.1e-3	1.4e-5	4.8e-4	4.8e-4	0.16826
V5	218.148	7.8935	0.15229	2.4e-4	3.5e-3	3.5e-3	5.9e-6	1.2e-3	1.2e-3	1.1e-5	4.8e-4	4.8e-4	0.16120
V6	218.148	9.7335	0.15918	1.1e-4	3.5e-3	3.5e-3	8.1e-6	1.4e-3	1.4e-3	7.2e-6	4.8e-4	4.8e-4	0.16940
V7	218.147	11.7910	0.18681	1.7e-4	3.5e-3	3.5e-3	1.1e-5	2.7e-3	2.7e-3	5.6e-6	4.8e-4	4.8e-4	0.19797
V8	218.148	13.0211	0.22283	1.4e-4	3.5e-3	3.5e-3	1.6e-5	2.8e-3	2.8e-3	8.8e-6	4.9e-4	4.9e-4	0.23321
V9	218.148	14.0359	0.28665	2.0e-4	3.6e-3	3.6e-3	2.2e-5	2.8e-3	2.8e-3	3.8e-5	5.7e-4[+]	5.7e-4[+]	0.29187
V10[*]	218.148	14.3563	0.33855	4.8e-5	3.2e-3	3.2e-3	9.5e-6	2.8e-3	2.8e-3	1.7e-5	9.4e-4[+]	9.4e-4[+]	0.33136
V11[*]	218.147	14.3873	0.34936	2.0e-4	3.3e-3	3.3e-3	7.4e-6	2.8e-3	2.8e-3	2.0e-5	1.2e-3[+]	1.2e-3[+]	0.33726
V12[*]	218.149	14.4111	0.36111	1.9e-4	3.3e-3	3.3e-3	1.5e-5	2.8e-3	2.8e-3	7.5e-5	1.8e-3[+]	1.8e-3[+]	0.34237
P2	233.143	1.0048[c]	0.99999	7.4e-5	6.8e-3	6.8e-3	1.1e-5	5.1e-4	5.1e-4				
V14	233.142	1.9677	0.56397	1.5e-4	7.3e-3	7.3e-3	2.3e-6	5.1e-4	5.1e-4	1.2e-4	5.1e-4	5.3e-4	0.56621
V15	233.142	2.9346	0.41117	2.1e-4	7.7e-3	7.7e-3	1.3e-5	5.2e-4	5.3e-4	3.3e-5	4.9e-4	4.9e-4	0.41571
V16	233.143	3.9408	0.33185	3.1e-4	6.8e-3	6.8e-3	2.5e-5	1.1e-3	1.1e-3	1.4e-5	4.9e-4	4.9e-4	0.33997
V17	233.143	5.9475	0.26280	7.5e-5	7.6e-3	7.6e-3	9.5e-5	1.1e-3	1.1e-3	4.7e-6	4.8e-4	4.8e-4	0.27331
V18	233.142	7.8335	0.24021	2.3e-4	7.5e-3	7.5e-3	3.5e-6	1.2e-3	1.2e-3	2.0e-5	4.8e-4	4.8e-4	0.25240
V19	233.141	8.8724	0.23715	3.2e-4	7.6e-3	7.6e-3	4.4e-6	1.3e-3	1.3e-3	2.2e-5	4.8e-4	4.8e-4	0.25033
V20	233.141	9.8514	0.23940	1.1e-4	7.5e-3	7.5e-3	7.7e-6	1.4e-3	1.4e-3	5.4e-6	4.8e-4	4.8e-4	0.25343
V21	233.141	11.8341	0.26143	1.6e-4	7.2e-3	7.2e-3	9.4e-6	2.7e-3	2.7e-3	1.0e-5	4.8e-4	4.8e-4	0.27633
V22	233.142	12.8248	0.28657	2.0e-4	7.2e-3	7.2e-3	1.1e-5	2.7e-3	2.7e-3	1.3e-5	4.9e-4	4.9e-4	0.30036
V23	233.142	13.6445	0.32548	1.6e-4	7.3e-3	7.3e-3	7.4e-6	2.7e-3	2.7e-3	1.5e-5	5.2e-4[+]	5.2e-4[+]	0.33416
V24[*]	233.144	14.1868	0.39244	2.0e-4	6.8e-3	6.8e-3	1.5e-5	2.8e-3	2.8e-3	2.8e-5	9.4e-4[+]	9.4e-4[+]	0.37661
V25[*]	233.144	14.2158	0.40299	3.9e-4	6.6e-3	6.6e-3	7.2e-6	2.8e-3	2.8e-3	2.7e-5	1.3e-3[+]	1.3e-3[+]	0.38020
V26[*]	233.145	14.2407	0.41751	1.2e-4	6.0e-3	6.0e-3	1.1e-5	2.8e-3	2.8e-3	1.1e-5	2.4e-3[+]	2.4e-3[+]	0.38354
P3	253.147	1.9699[d]	0.99999	1.5e-5	5.7e-3	5.7e-3	5.5e-6	5.1e-4	5.1e-4				
V28	253.147	2.9631	0.72731	8.7e-5	5.7e-3	5.7e-3	6.3e-5	5.3e-4	5.3e-4	9.5e-6	5.0e-4	5.0e-4	0.73135
V29	253.146	4.9363	0.51051	7.5e-5	5.7e-3	5.7e-3	1.5e-5	1.1e-3	1.1e-3	2.2e-5	4.9e-4	4.9e-4	0.51935
V30	253.146	6.9080	0.42654	1.6e-4	5.9e-3	5.9e-3	9.4e-6	1.1e-3	1.1e-3	2.7e-5	4.8e-4	4.8e-4	0.43955
V31	253.146	8.3057	0.39990	1.8e-4	5.9e-3	5.9e-3	1.1e-5	1.2e-3	1.2e-3	1.1e-5	4.8e-4	4.8e-4	0.41507
V32	253.148	9.6222	0.39110	6.1e-5	5.8e-3	5.8e-3	2.2e-5	1.4e-3	1.4e-3	8.6e-5	4.8e-4	4.9e-4	0.40751
V33	253.148	10.8461	0.39517	2.1e-4	5.6e-3	5.6e-3	2.3e-4	2.7e-3	2.7e-3	1.5e-5	4.8e-4	4.8e-4	0.41263
V34	253.146	11.8558	0.41081	6.8e-5	5.8e-3	5.8e-3	4.8e-5	2.7e-3	2.7e-3	1.2e-5	4.9e-4	4.9e-4	0.42773
V35	253.146	12.7677	0.44495	1.4e-4	5.7e-3	5.7e-3	8.4e-6	2.7e-3	2.7e-3	5.7e-6	5.2e-4[+]	5.2e-4[+]	0.45666
V36[*]	253.146	13.2762	0.50132	3.5e-4	5.8e-3	5.8e-3	4.2e-5	2.7e-3	2.7e-3	1.6e-5	8.6e-4[+]	8.6e-4[+]	0.49109
V37[*]	253.147	13.3023	0.50988	1.2e-4	6.0e-3	6.0e-3	2.2e-5	2.7e-3	2.7e-3	6.0e-5	1.1e-3[+]	1.1e-3[+]	0.49401
V38[*]	253.147	13.3200	0.51743	5.8e-5	5.8e-3	5.8e-3	6.6e-6	2.7e-3	2.7e-3	1.1e-5	1.6e-3[+]	1.6e-3[+]	0.49612
P4	273.147	3.4848[e]	0.99999	2.4e-5	1.5e-3	1.5e-3	9.9e-7	1.1e-3	1.1e-3				
V40	273.144	3.9433	0.91844	1.3e-4	2.2e-3	2.2e-3	1.7e-5	1.1e-3	1.1e-3	1.1e-4	5.1e-4	5.2e-4	0.92150
V41	273.145	5.0162	0.78625	2.1e-4	2.1e-3	2.1e-3	4.9e-5	1.1e-3	1.1e-3	3.6e-5	4.9e-4	4.9e-4	0.79225
V42	273.146	5.9256	0.71346	6.1e-5	2.5e-3	2.5e-3	2.5e-5	1.1e-3	1.1e-3	1.2e-5	4.9e-4	4.9e-4	0.72173
V43	273.146	6.9259	0.65904	8.1e-5	2.2e-3	2.2e-3	5.2e-5	1.1e-3	1.1e-3	1.2e-5	4.8e-4	4.8e-4	0.66945
V44	273.146	7.9107	0.62377	2.4e-4	2.3e-3	2.3e-3	5.1e-5	1.2e-3	1.2e-3	1.1e-5	4.8e-4	4.8e-4	0.63597
V45	273.146	8.8896	0.60275	9.9e-5	2.3e-3	2.3e-3	8.9e-5	1.3e-3	1.3e-3	1.0e-5	4.8e-4	4.8e-4	0.61637
V46	273.146	9.8539	0.59503	1.5e-4	2.5e-3	2.5e-3	2.0e-5	1.4e-3	1.4e-3	5.3e-6	4.8e-4	4.8e-4	0.60925
V47	273.146	10.8864	0.60684	1.7e-4	2.7e-3	2.7e-3	1.8e-5	2.7e-3	2.7e-3	7.8e-6	4.8e-4	4.8e-4	0.61857
V48	273.146	11.3312	0.62764	9.4e-5	2.4e-3	2.4e-3	1.7e-5	2.7e-3	2.7e-3	2.6e-5	5.3e-4[+]	5.4e-4[+]	0.63335
V49[*]	273.145	11.5578	0.66096	2.5e-5	2.6e-3	2.6e-3	2.3e-5	2.7e-3	2.7e-3	1.8e-5	1.1e-3[+]	1.1e-3[+]	0.64900
V50[*]	273.146	11.5780	0.67276	1.3e-4	2.4e-3	2.4e-3	1.5e-5	2.7e-3	2.7e-3	9.9e-5	3.1e-3[+]	3.1e-3[+]	0.65119
P5	288.139	5.0859[f]	0.99999	2.8e-4	1.8e-3	1.8e-3	2.9e-6	1.1e-3	1.1e-3				
V52	288.137	5.6498	0.94168	8.5e-4	1.7e-3	1.9e-3	3.5e-6	1.1e-3	1.1e-3	2.6e-5	4.9e-4	4.9e-4	0.94516
V53	288.142	7.0493	0.84273	2.1e-5	1.8e-3	1.8e-3	6.8e-6	1.1e-3	1.1e-3	3.7e-5	4.8e-4	4.8e-4	0.84963
V54	288.141	8.4289	0.79080	1.3e-3	1.8e-3	2.3e-3	1.4e-5	1.2e-3	1.2e-3	2.4e-5	4.8e-4	4.8e-4	0.79918
V55	288.137	8.8666	0.78344	5.1e-4	1.8e-3	1.8e-3	2.3e-5	1.3e-3	1.3e-3	1.7e-6	4.8e-4	4.8e-4	0.79132
V56	288.139	9.2573	0.78234	5.5e-4	1.7e-3	1.8e-3	8.7e-6	1.3e-3	1.3e-3	1.2e-6	4.8e-4	4.8e-4	0.78870
V57	288.138	9.5784	0.78942	4.3e-4	1.7e-3	1.8e-3	1.2e-5	1.4e-3	1.4e-3	2.8e-6	4.9e-4[+]	4.9e-4[+]	0.79159
V58	288.141	9.7066	0.79944	1.1e-4	1.7e-3	1.7e-3	2.0e-5	1.4e-3	1.4e-3	8.5e-6	5.1e-4[+]	5.1e-4[+]	0.79558
V59	288.141	9.7232	0.80207	4.1e-4	1.9e-3	1.9e-3	1.0e-5	1.4e-3	1.4e-3	9.5e-6	5.3e-4[+]	5.3e-4[+]	0.79633
V60	288.142	9.7447	0.80674	2.9e-5	1.9e-3	1.9e-3	3.9e-6	1.4e-3	1.4e-3	7.8e-5	6.4e-4[+]	6.5e-4[+]	0.79746
P6	298.137	6.4328[g]	0.99999	1.1e-4	3.0e-3	3.0e-3	8.6e-6	1.1e-3	1.1e-3				
V61	298.141	7.1110	0.95624	4.8e-5	3.2e-3	3.2e-3	2.8e-6	1.1e-3	1.1e-3	1.3e-5	4.8e-4	4.8e-4	0.95967
V62	298.135	7.4191	0.94072	7.8e-4	3.2e-3	3.3e-3	4.1e-6	1.1e-3	1.1e-3	2.7e-6	4.8e-4	4.8e-4	0.94483
V63	298.138	7.8392	0.92467	1.4e-3	3.1e-3	3.4e-3	1.4e-4	1.1e-3	1.1e-3	1.1e-5	4.8e-4	4.8e-4	0.92886
V64	298.140	8.0258	0.91978	3.9e-5	3.3e-3	3.3e-3	3.9e-6	1.1e-3	1.1e-3	8.6e-6	4.8e-4	4.8e-4	0.92365
V65	298.135	8.1339	0.91818	3.6e-4	3.0e-3	3.0e-3	6.7e-6	1.2e-3	1.2e-3	1.0e-5	4.8e-4	4.8e-4	0.92129
V66	298.135	8.2648	0.91898	7.1e-4	3.1e-3	3.2e-3	3.8e-6	1.2e-3	1.2e-3	9.2e-7	4.8e-4[+]	4.8e-4[+]	0.91966
V67	298.137	8.3019	0.92108	4.4e-4	3.2e-3	3.2e-3	9.0e-6	1.2e-3	1.2e-3	6.4e-6	4.9e-4[+]	4.9e-4[+]	0.91960
V68	298.136	8.3180	0.92389	1.0e-3	3.1e-3	3.3e-3	6.0e-6	1.2e-3	1.2e-3	1.0e-5	6.9e-4[+]	6.9e-4[+]	0.91965

[a] Sample standard deviation of the mean of the temperatures $s(\bar{T}_f)$, mean of the standard systematic uncertainty of the temperatures $\bar{u}_c(\bar{T})$, total standard uncertainty of the temperature $u_c(\bar{T}_f)$, sample standard deviation of the mean of the pressures $s(\bar{p}_f)$, mean of the standard systematic uncertainty of the pressures $\bar{u}_c(\bar{p})$, total standard uncertainty of the pressure $u_c(\bar{p}_f)$, sample standard deviation of the mean of the mole fractions $s(\bar{y}_{CO_2})$, mean of the total standard uncertainty of the mole fractions $\bar{u}_{tot}(y_{CO_2})$, final standard uncertainty of the mole fraction $u_c(\bar{y}_{CO_2})$, PR-MC-WS-NRTL Case 2 EOS calculated mole fraction $y_{CO_2,calc}(\bar{T}_f, \bar{p}_f)$ [b] Span-Wagner CO_2 vapor pressure is 0.5539 ± 0.0002 MPa. [c] Span-Wagner CO_2 vapor pressure is 1.0042 ± 0.0003 MPa. [d] Span-Wagner CO_2 vapor pressure is 1.9694 ± 0.0006 MPa. [e] Span-Wagner CO_2 vapor pressure is 3.4849 ± 0.0010 MPa. [f] Span-Wagner CO_2 vapor pressure is 5.0859 ± 0.0015 MPa. [g] Span-Wagner CO_2 vapor pressure is 6.4324 ± 0.0019 MPa. [*] Measured together with the supercritical data in Table 9 using the procedure in Section 2.3.2. [+] The derivatives $\partial y_{CO_2}/\partial p$ used in Eq. (7) to obtain $\bar{u}_{tot}(y_{CO_2})$ were calculated using the scaling law in Eq. (13) with the parameters in Table 11 instead of the PR-MC-WS-NRTL Case 2 fitted EOS. See Table A.3 for the values of the derivatives, and Section 5.3 for details.

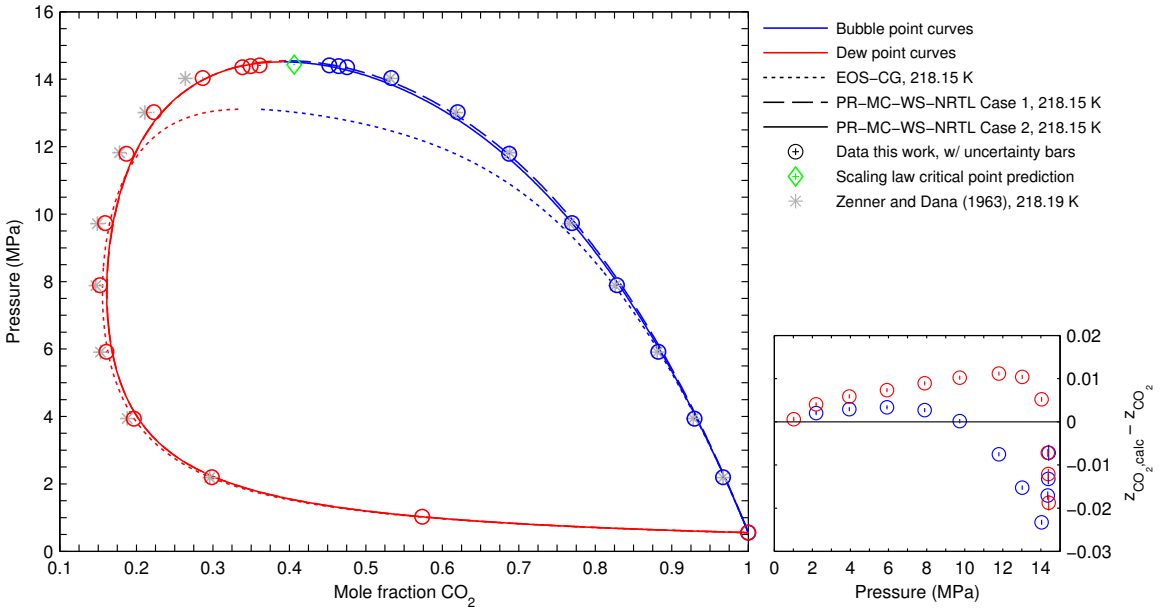

(a) Mean temperature of measurements in present work 218.148 K. VLE data from literature [18].

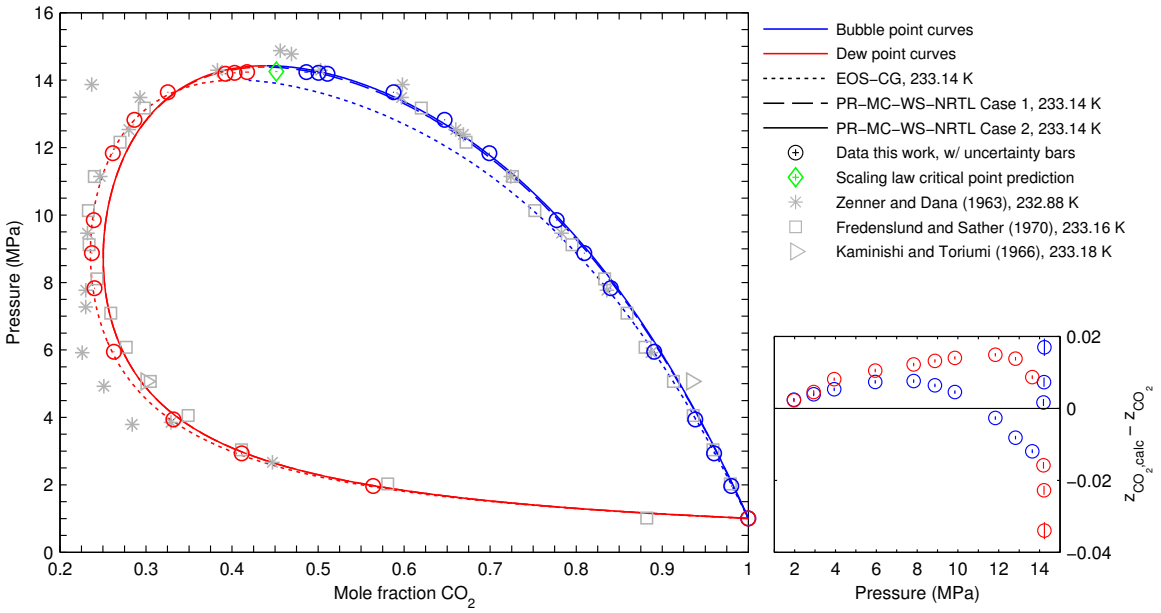

(b) Mean temperature of measurements in present work 233.143 K. VLE data from literature [18, 19, 20].

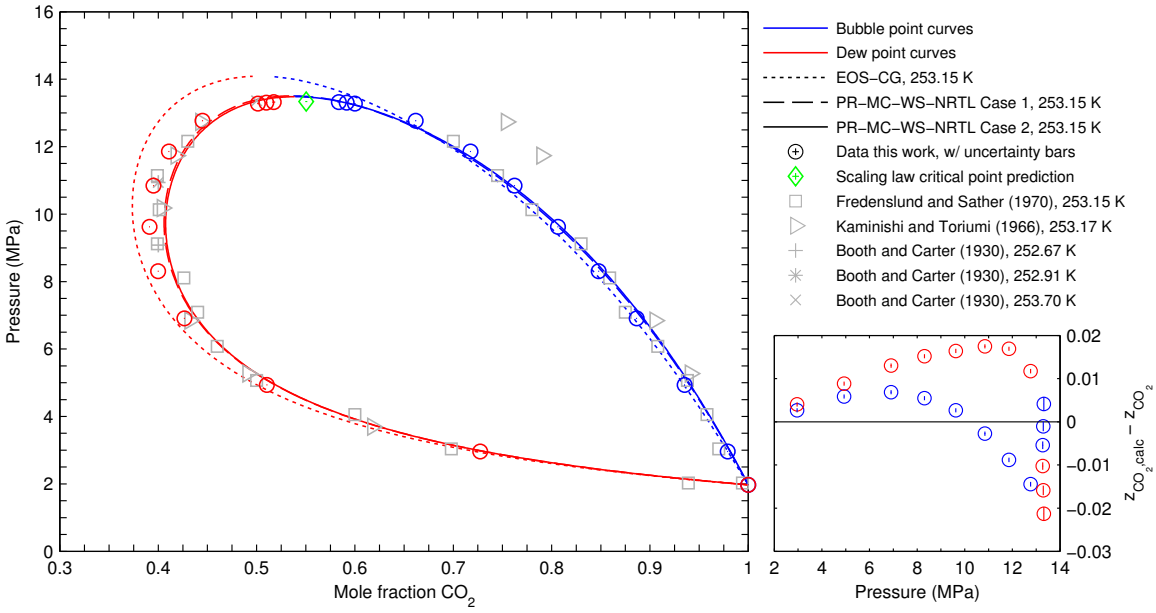

(c) Mean temperature of measurements in present work 253.147 K. VLE data from literature [19, 20, 21].

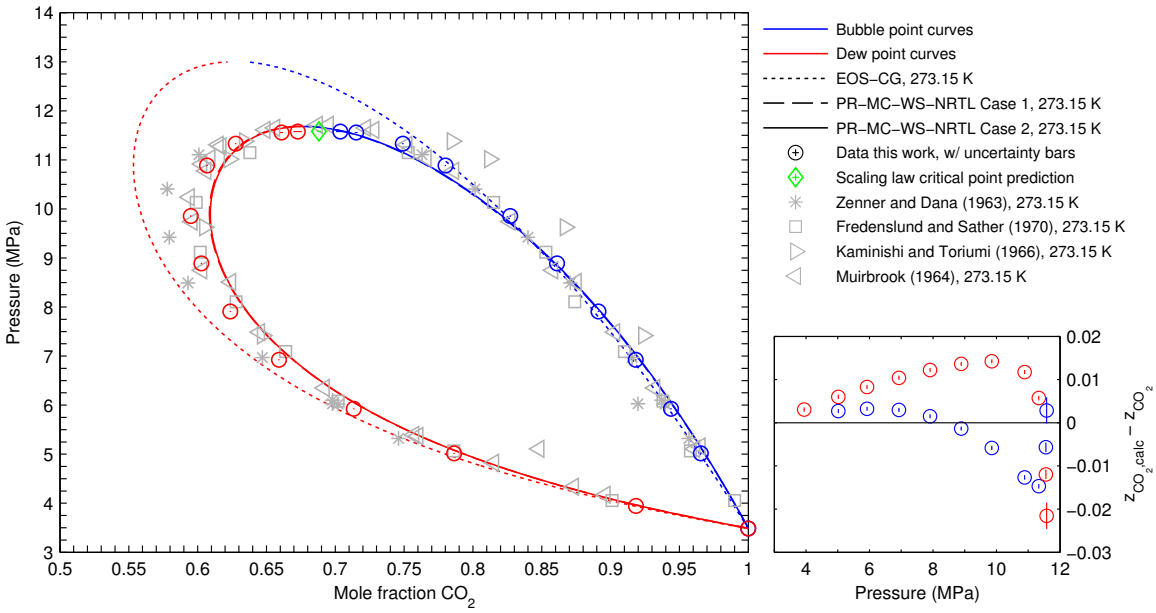

(d) Mean temperature of measurements in present work 273.146 K. VLE data from literature [18, 19, 20, 22].

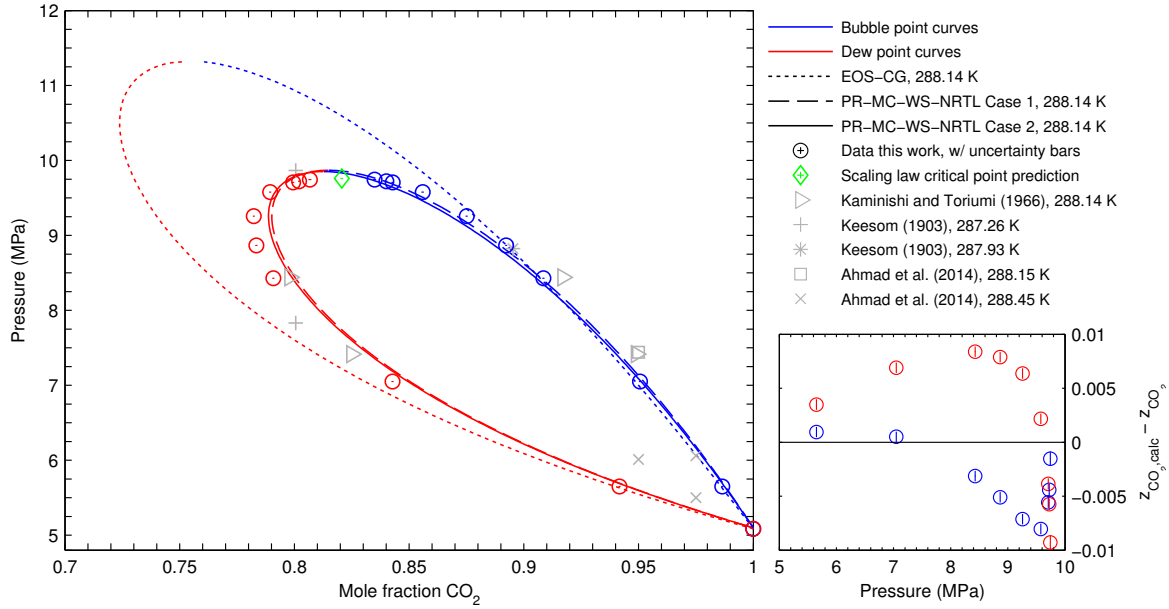

(e) Mean temperature of measurements in present work 288.139 K. VLE data from literature [20, 23, 24].

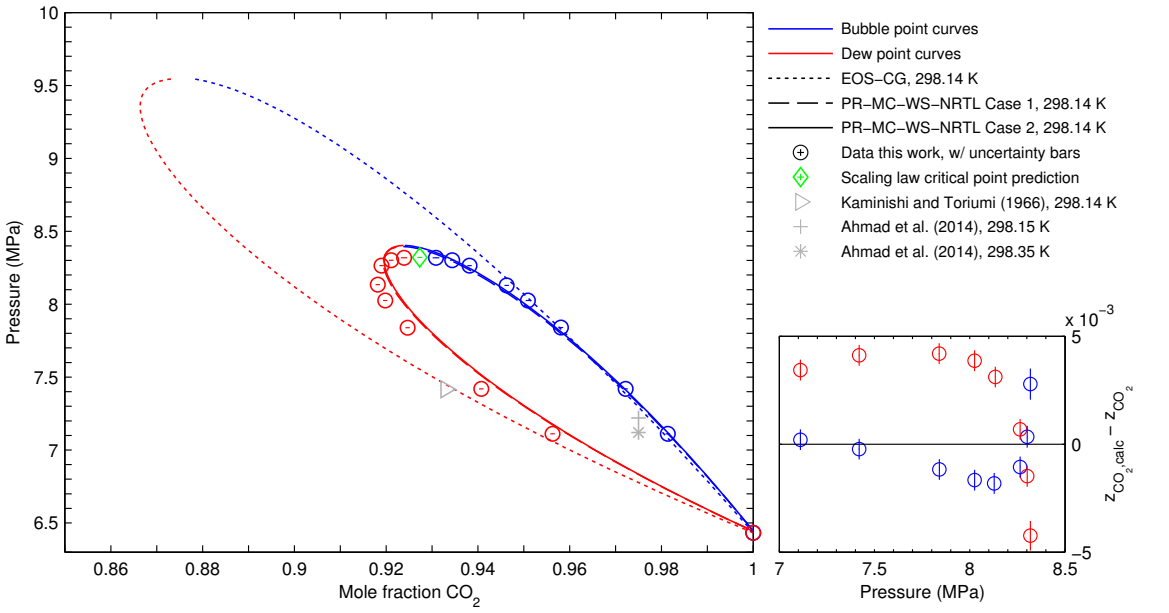

(f) Mean temperature of measurements in present work 298.136 K. VLE data from literature [20, 24].

Fig. 5. Left: Pressure-composition diagram based on EOS calculations at the different mean temperatures, VLE data from literature, and VLE measurements with estimated uncertainties from present work: $\bar{x}_{CO_2}$, $\bar{y}_{CO_2}$, $\bar{p}_f$, $u_c\left(\bar{x}_{CO_2}\right)$, $u_c\left(\bar{y}_{CO_2}\right)$ and $u_c\left(\bar{p}_f\right)$ from Tables 7 and 8. Please note that the uncertainty bars are very small compared to the scale of the plots. Critical point estimation and its uncertainties are from Section 5.3. Right: Plot of deviation between PR-MC-WS-NRTL Case 2 $z_{CO_2,calc}$ and VLE measurements from present work z_{CO_2}, where z_{CO_2} is equal to either x_{CO_2} or y_{CO_2}.

Table 9
Composition data at supercritical states for the liquid and vapor samplers for CO_2 (1) + O_2 (2) at mean temperature $\bar{T}_f$, mean pressure $\bar{p}_f$, and mean mole fraction $\bar{z}_{CO_2}$ [a].

	Data			Temperature			Pressure			Composition	
ID	$\bar{T}_f$ (K)	$\bar{p}_f$ (MPa)	$\bar{z}_{CO_2}$ (-)	$s(\bar{T}_f)$ (K)	$\bar{u}_c(\bar{T})$ (K)	$u_c(\bar{T}_f)$ (K)	$s(\bar{p}_f)$ (MPa)	$\bar{u}_c(\bar{p})$ (MPa)	$u_c(\bar{p}_f)$ (MPa)	$s(\bar{z}_{CO_2})$ (-)	$u_c(\bar{z}_{CO_2})$ (-)
L12	218.148	14.4390	0.39450	2.1e-4	3.4e-3	3.4e-3	1.2e-5	2.8e-3	2.8e-3	4.3e-6	4.8e-4
V13	218.147	14.4390	0.39472	1.4e-4	3.4e-3	3.4e-3	6.2e-6	2.8e-3	2.8e-3	9.0e-6	4.8e-4
L26	233.142	14.2617	0.44465	2.5e-4	7.4e-3	7.4e-3	1.3e-5	2.8e-3	2.8e-3	1.1e-5	4.8e-4
V27	233.142	14.2617	0.44445	7.7e-5	7.5e-3	7.5e-3	1.3e-5	2.8e-3	2.8e-3	9.3e-6	4.8e-4
L38	253.147	13.3560	0.55468	6.3e-5	5.9e-3	5.9e-3	3.5e-5	2.7e-3	2.7e-3	1.9e-5	4.8e-4
V39	253.148	13.3561	0.55470	3.3e-5	5.6e-3	5.6e-3	1.3e-4	2.7e-3	2.7e-3	1.3e-5	4.8e-4
L49	273.146	11.5976	0.68191	4.5e-4	2.6e-3	2.6e-3	9.5e-5	2.7e-3	2.7e-3	1.9e-5	4.8e-4
V51	273.145	11.5975	0.68219	1.2e-4	2.5e-3	2.5e-3	1.4e-5	2.7e-3	2.7e-3	5.5e-6	4.8e-4

[a] Samples taken using liquid sampler given with ID L, samples taken using vapor sampler given with ID V. Sample standard deviation of the mean of the temperatures $s(\bar{T}_f)$, mean of the standard systematic uncertainty of the temperatures $\bar{u}_c(\bar{T})$, total standard uncertainty of the temperature $u_c(\bar{T}_f)$, sample standard deviation of the mean of the pressures $s(\bar{p}_f)$, mean of the standard systematic uncertainty of the pressures $\bar{u}_c(\bar{p})$, total standard uncertainty of the pressure $u_c(\bar{p}_f)$, sample standard deviation of the mean of the mole fractions $s(\bar{z}_{CO_2})$. Standard uncertainty in mean of the mole fractions $u_c(\bar{z}_{CO_2}) = \sqrt{s^2(\bar{z}_{CO_2}) + \bar{u}^2(z_{CO_2})}$, where $\bar{u}(z_{CO_2})$ is the mean of $u(z_{CO_2})$ for the corresponding series in Table A.4.

Table 10
Available isothermal (ISOT) and synthetic (SYN) VLE literature data and the temperature, pressure and composition ranges.

Authors	Year	Type	T (K)	p (MPa)	Composition CO_2	No. of points
Zenner and Dana [18]	1963	ISOT	218.19, 232.88, 273.15	2.2-14.9	0.147-0.967	58
Kaminishi and Toriumi [20]	1966	ISOT	233.18, 253.17, 273.15, 288.14, 293.14, 298.14	3.7-12.7	0.300-0.949	30
Fredenslund and Sather [19]	1970	ISOT	223.16, 233.16, 243.16, 253.15, 263.15, 273.15, 283.15	1.0-13.2	0.180-0.994	143
Fredenslund et al. [25]	1972	ISOT	223.76	0.9-14.2	0.186-0.996	21
Engberg et al. [26]	2009	ISOT	240.9	1.9-7.2	0.301-0.986	20
Muirbrook [22]	1964	ISOT	273.15	4.2-11.7	0.594-0.965	33
Keesom [23]	1903	SYN	283.21-296.38	6.7-10.4	0.8006, 0.8953	36
Booth and Carter [21]	1930	SYN	212.76-259.91	3.6-14.3	0.2, 0.3, 0.4, 0.5	34[a]
Ahmad et al. [24]	2014	SYN	277.35-298.35	4.1-8.1	0.9493, 0.9506, 0.9745, 0.9751	22

[a] The authors did not report VLE data directly, only the observed phases present at different pressure-temperature states at constant total composition. VLE data points approximated as mean of state variables where difference in temperature or pressure was small across a liquid to vapor-liquid or vapor to vapor-liquid transition.

pairs in the critical region seemed to agree with their data at 14.3 MPa. Their data points at approximately 14.85 MPa did not agree with our critical point prediction (See Section 5.3 below). However, Zenner and Dana [18] indicated in their work that these two points were outside the two-phase region. The data by Fredenslund and Sather [19] agreed reasonably well with our data, except at lower pressures where the deviations between their dew point data and ours were somewhat larger. The two data points by Kaminishi and Toriumi [20] were not directly comparable with our data in terms of pressure, but their bubble point seemed to be slightly off in composition compared to our neighboring data points at 3.9 and 6.0 MPa.

At 253.15 K, the bubble point data by Fredenslund and Sather [19] agreed well with our data, while their dew point data did not agree that well, and their data showed more scatter than ours. The bubble point data by Kaminishi and Toriumi [20] showed large deviations from our data at high pressures, whereas their dew point data seemed to agree better. Although at slightly different temperatures than our data, the data by Booth and Carter [21] agreed well with our data at lower pressures, and very well with our data in the critical region.

At 273.15 K, the data by Zenner and Dana [18] showed a similar deviation pattern to our data as at 233.14 K: Their bubble points agreed well with our data, while their dew points did not agree very well with ours. The data by Fredenslund and Sather [19] agreed reasonably well with our data. The authors suggested that their bubble and dew points at 11.2 MPa might be erroneous, caused by entrainment. Our bubble and dew points neighboring these points were at respectively higher and lower CO_2 mole fractions, which indicated that this might be correct. Similarly to the data at 253.15 K, the bubble points by Kaminishi and Toriumi [20] did not agree very well with our data, while the dew points agreed better. The data by Muirbrook [22] agreed very well with our data, also in the critical region.

At 288.14 K, we found few literature data points to compare our measurements with. The four data points by Kaminishi and Toriumi [20] agreed better in terms of composition than at the lower temperatures. The data by Keesom [23], although at different temperatures than our data, agreed reasonably well with ours. Of the recent data by Ahmad et al. [24], the dew point data did not match our data very well. The reason for this could have been that the temperature uncertainty in the data by [24] was stated as 1 K, which was very high for measurements at these temperatures when considering the composition temperature derivatives given in Tables A.2 and A.3. The data situation at this temperature was improved considerably by the addition of our data.

At 298.14 K, the only data we were able to find in the literature was the dew point by Kaminishi and Toriumi [20], and the data by Ahmad et al. [24]. The data point by [20] deviated in composition from our data by approximately the same amount as the data by the same authors at 288.14 K. The bubble point by [24] seemed to agree well with our data,

while the dew point at a slightly higher temperature did not match well with our data. Similarly to at 288.14 K, the data situation was improved with our data.

In general, the agreement between our data and literature data varied significantly, also from one temperature to another by the same author. This highlighted the inconsistencies in the literature data noted in [3, 4, 5]. Compared with the existing literature data, the data in the present work described the VLE at the six measured temperatures with considerably less scatter, and included several measurements in the critical region at each temperature, thus forming a good basis for modeling the system. In addition, the VLE measurements at 288.14 and 298.14 K constituted the only complete isotherms at temperatures above 273.15 K.

5.3. Critical point estimation

The procedure for estimating the critical point in terms of pressure and composition for a binary mixture at a certain temperature utilizing scaling laws from statistical mechanics [27, 28, 29] was described for the use on CO_2+N_2 mixtures in [1]. The same procedure was used for estimating the critical points in the present work, the only exception being the estimation of the uncertainty in the critical composition, which is discussed below. The critical point for a binary mixture in terms of pressure and temperature is dependent on the composition. For a given temperature, the composition, if any, where the critical point is attained, is denoted the critical composition, with symbol $z_{CO_2,c}$, and the corresponding critical pressure, with symbol p_c, is identified as the point of maximum pressure in closed isothermal pressure-composition phase envelopes for a binary mixture, as seen in Figs. 5a to 5f.

Like in [1], the following scaling law was applied [30, 31]:

$$z_{CO_2} = \hat{z}_{CO_2,c} + \left(\lambda_1 - \epsilon\frac{\lambda_2}{2}\right)(\hat{p}_c - p) - \epsilon\frac{\mu}{2}(\hat{p}_c - p)^{\beta}\ , \quad \text{where} \quad \epsilon = \begin{cases} 1 \text{ for bubble points,} \\ -1 \text{ for dew points,} \end{cases} \tag{13}$$

and z_{CO_2} was the bubble point ($z_{CO_2} = x_{CO_2}$) or dew point ($z_{CO_2} = y_{CO_2}$) CO_2 mole fraction at pressure p. Keeping β fixed at 0.325 [32], the critical composition $z_{CO_2,c}$ and pressure p_c and the parameters λ_1, λ_2 and μ were fitted at each isotherm average temperature using the VLE data identified in Table 11. The regression was performed using the ordinary unweighted least squares method, giving the estimators $\hat{z}_{CO_2,c}$, $\hat{p}_c$, $\hat{\lambda}_1$, $\hat{\lambda}_2$ and $\hat{\mu}$ shown in Table 11.

The uncertainties in the estimated critical composition and pressure, respectively $u(\hat{z}_{CO_2,c})$ and $u(\hat{p}_c)$, were estimated according to Eqs. (16) and (17) in [1]. These estimates were based on the uncertainties in the composition and pressure of the VLE data used in the fitting, and the standard errors of regression of the critical composition and pressure, $S_E(\hat{z}_{CO_2,c})$ and $S_E(\hat{p}_c)$, respectively. The estimates for the uncertainty in the composition of the VLE data used in the fitting, $u_c(\bar{x}_{CO_2})$ and $u_c(\bar{y}_{CO_2})$, were calculated based on values for the composition derivatives with respect to pressure, $\partial z_{CO_2}/\partial p$, derived from Eq. (13). The values that were calculated using the scaling law are given in Tables A.2, A.3, 7 and 8, indicated with the marker symbol $^+$.

The estimated critical compositions and pressures with their corresponding uncertainties are given in Table 11, and are plotted together with the critical region VLE data and the supercritical state points from Table 9 in Fig. 6.

The standard errors of regression were very low compared to the corresponding uncertainties in the compositions and pressures in the VLE data used for each regression at all temperatures.

Attempts to increase or decrease the number of VLE points used to fit the parameters, compared to the sets of points stated in Table 11, did not result in changes in the critical compositions and pressures that were larger than the uncertainties in these fitted parameters. However, this was only valid if the VLE points closest to the mixture critical points were included in the fit. If fewer of these VLE points were included in the fit, the deviations in the estimated critical compositions and pressures from the estimates given in Table 11 became more pronounced. Two examples are given. First, if the eight VLE points identified as L6-9 and V7-10 in Tables 7 and 8 were used to fit the scaling law at 218.15 K, the estimated critical composition and pressure were respectively 0.4057 and 14.421 MPa. In this data set, the four VLE points closest to the mixture critical point were not included. The estimated critical composition did not change significantly, considering the uncertainty given in Table 11, $u(\hat{z}_{CO_2,c}) = 0.00115$. However, the estimated critical pressure decreased with 0.014 MPa. Second, if the data set contained the eight VLE points identified as L5-8 and V6-9 were used for the fit, the estimated critical composition and pressure were respectively 0.4052 and 14.346 MPa. In this data set, the six VLE points closest to the mixture critical point were not included. The estimated critical composition decreased slightly more compared to the estimate given in Table 11. Also, the estimated critical pressure decreased with 0.089 MPa.

The supercritical state point pairs at each temperature in Table 9 showed a small difference in composition. As indicated in Section 2.3.2, there was always a possibility that the content of the cell was in the two-phase region during these measurements, but sufficiently close to the critical point such that critical opalescence (see e.g. Ref. [33]) caused the cell phases to become indiscernible. However, the differences in composition shown in Table 9 were below the estimated uncertainty in the composition analysis, $4.8 \cdot 10^{-4}$. Hence, on this basis, it was not possible to conclude that this difference suggested an actual difference in composition, caused by the presence of two phases. In addition, as Fig. 6 shows, the supercritical state points at 218.15, 233.14, 253.15 and 273.15 K were all at higher pressures than the predicted critical pressures, which supported the assumption that these supercritical measurements were indeed outside the two-phase

region.

Based on this discussion, it was assumed that the estimates for the critical points were reasonable, and that the VLE measurements in the critical region also were reasonable, within their corresponding uncertainty estimates and their aforementioned limitations.

5.4. Model fitting

5.4.1. Introduction

In [1], the model for the CO_2+N_2 system in the equation of state called EOS-CG [3, 4] was fitted to the VLE data measured in [1]. The highly flexible structure of the GERG-2008 EOS [34], developed for natural gas mixtures, was used by Gernert and Span [3] to develop EOS-CG, which was fitted to data for the mixtures of some of the components expected in captured CO_2 in CCS processes [3]. The model and parameters used for the CO_2+N_2 system in EOS-CG were almost unchanged compared to that used in the GERG-2008 [3]. The EOS-CG model for the CO_2+O_2 system was an improvement compared to that of the GERG-2008 model. However, as noted in [3, 4], some restrictions on the number of fitting parameters and number of terms utilized in EOS-CG were set due to the inferior data situation. The quality of the description of the CO_2+O_2 system by EOS-CG was reduced accordingly.

The EOS-CG model calculations are plotted in Figs. 5a to 5f. The deviations between the model and the new data of this work were significant. The VLE data provided in the present work considerably improved the data situation for the CO_2+O_2 system, and can be used together with the other available literature data for VLE and properties such as density and speed of sound, to improve the model description of the system.

In this work, the parameters of the Peng-Robinson (PR) cubic EOS [35] with the alpha correction by Mathias and Copeman [36] (MC), the mixing rules by Wong and Sandler [37] (WS), and the NRTL [38] excess Gibbs energy model were fitted. This combination of EOS, alpha correction, mixing rule, and excess Gibbs energy model, designated here as PR-MC-WS-NRTL, has been used to fit VLE data of binary systems containing one supercritical component in our previous work [1] (CO_2+N_2) and in the work of Coquelet et al. [39] (CO_2+Ar).

The data in Tables 7 and 8 formed the basis for the model fitting. Similar to [1], the fitting was performed using orthogonal distance regression (ODR) [40], which consisted in our case of minimizing an objective function with weighting of the minimum deviation between data and model predictions in both composition $\bar{x}_{CO_2}$ and $\bar{y}_{CO_2}$, and in pressure $\bar{p}_f$, at a fixed temperature. The objective function can be stated as

$$S^2 = \frac{1}{n-n_p}\sum_i \left(\frac{p_{i,calc}-\bar{p}_{i,f}}{u_c(\bar{p}_{i,f})}\right)^2 + \frac{1}{n-n_p}\sum_i \left(\frac{z_{i,CO_2,calc}-\bar{z}_{i,CO_2}}{u(z_{CO_2})}\right)^2 , \quad (14)$$

where $\bar{z}_{CO_2}$ is equal to either $\bar{x}_{CO_2}$ or $\bar{y}_{CO_2}$, n is the total number of experimental data points, n_p is the number of parameters adjusted in the model fit and $u(z_{CO_2})$ is the composition uncertainty caused by the analysis given in Table 6. In addition to S, two other statistics were used to quantify the agreement between model and data: the absolute average deviation (AAD) and the bias (BIAS), whose formulas are given in Table 12.

5.4.2. Peng-Robinson EOS

The formulas and corresponding nomenclature used in the present work for the MC alpha correction [36], the WS mixing rules [37] and the NRTL [38] excess Gibbs energy model were given in [1] and are not reproduced here. The critical temperature and pressure used in the EOS phase equilibrium calculations for $i = CO_2$ or O_2 are given in Table 13, together with the parameters $c_{1,i}$, $c_{2,i}$ and $c_{3,i}$ used in the MC alpha correction.

The parameters of the PR-MC-WS-NRTL EOS consist of the Wong-Sandler binary interaction parameters, k_{ij}, the binary interaction parameters of the NRTL model, τ_{ij}, and the non-randomness parameters of the NRTL model, α_{ij}.

Like in [1], the following restrictions were put on the parameters:

$$\begin{aligned} k_{ij} &= k_{ji} , & k_{ii} &= 0 , \\ \alpha_{ij} &= \alpha_{ji} , & \alpha_{ii} &= 0 , \\ \tau_{ij} &\neq \tau_{ji} , & \tau_{ii} &= 0 . \end{aligned} \quad (15)$$

Furthermore, a constant value for $\alpha_{12} = \alpha_{21} = 0.3$ was assumed (cf. [1, 39]), based on the suggestions by Renon and Prausnitz [38] for a system of two non-polar components such as the CO_2+O_2 system. This leaves $n_p = 3$ adjustable parameters in the PR-MC-WS-NRTL model: k_{12}, τ_{12} and τ_{21}. These parameters were assumed to be temperature dependent, to obtain the best possible fit of the data. It was therefore of interest to fit the parameters to data at different temperatures, and try to determine a model for the temperature dependence of the parameters, enabling the use of the EOS over the whole temperature range of the data.

The parameters of the model were fitted to the data at each of the average temperatures 218.15, 233.14, 253.15, 273.15, 288.14 and 298.14 K. The fitted parameters for each temperature are given in Table 12 and plotted in Figs. 7a and 7b, denoted as Case 1. For the temperatures where there were several measurements close to the critical point, only the measurements at the highest pressure were included in the fit, in order to avoid a too strong emphasis on this region. An overview of the points that were excluded are given in Table 12.

With reference to Fig. 7a, the temperature dependencies of τ_{12} and τ_{21} could be approximately described by the function given in [41]:

$$\tau_{12}(T) = a_{\tau_{12}} + b_{\tau_{12}} \cdot \left| \left(T - T_{c,CO_2}\right)/T_{c,CO_2} \right|^{c_{\tau_{12}}} , \quad (16)$$

$$\tau_{21}(T) = a_{\tau_{21}} + b_{\tau_{21}} \cdot \left| \left(T - T_{c,CO_2}\right)/T_{c,CO_2} \right|^{c_{\tau_{21}}} . \quad (17)$$

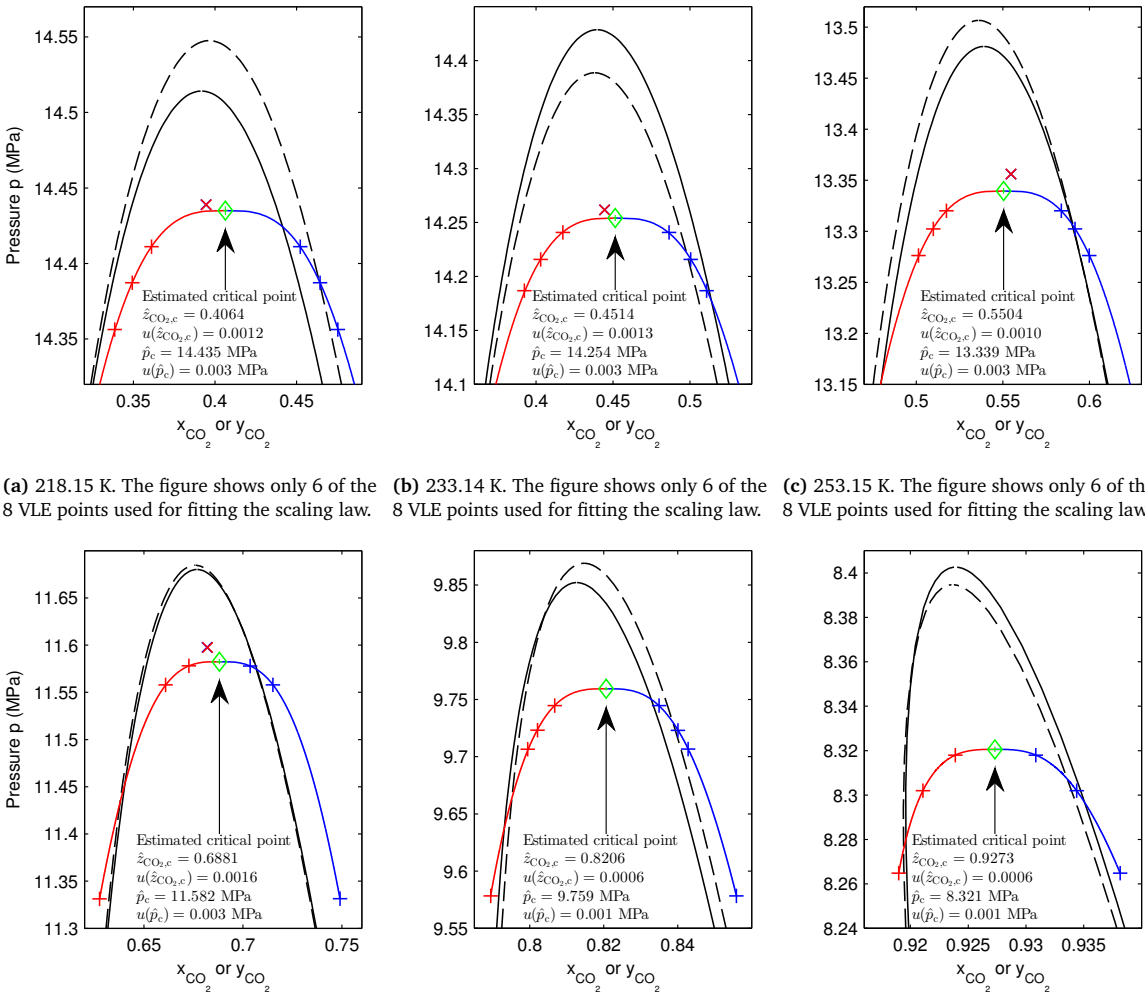

(a) 218.15 K. The figure shows only 6 of the 8 VLE points used for fitting the scaling law.

(b) 233.14 K. The figure shows only 6 of the 8 VLE points used for fitting the scaling law.

(c) 253.15 K. The figure shows only 6 of the 8 VLE points used for fitting the scaling law.

(d) 273.15 K.

(e) 288.14 K.

(f) 298.14 K.

Fig. 6. Comparison of the predictions of the pressure-composition phase behavior in the critical region by three different models: PR-MC-WS-NRTL Case 1 and Case 2 EOSs, and the scaling law model in Eq. (13). Please note that the scales of the graphs are very different from each other. Please refer to Table 11 for an overview of the VLE points used to fit the scaling law and the parameters at the different temperatures. Supercritical measurements are shown in Table 9.

Table 11
Parameters of the scaling law in Eq. (13) fitted to critical region data from this work at six different average temperatures.

T (K)	Used points[a]	n_p (-)	$\hat{\lambda}_1$ (MPa^{-1})	$\hat{\lambda}_2$ (MPa^{-1})	$\hat{\mu}$ ($MPa^{-\beta}$)	$\hat{z}_{CO_2,c}$ (-)	$\hat{p}_c$ (MPa)	$S_E(\hat{z}_{CO_2,c})$ (-)	$u(\hat{z}_{CO_2,c})$ (-)	$S_E(\hat{p}_c)$ (MPa)	$u(\hat{p}_c)$ (MPa)
218.148	L8-11, V9-12	8	$8.8655 \cdot 10^{-3}$	$-5.6184 \cdot 10^{-2}$	-0.30221	0.4064	14.435	$7.3 \cdot 10^{-5}$	0.00115	$3.6 \cdot 10^{-4}$	0.0028
233.143	L22-25, V23-26	8	$8.3022 \cdot 10^{-3}$	$-4.3134 \cdot 10^{-2}$	-0.27699	0.4514	14.254	$2.1 \cdot 10^{-4}$	0.00130	$6.3 \cdot 10^{-4}$	0.0028
253.147	L34-37, V35-38	8	$5.0483 \cdot 10^{-3}$	$-3.5444 \cdot 10^{-2}$	-0.23569	0.5504	13.339	$1.1 \cdot 10^{-4}$	0.00104	$6.3 \cdot 10^{-4}$	0.0028
273.146	L46-48, V48-50	6	$8.5843 \cdot 10^{-4}$	$-3.0614 \cdot 10^{-2}$	-0.17810	0.6881	11.582	$7.0 \cdot 10^{-5}$	0.00156	$1.3 \cdot 10^{-4}$	0.0027
288.139	L55-58, V57-60	8	$1.1095 \cdot 10^{-2}$	$-1.8503 \cdot 10^{-2}$	-0.11004	0.8206	9.759	$5.7 \cdot 10^{-5}$	0.00055	$5.1 \cdot 10^{-4}$	0.0015
298.136	L64-66, V66-68	6	$2.2534 \cdot 10^{-2}$	$-5.7951 \cdot 10^{-3}$	-0.048162	0.9273	8.321	$5.6 \cdot 10^{-6}$	0.00056	$2.5 \cdot 10^{-5}$	0.0012

[a] Data from Tables 7 and 8, identified with the given IDs.

Table 12
Optimal parameters k_{12}, τ_{12} and τ_{21} for the PR-MC-WS-NRTL model, fitted against data from the present work. Objective function S[c] and absolute average deviation AAD[d] and bias BIAS[e].

	Case 1[a]						Case 2[b]						Both cases
T (K)	k_{12}	τ_{12}	τ_{21}	S	AAD (%)	BIAS (%)	k_{12}	τ_{12}	τ_{21}	S	AAD (%)	BIAS (%)	Excluded points
218.148	0.306378	1.271116	0.362629	16.98	0.74	-0.26	0.3065	1.2536	0.3510	18.75	0.77	-0.02	L9-10, V10-11
233.143	0.308267	1.351550	0.161755	22.38	0.94	-0.34	0.3095	1.3578	0.1698	23.02	0.97	-0.45	L23-24, V24-25
253.147	0.315030	1.507658	-0.093799	24.48	0.96	-0.30	0.3135	1.5281	-0.0806	24.91	0.99	-0.47	L35-36, V36-37
273.146	0.317778	1.753552	-0.350178	20.70	0.80	-0.17	0.3175	1.7628	-0.3453	20.74	0.81	-0.22	L47, V49
288.139	0.322426	2.067354	-0.529082	11.90	0.44	-0.09	0.3205	2.0384	-0.5598	12.81	0.50	0.10	
298.136	0.320166	2.370883	-0.735367	5.89	0.22	-0.03	0.3225	2.3813	-0.7190	5.97	0.21	-0.07	

[a] $k_{12} = k_{21}$ varies freely, $\alpha = 0.3$ [b] $\alpha = 0.3$. τ_{12}, τ_{21} and $k_{12} = k_{21}$ calculated from Eqs. (16), (17) and (18) respectively using $a_{\tau_{12}} = 3.87841$, $b_{\tau_{12}} = -3.42853$, $c_{\tau_{12}} = 0.211545$, $a_{\tau_{21}} = -0.839864$, $b_{\tau_{21}} = 3.53709$, $c_{\tau_{21}} = 0.862063$, $a_{k_{12}} = 0.323688$, $b_{k_{12}} = 0.0606321$ and $T_{c,CO_2} = 304.19$ K from Table 13.

[c] Number of parameters fitted $n_p = 3$. [d] $\mathrm{AAD} = (100/n)\sum_i \left| z_{i,CO_2} - z_{i,CO_2,calc} \right|$ [e] $\mathrm{BIAS} = (100/n)\sum_i \left(z_{i,CO_2} - z_{i,CO_2,calc} \right)$

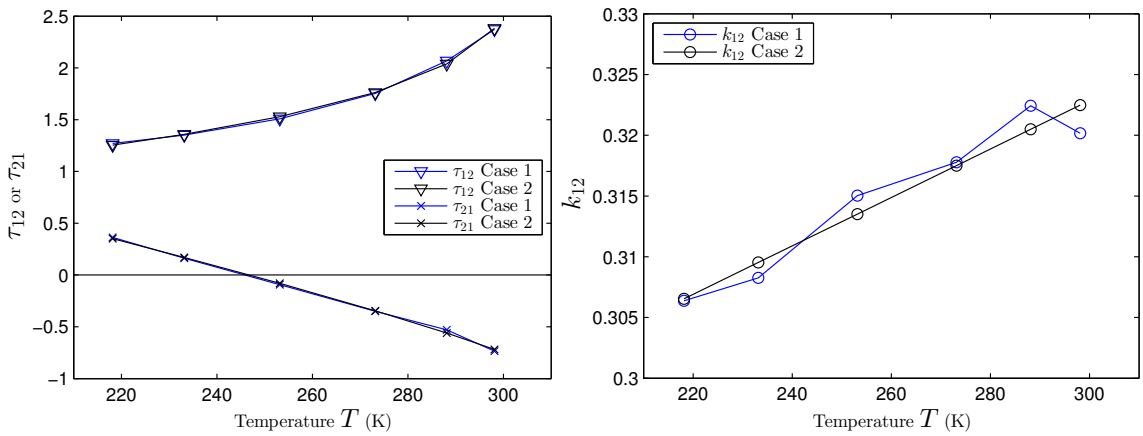

(a) Optimal values for τ_{12} and τ_{21} for the different temperature data sets in Table 12.

(b) Optimal values for k_{12} for the different temperature data sets in Table 12.

Fig. 7. Optimal values for τ_{12}, τ_{21} and k_{12} for the different temperature data sets in Table 12.

Table 13
Critical properties[a] and Mathias-Copeman coefficients[b] used in PR-MC-WS-NRTL EOS for CO_2 and O_2.

i	$T_{c,i}$ (K)	$p_{c,i}$ (MPa)	$c_{1,i}$	$c_{2,i}$	$c_{3,i}$
CO_2	304.19	7.381	0.7050	-0.3185	1.9012
O_2	154.58	5.043	0.4133	-0.0190	0.0944

[a] From Chiavone-Filho et al. [42]. Slightly different from the values used in [6] and [43]: $T_{c,CO_2} = 304.1282$ K, $p_{c,CO_2} = 7.3773$ MPa, $T_{c,O_2} = 154.581$ K, $p_{c,O_2} = 5.043$ MPa. [b] From Chiavone-Filho et al. [42].

Similarly, with reference to Fig. 7b, the temperature dependency of k_{12} was assumed to be described by a simple linear relationship:

$$k_{12}(T) = a_{k_{12}} + b_{k_{12}} \cdot \left(T - T_{c,CO_2}\right) / T_{c,CO_2} \,. \qquad (18)$$

With T_{c,CO_2} given in Table 13, the parameters $a_{\tau_{ij}}$, $b_{\tau_{ij}}$, $c_{\tau_{ij}}$, $a_{k_{12}}$ and $b_{k_{12}}$ in Eqs. (16), (17) and (18) were fitted using ordinary unweighted least squares to the optimal Case 1 parameters in Table 12. The fitted parameters of these equations and the calculated values of τ_{12}, τ_{21}, and k_{12} are given in the same table, denoted as Case 2. These calculated Case 2 EOS parameters are plotted in Figs. 7a and 7b with the optimal Case 1 parameters.

The VLE predictions of the PR-MC-WS-NRTL model using both the Case 1 and 2 parameters are shown in Figs. 5a to 5f together with the data from this work and literature. In addition, the deviations between the Case 2 calculated mole fractions and the experimental values are plotted in these figures. The objective function value, absolute average deviation and bias for both cases are given in Table 12.

With reference to Figs. 5a to 5f, the description of our measurements by the Case 2 model was very close to that of the Case 1 model, and this was reflected with only a minor increase in the values for S and AAD, as seen in Table 12. Therefore, for simplicity, only the Case 2 model will now be discussed. First, the model will be compared with our data, and, second, with the literature data in Table 10.

With reference to our measurement data, three aspects of the Case 2 model could be observed. First, except in the critical region, the vapor CO_2 compositions were slightly overestimated by the model, as seen in Figs. 5a to 5f. In fact, the deviations in composition were in general the largest for the vapor phase, as seen from the pressure-composition deviation plots in these figures. With reference to Table 12, the largest absolute average deviation (AAD), including both liquid and vapor measurements, was 0.01 in mole fraction, which was approximately 3 times larger than the maximum final standard uncertainty of the mole fractions, $u_c(\bar{z}_{CO_2})$, $3.1 \cdot 10^{-3}$. Second, the match between the Case 2 model critical points and those estimated by the scaling law in Section 5.3, was quite good, as seen in Figs. 6a to 6f. The critical pressures estimated by the PR-MC-WS-NRTL Case 2 model were approximately 1% higher than the pressures predicted by the scaling law, and the differences in critical compositions were less than 0.015. Third, as seen in the pressure-composition deviation plots in Figs. 5a to 5f, for each of the isotherms the deviation in composition seemed to develop in a similar manner as a function of pressure, with no apparent scatter. If there had been any apparent scatter, there would have been reason to suspect that the composition samples of the series that deviated from the pattern did not represent the composition at VLE. To be precise, the absence of scatter indicated that the samples represented the VLE composition, however not necessarily that the measured mole fractions for these samples were correct.

As the PR-MC-WS-NRTL Case 2 model was fitted against our data only, it was of interest to compare the model with the literature data in Table 10, and especially the data at other temperatures than those we measured. Table 14 shows the AAD and BIAS for the different VLE literature data in Table 10. Since the AAD and BIAS were calculated as the difference between experimental and calculated mole fractions, the values will in general be higher if a data set contained data in the critical region. The data sets that contained critical region data with proximity to the critical point comparable to our data are identified in Table 14. The AAD for these data sets were comparable to or higher than the AAD for our data at similar temperatures. The same was valid for the literature data sets in general, with a maximum AAD of 0.025 in mole fraction.

The synthetic VLE data sets in Tables 10 and 14 are plotted in a pressure-temperature phase diagram in Fig. 8, together with the PR-MC-WS-NRTL Case 2 VLE calculations at constant compositions. As seen from this figure, the data by Booth and Carter [21] and Ahmad et al. [24] deviated more from the model than the data by Keesom [23].

As it was not possible to find any literature data at temperatures above 298 K (see Table 10), it was difficult to determine how well the PR-MC-WS-NRTL Case 2 model extrapolates up to the critical temperature of CO_2 at 304.19 K.

It has been established that the PR-MC-WS-NRTL Case 2 model provides a fairly accurate description of the VLE for the CO_2+O_2 system given by our data from the temperatures 218 to 298 K, with and AAD of maximum 0.01 in mole fraction and an apparently good description of the critical locus. The most significant shortcoming of the model was the description of the vapor phase compositions, where the deviations were at their largest. With respect to the ability of the model to describe the literature data, the AAD were comparable or somewhat higher considering the lack of critical region data for most of the literature data sets.

6. Conclusions

This work reports accurate vapor-liquid equilibrium (VLE) data for the CO_2+O_2 binary system, at the temperatures 218.15, 233.14, 253.15, 273.15, 288.14 and 298.14 K.

The data measured in this study cover a large range of VLE liquid and vapor phase compositions, spanning CO_2 mole fractions from approximately 0.45 to 0.987 in the liquid phase, and from 0.15 to 0.956 in the vapor phase. The measured CO_2 vapor pressures at the six temperatures are consistent with the values calculated from the Span-Wagner EOS, considering the uncertainty in both the measured pressures and

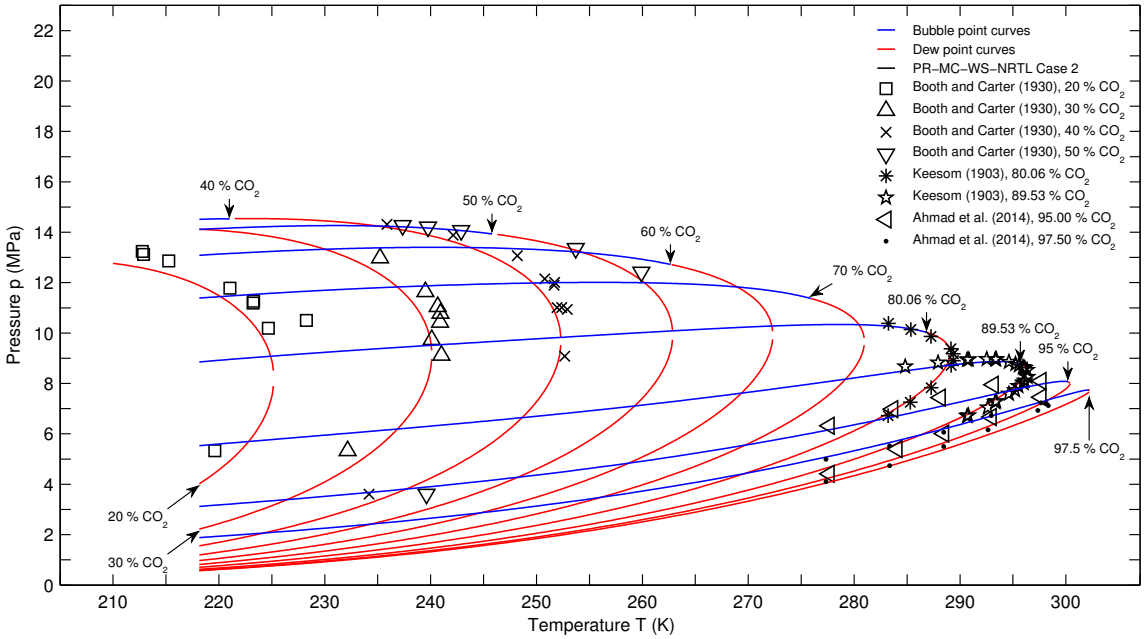

Fig. 8. Pressure-temperature phase diagram at constant compositions based on the PR-MC-WS-NRTL Case 2 model, and synthetic VLE data from literature [21, 23, 24].

that of the EOS. The agreement between our data and literature data varies significantly, also from one temperature to another by the same author. This highlights the inconsistencies in the literature data noted in [3, 4, 5]. As in [1], it was possible to perform very stable measurements close to the mixture critical point at each temperature, and these data formed the basis for the fitting of a scaling law, resulting in estimates for the critical points with low uncertainties. These critical point estimates were slightly lower in pressure than supercritical state point measurements performed at each temperature, which showed the consistency of the critical point estimates.

The Peng-Robinson (PR) cubic EOS [35] with the alpha correction by Mathias and Copeman [36] (MC), the mixing rules by Wong and Sandler [37] (WS), and the NRTL [38] excess Gibbs energy model was fitted to the data in the present work. Based on the parameters sets at each of the six temperatures, expressions for the temperature dependencies of the parameters were developed, resulting in an EOS that can be utilized for VLE calculations over the temperature range from 218 to 298 K and possibly be extrapolated to the critical temperature of CO_2 at 304.19 K. This model described our data quite accurately, and absolute average deviation of our data compared to this model was maximum 0.01 in mole fraction, and maximum 0.025 for the literature data. Additionally, the model matched well with the critical locus given by the scaling law predictions. The critical points calculated by the PR-MC-WS-NRTL model differed from the scaling law prediction by being approximately 1% higher in pressure, and differed in critical compositions with less than 0.015.

The data measured in the present work showed significantly less scatter than the data found in literature, and included measurements close to the mixture critical points for all six temperatures. This data set significantly improves the data situation for the CO_2+O_2 system. It can be used to enhance highly flexible multi-parameter equations of state such as EOS-CG [3, 4], which should be able to describe other thermodynamic properties of the system more accurately than the PR-MC-WS-NRTL model fit provided in the present work.

Acknowledgements

This publication has been produced with support from the research program CLIMIT and the BIGCCS Centre, performed under the Norwegian research program Centres for Environment-friendly Energy Research (FME). The authors acknowledge the following partners for their contributions: Gassco, Shell, Statoil, TOTAL, ENGIE and the Research Council of Norway (193816/S60 and 200005/S60).

The research leading to these results has also received funding from the European Community's Seventh Framework Programme (*FP7-ENERGY-20121-1-2STAGE*) under *grant agreement* n° *308809* (The IMPACTS project). The authors

acknowledge the project partners and the following funding partners for their contributions: Statoil Petroleum AS, Lundin Norway AS, Gas Natural Fenosa, MAN Diesel & Turbo SE and Vattenfall AB.

The authors would like to thank Dr. Morten Hammer, Dr. Geir Skaugen, Dr. Øivind Wilhelmsen, Eskil Aursand and Magnus Aashammer Gjennestad at SINTEF Energy Research for the in-house software used for VLE calculations and the model fitting. We would also like to thank Håvard Rekstad and Reidar Tellebon of NTNU, and Ingeborg Treu Røe who was a summer intern at SINTEF Energy Research, for their contributions.

Finally, the authors would like to thank Professor Roland Span of Ruhr-Universität Bochum and Dr. Johannes Gernert for the access to their literature data base [3].

Table 14
AAD and BIAS for the literature data in Table 10, calculated[a] using the PR-MC-WS-NRTL Case 2 model.

Authors	Type	T[b], z_{CO_2}[c] (K), (-)	AAD (%)	BIAS (%)	n[d]
Zenner and Dana [18]	ISOT	218.19	1.29	-0.76	16
		232.88	2.36	-1.70	22[g]
		273.15	1.49	-1.29	18
Kaminishi and Toriumi [20]	ISOT	233.18	1.02	1.02	2
		253.17	2.46	1.46	10
		273.15	2.16	1.89	8
		288.14	0.73	0.31	4
		293.14	0.82	0.13	5
		298.14	1.19	-1.19	1
Fredenslund and Sather [19]	ISOT	223.16	0.83	-0.79	26
		233.16	1.50	-0.93	25
		243.16	1.06	-0.99	22
		253.15	0.92	-0.57	22
		263.15	0.65	-0.13	20
		273.15	0.63	-0.30	16
		283.15	1.27	-0.76	12
Fredenslund et al. [25]	ISOT	223.76	1.79	1.24	21[g]
Engberg et al. [26]	ISOT	240.9	1.08	-1.08	20
Muirbrook [22]	ISOT	273.15	1.10	0.06	31[g]
Keesom [23]	SYN	0.8006	2.00	-1.77	10[g]
		0.8953	0.74	-0.40	26[g]
Booth and Carter [21]	SYN	0.2	1.67	-1.31	9
		0.3	1.27	-0.73	8
		0.4	1.56	-1.05	11[g]
		0.5	2.04	1.20	6[g]
Ahmad et al. [24]	SYN	0.9493[e]	2.38	2.38	5[g]
		0.9506[f]	0.90	0.90	5[g]
		0.9745[e]	1.01	1.01	6[g]
		0.9751[f]	0.22	-0.20	6[g]

[a] CO_2 mole fractions at VLE calculated at the temperature and pressure given in the literature data. [b] Temperature T if type is ISOT. [c] z_{CO_2} CO_2 mole fraction if type is SYN. [d] Number of temperature and pressure points that were in the VLE region according to the PR-MC-WS-NRTL Case 2 model. [e] Dew points. [f] Bubble points. [g] Data set contains critical region data.

List of symbols

g_L	local acceleration of gravity. See Appendix A.1 in [1]. ($m\,s^{-2}$)
h_i	$i = 1,2,3,4$, liq. Distance used in p_{hs} calculation. See Appendix A.1 in [1]. (m)
k_{ij}	WS binary interaction parameter between components i and j in Eq. (25) in [1]. (−)
M	molar mass ($kg\,mol^{-1}$)
p	pressure at VLE (MPa)
p_c	estimated critical pressure, defined in Section 5.3 (MPa)
p_i	absolute pressure of sensor i, where $i = 1,2,3,4$. See Appendix A.1 in [1]. (MPa)
p_{hs}	hydrostatic pressure. See Appendix A.1 in [1]. (MPa)
p_{11}	differential pressure. See Appendix A.1 in [1]. (MPa)
$\bar{p}$	pressure at VLE: mean pressure before one composition sample in Tables A.2 and A.3 (MPa)
$\bar{p}_f$	pressure at VLE: mean of the pressures $\bar{p}$ for a series of composition samples in Tables 7 and 8 (MPa)
R	resistance of SPRT at a temperature. See Appendix A.2 in [1]. (Ω)
R	universal gas constant = $8.3145\,J\,K^{-1}\,mol^{-1}$
R_{Ga}	resistance of SPRT at T_{Ga}. See Appendix A.2 in [1]. (Ω)
R_{H_2O}	resistance of SPRT at T_{H_2O}. See Appendix A.2 in [1]. (Ω)
R_{Hg}	resistance of SPRT at T_{Hg}. See Appendix A.2 in [1]. (Ω)
R_{ref}	resistance of reference normal. See Appendix A.2 in [1]. (Ω)
$s(z)$	sample standard deviation of variable z
$s(\bar{z})$	sample standard deviation of the mean of variable z
S	model fitting objective function to be minimized (−)
S_E	standard error of regression. See Section 5.3.
T_{04}	ITS-90 temperature of top flange SPRT (K)
T_{05}	ITS-90 temperature of bottom flange SPRT (K)
T	ITS-90 temperature at VLE (K)
$\bar{T}$	ITS-90 temperature at VLE: mean temperature before one composition sample in Tables A.2 and A.3 (K)
$\bar{T}_f$	ITS-90 temperature at VLE: mean of the temperatures $\bar{T}$ for a series of composition samples in Tables 7 and 8 (K)
T_{Ga}	ITS-90 temperature at gallium melting point. See Appendix A.2 in [1]. (K)
T_{H_2O}	ITS-90 temperature at water triple point. See Appendix A.2 in [1]. (K)
T_{Hg}	ITS-90 temperature at mercury triple point. See Appendix A.2 in [1]. (K)
$u(z)$	standard uncertainty of variable z
$u_c(z)$	combined standard uncertainty of variable z
$u_{tot}(z)$	total standard uncertainty of variable $z = x_{CO_2}$ or y_{CO_2}, from Eq. (7). (−)
W	ITS-90 ratio R/R_{H_2O}. See Appendix A.2 in [1]. (−)
W_b	thermometry bridge ratio R/R_{ref}. See Appendix A.2 in [1]. (−)
x_{CO_2}	liquid phase CO_2 mole fraction at VLE in Table A.2 (−)
$\bar{x}_{CO_2}$	liquid phase CO_2 mole fraction at VLE: mean mole fraction a series of composition samples in Table 7 (−)
$x_{CO_2,calc}$	liquid phase CO_2 mole fraction at VLE, calculated from the PR-MC-WS-NRTL Case 2 model. See Section 5.4.2. (−)
y_{CO_2}	vapor phase CO_2 mole fraction at VLE in Table A.3 (−)
$\bar{y}_{CO_2}$	vapor phase CO_2 mole fraction at VLE: mean mole fraction a series of composition samples in Table 8 (−)
$y_{CO_2,calc}$	vapor phase CO_2 mole fraction at VLE, calculated from the PR-MC-WS-NRTL Case 2 model. See Section 5.4.2. (−)
z_{CO_2}	liquid or vapor phase CO_2 mole fraction (−)
$z_{CO_2,c}$	estimated critical composition in terms of CO_2 mole fraction, defined in Section 5.3 (−)

Greek letters

α_{ij}	NRTL non-randomness parameter for binary interaction between components i and j in Eq. (26) in [1].
β	universal critical exponent of scaling law in Eq. (13)
λ_1, λ_2, μ	parameters of scaling law in Eq. (13).
ρ	density ($kg\,m^{-3}$)
ρ_i	density in the four different regions $i = 1,2,3,4$ used for calculation of p_{hs}. See Appendix A.1 in [1]. ($kg\,m^{-3}$)
$\rho_{4,1}$	density of pure CO_2 in Region 4 used for calculation of p_{hs}. See Appendix A.1 in [1]. ($kg\,m^{-3}$)
$\rho_{4,2}$	density of fluid in Region 4 used for calculation of p_{hs}. See Appendix A.1 in [1]. ($kg\,m^{-3}$)

τ_{ij}	NRTL parameter for binary interaction between components i and j in Eq. (26) in [1]. (−)

Subscripts

c	critical state

Superscripts

$\bar{}$	arithmetic mean

Abbreviations

AAD	absolute average deviation. See Section 5.4.1 and Table 12.
BIAS	bias. See Section 5.4.1 and Table 12.
CAD	computer-aided design
CCS	carbon capture, transport and storage
EOS	equation of state
EOS-CG	equation of state for combustion gases and combustion gas like mixtures [3, 4]
GC	gas chromatograph
GUM	ISO Guide for the Estimation of Uncertainty in Measurement [11]
ITS-90	International Temperature Scale of 1990 [44]
MC	Mathias-Copeman alpha correction [36]
NRTL	non-random two-liquid excess Gibbs energy model [38]
ODR	orthogonal distance regression
PR	Peng-Robinson EOS [35]
PR-MC-WS-NRTL	PR EOS with MC alpha correction and WS mixing rule with the NRTL excess Gibbs energy model
SPRT	standard platinum resistance thermometer
SW	Span-Wagner EOS for CO_2 [6]
TCD	thermal conductivity detector in GC
VLE	vapor-liquid equilibrium
WS	Wong-Sandler mixing rule [37]

Appendix A. Detailed experimental data

Detailed VLE data for the liquid phase samples are given in Table A.2, and for the vapor phase samples in Table A.3. Each row in the tables corresponds to one composition sample. A series of samples taken at the same VLE experiment is identified by the same ID.

For ease of reading, a summary of the symbols used in the tables will be given in Table A.1. The descriptions can also be found in the list of symbols.

Table A.1
Summary of symbols used in Tables A.2 and A.3.

Symbol	Description
ID	Identifier for a series of samples. L, V and P corresponds to liquid, vapor and CO_2 vapor pressure series, respectively. Marker * means that the series was measured using procedure in Section 2.3.2.
$\bar{T}$	Mean temperature before the sample is withdrawn from the cell. See Section 3.4.
$\bar{p}$	Mean pressure before the sample is withdrawn from the cell. See Section 3.4.
x_{CO_2}	Liquid phase CO_2 mole fraction of the sample.
y_{CO_2}	Vapor phase CO_2 mole fraction of the sample.
$s(T)$	Sample standard deviation of the measured temperatures used to calculate $\bar{T}$. See Eq. (7) in [1].
$s(\bar{T})$	Standard random uncertainty of $\bar{T}$, considering the autocorrelation of the measurements of T. See Eq. (6) in [1].
$\tilde{u}(T)$	Standard systematic uncertainty of $\bar{T}$. See Section 3.5 in [1].
$u_c(\bar{T})$	Combined standard uncertainty of $\bar{T}$. Calculated as $\sqrt{s^2(\bar{T}) + \tilde{u}^2(T)}$.
$s(p)$	Sample standard deviation of the measured pressures used to calculate $\bar{p}$. See Eq. (7) in [1].
$s(\bar{p})$	Standard random uncertainty of $\bar{p}$, considering the autocorrelation of the measurements of p. See Eq. (6) in [1].
$\tilde{u}(p)$	Standard systematic uncertainty of $\bar{p}$. See Section 3.5 in [1].
$u_c(\bar{p})$	Combined standard uncertainty of $\bar{p}$. Calculated as $\sqrt{s^2(\bar{p}) + \tilde{u}^2(p)}$.
$u(z_{CO_2})$[a]	Standard uncertainty of a sample from composition analysis alone. See Section 3.3 and Table 6.
$u_{tot}(z_{CO_2})$[a]	Total standard uncertainty of a sample, caused by additional contribution from the uncertainty in temperature and pressure. See Eq. (7). Marker $^+$ means that the derivative $\partial z_{CO_2}/\partial p$ used in Eq. (7) was calculated using the scaling law in Eq. (13) with the parameters in Table 11 instead of the PR-MC-WS-NRTL Case 2 fitted EOS.
$z_{CO_2,calc}$[a]	VLE CO_2 mole fraction at $(\bar{T}, \bar{p})$, calculated using the PR-MC-WS-NRTL Case 2 fitted EOS. See Section 5.4.2.
$\partial z_{CO_2}/\partial T$[a]	Partial derivative of phase composition at VLE with respect to temperature, calculated using the PR-MC-WS-NRTL Case 2 fitted EOS. Used in Eq. (7).
$\partial z_{CO_2}/\partial p$[a]	Partial derivative of phase composition at VLE with respect to pressure. Used in Eq. (7). Marker $^+$ means that the derivative was calculated using the scaling law in Eq. (13) with the parameters in Table 11 instead of the PR-MC-WS-NRTL Case 2 fitted EOS.

[a] z_{CO_2} equal to either x_{CO_2} or y_{CO_2}.

Table A.2
Liquid phase: Experimental VLE data for $CO_2 + O_2$ at mean temperature $\bar{T}$, mean pressure $\bar{p}$, and sample liquid phase mole fraction x_{CO_2}.

	Data			Temperature				Pressure				Composition			Composition derivatives	
ID	$\bar{T}$ (K)	$\bar{p}$ (MPa)	x_{CO_2} (-)	$s(T)$ (K)	$s(\bar{T})$ (K)	$\bar{u}(T)$ (K)	$u_c(\bar{T})$ (K)	$s(p)$ (MPa)	$s(\bar{p})$ (MPa)	$\bar{u}(p)$ (MPa)	$u_c(\bar{p})$ (MPa)	$u(x_{CO_2})$ (-)	$u_{tot}(x_{CO_2})$ (-)	$x_{CO_2,calc}$ (-)	$\partial x_{CO_2}/\partial T$ (K^{-1})	$\partial x_{CO_2}/\partial p$ (MPa^{-1})
P1	218.147	0.5546	0.99999	4.7e-4	7.3e-5	3.7e-3	3.7e-3	1.3e-5	1.1e-6	4.9e-4	4.9e-4					
L1	218.147	2.1957	0.96687	5.1e-4	1.1e-4	3.5e-3	3.6e-3	2.5e-5	6.0e-6	5.2e-4	5.2e-4	4.8e-4	4.8e-4	0.96887	0.00057	-0.01984
	218.147	2.1957	0.96688	8.8e-4	1.9e-4	3.5e-3	3.5e-3	3.2e-5	1.1e-5	5.2e-4	5.2e-4	4.8e-4	4.8e-4	0.96887	0.00057	-0.01984
	218.148	2.1957	0.96687	8.8e-4	3.3e-4	3.6e-3	3.6e-3	4.8e-5	1.6e-5	5.2e-4	5.2e-4	4.8e-4	4.8e-4	0.96887	0.00057	-0.01984
	218.148	2.1957	0.96688	5.3e-4	5.9e-5	3.4e-3	3.4e-3	2.8e-5	3.8e-6	5.2e-4	5.2e-4	4.8e-4	4.8e-4	0.96888	0.00057	-0.01984
	218.148	2.1958	0.96686	4.9e-4	1.4e-4	3.5e-3	3.5e-3	7.5e-5	1.6e-5	5.2e-4	5.2e-4	4.8e-4	4.8e-4	0.96887	0.00057	-0.01984
L2	218.148	3.9363	0.92960	8.9e-4	1.1e-4	3.7e-3	3.7e-3	1.4e-4	5.6e-5	1.1e-3	1.1e-3	4.8e-4	4.8e-4	0.93249	0.00073	-0.02205
	218.148	3.9363	0.92958	7.0e-4	8.4e-5	3.7e-3	3.7e-3	7.8e-5	6.9e-6	1.1e-3	1.1e-3	4.8e-4	4.8e-4	0.93249	0.00073	-0.02205
	218.148	3.9362	0.92957	7.5e-4	1.4e-4	3.8e-3	3.8e-3	1.5e-4	5.7e-5	1.1e-3	1.1e-3	4.8e-4	4.8e-4	0.93250	0.00073	-0.02205
	218.148	3.9362	0.92958	7.6e-4	1.3e-4	3.9e-3	3.9e-3	1.1e-4	3.8e-5	1.1e-3	1.1e-3	4.8e-4	4.8e-4	0.93250	0.00073	-0.02205
	218.148	3.9362	0.92957	6.6e-4	1.0e-4	3.7e-3	3.7e-3	5.3e-5	6.3e-6	1.1e-3	1.1e-3	4.8e-4	4.8e-4	0.93250	0.00073	-0.02205
	218.148	3.9363	0.92958	7.6e-4	9.5e-5	3.7e-3	3.7e-3	7.6e-5	2.2e-5	1.1e-3	1.1e-3	4.8e-4	4.8e-4	0.93249	0.00073	-0.02205
L3	218.147	5.9189	0.88227	7.6e-4	1.2e-4	3.6e-3	3.6e-3	1.2e-4	1.3e-5	1.1e-3	1.1e-3	4.8e-4	4.8e-4	0.88563	0.00091	-0.02541
	218.147	5.9190	0.88226	8.2e-4	8.2e-5	3.7e-3	3.7e-3	2.5e-4	1.5e-5	1.1e-3	1.1e-3	4.8e-4	4.8e-4	0.88562	0.00091	-0.02541
	218.147	5.9189	0.88227	2.0e-3	4.0e-4	3.4e-3	3.4e-3	1.2e-4	7.7e-6	1.1e-3	1.1e-3	4.8e-4	4.8e-4	0.88562	0.00091	-0.02541
	218.149	5.9189	0.88225	1.3e-3	3.4e-4	3.1e-3	3.2e-3	2.0e-4	2.9e-5	1.1e-3	1.1e-3	4.8e-4	4.8e-4	0.88563	0.00091	-0.02541
	218.149	5.9189	0.88226	9.5e-4	1.5e-4	3.2e-3	3.2e-3	1.4e-4	1.1e-5	1.1e-3	1.1e-3	4.8e-4	4.8e-4	0.88563	0.00091	-0.02541
	218.149	5.9189	0.88226	1.0e-3	2.0e-4	3.2e-3	3.2e-3	1.1e-4	1.1e-5	1.1e-3	1.1e-3	4.8e-4	4.8e-4	0.88563	0.00091	-0.02541
L4	218.148	7.8935	0.82833	3.9e-4	3.6e-5	3.4e-3	3.4e-3	1.1e-4	5.3e-6	1.2e-3	1.2e-3	4.8e-4	4.8e-4	0.83104	0.00110	-0.03021
	218.149	7.8935	0.82831	1.4e-3	2.4e-4	3.5e-3	3.5e-3	1.1e-4	3.2e-6	1.2e-3	1.2e-3	4.8e-4	4.8e-4	0.83104	0.00110	-0.03021
	218.148	7.8935	0.82831	7.6e-4	8.0e-5	3.5e-3	3.5e-3	1.1e-4	4.1e-6	1.2e-3	1.2e-3	4.8e-4	4.8e-4	0.83104	0.00110	-0.03021
	218.149	7.8935	0.82832	6.7e-4	6.7e-5	3.5e-3	3.5e-3	1.2e-4	6.3e-6	1.2e-3	1.2e-3	4.8e-4	4.8e-4	0.83104	0.00110	-0.03021
	218.148	7.8935	0.82834	7.4e-4	8.0e-5	3.5e-3	3.5e-3	1.0e-4	3.7e-6	1.2e-3	1.2e-3	4.8e-4	4.8e-4	0.83104	0.00110	-0.03021
L5	218.149	9.7335	0.76940	5.3e-4	1.0e-4	3.5e-3	3.5e-3	1.6e-4	6.8e-6	1.4e-3	1.4e-3	4.8e-4	4.8e-4	0.76955	0.00130	-0.03720
	218.148	9.7335	0.76941	4.6e-4	5.3e-5	3.4e-3	3.4e-3	1.2e-4	4.3e-6	1.4e-3	1.4e-3	4.8e-4	4.8e-4	0.76955	0.00130	-0.03720
	218.148	9.7335	0.76941	5.0e-4	7.2e-5	3.5e-3	3.5e-3	1.4e-4	8.9e-6	1.4e-3	1.4e-3	4.8e-4	4.8e-4	0.76955	0.00130	-0.03720
	218.148	9.7335	0.76941	9.1e-4	1.3e-4	3.4e-3	3.4e-3	1.3e-4	1.0e-5	1.4e-3	1.4e-3	4.8e-4	4.8e-4	0.76955	0.00130	-0.03720
	218.148	9.7335	0.76942	8.4e-4	9.5e-5	3.5e-3	3.5e-3	1.6e-4	7.5e-6	1.4e-3	1.4e-3	4.8e-4	4.8e-4	0.76955	0.00130	-0.03720
	218.148	9.7335	0.76941	6.6e-4	8.0e-5	3.4e-3	3.4e-3	1.2e-4	1.5e-5	1.4e-3	1.4e-3	4.8e-4	4.8e-4	0.76955	0.00130	-0.03720
L6	218.148	11.7910	0.68723	5.4e-4	5.9e-5	3.5e-3	3.5e-3	2.1e-4	1.7e-5	2.7e-3	2.7e-3	4.8e-4	5.0e-4	0.67972	0.00157	-0.05216
	218.148	11.7909	0.68722	8.5e-4	1.1e-4	3.5e-3	3.5e-3	2.5e-4	1.6e-5	2.7e-3	2.7e-3	4.8e-4	5.0e-4	0.67972	0.00157	-0.05216
	218.148	11.7910	0.68721	7.3e-4	1.2e-4	3.6e-3	3.6e-3	1.8e-4	6.9e-6	2.7e-3	2.7e-3	4.8e-4	5.0e-4	0.67972	0.00157	-0.05216
	218.148	11.7910	0.68723	6.4e-4	8.1e-5	3.6e-3	3.6e-3	2.0e-4	8.7e-6	2.7e-3	2.7e-3	4.8e-4	5.0e-4	0.67972	0.00157	-0.05216
	218.149	11.7909	0.68725	5.2e-4	1.0e-4	3.5e-3	3.5e-3	2.2e-4	1.2e-5	2.7e-3	2.7e-3	4.8e-4	5.0e-4	0.67972	0.00157	-0.05215
	218.148	11.7910	0.68722	5.0e-4	5.5e-5	3.5e-3	3.5e-3	2.0e-4	9.7e-6	2.7e-3	2.7e-3	4.8e-4	5.0e-4	0.67972	0.00157	-0.05216
L7	218.148	13.0211	0.61991	1.1e-3	1.7e-4	3.7e-3	3.7e-3	2.4e-4	1.1e-5	2.8e-3	2.8e-3	4.8e-4	5.2e-4	0.60471	0.00188	-0.07268
	218.149	13.0212	0.61993	6.7e-4	1.8e-4	3.4e-3	3.4e-3	2.1e-4	1.7e-5	2.8e-3	2.8e-3	4.8e-4	5.2e-4	0.60470	0.00188	-0.07268
	218.148	13.0212	0.61995	8.7e-4	2.7e-4	3.5e-3	3.5e-3	2.3e-4	1.5e-5	2.8e-3	2.8e-3	4.8e-4	5.2e-4	0.60470	0.00188	-0.07268
	218.148	13.0212	0.61994	9.8e-4	2.2e-4	3.5e-3	3.5e-3	2.0e-4	1.1e-5	2.8e-3	2.8e-3	4.8e-4	5.2e-4	0.60470	0.00188	-0.07268
	218.148	13.0211	0.61995	8.5e-4	1.1e-4	3.5e-3	3.5e-3	2.4e-4	2.4e-5	2.8e-3	2.8e-3	4.8e-4	5.2e-4	0.60471	0.00188	-0.07268
	218.148	13.0211	0.61996	6.4e-4	1.4e-4	3.6e-3	3.6e-3	2.1e-4	2.6e-5	2.8e-3	2.8e-3	4.8e-4	5.2e-4	0.60471	0.00188	-0.07268
L8	218.148	14.0359	0.53319	9.6e-4	1.0e-4	3.5e-3	3.5e-3	2.5e-4	2.1e-5	2.8e-3	2.8e-3	4.8e-4	$6.0e\text{-}4^{+}$	0.51002	0.00276	-0.12824^{+}
	218.149	14.0359	0.53324	8.0e-4	1.5e-4	3.6e-3	3.6e-3	2.1e-4	2.5e-5	2.8e-3	2.8e-3	4.8e-4	$6.0e\text{-}4^{+}$	0.51001	0.00276	-0.12825^{+}
	218.148	14.0358	0.53335	1.2e-3	4.7e-4	3.6e-3	3.6e-3	2.6e-4	1.4e-5	2.8e-3	2.8e-3	4.8e-4	$6.0e\text{-}4^{+}$	0.51003	0.00276	-0.12823^{+}
	218.147	14.0359	0.53333	1.4e-3	3.8e-4	3.7e-3	3.7e-3	2.4e-4	2.8e-5	2.8e-3	2.8e-3	4.8e-4	$6.0e\text{-}4^{+}$	0.51002	0.00276	-0.12824^{+}
	218.148	14.0358	0.53331	8.8e-4	9.0e-5	3.5e-3	3.6e-3	2.4e-4	3.0e-5	2.8e-3	2.8e-3	4.8e-4	$6.0e\text{-}4^{+}$	0.51002	0.00276	-0.12823^{+}
	218.148	14.0358	0.53333	1.1e-3	2.7e-4	3.6e-3	3.6e-3	2.3e-4	3.4e-5	2.8e-3	2.8e-3	4.8e-4	$6.0e\text{-}4^{+}$	0.51003	0.00276	-0.12823^{+}

L9*	218.148	14.3563	0.47535	6.4e-4	9.8e-5	3.4e-3	3.4e-3	2.9e-4	2.0e-5	2.8e-3	2.8e-3	4.8e-4	9.8e-4^{+}	0.45827	0.00403	-0.30998^{+}
	218.148	14.3563	0.47536	5.4e-4	8.8e-5	3.4e-3	3.4e-3	3.0e-4	2.1e-5	2.8e-3	2.8e-3	4.8e-4	9.8e-4^{+}	0.45827	0.00403	-0.31001^{+}
	218.148	14.3563	0.47533	6.1e-4	4.0e-5	3.2e-3	3.2e-3	2.7e-4	1.8e-5	2.8e-3	2.8e-3	4.8e-4	9.8e-4^{+}	0.45826	0.00403	-0.31002^{+}
	218.148	14.3564	0.47536	1.0e-3	1.4e-4	3.2e-3	3.2e-3	2.4e-4	2.9e-5	2.8e-3	2.8e-3	4.8e-4	9.8e-4^{+}	0.45825	0.00403	-0.31013^{+}
	218.148	14.3563	0.47536	6.1e-4	2.0e-4	3.2e-3	3.2e-3	1.2e-4	4.6e-6	2.8e-3	2.8e-3	4.8e-4	9.8e-4^{+}	0.45827	0.00403	-0.30996^{+}
L10*	218.149	14.3873	0.46438	6.3e-4	2.2e-4	3.4e-3	3.4e-3	2.6e-4	2.4e-5	2.8e-3	2.8e-3	4.8e-4	1.3e-3^{+}	0.45116	0.00435	-0.41964^{+}
	218.149	14.3873	0.46441	7.0e-4	1.8e-4	3.3e-3	3.3e-3	2.4e-4	1.8e-5	2.8e-3	2.8e-3	4.8e-4	1.3e-3^{+}	0.45117	0.00435	-0.41955^{+}
	218.149	14.3873	0.46440	6.3e-4	1.2e-4	3.2e-3	3.3e-3	2.0e-4	8.1e-6	2.8e-3	2.8e-3	4.8e-4	1.3e-3^{+}	0.45116	0.00435	-0.41961^{+}
	218.149	14.3873	0.46441	6.4e-4	8.4e-5	3.4e-3	3.4e-3	2.9e-4	2.5e-5	2.8e-3	2.8e-3	4.8e-4	1.3e-3^{+}	0.45117	0.00435	-0.41946^{+}
	218.148	14.3874	0.46438	6.2e-4	8.0e-5	3.5e-3	3.5e-3	2.2e-4	1.4e-5	2.8e-3	2.8e-3	4.8e-4	1.3e-3^{+}	0.45114	0.00435	-0.42010^{+}
	218.148	14.3873	0.46440	6.2e-4	6.2e-5	3.4e-3	3.4e-3	2.8e-4	3.8e-5	2.8e-3	2.8e-3	4.8e-4	1.3e-3^{+}	0.45117	0.00435	-0.41953^{+}
L11*	218.148	14.4110	0.45222	1.5e-3	3.6e-4	3.4e-3	3.4e-3	3.0e-4	3.6e-5	2.8e-3	2.8e-3	4.8e-4	1.9e-3^{+}	0.44514	0.00467	-0.64579^{+}
	218.149	14.4111	0.45231	8.6e-4	1.3e-4	3.4e-3	3.4e-3	2.6e-4	1.3e-5	2.8e-3	2.8e-3	4.8e-4	1.9e-3^{+}	0.44512	0.00467	-0.64692^{+}
	218.149	14.4111	0.45231	8.3e-4	1.3e-4	3.4e-3	3.4e-3	2.7e-4	3.1e-5	2.8e-3	2.8e-3	4.8e-4	1.9e-3^{+}	0.44511	0.00467	-0.64770^{+}
	218.149	14.4111	0.45233	8.9e-4	1.3e-4	3.3e-3	3.3e-3	2.4e-4	1.6e-5	2.8e-3	2.8e-3	4.8e-4	1.9e-3^{+}	0.44513	0.00467	-0.64630^{+}
	218.149	14.4111	0.45235	7.8e-4	1.1e-4	3.3e-3	3.3e-3	2.4e-4	1.3e-5	2.8e-3	2.8e-3	4.8e-4	1.9e-3^{+}	0.44512	0.00467	-0.64703^{+}
	218.149	14.4111	0.45240	6.8e-4	1.0e-4	3.3e-3	3.3e-3	2.8e-4	1.9e-5	2.8e-3	2.8e-3	4.8e-4	1.9e-3^{+}	0.44512	0.00467	-0.64703^{+}
P2	233.143	1.0048	0.99999	9.7e-4	7.4e-5	6.8e-3	6.8e-3	4.3e-5	1.1e-5	5.1e-4	5.1e-4					
L13	233.143	1.9677	0.98003	9.0e-4	1.5e-4	7.3e-3	7.3e-3	4.3e-5	7.6e-6	5.1e-4	5.1e-4	4.8e-4	4.8e-4	0.98262	0.00070	-0.01860
	233.142	1.9677	0.98022	7.6e-4	1.3e-4	7.0e-3	7.0e-3	4.9e-5	1.1e-5	5.1e-4	5.1e-4	4.8e-4	4.8e-4	0.98262	0.00070	-0.01860
	233.142	1.9677	0.98046	9.1e-4	1.0e-4	7.2e-3	7.2e-3	2.4e-5	5.6e-6	5.1e-4	5.1e-4	4.8e-4	4.8e-4	0.98262	0.00070	-0.01860
	233.142	1.9677	0.98020	1.1e-3	1.9e-4	7.4e-3	7.4e-3	2.8e-5	7.7e-6	5.1e-4	5.1e-4	4.8e-4	4.8e-4	0.98262	0.00070	-0.01860
L14	233.141	2.9346	0.96022	1.0e-3	1.5e-4	7.6e-3	7.6e-3	1.1e-4	4.7e-5	5.3e-4	5.3e-4	4.8e-4	4.8e-4	0.96410	0.00075	-0.01973
	233.141	2.9345	0.96022	1.1e-3	1.9e-4	7.9e-3	7.9e-3	2.0e-4	7.4e-5	5.3e-4	5.3e-4	4.8e-4	4.8e-4	0.96410	0.00075	-0.01973
	233.141	2.9345	0.96019	7.0e-4	6.9e-5	7.6e-3	7.6e-3	4.4e-5	1.5e-5	5.2e-4	5.2e-4	4.8e-4	4.8e-4	0.96410	0.00075	-0.01973
	233.141	2.9345	0.96019	8.7e-4	9.4e-5	8.1e-3	8.1e-3	1.2e-4	1.8e-5	5.3e-4	5.3e-4	4.8e-4	4.8e-4	0.96410	0.00075	-0.01973
	233.141	2.9345	0.96021	9.6e-4	3.2e-4	7.7e-3	7.7e-3	2.9e-5	2.1e-6	5.2e-4	5.2e-4	4.8e-4	4.8e-4	0.96410	0.00075	-0.01973
	233.141	2.9346	0.96020	1.0e-3	1.1e-4	7.7e-3	7.7e-3	6.1e-5	8.5e-6	5.3e-4	5.3e-4	4.8e-4	4.8e-4	0.96409	0.00075	-0.01973
L15	233.143	3.9407	0.93831	1.5e-3	2.1e-4	6.7e-3	6.7e-3	7.3e-4	8.4e-5	1.1e-3	1.1e-3	4.8e-4	4.8e-4	0.94358	0.00079	-0.02108
	233.143	3.9407	0.93830	1.3e-3	4.1e-4	6.6e-3	6.6e-3	5.8e-4	8.9e-5	1.1e-3	1.1e-3	4.8e-4	4.8e-4	0.94358	0.00079	-0.02108
	233.142	3.9409	0.93829	1.1e-3	1.6e-4	6.9e-3	6.9e-3	6.5e-4	9.5e-5	1.1e-3	1.1e-3	4.8e-4	4.8e-4	0.94358	0.00079	-0.02108
	233.143	3.9409	0.93829	1.2e-3	2.5e-4	6.8e-3	6.8e-3	6.1e-4	8.2e-5	1.1e-3	1.1e-3	4.8e-4	4.8e-4	0.94358	0.00079	-0.02108
	233.142	3.9406	0.93828	9.4e-4	1.4e-4	6.8e-3	6.8e-3	7.2e-4	8.4e-5	1.1e-3	1.1e-3	4.8e-4	4.8e-4	0.94358	0.00079	-0.02108
	233.142	3.9408	0.93829	1.2e-3	1.3e-4	7.2e-3	7.2e-3	6.3e-4	1.1e-4	1.1e-3	1.1e-3	4.8e-4	4.8e-4	0.94358	0.00079	-0.02108
L16	233.142	5.9478	0.89066	1.1e-3	3.1e-4	7.0e-3	7.1e-3	1.2e-4	1.3e-5	1.1e-3	1.1e-3	4.8e-4	4.8e-4	0.89802	0.00087	-0.02451
	233.143	5.9477	0.89066	7.8e-4	2.1e-4	7.0e-3	7.1e-3	1.3e-4	1.6e-5	1.1e-3	1.1e-3	4.8e-4	4.8e-4	0.89803	0.00087	-0.02451
	233.143	5.9477	0.89068	1.3e-3	2.9e-4	7.2e-3	7.2e-3	7.8e-5	5.9e-6	1.1e-3	1.1e-3	4.8e-4	4.8e-4	0.89803	0.00087	-0.02451
	233.144	5.9478	0.89068	7.8e-4	1.1e-4	7.2e-3	7.2e-3	1.1e-4	1.5e-5	1.1e-3	1.1e-3	4.8e-4	4.8e-4	0.89803	0.00087	-0.02451
	233.144	5.9477	0.89068	9.9e-4	1.5e-4	7.8e-3	7.8e-3	1.0e-4	1.6e-5	1.1e-3	1.1e-3	4.8e-4	4.8e-4	0.89803	0.00087	-0.02451
	233.144	5.9477	0.89066	7.6e-4	1.0e-4	7.2e-3	7.2e-3	1.2e-4	1.0e-5	1.1e-3	1.1e-3	4.8e-4	4.8e-4	0.89803	0.00087	-0.02451
L17	233.143	7.8334	0.84019	1.2e-3	3.2e-4	7.7e-3	7.7e-3	2.1e-4	1.5e-5	1.2e-3	1.2e-3	4.8e-4	4.8e-4	0.84775	0.00094	-0.02911
	233.142	7.8335	0.84017	1.1e-3	3.3e-4	7.5e-3	7.6e-3	2.6e-4	3.0e-5	1.2e-3	1.2e-3	4.8e-4	4.8e-4	0.84775	0.00094	-0.02911
	233.143	7.8334	0.84017	8.3e-4	8.3e-5	7.7e-3	7.7e-3	2.3e-4	1.3e-5	1.2e-3	1.2e-3	4.8e-4	4.8e-4	0.84775	0.00094	-0.02911
	233.144	7.8334	0.84018	1.4e-3	4.3e-4	7.5e-3	7.5e-3	1.9e-4	1.4e-5	1.2e-3	1.2e-3	4.8e-4	4.8e-4	0.84775	0.00094	-0.02911
	233.143	7.8334	0.84018	1.6e-3	6.5e-4	7.5e-3	7.5e-3	2.3e-4	1.9e-5	1.2e-3	1.2e-3	4.8e-4	4.8e-4	0.84775	0.00094	-0.02911
	233.142	7.8334	0.84017	7.8e-4	2.0e-4	7.3e-3	7.3e-3	2.1e-4	2.2e-5	1.2e-3	1.2e-3	4.8e-4	4.8e-4	0.84775	0.00094	-0.02911
	233.142	7.8335	0.84016	9.9e-4	9.6e-5	7.5e-3	7.5e-3	1.6e-4	8.7e-6	1.2e-3	1.2e-3	4.8e-4	4.8e-4	0.84775	0.00094	-0.02911
L18	233.141	8.8724	0.80941	2.0e-3	6.3e-4	7.3e-3	7.4e-3	2.2e-4	9.3e-6	1.3e-3	1.3e-3	4.8e-4	4.8e-4	0.81577	0.00096	-0.03259
	233.143	8.8724	0.80934	1.6e-3	3.0e-4	7.2e-3	7.2e-3	2.0e-4	1.1e-5	1.3e-3	1.3e-3	4.8e-4	4.8e-4	0.81577	0.00096	-0.03259
	233.141	8.8724	0.80940	1.8e-3	2.9e-4	7.9e-3	7.9e-3	1.4e-4	8.0e-6	1.3e-3	1.3e-3	4.8e-4	4.8e-4	0.81577	0.00096	-0.03259
	233.141	8.8724	0.80941	1.2e-3	1.6e-4	7.6e-3	7.6e-3	1.6e-4	1.4e-5	1.3e-3	1.3e-3	4.8e-4	4.8e-4	0.81577	0.00096	-0.03259
L19	233.142	9.8513	0.77736	1.6e-3	4.9e-4	7.1e-3	7.1e-3	2.0e-4	2.2e-5	1.4e-3	1.4e-3	4.8e-4	4.8e-4	0.78187	0.00098	-0.03685
	233.143	9.8514	0.77735	1.1e-3	2.0e-4	7.1e-3	7.2e-3	2.5e-4	2.8e-5	1.4e-3	1.4e-3	4.8e-4	4.8e-4	0.78187	0.00098	-0.03686
	233.141	9.8514	0.77734	1.2e-3	1.9e-4	7.0e-3	7.0e-3	1.4e-4	6.7e-6	1.4e-3	1.4e-3	4.8e-4	4.8e-4	0.78187	0.00098	-0.03685

	233.141	9.8514	0.77738	9.7e-4	1.9e-4	7.2e-3	7.2e-3	1.4e-4	4.6e-6	1.4e-3	1.4e-3	4.8e-4	4.8e-4	0.78187	0.00098	-0.03686
L20	233.140	11.8341	0.69898	1.1e-3	1.2e-4	7.3e-3	7.3e-3	3.7e-4	9.9e-6	2.7e-3	2.7e-3	4.8e-4	5.0e-4	0.69628	0.00098	-0.05132
	233.140	11.8342	0.69897	7.0e-4	6.2e-5	7.7e-3	7.7e-3	3.6e-4	1.7e-5	2.7e-3	2.7e-3	4.8e-4	5.0e-4	0.69628	0.00098	-0.05132
	233.140	11.8342	0.69895	1.1e-3	2.4e-4	7.2e-3	7.2e-3	2.2e-4	1.5e-5	2.7e-3	2.7e-3	4.8e-4	5.0e-4	0.69628	0.00098	-0.05132
	233.139	11.8342	0.69897	1.3e-3	4.3e-4	7.2e-3	7.3e-3	2.2e-4	2.0e-5	2.7e-3	2.7e-3	4.8e-4	5.0e-4	0.69628	0.00098	-0.05132
	233.140	11.8341	0.69897	1.9e-3	4.3e-4	6.8e-3	6.8e-3	2.7e-4	5.7e-5	2.7e-3	2.7e-3	4.8e-4	5.0e-4	0.69628	0.00098	-0.05132
L21	233.143	12.8248	0.64712	7.4e-4	1.2e-4	7.0e-3	7.0e-3	2.4e-4	1.5e-5	2.7e-3	2.7e-3	4.8e-4	5.1e-4	0.63897	0.00093	-0.06595
	233.142	12.8248	0.64708	9.1e-4	8.9e-5	6.7e-3	6.7e-3	2.6e-4	1.5e-5	2.7e-3	2.7e-3	4.8e-4	5.1e-4	0.63897	0.00093	-0.06594
	233.143	12.8248	0.64712	1.3e-3	3.9e-4	7.1e-3	7.1e-3	2.3e-4	1.4e-5	2.7e-3	2.7e-3	4.8e-4	5.1e-4	0.63897	0.00093	-0.06594
	233.142	12.8248	0.64711	6.1e-4	3.2e-5	6.6e-3	6.6e-3	1.9e-4	1.1e-5	2.7e-3	2.7e-3	4.8e-4	5.1e-4	0.63897	0.00093	-0.06595
	233.143	12.8248	0.64711	1.0e-3	1.9e-4	7.0e-3	7.0e-3	1.8e-4	2.2e-5	2.7e-3	2.7e-3	4.8e-4	5.1e-4	0.63897	0.00093	-0.06591
L22	233.141	13.6445	0.58764	1.7e-3	6.8e-4	7.2e-3	7.2e-3	2.5e-4	2.0e-5	2.7e-3	2.7e-3	4.8e-4	5.4e-4^{+}	0.57569	0.00070	-0.09273^{+}
	233.143	13.6445	0.58764	8.5e-4	1.2e-4	7.4e-3	7.4e-3	2.8e-4	1.9e-5	2.8e-3	2.8e-3	4.8e-4	5.4e-4^{+}	0.57569	0.00070	-0.09273^{+}
	233.144	13.6445	0.58761	1.5e-3	3.0e-4	7.1e-3	7.2e-3	2.6e-4	2.7e-5	2.8e-3	2.8e-3	4.8e-4	5.4e-4^{+}	0.57569	0.00070	-0.09273^{+}
	233.143	13.6445	0.58760	5.8e-4	4.1e-5	6.8e-3	6.8e-3	2.5e-4	9.0e-6	2.8e-3	2.8e-3	4.8e-4	5.4e-4^{+}	0.57569	0.00070	-0.09273^{+}
	233.143	13.6445	0.58759	6.2e-4	1.5e-4	7.3e-3	7.3e-3	2.7e-4	2.1e-5	2.8e-3	2.8e-3	4.8e-4	5.4e-4^{+}	0.57569	0.00070	-0.09273^{+}
	233.141	13.6444	0.58762	2.0e-3	5.3e-4	7.4e-3	7.4e-3	2.1e-4	9.9e-6	2.7e-3	2.7e-3	4.8e-4	5.4e-4^{+}	0.57569	0.00070	-0.09273^{+}
L23*	233.144	14.1868	0.51082	7.6e-4	1.1e-4	6.9e-3	6.9e-3	2.4e-4	1.7e-5	2.8e-3	2.8e-3	4.8e-4	9.7e-4^{+}	0.51244	-0.00036	-0.30787^{+}
	233.144	14.1868	0.51081	7.7e-4	1.4e-4	6.8e-3	6.8e-3	1.8e-4	1.1e-5	2.8e-3	2.8e-3	4.8e-4	9.7e-4^{+}	0.51244	-0.00036	-0.30779^{+}
	233.144	14.1868	0.51081	4.8e-4	6.8e-5	6.9e-3	6.9e-3	2.6e-4	3.4e-5	2.8e-3	2.8e-3	4.8e-4	9.8e-4^{+}	0.51244	-0.00036	-0.30788^{+}
	233.144	14.1868	0.51080	6.3e-4	1.9e-4	7.1e-3	7.1e-3	3.1e-4	2.1e-5	2.8e-3	2.8e-3	4.8e-4	9.8e-4^{+}	0.51244	-0.00036	-0.30788^{+}
	233.144	14.1867	0.51082	5.1e-4	4.5e-5	6.9e-3	6.9e-3	2.7e-4	1.8e-5	2.8e-3	2.8e-3	4.8e-4	9.7e-4^{+}	0.51245	-0.00035	-0.30771^{+}
	233.144	14.1868	0.51080	6.8e-4	6.3e-5	6.8e-3	6.8e-3	3.1e-4	1.8e-5	2.8e-3	2.8e-3	4.8e-4	9.8e-4^{+}	0.51244	-0.00036	-0.30783^{+}
L24*	233.144	14.2158	0.50043	6.1e-4	9.8e-5	7.0e-3	7.0e-3	2.6e-4	2.5e-5	2.8e-3	2.8e-3	4.8e-4	1.3e-3^{+}	0.50770	-0.00054	-0.43666^{+}
	233.144	14.2158	0.50045	6.6e-4	1.6e-4	6.4e-3	6.4e-3	2.5e-4	2.0e-5	2.8e-3	2.8e-3	4.8e-4	1.3e-3^{+}	0.50771	-0.00054	-0.43628^{+}
	233.144	14.2158	0.50044	6.9e-4	1.6e-4	6.9e-3	6.9e-3	2.9e-4	4.4e-5	2.8e-3	2.8e-3	4.8e-4	1.3e-3^{+}	0.50770	-0.00054	-0.43663^{+}
	233.144	14.2157	0.50043	6.3e-4	9.8e-5	6.8e-3	6.8e-3	2.7e-4	2.0e-5	2.8e-3	2.8e-3	4.8e-4	1.3e-3^{+}	0.50772	-0.00054	-0.43584^{+}
	233.144	14.2158	0.50044	6.2e-4	1.5e-4	6.7e-3	6.7e-3	2.2e-4	1.8e-5	2.8e-3	2.8e-3	4.8e-4	1.3e-3^{+}	0.50771	-0.00054	-0.43625^{+}
	233.144	14.2158	0.50045	4.7e-4	7.7e-5	6.7e-3	6.7e-3	1.9e-4	1.4e-5	2.8e-3	2.8e-3	4.8e-4	1.3e-3^{+}	0.50771	-0.00054	-0.43619^{+}
L25*	233.146	14.2408	0.48640	1.4e-3	4.7e-4	5.9e-3	5.9e-3	2.2e-4	1.7e-5	2.8e-3	2.8e-3	4.8e-4	2.4e-3^{+}	0.50338	-0.00074	-0.85676^{+}
	233.146	14.2408	0.48639	7.9e-4	1.2e-4	6.1e-3	6.1e-3	2.5e-4	2.8e-5	2.8e-3	2.8e-3	4.8e-4	2.4e-3^{+}	0.50338	-0.00074	-0.85715^{+}
	233.146	14.2407	0.48640	6.2e-4	1.0e-4	6.0e-3	6.0e-3	2.4e-4	1.2e-5	2.8e-3	2.8e-3	4.8e-4	2.4e-3^{+}	0.50339	-0.00074	-0.85446^{+}
	233.146	14.2407	0.48642	8.2e-4	3.0e-4	6.0e-3	6.0e-3	1.6e-4	1.3e-5	2.8e-3	2.8e-3	4.8e-4	2.4e-3^{+}	0.50339	-0.00074	-0.85608^{+}
	233.146	14.2407	0.48642	9.3e-4	1.8e-4	6.0e-3	6.0e-3	2.3e-4	1.7e-5	2.8e-3	2.8e-3	4.8e-4	2.4e-3^{+}	0.50339	-0.00074	-0.85516^{+}
	233.148	14.2407	0.48640	1.4e-3	6.2e-4	6.0e-3	6.0e-3	1.8e-4	8.4e-6	2.8e-3	2.8e-3	4.8e-4	2.4e-3^{+}	0.50339	-0.00074	-0.85451^{+}
P3	253.147	1.9699	0.99999	8.5e-4	1.5e-5	5.7e-3	5.7e-3	3.7e-5	5.5e-6	5.1e-4	5.1e-4					
L27	253.146	2.9632	0.97897	8.9e-4	1.7e-4	5.9e-3	5.9e-3	4.1e-5	7.5e-6	5.2e-4	5.2e-4	4.8e-4	4.8e-4	0.98168	0.00111	-0.01913
	253.147	2.9633	0.97902	9.6e-4	2.2e-4	5.8e-3	5.8e-3	1.1e-4	4.4e-5	5.2e-4	5.2e-4	4.8e-4	4.8e-4	0.98167	0.00111	-0.01913
	253.146	2.9633	0.97901	8.1e-4	1.1e-4	5.8e-3	5.8e-3	2.8e-5	3.5e-6	5.2e-4	5.2e-4	4.8e-4	4.8e-4	0.98167	0.00111	-0.01913
	253.147	2.9632	0.97897	8.2e-4	1.1e-4	5.7e-3	5.7e-3	3.6e-5	6.0e-6	5.2e-4	5.2e-4	4.8e-4	4.8e-4	0.98167	0.00111	-0.01913
L28	253.146	4.9363	0.93518	9.3e-4	2.0e-4	6.0e-3	6.0e-3	1.4e-4	5.1e-5	1.1e-3	1.1e-3	4.8e-4	4.8e-4	0.94105	0.00114	-0.02220
	253.146	4.9367	0.93519	9.4e-4	1.7e-4	6.3e-3	6.3e-3	8.1e-5	2.4e-5	1.1e-3	1.1e-3	4.8e-4	4.8e-4	0.94104	0.00114	-0.02220
	253.146	4.9364	0.93519	1.1e-3	1.5e-4	6.1e-3	6.1e-3	6.4e-5	7.1e-6	1.1e-3	1.1e-3	4.8e-4	4.8e-4	0.94105	0.00114	-0.02220
	253.146	4.9363	0.93518	9.1e-4	1.0e-4	5.3e-3	5.3e-3	1.7e-4	6.1e-5	1.1e-3	1.1e-3	4.8e-4	4.8e-4	0.94105	0.00114	-0.02220
	253.146	4.9368	0.93518	1.1e-3	2.7e-4	6.1e-3	6.1e-3	7.7e-5	2.4e-5	1.1e-3	1.1e-3	4.8e-4	4.8e-4	0.94104	0.00114	-0.02220
L29	253.146	6.9082	0.88642	7.2e-4	8.5e-5	5.9e-3	5.9e-3	2.1e-4	6.5e-5	1.1e-3	1.1e-3	4.8e-4	4.8e-4	0.89326	0.00113	-0.02653
	253.146	6.9080	0.88638	1.3e-3	3.5e-4	6.0e-3	6.0e-3	2.1e-4	7.8e-5	1.1e-3	1.1e-3	4.8e-4	4.8e-4	0.89327	0.00113	-0.02653
	253.147	6.9080	0.88643	9.1e-4	2.1e-4	5.8e-3	5.8e-3	1.1e-4	1.2e-5	1.1e-3	1.1e-3	4.8e-4	4.8e-4	0.89327	0.00113	-0.02653
	253.146	6.9080	0.88640	1.1e-3	1.2e-4	6.2e-3	6.2e-3	8.7e-5	2.3e-5	1.1e-3	1.1e-3	4.8e-4	4.8e-4	0.89327	0.00113	-0.02653
	253.146	6.9080	0.88639	5.4e-4	7.5e-5	6.1e-3	6.1e-3	2.2e-4	8.8e-5	1.1e-3	1.1e-3	4.8e-4	4.8e-4	0.89327	0.00113	-0.02653
L30	253.146	8.3058	0.84781	8.0e-4	1.2e-4	6.1e-3	6.1e-3	1.8e-4	5.1e-5	1.2e-3	1.2e-3	4.8e-4	4.8e-4	0.85331	0.00109	-0.03088
	253.146	8.3057	0.84783	1.4e-3	1.9e-4	5.7e-3	5.7e-3	2.5e-4	7.7e-5	1.2e-3	1.2e-3	4.8e-4	4.8e-4	0.85331	0.00109	-0.03088
	253.145	8.3057	0.84784	9.0e-4	1.7e-4	5.9e-3	5.9e-3	1.2e-4	3.1e-5	1.2e-3	1.2e-3	4.8e-4	4.8e-4	0.85331	0.00109	-0.03088
	253.146	8.3058	0.84783	1.1e-3	2.8e-4	6.1e-3	6.1e-3	1.4e-4	1.7e-5	1.2e-3	1.2e-3	4.8e-4	4.8e-4	0.85331	0.00109	-0.03088

	253.146	8.3058	0.84783	5.9e-4	5.5e-5	5.9e-3	5.9e-3	1.7e-4	4.6e-5	1.2e-3	1.2e-3	4.8e-4	4.8e-4	0.85331	0.00109	-0.03088
L31	253.148	9.6222	0.80638	7.4e-4	1.1e-4	5.7e-3	5.7e-3	6.8e-4	3.1e-4	1.4e-3	1.5e-3	4.8e-4	4.8e-4	0.80907	0.00098	-0.03670
	253.148	9.6241	0.80640	1.0e-3	1.8e-4	5.9e-3	5.9e-3	1.5e-3	7.0e-4	1.5e-3	1.7e-3	4.8e-4	4.8e-4	0.80900	0.00098	-0.03671
	253.148	9.6222	0.80643	6.4e-4	1.2e-4	5.9e-3	5.9e-3	1.0e-3	3.5e-4	1.4e-3	1.5e-3	4.8e-4	4.8e-4	0.80907	0.00098	-0.03670
	253.148	9.6222	0.80641	7.7e-4	1.2e-4	5.7e-3	5.7e-3	2.3e-4	2.9e-5	1.4e-3	1.4e-3	4.8e-4	4.8e-4	0.80908	0.00098	-0.03670
	253.148	9.6221	0.80640	9.1e-4	9.0e-5	5.3e-3	5.3e-3	5.7e-4	1.6e-4	1.4e-3	1.4e-3	4.8e-4	4.8e-4	0.80908	0.00098	-0.03670
L32	253.147	10.8464	0.76222	6.3e-4	6.4e-5	6.1e-3	6.1e-3	2.5e-4	5.2e-5	2.7e-3	2.7e-3	4.8e-4	4.9e-4	0.75947	0.00076	-0.04501
	253.147	10.8462	0.76219	4.9e-4	7.3e-5	5.8e-3	5.8e-3	4.0e-4	5.5e-5	2.7e-3	2.7e-3	4.8e-4	4.9e-4	0.75948	0.00076	-0.04501
	253.147	10.8463	0.76223	6.1e-4	1.0e-4	6.0e-3	6.0e-3	3.2e-4	6.8e-5	2.7e-3	2.7e-3	4.8e-4	4.9e-4	0.75948	0.00076	-0.04501
	253.147	10.8463	0.76222	6.0e-4	7.8e-5	5.7e-3	5.7e-3	1.7e-4	3.7e-5	2.7e-3	2.7e-3	4.8e-4	4.9e-4	0.75947	0.00076	-0.04501
	253.148	10.8463	0.76221	9.9e-4	3.2e-4	5.6e-3	5.6e-3	3.4e-4	4.8e-5	2.7e-3	2.7e-3	4.8e-4	4.9e-4	0.75948	0.00076	-0.04501
L33	253.146	11.8557	0.71750	9.0e-4	1.0e-4	5.6e-3	5.6e-3	1.8e-4	3.1e-5	2.7e-3	2.7e-3	4.8e-4	5.0e-4	0.70865	0.00032	-0.05692
	253.146	11.8557	0.71745	1.1e-3	1.4e-4	5.9e-3	5.9e-3	3.3e-4	6.5e-5	2.7e-3	2.7e-3	4.8e-4	5.0e-4	0.70865	0.00032	-0.05692
	253.146	11.8557	0.71746	6.9e-4	5.8e-5	6.2e-3	6.2e-3	3.4e-4	4.2e-5	2.7e-3	2.7e-3	4.8e-4	5.0e-4	0.70865	0.00032	-0.05692
	253.146	11.8557	0.71749	1.0e-3	1.5e-4	6.1e-3	6.1e-3	3.8e-4	6.5e-5	2.7e-3	2.7e-3	4.8e-4	5.0e-4	0.70866	0.00032	-0.05693
	253.146	11.8556	0.71747	1.0e-3	2.3e-4	6.1e-3	6.1e-3	3.0e-4	5.9e-5	2.7e-3	2.7e-3	4.8e-4	5.0e-4	0.70866	0.00032	-0.05691
L34	253.146	12.7679	0.66172	8.2e-4	9.1e-5	5.7e-3	5.7e-3	5.0e-4	7.5e-5	2.7e-3	2.7e-3	4.8e-4	5.2e-4^{+}	0.64727	-0.00094	-0.07864^{+}
	253.146	12.7678	0.66174	7.6e-4	9.2e-5	5.8e-3	5.8e-3	4.0e-4	6.3e-5	2.7e-3	2.7e-3	4.8e-4	5.2e-4^{+}	0.64728	-0.00094	-0.07863^{+}
	253.146	12.7677	0.66172	6.3e-4	1.3e-4	5.9e-3	5.9e-3	2.7e-4	3.0e-5	2.7e-3	2.7e-3	4.8e-4	5.2e-4^{+}	0.64729	-0.00094	-0.07863^{+}
	253.146	12.7678	0.66174	7.5e-4	5.6e-5	5.6e-3	5.6e-3	3.4e-4	5.4e-5	2.7e-3	2.7e-3	4.8e-4	5.2e-4^{+}	0.64728	-0.00094	-0.07863^{+}
L35*	253.146	13.2763	0.59985	8.1e-4	1.1e-4	5.9e-3	5.9e-3	5.8e-4	6.2e-5	2.7e-3	2.7e-3	4.8e-4	8.8e-4^{+}	0.59446	-0.00471	-0.26976^{+}
	253.146	13.2762	0.59987	8.8e-4	1.1e-4	5.5e-3	5.5e-3	5.3e-4	7.8e-5	2.7e-3	2.7e-3	4.8e-4	8.8e-4^{+}	0.59446	-0.00471	-0.26960^{+}
	253.147	13.2762	0.59989	1.2e-3	4.1e-4	5.5e-3	5.6e-3	2.7e-4	4.8e-5	2.7e-3	2.7e-3	4.8e-4	8.8e-4^{+}	0.59446	-0.00471	-0.26955^{+}
	253.146	13.2763	0.59988	7.4e-4	1.5e-4	6.0e-3	6.0e-3	3.5e-4	5.6e-5	2.7e-3	2.7e-3	4.8e-4	8.8e-4^{+}	0.59445	-0.00471	-0.26977^{+}
	253.146	13.2762	0.59989	6.9e-4	9.9e-5	5.6e-3	5.6e-3	2.8e-4	6.5e-5	2.7e-3	2.7e-3	4.8e-4	8.8e-4^{+}	0.59446	-0.00471	-0.26965^{+}
L36*	253.147	13.3024	0.59159	9.4e-4	2.2e-4	5.8e-3	5.8e-3	5.8e-4	8.0e-5	2.7e-3	2.7e-3	4.8e-4	1.1e-3^{+}	0.59060	-0.00531	-0.37659^{+}
	253.147	13.3024	0.59163	5.8e-4	9.6e-5	6.1e-3	6.1e-3	4.6e-4	9.1e-5	2.7e-3	2.7e-3	4.8e-4	1.1e-3^{+}	0.59060	-0.00531	-0.37660^{+}
	253.147	13.3023	0.59166	4.8e-4	4.9e-5	5.7e-3	5.7e-3	5.2e-4	8.0e-5	2.7e-3	2.7e-3	4.8e-4	1.1e-3^{+}	0.59060	-0.00531	-0.37652^{+}
	253.147	13.3024	0.59167	7.7e-4	1.0e-4	5.8e-3	5.8e-3	5.2e-4	9.9e-5	2.7e-3	2.7e-3	4.8e-4	1.1e-3^{+}	0.59059	-0.00531	-0.37699^{+}
	253.147	13.3023	0.59169	9.0e-4	1.3e-4	5.7e-3	5.7e-3	3.3e-4	5.1e-5	2.7e-3	2.7e-3	4.8e-4	1.1e-3^{+}	0.59060	-0.00531	-0.37628^{+}
L37*	253.147	13.3199	0.58367	8.7e-4	2.5e-4	5.9e-3	5.9e-3	6.8e-4	1.6e-4	2.7e-3	2.8e-3	4.8e-4	1.6e-3^{+}	0.58787	-0.00579	-0.56725^{+}
	253.147	13.3202	0.58368	6.8e-4	1.2e-4	5.9e-3	5.9e-3	1.3e-4	2.9e-5	2.7e-3	2.7e-3	4.8e-4	1.6e-3^{+}	0.58781	-0.00581	-0.57410^{+}
	253.148	13.3200	0.58373	7.9e-4	8.7e-5	5.6e-3	5.6e-3	5.4e-4	8.5e-5	2.7e-3	2.7e-3	4.8e-4	1.6e-3^{+}	0.58784	-0.00580	-0.57029^{+}
	253.148	13.3201	0.58372	9.0e-4	2.4e-4	5.6e-3	5.6e-3	6.3e-4	6.6e-5	2.7e-3	2.7e-3	4.8e-4	1.6e-3^{+}	0.58783	-0.00580	-0.57117^{+}
	253.147	13.3200	0.58376	5.4e-4	6.6e-5	6.0e-3	6.0e-3	6.1e-4	1.3e-4	2.7e-3	2.7e-3	4.8e-4	1.6e-3^{+}	0.58784	-0.00580	-0.57030^{+}
P4	273.147	3.4848	0.99999	7.2e-4	2.4e-5	1.5e-3	1.5e-3	5.6e-5	9.9e-7	1.1e-3	1.1e-3					
L39	273.145	5.0161	0.96558	1.1e-3	3.5e-4	2.3e-3	2.4e-3	2.0e-4	8.9e-5	1.1e-3	1.1e-3	4.8e-4	4.8e-4	0.96828	0.00183	-0.02227
	273.145	5.0162	0.96558	1.0e-3	1.7e-4	1.6e-3	1.6e-3	1.2e-4	3.1e-5	1.1e-3	1.1e-3	4.8e-4	4.8e-4	0.96828	0.00183	-0.02227
	273.145	5.0161	0.96557	1.1e-3	1.1e-4	2.3e-3	2.3e-3	7.9e-5	1.9e-5	1.1e-3	1.1e-3	4.8e-4	4.8e-4	0.96828	0.00183	-0.02227
	273.145	5.0161	0.96559	7.6e-4	6.9e-5	1.9e-3	1.9e-3	8.2e-5	1.3e-5	1.1e-3	1.1e-3	4.8e-4	4.8e-4	0.96828	0.00183	-0.02227
	273.145	5.0160	0.96559	9.9e-4	2.2e-4	1.7e-3	1.7e-3	1.9e-4	7.5e-5	1.1e-3	1.1e-3	4.8e-4	4.8e-4	0.96828	0.00183	-0.02227
	273.145	5.0160	0.96559	6.5e-4	6.0e-5	2.0e-3	2.0e-3	6.4e-5	5.5e-6	1.1e-3	1.1e-3	4.8e-4	4.8e-4	0.96828	0.00183	-0.02227
L40	273.147	5.9255	0.94386	6.1e-4	6.9e-5	2.2e-3	2.2e-3	1.0e-4	1.3e-5	1.1e-3	1.1e-3	4.8e-4	4.8e-4	0.94709	0.00183	-0.02441
	273.146	5.9255	0.94385	5.8e-4	1.5e-4	2.9e-3	2.9e-3	9.8e-5	2.7e-5	1.1e-3	1.1e-3	4.8e-4	4.8e-4	0.94709	0.00183	-0.02441
	273.146	5.9256	0.94385	4.7e-4	6.1e-5	2.4e-3	2.4e-3	8.6e-5	1.7e-5	1.1e-3	1.1e-3	4.8e-4	4.8e-4	0.94708	0.00183	-0.02441
	273.146	5.9255	0.94384	6.0e-4	6.8e-5	2.7e-3	2.7e-3	1.3e-4	4.3e-5	1.1e-3	1.1e-3	4.8e-4	4.8e-4	0.94709	0.00183	-0.02441
	273.147	5.9255	0.94385	5.1e-4	1.2e-4	2.2e-3	2.2e-3	7.4e-5	1.3e-5	1.1e-3	1.1e-3	4.8e-4	4.8e-4	0.94709	0.00183	-0.02441
	273.146	5.9256	0.94385	8.1e-4	1.8e-4	2.6e-3	2.6e-3	7.3e-5	1.4e-5	1.1e-3	1.1e-3	4.8e-4	4.8e-4	0.94709	0.00183	-0.02441
L41	273.146	6.9257	0.91830	7.2e-4	2.0e-4	2.5e-3	2.5e-3	2.1e-4	5.1e-5	1.1e-3	1.1e-3	4.8e-4	4.8e-4	0.92127	0.00180	-0.02733
	273.146	6.9258	0.91829	5.4e-4	1.2e-4	2.2e-3	2.2e-3	3.1e-4	8.2e-5	1.1e-3	1.1e-3	4.8e-4	4.8e-4	0.92127	0.00180	-0.02733
	273.146	6.9258	0.91829	9.0e-4	1.0e-4	2.4e-3	2.4e-3	1.9e-4	3.8e-5	1.1e-3	1.1e-3	4.8e-4	4.8e-4	0.92127	0.00180	-0.02733
	273.146	6.9259	0.91829	7.2e-4	5.8e-5	2.7e-3	2.7e-3	2.3e-4	4.0e-5	1.1e-3	1.1e-3	4.8e-4	4.8e-4	0.92127	0.00180	-0.02733
	273.146	6.9258	0.91829	6.2e-4	4.3e-5	2.3e-3	2.3e-3	2.8e-4	2.8e-5	1.1e-3	1.1e-3	4.8e-4	4.8e-4	0.92127	0.00180	-0.02733
L42	273.146	7.9106	0.89112	7.3e-4	1.4e-4	2.5e-3	2.5e-3	3.7e-4	7.1e-5	1.2e-3	1.2e-3	4.8e-4	4.8e-4	0.89260	0.00171	-0.03108

	273.146	7.9108	0.89110	7.2e-4	1.7e-4	2.3e-3	2.3e-3	4.8e-4	1.5e-4	1.2e-3	1.2e-3	4.8e-4	4.8e-4	0.89259	0.00171	-0.03108
	273.146	7.9107	0.89111	5.5e-4	5.4e-5	2.3e-3	2.4e-3	2.7e-4	5.0e-5	1.2e-3	1.2e-3	4.8e-4	4.8e-4	0.89260	0.00171	-0.03108
	273.146	7.9107	0.89109	9.4e-4	1.5e-4	2.7e-3	2.7e-3	2.6e-4	6.5e-5	1.2e-3	1.2e-3	4.8e-4	4.8e-4	0.89259	0.00171	-0.03108
	273.147	7.9106	0.89108	5.8e-4	8.7e-5	2.1e-3	2.1e-3	2.3e-4	4.7e-5	1.2e-3	1.2e-3	4.8e-4	4.8e-4	0.89260	0.00171	-0.03108
L43	273.147	8.8895	0.86116	6.7e-4	1.4e-4	2.5e-3	2.5e-3	7.1e-4	1.3e-4	1.3e-3	1.3e-3	4.8e-4	4.8e-4	0.85979	0.00153	-0.03628
	273.146	8.8895	0.86116	5.5e-4	8.2e-5	2.5e-3	2.5e-3	3.8e-4	1.0e-4	1.3e-3	1.3e-3	4.8e-4	4.8e-4	0.85979	0.00153	-0.03628
	273.147	8.8894	0.86112	5.7e-4	8.8e-5	2.1e-3	2.1e-3	3.2e-4	4.8e-5	1.3e-3	1.3e-3	4.8e-4	4.8e-4	0.85979	0.00153	-0.03628
	273.146	8.8892	0.86110	7.1e-4	1.0e-4	2.5e-3	2.5e-3	6.1e-4	9.5e-5	1.3e-3	1.3e-3	4.8e-4	4.8e-4	0.85980	0.00153	-0.03628
	273.146	8.8893	0.86110	6.7e-4	9.4e-5	2.4e-3	2.4e-3	4.4e-4	9.1e-5	1.3e-3	1.3e-3	4.8e-4	4.8e-4	0.85979	0.00153	-0.03628
L44	273.145	9.8539	0.82709	8.6e-4	1.2e-4	2.3e-3	2.3e-3	6.3e-4	7.3e-5	1.4e-3	1.4e-3	4.8e-4	4.8e-4	0.82127	0.00111	-0.04432
	273.145	9.8532	0.82712	9.8e-4	2.0e-4	2.1e-3	2.1e-3	2.2e-4	3.1e-5	1.4e-3	1.4e-3	4.8e-4	4.8e-4	0.82130	0.00111	-0.04431
	273.144	9.8540	0.82711	1.4e-3	3.4e-4	2.7e-3	2.7e-3	4.7e-4	8.5e-5	1.4e-3	1.4e-3	4.8e-4	4.8e-4	0.82126	0.00111	-0.04432
	273.145	9.8538	0.82710	7.6e-4	2.1e-4	2.5e-3	2.5e-3	3.2e-4	8.1e-5	1.4e-3	1.4e-3	4.8e-4	4.8e-4	0.82127	0.00111	-0.04432
	273.145	9.8538	0.82709	8.3e-4	1.1e-4	2.3e-3	2.3e-3	1.8e-4	1.8e-5	1.4e-3	1.4e-3	4.8e-4	4.8e-4	0.82128	0.00111	-0.04432
L45	273.147	10.8865	0.78023	6.5e-4	1.2e-4	2.5e-3	2.5e-3	2.9e-4	8.0e-5	2.7e-3	2.7e-3	4.8e-4	5.1e-4	0.76737	-0.00031	-0.06367
	273.146	10.8864	0.78016	4.3e-4	4.7e-5	2.5e-3	2.5e-3	2.4e-4	2.9e-5	2.7e-3	2.7e-3	4.8e-4	5.1e-4	0.76738	-0.00031	-0.06367
	273.147	10.8865	0.77987	4.6e-4	3.9e-5	2.2e-3	2.2e-3	2.3e-4	4.3e-5	2.7e-3	2.7e-3	4.8e-4	5.1e-4	0.76737	-0.00031	-0.06367
	273.147	10.8864	0.77996	6.7e-4	4.0e-5	2.6e-3	2.6e-3	2.1e-4	3.1e-5	2.7e-3	2.7e-3	4.8e-4	5.1e-4	0.76737	-0.00031	-0.06367
	273.147	10.8864	0.77995	4.6e-4	6.3e-5	2.3e-3	2.3e-3	2.7e-4	5.4e-5	2.7e-3	2.7e-3	4.8e-4	5.1e-4	0.76738	-0.00031	-0.06367
L46	273.147	11.3315	0.74889	6.2e-4	1.5e-4	2.2e-3	2.2e-3	4.5e-4	8.3e-5	2.7e-3	2.7e-3	4.8e-4	5.4e-4^{+}	0.73427	-0.00275	-0.08975^{+}
	273.146	11.3311	0.74904	5.2e-4	5.1e-5	2.4e-3	2.4e-3	1.4e-4	3.2e-5	2.7e-3	2.7e-3	4.8e-4	5.4e-4^{+}	0.73431	-0.00274	-0.08967^{+}
	273.146	11.3318	0.74903	6.0e-4	8.3e-5	2.0e-3	2.0e-3	1.5e-4	2.5e-5	2.7e-3	2.7e-3	4.8e-4	5.4e-4^{+}	0.73425	-0.00275	-0.08981^{+}
	273.146	11.3313	0.74900	9.2e-4	1.3e-4	2.4e-3	2.4e-3	2.4e-4	5.2e-5	2.7e-3	2.7e-3	4.8e-4	5.4e-4^{+}	0.73429	-0.00274	-0.08971^{+}
	273.146	11.3313	0.74901	6.2e-4	1.0e-4	2.4e-3	2.4e-3	2.8e-4	5.0e-5	2.7e-3	2.7e-3	4.8e-4	5.4e-4^{+}	0.73429	-0.00274	-0.08971^{+}
L47*	273.144	11.5579	0.71517	9.0e-4	7.4e-5	2.9e-3	2.9e-3	2.1e-4	3.4e-5	2.7e-3	2.7e-3	4.8e-4	1.1e-3^{+}	0.70945	-0.00803	-0.36948^{+}
	273.145	11.5579	0.71516	7.6e-4	1.0e-4	2.5e-3	2.5e-3	1.7e-4	5.1e-5	2.7e-3	2.7e-3	4.8e-4	1.1e-3^{+}	0.70945	-0.00804	-0.36924^{+}
	273.145	11.5579	0.71515	7.6e-4	2.3e-4	2.5e-3	2.6e-3	1.6e-4	2.9e-5	2.7e-3	2.7e-3	4.8e-4	1.1e-3^{+}	0.70944	-0.00804	-0.36946^{+}
	273.145	11.5578	0.71509	7.4e-4	9.1e-5	2.5e-3	2.5e-3	1.8e-4	5.2e-5	2.7e-3	2.7e-3	4.8e-4	1.1e-3^{+}	0.70946	-0.00803	-0.36866^{+}
	273.145	11.5579	0.71511	6.5e-4	6.7e-5	2.4e-3	2.4e-3	2.7e-4	4.2e-5	2.7e-3	2.7e-3	4.8e-4	1.1e-3^{+}	0.70945	-0.00804	-0.36906^{+}
L48*	273.145	11.5779	0.70323	6.9e-4	5.7e-5	2.4e-3	2.4e-3	3.3e-4	6.4e-5	2.7e-3	2.7e-3	4.8e-4	3.0e-3^{+}	0.70648	-0.00928	-1.12188^{+}
	273.146	11.5780	0.70342	7.0e-4	7.4e-5	2.5e-3	2.5e-3	1.7e-4	4.3e-5	2.7e-3	2.7e-3	4.8e-4	3.0e-3^{+}	0.70648	-0.00928	-1.12681^{+}
	273.146	11.5779	0.70374	6.1e-4	5.9e-5	2.2e-3	2.2e-3	1.0e-4	8.1e-6	2.7e-3	2.7e-3	4.8e-4	3.0e-3^{+}	0.70647	-0.00928	-1.12323^{+}
	273.146	11.5780	0.70385	5.7e-4	6.5e-5	2.1e-3	2.1e-3	1.8e-4	3.1e-5	2.7e-3	2.7e-3	4.8e-4	3.0e-3^{+}	0.70647	-0.00928	-1.12771^{+}
	273.145	11.5779	0.70392	7.7e-4	7.8e-5	2.5e-3	2.5e-3	2.4e-4	4.0e-5	2.7e-3	2.7e-3	4.8e-4	3.0e-3^{+}	0.70648	-0.00928	-1.12423^{+}
P5	288.139	5.0859	0.99999	6.9e-4	2.8e-4	1.8e-3	1.8e-3	5.7e-5	2.9e-6	1.1e-3	1.1e-3					
L50	288.135	5.6497	0.98646	5.5e-4	7.9e-5	1.6e-3	1.6e-3	7.8e-5	7.3e-6	1.1e-3	1.1e-3	4.8e-4	4.8e-4	0.98744	0.00274	-0.02353
	288.139	5.6498	0.98646	1.2e-3	4.7e-4	1.8e-3	1.8e-3	1.1e-4	1.5e-5	1.1e-3	1.1e-3	4.8e-4	4.8e-4	0.98745	0.00274	-0.02353
	288.135	5.6498	0.98646	4.6e-4	4.9e-5	1.7e-3	1.7e-3	8.2e-5	1.1e-5	1.1e-3	1.1e-3	4.8e-4	4.8e-4	0.98743	0.00274	-0.02353
	288.138	5.6498	0.98654	2.1e-3	5.7e-4	1.6e-3	1.7e-3	7.5e-5	4.5e-6	1.1e-3	1.1e-3	4.8e-4	4.8e-4	0.98744	0.00274	-0.02353
	288.138	5.6498	0.98654	1.1e-3	3.0e-4	1.8e-3	1.8e-3	8.0e-5	1.4e-5	1.1e-3	1.1e-3	4.8e-4	4.8e-4	0.98744	0.00274	-0.02353
L51	288.137	7.0494	0.95060	1.0e-3	2.9e-4	1.5e-3	1.5e-3	1.3e-4	1.3e-5	1.1e-3	1.1e-3	4.8e-4	4.8e-4	0.95110	0.00273	-0.02882
	288.137	7.0493	0.95060	7.4e-4	2.3e-4	1.5e-3	1.5e-3	1.5e-4	8.9e-6	1.1e-3	1.1e-3	4.8e-4	4.8e-4	0.95110	0.00273	-0.02882
	288.138	7.0493	0.95060	1.0e-3	2.9e-4	1.7e-3	1.7e-3	1.4e-4	8.2e-6	1.1e-3	1.1e-3	4.8e-4	4.8e-4	0.95110	0.00273	-0.02882
	288.136	7.0494	0.95060	3.8e-4	6.8e-5	1.6e-3	1.6e-3	9.8e-5	3.8e-6	1.1e-3	1.1e-3	4.8e-4	4.8e-4	0.95110	0.00273	-0.02882
	288.135	7.0493	0.95060	8.5e-4	2.6e-4	1.6e-3	1.6e-3	1.1e-4	1.1e-5	1.1e-3	1.1e-3	4.8e-4	4.8e-4	0.95110	0.00273	-0.02882
	288.135	7.0494	0.95059	7.6e-4	2.0e-4	1.5e-3	1.5e-3	1.1e-4	1.0e-5	1.1e-3	1.1e-3	4.8e-4	4.8e-4	0.95110	0.00273	-0.02882
L52	288.136	8.4289	0.90854	1.9e-3	8.3e-4	1.5e-3	1.7e-3	2.3e-4	8.9e-6	1.2e-3	1.2e-3	4.8e-4	4.8e-4	0.90541	0.00234	-0.03878
	288.134	8.4290	0.90854	9.8e-4	1.3e-4	1.6e-3	1.6e-3	2.1e-4	1.0e-5	1.2e-3	1.2e-3	4.8e-4	4.8e-4	0.90541	0.00234	-0.03878
	288.137	8.4289	0.90854	1.7e-3	5.5e-4	1.5e-3	1.6e-3	2.9e-4	1.9e-5	1.2e-3	1.2e-3	4.8e-4	4.8e-4	0.90542	0.00234	-0.03878
	288.134	8.4289	0.90854	7.3e-4	9.6e-5	1.6e-3	1.6e-3	2.0e-4	1.4e-5	1.2e-3	1.2e-3	4.8e-4	4.8e-4	0.90541	0.00234	-0.03878
	288.132	8.4289	0.90855	7.5e-4	7.4e-5	1.4e-3	1.4e-3	1.8e-4	8.2e-6	1.2e-3	1.2e-3	4.8e-4	4.8e-4	0.90540	0.00234	-0.03878
	288.134	8.4289	0.90855	8.8e-4	1.7e-4	1.5e-3	1.5e-3	1.8e-4	1.5e-5	1.2e-3	1.2e-3	4.8e-4	4.8e-4	0.90541	0.00234	-0.03878
L53	288.136	8.8666	0.89229	1.4e-3	3.9e-4	1.7e-3	1.7e-3	1.4e-4	2.0e-5	1.3e-3	1.3e-3	4.8e-4	4.8e-4	0.88720	0.00191	-0.04495
	288.139	8.8666	0.89230	7.3e-4	1.2e-4	1.7e-3	1.7e-3	1.2e-4	6.0e-6	1.3e-3	1.3e-3	4.8e-4	4.8e-4	0.88720	0.00191	-0.04495

	288.136	8.8666	0.89231	5.6e-4	7.4e-5	1.7e-3	1.7e-3	1.6e-4	1.4e-5	1.3e-3	1.3e-3	4.8e-4	4.8e-4	0.88720	0.00191	-0.04495
L54	288.139	9.2573	0.87507	5.9e-4	3.5e-5	1.5e-3	1.5e-3	1.8e-4	1.1e-5	1.3e-3	1.3e-3	4.8e-4	4.8e-4	0.86795	0.00106	-0.05470
	288.138	9.2573	0.87510	7.8e-4	2.4e-4	1.4e-3	1.4e-3	1.7e-4	6.7e-6	1.3e-3	1.3e-3	4.8e-4	4.8e-4	0.86795	0.00106	-0.05470
	288.138	9.2573	0.87508	4.6e-4	3.3e-5	1.7e-3	1.7e-3	1.4e-4	5.5e-6	1.3e-3	1.3e-3	4.8e-4	4.8e-4	0.86795	0.00106	-0.05470
	288.138	9.2573	0.87507	1.2e-3	2.6e-4	1.5e-3	1.5e-3	2.1e-4	2.2e-5	1.3e-3	1.3e-3	4.8e-4	4.8e-4	0.86795	0.00106	-0.05470
	288.138	9.2573	0.87507	9.9e-4	1.8e-4	1.7e-3	1.7e-3	1.5e-4	7.4e-6	1.3e-3	1.3e-3	4.8e-4	4.8e-4	0.86795	0.00106	-0.05470
	288.138	9.2573	0.87506	5.3e-4	5.2e-5	1.7e-3	1.7e-3	1.7e-4	8.5e-6	1.3e-3	1.3e-3	4.8e-4	4.8e-4	0.86795	0.00106	-0.05470
L55	288.137	9.5784	0.85588	5.7e-4	9.7e-5	1.7e-3	1.7e-3	1.2e-4	1.7e-5	1.4e-3	1.4e-3	4.8e-4	4.9e-4^{+}	0.84787	-0.00098	-0.07705^{+}
	288.137	9.5784	0.85590	4.4e-4	7.6e-5	1.8e-3	1.8e-3	1.1e-4	4.8e-6	1.4e-3	1.4e-3	4.8e-4	4.9e-4^{+}	0.84787	-0.00098	-0.07704^{+}
	288.140	9.5785	0.85591	1.4e-3	6.2e-4	1.8e-3	1.9e-3	1.2e-4	8.2e-6	1.4e-3	1.4e-3	4.8e-4	4.9e-4^{+}	0.84786	-0.00099	-0.07705^{+}
	288.141	9.5784	0.85589	3.1e-4	3.2e-5	1.9e-3	1.9e-3	1.1e-4	5.1e-6	1.4e-3	1.4e-3	4.8e-4	4.9e-4^{+}	0.84786	-0.00099	-0.07705^{+}
L56	288.135	9.7067	0.84280	9.8e-4	2.0e-4	1.9e-3	1.9e-3	2.1e-4	3.1e-5	1.4e-3	1.4e-3	4.8e-4	5.2e-4^{+}	0.83726	-0.00349	-0.15076^{+}
	288.135	9.7067	0.84282	5.6e-4	1.4e-4	1.6e-3	1.6e-3	1.9e-4	2.4e-5	1.4e-3	1.4e-3	4.8e-4	5.2e-4^{+}	0.83726	-0.00349	-0.15074^{+}
	288.136	9.7067	0.84282	6.0e-4	9.3e-5	1.5e-3	1.5e-3	1.6e-4	1.4e-5	1.4e-3	1.4e-3	4.8e-4	5.2e-4^{+}	0.83726	-0.00349	-0.15075^{+}
	288.140	9.7067	0.84283	1.8e-3	5.5e-4	1.8e-3	1.9e-3	1.5e-4	2.4e-5	1.4e-3	1.4e-3	4.8e-4	5.2e-4^{+}	0.83725	-0.00351	-0.15070^{+}
	288.141	9.7066	0.84282	3.0e-4	1.8e-5	1.8e-3	1.8e-3	1.4e-4	6.2e-6	1.4e-3	1.4e-3	4.8e-4	5.2e-4^{+}	0.83725	-0.00351	-0.15056^{+}
	288.141	9.7066	0.84284	3.9e-4	2.0e-5	1.7e-3	1.7e-3	1.3e-4	8.9e-6	1.4e-3	1.4e-3	4.8e-4	5.2e-4^{+}	0.83726	-0.00351	-0.15053^{+}
L57	288.141	9.7231	0.84006	2.2e-4	2.0e-5	1.9e-3	1.9e-3	1.5e-4	1.2e-5	1.4e-3	1.4e-3	4.8e-4	5.5e-4^{+}	0.83565	-0.00410	-0.18809^{+}
	288.141	9.7230	0.84007	2.8e-4	2.6e-5	1.8e-3	1.8e-3	1.3e-4	1.4e-5	1.4e-3	1.4e-3	4.8e-4	5.5e-4^{+}	0.83565	-0.00410	-0.18797^{+}
	288.141	9.7230	0.84006	2.6e-4	2.3e-5	1.8e-3	1.8e-3	1.4e-4	8.7e-6	1.4e-3	1.4e-3	4.8e-4	5.5e-4^{+}	0.83565	-0.00410	-0.18791^{+}
	288.141	9.7231	0.84005	1.5e-4	2.8e-5	1.9e-3	1.9e-3	1.2e-4	7.7e-6	1.4e-3	1.4e-3	4.8e-4	5.5e-4^{+}	0.83565	-0.00410	-0.18803^{+}
L58	288.134	9.7447	0.83482	6.9e-4	7.6e-5	1.5e-3	1.5e-3	2.0e-4	8.6e-6	1.4e-3	1.4e-3	4.8e-4	6.6e-4^{+}	0.83345	-0.00503	-0.32930^{+}
	288.135	9.7447	0.83498	4.8e-4	8.1e-5	1.6e-3	1.6e-3	1.9e-4	8.5e-6	1.4e-3	1.4e-3	4.8e-4	6.6e-4^{+}	0.83345	-0.00503	-0.32919^{+}
	288.140	9.7447	0.83499	3.4e-3	1.4e-3	1.8e-3	2.3e-3	1.5e-4	7.1e-6	1.4e-3	1.4e-3	4.8e-4	6.6e-4^{+}	0.83343	-0.00506	-0.32930^{+}
	288.142	9.7447	0.83497	2.7e-4	6.2e-5	2.0e-3	2.0e-3	1.6e-4	9.3e-6	1.4e-3	1.4e-3	4.8e-4	6.6e-4^{+}	0.83341	-0.00508	-0.32986^{+}
	288.142	9.7447	0.83497	2.9e-4	3.5e-5	1.9e-3	1.9e-3	1.5e-4	1.7e-5	1.4e-3	1.4e-3	4.8e-4	6.6e-4^{+}	0.83341	-0.00508	-0.32928^{+}
	288.142	9.7447	0.83497	3.1e-4	5.7e-5	2.0e-3	2.0e-3	1.5e-4	8.1e-6	1.4e-3	1.4e-3	4.8e-4	6.6e-4^{+}	0.83342	-0.00508	-0.32893^{+}
P6	298.137	6.4328	0.99999	7.5e-4	1.1e-4	3.0e-3	3.0e-3	9.4e-5	8.6e-6	1.1e-3	1.1e-3					
L59	298.134	7.1110	0.98138	1.6e-3	6.2e-4	3.0e-3	3.0e-3	1.0e-4	2.3e-5	1.1e-3	1.1e-3	4.8e-4	4.8e-4	0.98158	0.00383	-0.02989
	298.133	7.1110	0.98137	6.5e-4	7.8e-5	3.0e-3	3.0e-3	1.0e-4	1.1e-5	1.1e-3	1.1e-3	4.8e-4	4.8e-4	0.98157	0.00383	-0.02989
	298.132	7.1110	0.98137	6.5e-4	5.9e-5	3.0e-3	3.0e-3	9.0e-5	2.3e-5	1.1e-3	1.1e-3	4.8e-4	4.8e-4	0.98157	0.00383	-0.02989
	298.132	7.1111	0.98137	7.4e-4	2.4e-4	2.8e-3	2.9e-3	9.1e-5	1.1e-5	1.1e-3	1.1e-3	4.8e-4	4.8e-4	0.98157	0.00383	-0.02989
	298.133	7.1110	0.98137	6.9e-4	1.2e-4	3.1e-3	3.1e-3	9.1e-5	9.8e-6	1.1e-3	1.1e-3	4.8e-4	4.8e-4	0.98158	0.00383	-0.02989
	298.136	7.1110	0.98138	3.0e-3	1.3e-3	3.1e-3	3.4e-3	8.8e-5	1.2e-5	1.1e-3	1.1e-3	4.8e-4	4.8e-4	0.98159	0.00383	-0.02989
L60	298.135	7.4191	0.97218	8.7e-4	3.3e-4	3.2e-3	3.2e-3	1.1e-4	8.6e-6	1.1e-3	1.1e-3	4.8e-4	4.8e-4	0.97195	0.00379	-0.03281
	298.134	7.4191	0.97218	6.3e-4	1.0e-4	3.1e-3	3.1e-3	9.7e-5	1.2e-5	1.1e-3	1.1e-3	4.8e-4	4.8e-4	0.97195	0.00379	-0.03281
	298.135	7.4191	0.97218	6.1e-4	1.3e-4	3.0e-3	3.0e-3	1.0e-4	6.0e-6	1.1e-3	1.1e-3	4.8e-4	4.8e-4	0.97195	0.00379	-0.03281
	298.134	7.4191	0.97218	5.6e-4	5.0e-5	3.1e-3	3.1e-3	8.9e-5	8.4e-6	1.1e-3	1.1e-3	4.8e-4	4.8e-4	0.97194	0.00379	-0.03281
	298.137	7.4191	0.97218	4.9e-4	1.4e-4	3.2e-3	3.2e-3	9.0e-5	7.2e-6	1.1e-3	1.1e-3	4.8e-4	4.8e-4	0.97196	0.00379	-0.03281
	298.136	7.4191	0.97218	4.4e-4	3.8e-5	3.2e-3	3.2e-3	9.5e-5	1.3e-5	1.1e-3	1.1e-3	4.8e-4	4.8e-4	0.97195	0.00379	-0.03281
L61	298.139	7.8406	0.95810	1.7e-3	3.8e-4	3.0e-3	3.0e-3	7.1e-4	8.9e-5	1.2e-3	1.2e-3	4.8e-4	4.8e-4	0.95692	0.00349	-0.03927
	298.133	7.8403	0.95809	1.8e-3	4.6e-4	2.9e-3	3.0e-3	3.2e-4	9.0e-5	1.1e-3	1.1e-3	4.8e-4	4.8e-4	0.95692	0.00349	-0.03925
	298.134	7.8404	0.95809	7.5e-4	1.1e-4	2.9e-3	2.9e-3	1.2e-4	2.1e-5	1.1e-3	1.1e-3	4.8e-4	4.8e-4	0.95692	0.00349	-0.03926
	298.133	7.8402	0.95809	9.1e-4	2.2e-4	2.9e-3	2.9e-3	1.1e-4	1.7e-5	1.1e-3	1.1e-3	4.8e-4	4.8e-4	0.95692	0.00349	-0.03925
	298.133	7.8400	0.95810	8.7e-4	3.0e-4	3.0e-3	3.0e-3	1.3e-4	1.7e-5	1.1e-3	1.1e-3	4.8e-4	4.8e-4	0.95693	0.00349	-0.03925
L62	298.132	8.0258	0.95086	4.7e-4	5.0e-5	3.1e-3	3.1e-3	1.3e-4	1.8e-5	1.1e-3	1.1e-3	4.8e-4	4.8e-4	0.94920	0.00310	-0.04439
	298.132	8.0258	0.95086	8.1e-4	2.9e-4	3.1e-3	3.1e-3	1.3e-4	1.3e-5	1.1e-3	1.1e-3	4.8e-4	4.8e-4	0.94919	0.00310	-0.04439
	298.133	8.0258	0.95087	4.8e-4	4.9e-5	3.1e-3	3.1e-3	1.4e-4	1.0e-5	1.1e-3	1.1e-3	4.8e-4	4.8e-4	0.94920	0.00310	-0.04439
	298.133	8.0258	0.95087	8.2e-4	1.8e-4	3.2e-3	3.2e-3	1.2e-4	7.4e-6	1.1e-3	1.1e-3	4.8e-4	4.8e-4	0.94920	0.00310	-0.04439
	298.137	8.0258	0.95087	2.7e-3	1.2e-3	3.2e-3	3.5e-3	1.1e-4	9.9e-6	1.1e-3	1.1e-3	4.8e-4	4.8e-4	0.94921	0.00310	-0.04440
	298.140	8.0258	0.95088	2.0e-4	2.8e-5	3.4e-3	3.4e-3	1.2e-4	9.5e-6	1.1e-3	1.1e-3	4.8e-4	4.8e-4	0.94922	0.00310	-0.04442
L63	298.136	8.1284	0.94625	6.0e-4	1.8e-4	3.0e-3	3.1e-3	1.3e-4	2.3e-5	1.2e-3	1.2e-3	4.8e-4	4.8e-4	0.94443	0.00267	-0.04892
	298.135	8.1284	0.94625	6.4e-4	8.4e-5	3.1e-3	3.1e-3	1.2e-4	2.2e-5	1.2e-3	1.2e-3	4.8e-4	4.8e-4	0.94443	0.00267	-0.04892
	298.135	8.1284	0.94625	5.5e-4	7.2e-5	3.1e-3	3.1e-3	1.4e-4	2.8e-5	1.2e-3	1.2e-3	4.8e-4	4.8e-4	0.94443	0.00267	-0.04891

	298.135	8.1285	0.94625	5.3e-4	4.4e-5	3.0e-3	3.0e-3	1.3e-4	2.1e-5	1.2e-3	1.2e-3	4.8e-4	4.8e-4	0.94443	0.00267	-0.04891
	298.134	8.1285	0.94625	4.2e-4	3.5e-5	3.0e-3	3.0e-3	1.6e-4	2.5e-5	1.2e-3	1.2e-3	4.8e-4	4.8e-4	0.94443	0.00267	-0.04891
	298.134	8.1284	0.94625	4.5e-4	8.3e-5	2.9e-3	2.9e-3	1.2e-4	2.0e-5	1.2e-3	1.2e-3	4.8e-4	4.8e-4	0.94443	0.00267	-0.04891
L64	298.136	8.2648	0.93816	7.8e-4	2.3e-4	3.3e-3	3.3e-3	1.4e-4	3.2e-5	1.2e-3	1.2e-3	4.8e-4	4.9e-4^{+}	0.93709	0.00133	-0.08034^{+}
	298.136	8.2648	0.93815	7.9e-4	1.4e-4	3.1e-3	3.1e-3	1.5e-4	1.6e-5	1.2e-3	1.2e-3	4.8e-4	4.9e-4^{+}	0.93709	0.00133	-0.08037^{+}
	298.135	8.2648	0.93815	6.1e-4	4.5e-5	3.2e-3	3.2e-3	1.2e-4	2.5e-5	1.2e-3	1.2e-3	4.8e-4	4.9e-4^{+}	0.93709	0.00133	-0.08037^{+}
	298.135	8.2648	0.93815	5.5e-4	7.1e-5	3.1e-3	3.2e-3	1.2e-4	1.3e-5	1.2e-3	1.2e-3	4.8e-4	4.9e-4^{+}	0.93709	0.00134	-0.08036^{+}
	298.135	8.2648	0.93815	5.3e-4	8.3e-5	3.2e-3	3.2e-3	1.2e-4	2.0e-5	1.2e-3	1.2e-3	4.8e-4	4.9e-4^{+}	0.93709	0.00133	-0.08036^{+}
	298.135	8.2648	0.93816	5.2e-4	6.8e-5	3.1e-3	3.1e-3	1.1e-4	1.1e-5	1.2e-3	1.2e-3	4.8e-4	4.9e-4^{+}	0.93709	0.00134	-0.08033^{+}
L65	298.135	8.3020	0.93438	5.4e-4	5.1e-5	3.3e-3	3.3e-3	1.8e-4	2.7e-5	1.2e-3	1.2e-3	4.8e-4	5.1e-4^{+}	0.93473	0.00051	-0.14060^{+}
	298.135	8.3020	0.93439	3.9e-4	3.6e-5	3.3e-3	3.3e-3	1.4e-4	2.1e-5	1.2e-3	1.2e-3	4.8e-4	5.1e-4^{+}	0.93473	0.00050	-0.14069^{+}
	298.138	8.3019	0.93439	1.2e-3	3.0e-4	3.2e-3	3.2e-3	1.0e-4	1.3e-5	1.2e-3	1.2e-3	4.8e-4	5.1e-4^{+}	0.93474	0.00050	-0.14043^{+}
	298.138	8.3019	0.93438	5.1e-4	6.8e-5	3.2e-3	3.2e-3	1.4e-4	2.3e-5	1.2e-3	1.2e-3	4.8e-4	5.1e-4^{+}	0.93474	0.00069	-0.14048^{+}
	298.135	8.3019	0.93440	1.0e-3	3.8e-4	3.2e-3	3.2e-3	1.6e-4	4.3e-5	1.2e-3	1.2e-3	4.8e-4	5.1e-4^{+}	0.93474	0.00051	-0.14053^{+}
	298.136	8.3019	0.93441	2.0e-3	8.8e-4	3.2e-3	3.3e-3	1.4e-4	2.4e-5	1.2e-3	1.2e-3	4.8e-4	5.1e-4^{+}	0.93474	0.00051	-0.14043^{+}
L66	298.133	8.3180	0.93085	1.0e-3	3.0e-4	3.0e-3	3.0e-3	1.2e-4	7.7e-6	1.2e-3	1.2e-3	4.8e-4	7.2e-4^{+}	0.93363	-0.00001	-0.46243^{+}
	298.135	8.3180	0.93077	9.8e-4	1.2e-4	3.2e-3	3.2e-3	1.0e-4	1.2e-5	1.2e-3	1.2e-3	4.8e-4	7.2e-4^{+}	0.93363	-0.00001	-0.46047^{+}
	298.133	8.3180	0.93090	8.4e-4	6.1e-5	3.2e-3	3.2e-3	1.1e-4	1.1e-5	1.2e-3	1.2e-3	4.8e-4	7.2e-4^{+}	0.93363	-0.00000	-0.46319^{+}
	298.134	8.3180	0.93082	2.2e-3	8.8e-4	3.2e-3	3.3e-3	1.3e-4	1.4e-5	1.2e-3	1.2e-3	4.8e-4	7.2e-4^{+}	0.93363	-0.00001	-0.46008^{+}
	298.134	8.3180	0.93096	6.6e-4	1.4e-4	3.0e-3	3.0e-3	1.3e-4	1.5e-5	1.2e-3	1.2e-3	4.8e-4	7.2e-4^{+}	0.93363	-0.00001	-0.46153^{+}
	298.136	8.3180	0.93081	1.3e-3	4.7e-4	3.1e-3	3.1e-3	1.1e-4	9.9e-6	1.2e-3	1.2e-3	4.8e-4	7.2e-4^{+}	0.93363	-0.00002	-0.46044^{+}

Table A.3
Vapor phase: Experimental VLE data for $CO_2 + O_2$ at mean temperature $\bar{T}$, mean pressure $\bar{p}$, and sample vapor phase mole fraction y_{CO_2}.

	Data			Temperature				Pressure				Composition			Composition derivatives	
ID	$\bar{T}$ (K)	$\bar{p}$ (MPa)	y_{CO_2} (-)	$s(T)$ (K)	$s(\bar{T})$ (K)	$\bar{u}(T)$ (K)	$u_c(\bar{T})$ (K)	$s(p)$ (MPa)	$s(\bar{p})$ (MPa)	$\bar{u}(p)$ (MPa)	$u_c(\bar{p})$ (MPa)	$u(y_{CO_2})$ (-)	$u_{tot}(y_{CO_2})$ (-)	$y_{CO_2,calc}$ (-)	$\partial y_{CO_2}/\partial T$ (K^{-1})	$\partial y_{CO_2}/\partial p$ (MPa^{-1})
P1	218.147	0.5546	0.99999	4.7e-4	7.3e-5	3.7e-3	3.7e-3	1.3e-5	1.1e-6	4.9e-4	4.9e-4					
V1	218.148	1.0238	0.57407	8.9e-4	1.4e-4	3.4e-3	3.4e-3	2.3e-5	7.2e-6	5.1e-4	5.1e-4	4.8e-4	5.5e-4	0.57409	0.02295	-0.49749
	218.148	1.0238	0.57376	8.9e-4	1.2e-4	3.5e-3	3.5e-3	2.8e-5	1.1e-5	5.1e-4	5.1e-4	4.8e-4	5.5e-4	0.57411	0.02295	-0.49753
	218.148	1.0238	0.57373	1.1e-3	1.6e-4	3.4e-3	3.4e-3	3.1e-5	1.3e-5	5.1e-4	5.1e-4	4.8e-4	5.5e-4	0.57412	0.02295	-0.49755
	218.148	1.0237	0.57348	1.2e-3	1.8e-4	3.3e-3	3.3e-3	3.3e-5	1.4e-5	5.1e-4	5.1e-4	4.8e-4	5.5e-4	0.57413	0.02295	-0.49758
	218.148	1.0237	0.57340	1.0e-3	1.7e-4	3.4e-3	3.4e-3	2.6e-5	8.6e-6	5.1e-4	5.1e-4	4.8e-4	5.5e-4	0.57417	0.02295	-0.49764
	218.148	1.0236	0.57325	8.8e-4	1.1e-4	3.2e-3	3.2e-3	3.4e-5	1.5e-5	5.1e-4	5.1e-4	4.8e-4	5.5e-4	0.57419	0.02295	-0.49768
	218.148	1.0236	0.57344	1.4e-3	2.0e-4	3.4e-3	3.5e-3	3.1e-5	1.3e-5	5.1e-4	5.1e-4	4.8e-4	5.5e-4	0.57421	0.02295	-0.49772
	218.148	1.0236	0.57323	9.7e-4	1.9e-4	3.3e-3	3.3e-3	3.7e-5	1.6e-5	5.1e-4	5.1e-4	4.8e-4	5.5e-4	0.57423	0.02296	-0.49775
V2	218.148	2.1957	0.29873	4.7e-4	1.2e-4	3.5e-3	3.5e-3	3.3e-5	1.1e-5	5.2e-4	5.2e-4	4.8e-4	4.8e-4	0.30251	0.01191	-0.10668
	218.147	2.1957	0.29847	7.5e-4	1.6e-4	3.5e-3	3.5e-3	2.2e-5	2.3e-6	5.2e-4	5.2e-4	4.8e-4	4.8e-4	0.30251	0.01191	-0.10668
	218.148	2.1957	0.29849	4.4e-4	6.2e-5	3.4e-3	3.4e-3	3.3e-5	7.7e-6	5.2e-4	5.2e-4	4.8e-4	4.8e-4	0.30252	0.01191	-0.10668
	218.148	2.1957	0.29844	5.2e-4	1.0e-4	3.4e-3	3.4e-3	4.6e-5	1.7e-5	5.2e-4	5.2e-4	4.8e-4	4.8e-4	0.30252	0.01191	-0.10669
	218.148	2.1957	0.29842	4.2e-4	3.1e-5	3.4e-3	3.4e-3	7.5e-5	3.2e-5	5.2e-4	5.2e-4	4.8e-4	4.8e-4	0.30252	0.01191	-0.10669
	218.148	2.1956	0.29839	4.9e-4	5.9e-5	3.5e-3	3.5e-3	6.5e-5	3.0e-5	5.2e-4	5.2e-4	4.8e-4	4.8e-4	0.30253	0.01191	-0.10669
V3	218.148	3.9361	0.19677	7.6e-4	1.5e-4	3.9e-3	3.9e-3	5.3e-5	1.1e-5	1.1e-3	1.1e-3	4.8e-4	4.8e-4	0.20251	0.00762	-0.02965
	218.148	3.9362	0.19668	9.3e-4	1.3e-4	3.7e-3	3.7e-3	5.2e-5	6.4e-6	1.1e-3	1.1e-3	4.8e-4	4.8e-4	0.20251	0.00762	-0.02965
	218.148	3.9362	0.19662	1.1e-3	2.4e-4	3.6e-3	3.6e-3	6.3e-5	1.8e-5	1.1e-3	1.1e-3	4.8e-4	4.8e-4	0.20251	0.00762	-0.02965
	218.148	3.9362	0.19656	1.1e-3	2.2e-4	3.8e-3	3.8e-3	6.0e-5	9.0e-6	1.1e-3	1.1e-3	4.8e-4	4.8e-4	0.20251	0.00762	-0.02965
	218.148	3.9362	0.19654	8.8e-4	1.2e-4	3.8e-3	3.8e-3	5.2e-5	7.5e-6	1.1e-3	1.1e-3	4.8e-4	4.8e-4	0.20251	0.00762	-0.02965
V4	218.150	5.9189	0.16098	6.2e-4	8.5e-5	3.2e-3	3.2e-3	8.2e-5	5.0e-6	1.1e-3	1.1e-3	4.8e-4	4.8e-4	0.16825	0.00589	-0.00866
	218.150	5.9189	0.16093	8.8e-4	1.3e-4	3.3e-3	3.3e-3	1.1e-4	8.8e-6	1.1e-3	1.1e-3	4.8e-4	4.8e-4	0.16826	0.00589	-0.00866
	218.150	5.9189	0.16094	5.3e-4	7.7e-5	3.2e-3	3.2e-3	8.9e-5	6.6e-6	1.1e-3	1.1e-3	4.8e-4	4.8e-4	0.16826	0.00589	-0.00866
	218.150	5.9189	0.16091	8.6e-4	1.5e-4	3.2e-3	3.2e-3	8.1e-5	5.4e-6	1.1e-3	1.1e-3	4.8e-4	4.8e-4	0.16826	0.00589	-0.00866
	218.150	5.9189	0.16089	8.0e-4	1.1e-4	3.2e-3	3.2e-3	8.6e-5	9.2e-6	1.1e-3	1.1e-3	4.8e-4	4.8e-4	0.16825	0.00589	-0.00866
V5	218.148	7.8935	0.15232	6.1e-4	4.1e-5	3.5e-3	3.5e-3	1.0e-4	3.9e-6	1.2e-3	1.2e-3	4.8e-4	4.8e-4	0.16120	0.00510	0.00080
	218.148	7.8935	0.15231	6.7e-4	1.2e-4	3.4e-3	3.4e-3	1.0e-4	4.6e-6	1.2e-3	1.2e-3	4.8e-4	4.8e-4	0.16120	0.00510	0.00080
	218.148	7.8935	0.15230	7.9e-4	2.6e-4	3.4e-3	3.4e-3	9.1e-5	5.3e-6	1.2e-3	1.2e-3	4.8e-4	4.8e-4	0.16120	0.00510	0.00080
	218.147	7.8935	0.15227	7.6e-4	1.6e-4	3.4e-3	3.4e-3	9.5e-5	1.2e-5	1.2e-3	1.2e-3	4.8e-4	4.8e-4	0.16120	0.00510	0.00080
	218.149	7.8935	0.15225	4.3e-4	6.0e-5	3.5e-3	3.5e-3	1.1e-4	2.3e-5	1.2e-3	1.2e-3	4.8e-4	4.8e-4	0.16121	0.00510	0.00080
	218.148	7.8935	0.15227	5.5e-4	1.1e-4	3.5e-3	3.5e-3	1.0e-4	1.3e-5	1.2e-3	1.2e-3	4.8e-4	4.8e-4	0.16120	0.00510	0.00080
V6	218.148	9.7335	0.15919	7.7e-4	2.3e-4	3.4e-3	3.4e-3	1.3e-4	7.8e-6	1.4e-3	1.4e-3	4.8e-4	4.8e-4	0.16940	0.00466	0.00826
	218.148	9.7336	0.15919	7.1e-4	1.2e-4	3.5e-3	3.5e-3	1.2e-4	1.0e-5	1.4e-3	1.4e-3	4.8e-4	4.8e-4	0.16941	0.00466	0.00826
	218.148	9.7335	0.15917	6.4e-4	1.1e-4	3.5e-3	3.5e-3	1.2e-4	6.8e-6	1.4e-3	1.4e-3	4.8e-4	4.8e-4	0.16940	0.00466	0.00826
	218.148	9.7335	0.15919	7.5e-4	1.4e-4	3.5e-3	3.5e-3	1.3e-4	7.1e-6	1.4e-3	1.4e-3	4.8e-4	4.8e-4	0.16940	0.00466	0.00826
	218.148	9.7335	0.15916	5.7e-4	9.4e-5	3.5e-3	3.5e-3	1.3e-4	1.6e-5	1.4e-3	1.4e-3	4.8e-4	4.8e-4	0.16940	0.00466	0.00826
V7	218.148	11.7910	0.18682	7.0e-4	6.4e-5	3.6e-3	3.6e-3	1.9e-4	1.1e-5	2.7e-3	2.7e-3	4.8e-4	4.8e-4	0.19797	0.00416	0.02109
	218.148	11.7910	0.18681	5.8e-4	6.6e-5	3.5e-3	3.5e-3	1.7e-4	2.0e-5	2.7e-3	2.7e-3	4.8e-4	4.8e-4	0.19797	0.00416	0.02109
	218.147	11.7910	0.18681	7.5e-4	1.5e-4	3.4e-3	3.4e-3	1.7e-4	8.4e-6	2.7e-3	2.7e-3	4.8e-4	4.8e-4	0.19797	0.00416	0.02109
	218.147	11.7910	0.18683	1.0e-3	1.1e-4	3.5e-3	3.5e-3	1.5e-4	1.9e-5	2.7e-3	2.7e-3	4.8e-4	4.8e-4	0.19796	0.00416	0.02109
	218.147	11.7910	0.18679	8.2e-4	1.0e-4	3.5e-3	3.5e-3	1.4e-4	9.0e-6	2.7e-3	2.7e-3	4.8e-4	4.8e-4	0.19797	0.00416	0.02109
	218.148	11.7910	0.18683	5.2e-4	6.8e-5	3.7e-3	3.7e-3	1.5e-4	6.5e-6	2.7e-3	2.7e-3	4.8e-4	4.8e-4	0.19797	0.00416	0.02109
	218.148	11.7910	0.18679	7.6e-4	2.0e-4	3.4e-3	3.4e-3	1.6e-4	2.5e-5	2.7e-3	2.7e-3	4.8e-4	4.8e-4	0.19797	0.00416	0.02109
V8	218.148	13.0212	0.22285	7.3e-4	1.7e-4	3.6e-3	3.6e-3	1.7e-4	1.7e-5	2.8e-3	2.8e-3	4.8e-4	4.9e-4	0.23322	0.00358	0.03885
	218.149	13.0211	0.22281	8.3e-4	2.8e-4	3.6e-3	3.6e-3	1.5e-4	6.3e-6	2.8e-3	2.8e-3	4.8e-4	4.9e-4	0.23322	0.00358	0.03886
	218.148	13.0211	0.22282	6.4e-4	8.2e-5	3.5e-3	3.5e-3	2.0e-4	2.9e-5	2.8e-3	2.8e-3	4.8e-4	4.9e-4	0.23321	0.00358	0.03885
	218.148	13.0211	0.22283	8.0e-4	1.6e-4	3.4e-3	3.4e-3	1.8e-4	8.3e-6	2.8e-3	2.8e-3	4.8e-4	4.9e-4	0.23321	0.00358	0.03885

V9	218.148	14.0360	0.28671	6.9e-4	1.1e-4	3.7e-3	3.7e-3	1.8e-4	2.1e-5	2.8e-3	2.8e-3	4.8e-4	5.7e-4^{+}	0.29187	0.00229	0.11052^{+}
	218.147	14.0359	0.28671	8.7e-4	1.0e-4	3.6e-3	3.6e-3	2.3e-4	1.7e-5	2.8e-3	2.8e-3	4.8e-4	5.7e-4^{+}	0.29187	0.00229	0.11051^{+}
	218.148	14.0359	0.28663	6.4e-4	8.3e-5	3.6e-3	3.6e-3	1.8e-4	1.2e-5	2.8e-3	2.8e-3	4.8e-4	5.7e-4^{+}	0.29187	0.00229	0.11052^{+}
	218.148	14.0359	0.28655	7.1e-4	8.4e-5	3.5e-3	3.5e-3	1.9e-4	7.4e-6	2.8e-3	2.8e-3	4.8e-4	5.7e-4^{+}	0.29186	0.00229	0.11050^{+}
V10*	218.148	14.3562	0.33858	6.8e-4	8.9e-5	3.2e-3	3.2e-3	2.4e-4	2.0e-5	2.8e-3	2.8e-3	4.8e-4	9.4e-4^{+}	0.33135	0.00084	0.29213^{+}
	218.148	14.3563	0.33861	7.3e-4	1.2e-4	3.1e-3	3.1e-3	1.8e-4	1.1e-5	2.8e-3	2.8e-3	4.8e-4	9.4e-4^{+}	0.33136	0.00084	0.29221^{+}
	218.148	14.3563	0.33855	7.6e-4	2.3e-4	3.2e-3	3.2e-3	1.8e-4	2.0e-5	2.8e-3	2.8e-3	4.8e-4	9.4e-4^{+}	0.33136	0.00084	0.29218^{+}
	218.148	14.3563	0.33850	7.5e-4	2.2e-4	3.2e-3	3.2e-3	1.8e-4	7.7e-6	2.8e-3	2.8e-3	4.8e-4	9.4e-4^{+}	0.33136	0.00084	0.29216^{+}
	218.148	14.3562	0.33858	5.2e-4	1.2e-4	3.1e-3	3.1e-3	1.7e-4	1.1e-5	2.8e-3	2.8e-3	4.8e-4	9.4e-4^{+}	0.33135	0.00084	0.29204^{+}
	218.148	14.3562	0.33853	5.7e-4	1.1e-4	3.1e-3	3.1e-3	2.0e-4	1.2e-5	2.8e-3	2.8e-3	4.8e-4	9.4e-4^{+}	0.33136	0.00084	0.29215^{+}
	218.148	14.3563	0.33849	4.9e-4	8.5e-5	3.2e-3	3.2e-3	2.0e-4	1.6e-5	2.8e-3	2.8e-3	4.8e-4	9.4e-4^{+}	0.33136	0.00084	0.29221^{+}
V11*	218.148	14.3873	0.34939	6.1e-4	8.4e-5	3.1e-3	3.1e-3	2.4e-4	1.7e-5	2.8e-3	2.8e-3	4.8e-4	1.2e-3^{+}	0.33726	0.00050	0.40199^{+}
	218.147	14.3873	0.34927	1.2e-3	2.6e-4	3.4e-3	3.4e-3	2.1e-4	8.8e-6	2.8e-3	2.8e-3	4.8e-4	1.2e-3^{+}	0.33726	0.00050	0.40215^{+}
	218.147	14.3873	0.34937	9.9e-4	1.3e-4	3.3e-3	3.3e-3	1.6e-4	9.6e-6	2.8e-3	2.8e-3	4.8e-4	1.2e-3^{+}	0.33726	0.00050	0.40196^{+}
	218.147	14.3873	0.34939	9.0e-4	2.3e-4	3.2e-3	3.2e-3	2.2e-4	1.1e-5	2.8e-3	2.8e-3	4.8e-4	1.2e-3^{+}	0.33726	0.00050	0.40201^{+}
	218.147	14.3873	0.34933	8.3e-4	8.0e-5	3.3e-3	3.3e-3	2.2e-4	3.3e-5	2.8e-3	2.8e-3	4.8e-4	1.2e-3^{+}	0.33725	0.00050	0.40185^{+}
	218.147	14.3873	0.34939	9.6e-4	2.4e-4	3.3e-3	3.3e-3	2.2e-4	3.1e-5	2.8e-3	2.8e-3	4.8e-4	1.2e-3^{+}	0.33726	0.00050	0.40203^{+}
V12*	218.149	14.4111	0.36118	6.4e-4	1.1e-4	3.4e-3	3.4e-3	2.0e-4	1.1e-5	2.8e-3	2.8e-3	4.8e-4	1.8e-3^{+}	0.34236	0.00017	0.62899^{+}
	218.148	14.4111	0.36122	1.0e-3	3.6e-4	3.2e-3	3.3e-3	2.1e-4	8.4e-6	2.8e-3	2.8e-3	4.8e-4	1.8e-3^{+}	0.34236	0.00017	0.62908^{+}
	218.149	14.4111	0.36122	9.2e-4	2.2e-4	3.4e-3	3.4e-3	1.6e-4	1.3e-5	2.8e-3	2.8e-3	4.8e-4	1.8e-3^{+}	0.34237	0.00032	0.62982^{+}
	218.150	14.4111	0.36115	9.3e-4	2.8e-4	3.4e-3	3.5e-3	1.8e-4	8.8e-6	2.8e-3	2.8e-3	4.8e-4	1.8e-3^{+}	0.34237	0.00017	0.62952^{+}
	218.149	14.4111	0.36117	1.1e-3	1.9e-4	3.3e-3	3.3e-3	1.9e-4	1.5e-5	2.8e-3	2.8e-3	4.8e-4	1.8e-3^{+}	0.34236	0.00017	0.62884^{+}
	218.149	14.4111	0.36113	1.0e-3	2.1e-4	3.3e-3	3.3e-3	1.8e-4	7.7e-6	2.8e-3	2.8e-3	4.8e-4	1.8e-3^{+}	0.34236	0.00017	0.62915^{+}
	218.150	14.4112	0.36067	9.1e-4	2.3e-4	3.3e-3	3.3e-3	1.7e-4	3.5e-6	2.8e-3	2.8e-3	4.8e-4	1.8e-3^{+}	0.34239	0.00017	0.63082^{+}
P2	233.143	1.0048	0.99999	9.7e-4	7.4e-5	6.8e-3	6.8e-3	4.3e-5	1.1e-5	5.1e-4	5.1e-4					
V14	233.143	1.9677	0.56443	9.5e-4	1.6e-4	7.4e-3	7.4e-3	3.5e-5	1.2e-5	5.1e-4	5.1e-4	4.8e-4	5.1e-4	0.56621	0.01852	-0.23333
	233.143	1.9677	0.56407	1.1e-3	1.5e-4	7.1e-3	7.1e-3	2.2e-5	2.5e-6	5.1e-4	5.1e-4	4.8e-4	5.1e-4	0.56621	0.01852	-0.23333
	233.143	1.9677	0.56405	1.1e-3	2.1e-4	7.2e-3	7.2e-3	2.1e-5	2.1e-6	5.1e-4	5.1e-4	4.8e-4	5.1e-4	0.56621	0.01852	-0.23333
	233.142	1.9677	0.56395	1.1e-3	1.3e-4	7.2e-3	7.3e-3	2.0e-5	2.1e-6	5.1e-4	5.1e-4	4.8e-4	5.1e-4	0.56621	0.01852	-0.23333
	233.142	1.9677	0.56369	1.1e-3	1.7e-4	7.4e-3	7.4e-3	2.8e-5	7.9e-6	5.1e-4	5.1e-4	4.8e-4	5.1e-4	0.56620	0.01852	-0.23333
	233.142	1.9677	0.56362	1.1e-3	1.5e-4	7.7e-3	7.7e-3	2.0e-5	2.3e-6	5.1e-4	5.1e-4	4.8e-4	5.1e-4	0.56620	0.01852	-0.23333
V15	233.141	2.9346	0.41129	1.3e-3	3.2e-4	7.8e-3	7.8e-3	9.9e-5	4.3e-5	5.3e-4	5.3e-4	4.8e-4	4.9e-4	0.41569	0.01345	-0.10307
	233.141	2.9346	0.41115	1.3e-3	2.3e-4	7.4e-3	7.4e-3	2.6e-5	6.1e-6	5.2e-4	5.2e-4	4.8e-4	4.9e-4	0.41570	0.01345	-0.10308
	233.143	2.9345	0.41116	9.7e-4	1.2e-4	8.1e-3	8.1e-3	2.4e-5	2.7e-6	5.2e-4	5.2e-4	4.8e-4	4.9e-4	0.41572	0.01345	-0.10308
	233.142	2.9346	0.41126	6.0e-4	6.3e-5	7.5e-3	7.5e-3	2.5e-5	4.7e-6	5.2e-4	5.2e-4	4.8e-4	4.9e-4	0.41571	0.01345	-0.10308
	233.142	2.9345	0.41118	6.2e-4	5.4e-5	7.7e-3	7.7e-3	2.6e-5	6.3e-6	5.2e-4	5.2e-4	4.8e-4	4.9e-4	0.41571	0.01345	-0.10308
	233.142	2.9345	0.41106	1.2e-3	3.3e-4	8.0e-3	8.0e-3	2.5e-5	5.5e-6	5.2e-4	5.2e-4	4.8e-4	4.9e-4	0.41572	0.01345	-0.10308
	233.142	2.9345	0.41107	8.7e-4	9.6e-5	7.8e-3	7.8e-3	6.8e-5	1.6e-5	5.2e-4	5.3e-4	4.8e-4	4.9e-4	0.41571	0.01345	-0.10308
V16	233.141	3.9408	0.33186	1.8e-3	5.7e-4	6.8e-3	6.8e-3	3.0e-4	7.1e-5	1.1e-3	1.1e-3	4.8e-4	4.9e-4	0.33995	0.01079	-0.05441
	233.143	3.9407	0.33186	9.8e-4	1.1e-4	6.9e-3	6.9e-3	2.5e-4	5.8e-5	1.1e-3	1.1e-3	4.8e-4	4.9e-4	0.33996	0.01079	-0.05442
	233.143	3.9407	0.33179	1.0e-3	2.4e-4	6.6e-3	6.6e-3	6.7e-5	1.2e-5	1.1e-3	1.1e-3	4.8e-4	4.9e-4	0.33997	0.01079	-0.05442
	233.143	3.9409	0.33190	9.3e-4	1.1e-4	6.6e-3	6.6e-3	7.6e-5	2.7e-5	1.1e-3	1.1e-3	4.8e-4	4.9e-4	0.33996	0.01079	-0.05441
	233.144	3.9408	0.33184	8.5e-4	1.7e-4	6.8e-3	6.8e-3	6.0e-5	1.2e-5	1.1e-3	1.1e-3	4.8e-4	4.9e-4	0.33997	0.01079	-0.05442
	233.143	3.9408	0.33188	6.2e-4	1.2e-4	7.1e-3	7.1e-3	5.8e-5	1.1e-5	1.1e-3	1.1e-3	4.8e-4	4.9e-4	0.33997	0.01079	-0.05441
V17	233.144	5.9477	0.26280	9.3e-4	2.4e-4	8.0e-3	8.0e-3	8.7e-5	1.2e-5	1.1e-3	1.1e-3	4.8e-4	4.8e-4	0.27331	0.00821	-0.01872
	233.143	5.9476	0.26279	7.5e-4	7.4e-5	7.4e-3	7.4e-3	2.9e-4	1.0e-4	1.1e-3	1.1e-3	4.8e-4	4.8e-4	0.27331	0.00821	-0.01872
	233.143	5.9475	0.26279	7.0e-4	1.2e-4	7.6e-3	7.6e-3	3.2e-4	1.3e-4	1.1e-3	1.1e-3	4.8e-4	4.8e-4	0.27331	0.00821	-0.01872
	233.143	5.9474	0.26282	6.5e-4	7.7e-5	7.4e-3	7.4e-3	4.3e-4	1.9e-4	1.1e-3	1.1e-3	4.8e-4	4.8e-4	0.27331	0.00821	-0.01872
	233.144	5.9472	0.26280	8.4e-4	2.7e-4	7.8e-3	7.8e-3	5.7e-4	2.7e-4	1.1e-3	1.2e-3	4.8e-4	4.8e-4	0.27332	0.00821	-0.01872
V18	233.141	7.8335	0.24023	2.1e-3	7.1e-4	7.6e-3	7.6e-3	1.5e-4	1.2e-5	1.2e-3	1.2e-3	4.8e-4	4.8e-4	0.25239	0.00708	-0.00479
	233.142	7.8335	0.24025	1.3e-3	3.4e-4	7.5e-3	7.5e-3	1.5e-4	1.3e-5	1.2e-3	1.2e-3	4.8e-4	4.8e-4	0.25240	0.00708	-0.00479
	233.142	7.8335	0.24023	8.7e-4	1.2e-4	7.8e-3	7.8e-3	1.3e-4	6.3e-6	1.2e-3	1.2e-3	4.8e-4	4.8e-4	0.25240	0.00708	-0.00479
	233.142	7.8334	0.24020	1.1e-3	1.8e-4	7.4e-3	7.4e-3	1.1e-4	7.2e-6	1.2e-3	1.2e-3	4.8e-4	4.8e-4	0.25240	0.00708	-0.00479
	233.142	7.8335	0.24014	1.0e-3	2.8e-4	7.4e-3	7.4e-3	1.2e-4	5.5e-6	1.2e-3	1.2e-3	4.8e-4	4.8e-4	0.25240	0.00708	-0.00479

V19	233.140	8.8724	0.23720	1.3e-3	1.9e-4	7.5e-3	7.5e-3	1.9e-4	9.2e-6	1.3e-3	1.3e-3	4.8e-4	4.8e-4	0.25032	0.00671	0.00070
	233.140	8.8724	0.23719	1.1e-3	2.7e-4	7.1e-3	7.1e-3	1.4e-4	1.4e-5	1.3e-3	1.3e-3	4.8e-4	4.8e-4	0.25032	0.00671	0.00070
	233.141	8.8724	0.23720	1.0e-3	9.7e-5	7.8e-3	7.8e-3	1.2e-4	1.1e-5	1.3e-3	1.3e-3	4.8e-4	4.8e-4	0.25033	0.00671	0.00070
	233.141	8.8724	0.23715	8.7e-4	1.6e-4	7.6e-3	7.6e-3	1.4e-4	9.4e-6	1.3e-3	1.3e-3	4.8e-4	4.8e-4	0.25033	0.00671	0.00070
	233.142	8.8724	0.23710	7.5e-4	1.1e-4	7.7e-3	7.7e-3	1.3e-4	8.5e-6	1.3e-3	1.3e-3	4.8e-4	4.8e-4	0.25034	0.00671	0.00070
	233.142	8.8724	0.23708	8.3e-4	1.0e-4	7.7e-3	7.7e-3	1.3e-4	4.4e-6	1.3e-3	1.3e-3	4.8e-4	4.8e-4	0.25034	0.00671	0.00070
V20	233.141	9.8514	0.23940	1.0e-3	1.4e-4	7.4e-3	7.4e-3	1.6e-4	1.0e-5	1.4e-3	1.4e-3	4.8e-4	4.8e-4	0.25343	0.00645	0.00566
	233.140	9.8513	0.23942	1.5e-3	4.3e-4	7.4e-3	7.4e-3	2.1e-4	1.0e-5	1.4e-3	1.4e-3	4.8e-4	4.8e-4	0.25342	0.00645	0.00566
	233.141	9.8514	0.23938	8.8e-4	1.1e-4	7.7e-3	7.7e-3	1.3e-4	4.6e-6	1.4e-3	1.4e-3	4.8e-4	4.8e-4	0.25343	0.00645	0.00566
	233.141	9.8514	0.23940	8.3e-4	8.5e-5	7.5e-3	7.5e-3	1.5e-4	1.0e-5	1.4e-3	1.4e-3	4.8e-4	4.8e-4	0.25343	0.00645	0.00566
	233.140	9.8514	0.23941	9.6e-4	1.3e-4	7.7e-3	7.7e-3	1.5e-4	1.0e-5	1.4e-3	1.4e-3	4.8e-4	4.8e-4	0.25343	0.00645	0.00566
	233.141	9.8513	0.23939	1.0e-3	1.2e-4	7.4e-3	7.4e-3	1.5e-4	7.2e-6	1.4e-3	1.4e-3	4.8e-4	4.8e-4	0.25343	0.00645	0.00566
V21	233.141	11.8342	0.26146	1.3e-3	2.0e-4	6.9e-3	7.0e-3	2.0e-4	1.0e-5	2.7e-3	2.7e-3	4.8e-4	4.8e-4	0.27633	0.00616	0.01869
	233.140	11.8341	0.26145	1.0e-3	2.8e-4	7.4e-3	7.4e-3	1.7e-4	9.8e-6	2.7e-3	2.7e-3	4.8e-4	4.8e-4	0.27633	0.00616	0.01869
	233.140	11.8341	0.26139	1.0e-3	6.9e-5	7.1e-3	7.1e-3	1.8e-4	1.8e-5	2.7e-3	2.7e-3	4.8e-4	4.8e-4	0.27633	0.00616	0.01869
	233.141	11.8341	0.26144	7.1e-4	8.4e-5	7.5e-3	7.5e-3	1.6e-4	6.1e-6	2.7e-3	2.7e-3	4.8e-4	4.8e-4	0.27633	0.00616	0.01869
	233.141	11.8341	0.26143	1.4e-3	1.9e-4	7.1e-3	7.1e-3	1.7e-4	9.4e-6	2.7e-3	2.7e-3	4.8e-4	4.8e-4	0.27633	0.00616	0.01869
	233.141	11.8341	0.26142	8.3e-4	1.5e-4	7.3e-3	7.3e-3	1.5e-4	8.6e-6	2.7e-3	2.7e-3	4.8e-4	4.8e-4	0.27633	0.00616	0.01869
V22	233.143	12.8248	0.28660	7.0e-4	6.5e-5	7.2e-3	7.2e-3	2.4e-4	1.7e-5	2.7e-3	2.7e-3	4.8e-4	4.9e-4	0.30037	0.00615	0.03119
	233.143	12.8248	0.28657	1.0e-3	2.1e-4	7.4e-3	7.4e-3	2.4e-4	1.2e-5	2.7e-3	2.7e-3	4.8e-4	4.9e-4	0.30036	0.00615	0.03120
	233.142	12.8248	0.28655	7.7e-4	1.4e-4	7.1e-3	7.1e-3	1.5e-4	1.9e-5	2.7e-3	2.7e-3	4.8e-4	4.9e-4	0.30036	0.00615	0.03119
	233.142	12.8248	0.28653	6.2e-4	9.3e-5	7.2e-3	7.2e-3	1.7e-4	7.8e-6	2.7e-3	2.7e-3	4.8e-4	4.9e-4	0.30036	0.00615	0.03118
	233.142	12.8248	0.28659	6.6e-4	6.0e-5	7.2e-3	7.2e-3	2.1e-4	1.3e-5	2.7e-3	2.7e-3	4.8e-4	4.9e-4	0.30036	0.00615	0.03119
V23	233.142	13.6445	0.32553	9.3e-4	1.2e-4	7.1e-3	7.1e-3	2.4e-4	1.5e-5	2.8e-3	2.8e-3	4.8e-4	5.2e-4^{+}	0.33416	0.00638	0.07613^{+}
	233.142	13.6445	0.32550	9.9e-4	1.7e-4	7.4e-3	7.4e-3	2.8e-4	2.5e-5	2.8e-3	2.8e-3	4.8e-4	5.2e-4^{+}	0.33416	0.00638	0.07612^{+}
	233.141	13.6445	0.32544	8.7e-4	9.5e-5	7.4e-3	7.4e-3	1.8e-4	5.4e-6	2.7e-3	2.7e-3	4.8e-4	5.2e-4^{+}	0.33415	0.00638	0.07613^{+}
	233.142	13.6445	0.32546	1.1e-3	1.8e-4	7.3e-3	7.3e-3	1.6e-4	8.9e-6	2.7e-3	2.7e-3	4.8e-4	5.2e-4^{+}	0.33416	0.00638	0.07613^{+}
	233.141	13.6445	0.32551	1.0e-3	1.4e-4	7.3e-3	7.3e-3	1.5e-4	1.0e-5	2.7e-3	2.7e-3	4.8e-4	5.2e-4^{+}	0.33416	0.00638	0.07613^{+}
	233.142	13.6445	0.32545	1.0e-3	1.5e-4	7.1e-3	7.1e-3	1.9e-4	8.6e-6	2.7e-3	2.7e-3	4.8e-4	5.2e-4^{+}	0.33416	0.00638	0.07613^{+}
V24*	233.144	14.1867	0.39251	5.9e-4	1.4e-4	6.8e-3	6.8e-3	2.1e-4	1.2e-5	2.8e-3	2.8e-3	4.8e-4	9.4e-4^{+}	0.37661	0.00747	0.29114^{+}
	233.144	14.1867	0.39244	9.8e-4	1.4e-4	6.9e-3	6.9e-3	2.8e-4	1.3e-5	2.8e-3	2.8e-3	4.8e-4	9.4e-4^{+}	0.37661	0.00747	0.29115^{+}
	233.144	14.1867	0.39238	8.0e-4	1.5e-4	6.7e-3	6.7e-3	2.4e-4	1.5e-5	2.8e-3	2.8e-3	4.8e-4	9.4e-4^{+}	0.37661	0.00747	0.29115^{+}
	233.144	14.1868	0.39253	8.1e-4	1.5e-4	6.8e-3	6.8e-3	2.9e-4	2.9e-5	2.8e-3	2.8e-3	4.8e-4	9.4e-4^{+}	0.37661	0.00747	0.29120^{+}
	233.144	14.1868	0.39242	6.1e-4	1.1e-4	7.0e-3	7.0e-3	2.0e-4	1.3e-5	2.8e-3	2.8e-3	4.8e-4	9.4e-4^{+}	0.37662	0.00747	0.29139^{+}
	233.143	14.1868	0.39236	1.7e-3	6.0e-4	6.7e-3	6.8e-3	2.0e-4	1.2e-5	2.8e-3	2.8e-3	4.8e-4	9.4e-4^{+}	0.37661	0.00747	0.29132^{+}
V25*	233.144	14.2158	0.40310	5.5e-4	9.8e-5	6.7e-3	6.7e-3	2.0e-4	1.2e-5	2.8e-3	2.8e-3	4.8e-4	1.3e-3^{+}	0.38020	0.00766	0.41949^{+}
	233.145	14.2158	0.40303	1.0e-3	3.1e-4	6.7e-3	6.7e-3	2.0e-4	8.4e-6	2.8e-3	2.8e-3	4.8e-4	1.3e-3^{+}	0.38021	0.00766	0.41962^{+}
	233.145	14.2158	0.40299	8.5e-4	1.9e-4	6.5e-3	6.5e-3	1.6e-4	1.1e-5	2.8e-3	2.8e-3	4.8e-4	1.3e-3^{+}	0.38021	0.00766	0.41970^{+}
	233.144	14.2158	0.40298	7.8e-4	2.2e-4	6.7e-3	6.7e-3	2.2e-4	1.7e-5	2.8e-3	2.8e-3	4.8e-4	1.3e-3^{+}	0.38021	0.00766	0.41959^{+}
	233.143	14.2158	0.40290	1.9e-3	4.1e-4	6.5e-3	6.5e-3	2.3e-4	1.8e-5	2.8e-3	2.8e-3	4.8e-4	1.3e-3^{+}	0.38019	0.00766	0.41959^{+}
	233.145	14.2158	0.40296	4.9e-4	4.0e-5	6.4e-3	6.4e-3	2.2e-4	2.8e-5	2.8e-3	2.8e-3	4.8e-4	1.3e-3^{+}	0.38021	0.00766	0.41986^{+}
V26*	233.145	14.2408	0.41751	6.7e-4	7.1e-5	6.0e-3	6.0e-3	2.0e-4	1.7e-5	2.8e-3	2.8e-3	4.8e-4	2.4e-3^{+}	0.38355	0.00786	0.84058^{+}
	233.146	14.2407	0.41756	6.6e-4	1.3e-4	5.9e-3	5.9e-3	2.0e-4	1.1e-5	2.8e-3	2.8e-3	4.8e-4	2.4e-3^{+}	0.38354	0.00786	0.83931^{+}
	233.146	14.2407	0.41751	5.2e-4	5.4e-5	6.0e-3	6.0e-3	1.8e-4	1.5e-5	2.8e-3	2.8e-3	4.8e-4	2.4e-3^{+}	0.38354	0.00786	0.83833^{+}
	233.145	14.2407	0.41752	5.5e-4	1.2e-4	6.0e-3	6.0e-3	2.2e-4	1.5e-5	2.8e-3	2.8e-3	4.8e-4	2.4e-3^{+}	0.38353	0.00786	0.83708^{+}
	233.145	14.2407	0.41750	4.7e-4	8.4e-5	5.9e-3	5.9e-3	1.8e-4	9.4e-6	2.8e-3	2.8e-3	4.8e-4	2.4e-3^{+}	0.38354	0.00786	0.83851^{+}
	233.145	14.2407	0.41747	6.6e-4	1.0e-4	6.1e-3	6.1e-3	1.5e-4	7.6e-6	2.8e-3	2.8e-3	4.8e-4	2.4e-3^{+}	0.38354	0.00786	0.83871^{+}
P3	253.147	1.9699	0.99999	8.5e-4	1.5e-5	5.7e-3	5.7e-3	3.7e-5	5.5e-6	5.1e-4	5.1e-4					
V28	253.146	2.9634	0.72728	1.0e-3	1.4e-4	5.8e-3	5.8e-3	8.1e-5	1.3e-5	5.2e-4	5.2e-4	4.8e-4	5.0e-4	0.73129	0.01824	-0.18197
	253.147	2.9630	0.72729	7.9e-4	1.9e-4	5.4e-3	5.4e-3	1.6e-4	7.1e-5	5.2e-4	5.3e-4	4.8e-4	5.0e-4	0.73136	0.01824	-0.18201
	253.146	2.9630	0.72731	7.4e-4	7.6e-5	6.0e-3	6.0e-3	1.4e-4	5.5e-5	5.2e-4	5.3e-4	4.8e-4	5.0e-4	0.73135	0.01824	-0.18201
	253.147	2.9630	0.72735	5.8e-4	4.5e-5	5.6e-3	5.6e-3	1.3e-4	5.5e-5	5.2e-4	5.3e-4	4.8e-4	5.0e-4	0.73136	0.01824	-0.18201
	253.147	2.9630	0.72732	6.7e-4	1.1e-4	6.0e-3	6.0e-3	1.3e-4	5.6e-5	5.2e-4	5.3e-4	4.8e-4	5.0e-4	0.73136	0.01824	-0.18201
	253.146	2.9630	0.72730	9.2e-4	2.7e-4	5.7e-3	5.7e-3	1.3e-4	5.3e-5	5.2e-4	5.3e-4	4.8e-4	5.0e-4	0.73136	0.01824	-0.18202

V29	253.146	4.9363	0.51059	8.8e-4	8.5e-5	5.5e-3	5.5e-3	1.8e-4	6.2e-5	1.1e-3	1.1e-3	4.8e-4	4.9e-4	0.51935	0.01278	-0.06146
	253.146	4.9364	0.51053	1.2e-3	2.2e-4	5.8e-3	5.8e-3	9.5e-5	2.8e-5	1.1e-3	1.1e-3	4.8e-4	4.9e-4	0.51934	0.01278	-0.06146
	253.146	4.9363	0.51049	9.8e-4	1.9e-4	5.7e-3	5.7e-3	9.1e-5	1.7e-5	1.1e-3	1.1e-3	4.8e-4	4.9e-4	0.51935	0.01278	-0.06146
	253.146	4.9363	0.51047	1.2e-3	1.7e-4	5.7e-3	5.7e-3	9.7e-5	2.5e-5	1.1e-3	1.1e-3	4.8e-4	4.9e-4	0.51935	0.01278	-0.06146
	253.146	4.9363	0.51047	9.5e-4	1.4e-4	5.9e-3	5.9e-3	6.6e-5	9.7e-6	1.1e-3	1.1e-3	4.8e-4	4.9e-4	0.51934	0.01278	-0.06146
V30	253.146	6.9080	0.42662	9.8e-4	2.5e-4	5.7e-3	5.7e-3	1.4e-4	4.5e-5	1.1e-3	1.1e-3	4.8e-4	4.8e-4	0.43955	0.01042	-0.02485
	253.146	6.9080	0.42662	1.1e-3	1.1e-4	6.0e-3	6.0e-3	1.6e-4	3.3e-5	1.1e-3	1.1e-3	4.8e-4	4.8e-4	0.43955	0.01042	-0.02485
	253.146	6.9080	0.42651	1.2e-3	1.9e-4	6.0e-3	6.0e-3	1.2e-4	2.8e-5	1.1e-3	1.1e-3	4.8e-4	4.8e-4	0.43955	0.01042	-0.02485
	253.145	6.9080	0.42650	1.3e-3	2.5e-4	5.9e-3	5.9e-3	1.6e-4	3.9e-5	1.1e-3	1.1e-3	4.8e-4	4.8e-4	0.43954	0.01041	-0.02485
	253.146	6.9080	0.42648	1.2e-3	1.5e-4	5.4e-3	5.4e-3	1.1e-4	1.7e-5	1.1e-3	1.1e-3	4.8e-4	4.8e-4	0.43955	0.01042	-0.02485
	253.146	6.9080	0.42649	1.4e-3	1.3e-4	6.2e-3	6.2e-3	1.0e-4	1.9e-5	1.1e-3	1.1e-3	4.8e-4	4.8e-4	0.43954	0.01042	-0.02485
V31	253.146	8.3057	0.39991	1.2e-3	1.2e-4	5.7e-3	5.7e-3	1.2e-4	2.3e-5	1.2e-3	1.2e-3	4.8e-4	4.8e-4	0.41508	0.00950	-0.01100
	253.145	8.3057	0.39991	1.1e-3	2.0e-4	5.8e-3	5.8e-3	1.2e-4	1.2e-5	1.2e-3	1.2e-3	4.8e-4	4.8e-4	0.41507	0.00950	-0.01100
	253.146	8.3057	0.39990	8.8e-4	6.4e-5	6.1e-3	6.1e-3	1.5e-4	2.1e-5	1.2e-3	1.2e-3	4.8e-4	4.8e-4	0.41507	0.00950	-0.01100
	253.146	8.3058	0.39986	1.1e-3	1.6e-4	5.8e-3	5.8e-3	1.6e-4	3.4e-5	1.2e-3	1.2e-3	4.8e-4	4.8e-4	0.41507	0.00950	-0.01100
V32	253.147	9.6222	0.39145	5.6e-4	1.5e-4	5.9e-3	5.9e-3	3.2e-4	8.4e-5	1.4e-3	1.4e-3	4.8e-4	4.8e-4	0.40750	0.00900	-0.00069
	253.148	9.6223	0.39124	6.4e-4	8.3e-5	5.7e-3	5.7e-3	2.7e-4	1.1e-4	1.4e-3	1.4e-3	4.8e-4	4.8e-4	0.40751	0.00900	-0.00069
	253.148	9.6222	0.39110	4.7e-4	3.8e-5	5.9e-3	5.9e-3	2.5e-4	3.9e-5	1.4e-3	1.4e-3	4.8e-4	4.8e-4	0.40750	0.00900	-0.00069
	253.148	9.6222	0.39098	8.9e-4	1.1e-4	5.9e-3	5.9e-3	2.9e-4	1.0e-4	1.4e-3	1.4e-3	4.8e-4	4.8e-4	0.40751	0.00900	-0.00069
	253.147	9.6223	0.39092	6.5e-4	1.7e-4	5.8e-3	5.8e-3	1.7e-4	3.4e-5	1.4e-3	1.4e-3	4.8e-4	4.8e-4	0.40750	0.00900	-0.00069
	253.148	9.6222	0.39092	1.1e-3	3.1e-4	5.8e-3	5.8e-3	2.2e-4	7.3e-5	1.4e-3	1.4e-3	4.8e-4	4.8e-4	0.40751	0.00900	-0.00069
V33	253.148	10.8464	0.39521	5.7e-4	1.5e-4	5.3e-3	5.3e-3	3.3e-4	5.2e-5	2.7e-3	2.7e-3	4.8e-4	4.8e-4	0.41264	0.00882	0.00943
	253.148	10.8464	0.39516	1.1e-3	3.1e-4	5.4e-3	5.4e-3	2.1e-4	6.6e-5	2.7e-3	2.7e-3	4.8e-4	4.8e-4	0.41264	0.00882	0.00943
	253.148	10.8463	0.39515	6.2e-4	1.7e-4	5.7e-3	5.7e-3	2.6e-4	8.1e-5	2.7e-3	2.7e-3	4.8e-4	4.8e-4	0.41264	0.00882	0.00943
	253.147	10.8454	0.39516	3.1e-4	2.7e-5	6.0e-3	6.0e-3	1.1e-4	1.5e-5	2.7e-3	2.7e-3	4.8e-4	4.8e-4	0.41262	0.00882	0.00942
V34	253.146	11.8558	0.41082	1.1e-3	1.8e-4	6.0e-3	6.0e-3	3.2e-4	6.7e-5	2.7e-3	2.7e-3	4.8e-4	4.9e-4	0.42773	0.00903	0.02158
	253.146	11.8557	0.41078	1.0e-3	2.0e-4	5.8e-3	5.8e-3	3.9e-4	5.3e-5	2.7e-3	2.7e-3	4.8e-4	4.9e-4	0.42772	0.00903	0.02158
	253.146	11.8557	0.41085	8.0e-4	1.3e-4	5.6e-3	5.6e-3	1.2e-4	1.4e-5	2.7e-3	2.7e-3	4.8e-4	4.9e-4	0.42773	0.00903	0.02158
	253.146	11.8559	0.41080	1.1e-3	1.7e-4	5.6e-3	5.6e-3	2.9e-4	5.0e-5	2.7e-3	2.7e-3	4.8e-4	4.9e-4	0.42773	0.00903	0.02158
	253.146	11.8558	0.41079	9.2e-4	2.4e-4	5.9e-3	5.9e-3	2.2e-4	3.9e-5	2.7e-3	2.7e-3	4.8e-4	4.9e-4	0.42773	0.00903	0.02158
V35	253.146	12.7677	0.44494	5.3e-4	8.7e-5	5.9e-3	5.9e-3	2.9e-4	8.0e-5	2.7e-3	2.7e-3	4.8e-4	5.2e-4^{+}	0.45666	0.01016	0.06853^{+}
	253.146	12.7677	0.44495	7.1e-4	6.7e-5	5.8e-3	5.8e-3	2.2e-4	3.2e-5	2.7e-3	2.7e-3	4.8e-4	5.2e-4^{+}	0.45666	0.01016	0.06853^{+}
	253.146	12.7677	0.44496	1.1e-3	1.6e-4	5.5e-3	5.5e-3	3.7e-4	5.3e-5	2.7e-3	2.7e-3	4.8e-4	5.2e-4^{+}	0.45667	0.01016	0.06853^{+}
V36*	253.145	13.2761	0.50134	9.0e-4	1.7e-4	5.7e-3	5.7e-3	3.3e-4	6.1e-5	2.7e-3	2.7e-3	4.8e-4	8.6e-4^{+}	0.49107	0.01389	0.25936^{+}
	253.147	13.2763	0.50133	8.2e-4	1.4e-4	5.7e-3	5.7e-3	2.0e-4	2.5e-5	2.7e-3	2.7e-3	4.8e-4	8.6e-4^{+}	0.49111	0.01389	0.25974^{+}
	253.146	13.2762	0.50129	1.1e-3	1.1e-4	6.1e-3	6.1e-3	2.5e-4	3.9e-5	2.7e-3	2.7e-3	4.8e-4	8.6e-4^{+}	0.49109	0.01389	0.25953^{+}
V37*	253.147	13.3024	0.51003	6.4e-4	1.0e-4	6.1e-3	6.1e-3	3.2e-4	5.2e-5	2.7e-3	2.7e-3	4.8e-4	1.1e-3^{+}	0.49401	0.01449	0.36676^{+}
	253.147	13.3023	0.50991	6.3e-4	1.2e-4	6.1e-3	6.1e-3	2.6e-4	6.5e-5	2.7e-3	2.7e-3	4.8e-4	1.1e-3^{+}	0.49401	0.01449	0.36640^{+}
	253.147	13.3023	0.50980	5.4e-4	6.2e-5	5.8e-3	5.8e-3	3.2e-4	6.4e-5	2.7e-3	2.7e-3	4.8e-4	1.1e-3^{+}	0.49400	0.01449	0.36611^{+}
	253.147	13.3023	0.50977	6.5e-4	9.5e-5	6.0e-3	6.0e-3	3.2e-4	5.7e-5	2.7e-3	2.7e-3	4.8e-4	1.1e-3^{+}	0.49401	0.01449	0.36622^{+}
V38*	253.147	13.3200	0.51746	7.7e-4	8.3e-5	5.9e-3	5.9e-3	6.4e-4	1.3e-4	2.7e-3	2.7e-3	4.8e-4	1.6e-3^{+}	0.49613	0.01498	0.56042^{+}
	253.147	13.3200	0.51740	7.8e-4	6.8e-5	5.9e-3	5.9e-3	5.4e-4	9.5e-5	2.7e-3	2.7e-3	4.8e-4	1.6e-3^{+}	0.49612	0.01498	0.56009^{+}
	253.147	13.3200	0.51744	8.5e-4	2.5e-4	5.4e-3	5.4e-3	6.6e-4	1.3e-4	2.7e-3	2.7e-3	4.8e-4	1.6e-3^{+}	0.49612	0.01498	0.55985^{+}
	253.147	13.3200	0.51741	7.0e-4	8.0e-5	5.8e-3	5.8e-3	5.3e-4	9.0e-5	2.7e-3	2.7e-3	4.8e-4	1.6e-3^{+}	0.49612	0.01498	0.55978^{+}
	253.147	13.3200	0.51742	6.8e-4	7.3e-5	5.9e-3	5.9e-3	6.4e-4	1.0e-4	2.7e-3	2.7e-3	4.8e-4	1.6e-3^{+}	0.49612	0.01498	0.56033^{+}
P4	273.147	3.4848	0.99999	7.2e-4	2.4e-5	1.5e-3	1.5e-3	5.6e-5	9.9e-7	1.1e-3	1.1e-3					
V40	273.145	3.9434	0.91884	1.0e-3	1.3e-4	2.3e-3	2.3e-3	7.1e-5	9.6e-6	1.1e-3	1.1e-3	4.8e-4	5.1e-4	0.92150	0.01688	-0.15393
	273.144	3.9433	0.91876	1.2e-3	1.8e-4	2.2e-3	2.2e-3	1.3e-4	4.6e-5	1.1e-3	1.1e-3	4.8e-4	5.1e-4	0.92150	0.01688	-0.15394
	273.144	3.9434	0.91829	1.5e-3	2.4e-4	2.2e-3	2.2e-3	6.8e-5	1.5e-5	1.1e-3	1.1e-3	4.8e-4	5.1e-4	0.92149	0.01688	-0.15393
	273.144	3.9433	0.91828	1.3e-3	1.8e-4	2.0e-3	2.0e-3	5.1e-5	4.7e-6	1.1e-3	1.1e-3	4.8e-4	5.1e-4	0.92149	0.01688	-0.15393
	273.144	3.9433	0.91824	1.4e-3	1.5e-4	2.6e-3	2.6e-3	6.4e-5	1.9e-5	1.1e-3	1.1e-3	4.8e-4	5.1e-4	0.92150	0.01688	-0.15394
	273.144	3.9434	0.91825	9.4e-4	1.1e-4	2.1e-3	2.1e-3	8.8e-5	3.2e-5	1.1e-3	1.1e-3	4.8e-4	5.1e-4	0.92150	0.01688	-0.15393
V41	273.144	5.0162	0.78639	1.3e-3	3.4e-4	2.4e-3	2.5e-3	1.3e-4	4.2e-5	1.1e-3	1.1e-3	4.8e-4	4.9e-4	0.79224	0.01471	-0.09350
	273.144	5.0162	0.78629	1.3e-3	1.3e-4	1.9e-3	1.9e-3	1.9e-4	8.2e-5	1.1e-3	1.1e-3	4.8e-4	4.9e-4	0.79224	0.01471	-0.09350

	273.145	5.0161	0.78627	1.0e-3	1.7e-4	1.9e-3	1.9e-3	6.6e-5	6.3e-6	1.1e-3	1.1e-3	4.8e-4	4.9e-4	0.79226	0.01471	-0.09351
	273.145	5.0162	0.78619	8.3e-4	1.3e-4	2.3e-3	2.3e-3	1.1e-4	3.0e-5	1.1e-3	1.1e-3	4.8e-4	4.9e-4	0.79225	0.01471	-0.09350
	273.145	5.0164	0.78620	9.1e-4	3.1e-4	2.1e-3	2.1e-3	1.8e-4	7.3e-5	1.1e-3	1.1e-3	4.8e-4	4.9e-4	0.79224	0.01471	-0.09350
	273.145	5.0160	0.78615	7.2e-4	1.6e-4	2.0e-3	2.0e-3	1.6e-4	4.7e-5	1.1e-3	1.1e-3	4.8e-4	4.9e-4	0.79227	0.01471	-0.09351
V42	273.146	5.9256	0.71350	8.1e-4	1.6e-4	2.6e-3	2.6e-3	1.0e-4	3.7e-5	1.1e-3	1.1e-3	4.8e-4	4.9e-4	0.72173	0.01340	-0.06380
	273.146	5.9255	0.71347	7.7e-4	1.1e-4	2.7e-3	2.7e-3	1.9e-4	6.7e-5	1.1e-3	1.1e-3	4.8e-4	4.9e-4	0.72173	0.01340	-0.06380
	273.146	5.9256	0.71345	4.9e-4	8.3e-5	2.5e-3	2.5e-3	9.3e-5	1.1e-5	1.1e-3	1.1e-3	4.8e-4	4.9e-4	0.72173	0.01340	-0.06379
	273.146	5.9256	0.71344	8.1e-4	2.2e-4	2.5e-3	2.5e-3	1.1e-4	3.4e-5	1.1e-3	1.1e-3	4.8e-4	4.9e-4	0.72172	0.01340	-0.06379
	273.146	5.9255	0.71343	6.7e-4	8.6e-5	2.1e-3	2.1e-3	9.6e-5	2.5e-5	1.1e-3	1.1e-3	4.8e-4	4.8e-4	0.72174	0.01340	-0.06380
V43	273.146	6.9260	0.65908	5.8e-4	7.9e-5	2.2e-3	2.2e-3	1.1e-4	3.0e-5	1.1e-3	1.1e-3	4.8e-4	4.8e-4	0.66945	0.01236	-0.04209
	273.146	6.9258	0.65903	5.6e-4	9.4e-5	2.2e-3	2.2e-3	3.2e-4	1.1e-4	1.1e-3	1.1e-3	4.8e-4	4.8e-4	0.66946	0.01236	-0.04209
	273.146	6.9260	0.65901	4.8e-4	4.5e-5	2.4e-3	2.4e-3	2.1e-4	8.9e-5	1.1e-3	1.1e-3	4.8e-4	4.8e-4	0.66944	0.01236	-0.04208
	273.146	6.9259	0.65903	6.7e-4	7.1e-5	2.0e-3	2.0e-3	1.3e-4	4.2e-5	1.1e-3	1.1e-3	4.8e-4	4.8e-4	0.66946	0.01236	-0.04209
	273.146	6.9257	0.65904	5.3e-4	5.1e-5	2.3e-3	2.3e-3	2.5e-4	8.3e-5	1.1e-3	1.1e-3	4.8e-4	4.8e-4	0.66946	0.01236	-0.04209
V44	273.145	7.9107	0.62381	9.5e-4	2.7e-4	2.8e-3	2.8e-3	2.5e-4	5.8e-5	1.2e-3	1.2e-3	4.8e-4	4.8e-4	0.63597	0.01165	-0.02656
	273.147	7.9107	0.62380	1.1e-3	3.5e-4	2.0e-3	2.1e-3	3.5e-4	8.7e-5	1.2e-3	1.2e-3	4.8e-4	4.8e-4	0.63598	0.01165	-0.02656
	273.146	7.9106	0.62376	7.8e-4	1.2e-4	2.3e-3	2.3e-3	3.2e-4	7.0e-5	1.2e-3	1.2e-3	4.8e-4	4.8e-4	0.63598	0.01165	-0.02657
	273.146	7.9106	0.62375	8.2e-4	2.5e-4	2.4e-3	2.4e-3	1.4e-4	3.8e-5	1.2e-3	1.2e-3	4.8e-4	4.8e-4	0.63597	0.01165	-0.02657
	273.147	7.9109	0.62376	7.1e-4	8.0e-5	2.0e-3	2.0e-3	2.5e-4	9.6e-5	1.2e-3	1.2e-3	4.8e-4	4.8e-4	0.63597	0.01165	-0.02656
V45	273.147	8.8895	0.60277	8.4e-4	1.3e-4	2.3e-3	2.3e-3	4.1e-4	8.4e-5	1.3e-3	1.3e-3	4.8e-4	4.8e-4	0.61637	0.01123	-0.01370
	273.146	8.8898	0.60274	8.1e-4	2.8e-4	2.4e-3	2.5e-3	4.3e-4	6.6e-5	1.3e-3	1.3e-3	4.8e-4	4.8e-4	0.61636	0.01123	-0.01370
	273.147	8.8896	0.60273	4.0e-4	5.2e-5	2.0e-3	2.0e-3	3.9e-4	5.0e-5	1.3e-3	1.3e-3	4.8e-4	4.8e-4	0.61637	0.01123	-0.01370
	273.146	8.8894	0.60277	7.6e-4	2.9e-4	2.3e-3	2.3e-3	3.1e-4	6.1e-5	1.3e-3	1.3e-3	4.8e-4	4.8e-4	0.61637	0.01123	-0.01370
V46	273.146	9.8539	0.59504	6.7e-4	4.7e-5	2.7e-3	2.7e-3	2.4e-4	7.9e-5	1.4e-3	1.4e-3	4.8e-4	4.8e-4	0.60925	0.01118	-0.00068
	273.147	9.8539	0.59501	7.2e-4	1.2e-4	2.2e-3	2.2e-3	2.5e-4	4.3e-5	1.4e-3	1.4e-3	4.8e-4	4.8e-4	0.60926	0.01118	-0.00068
	273.147	9.8539	0.59503	9.7e-4	2.9e-4	2.3e-3	2.4e-3	3.3e-4	4.4e-5	1.4e-3	1.4e-3	4.8e-4	4.8e-4	0.60926	0.01118	-0.00068
	273.146	9.8538	0.59504	5.8e-4	6.7e-5	2.5e-3	2.5e-3	3.3e-4	6.3e-5	1.4e-3	1.4e-3	4.8e-4	4.8e-4	0.60925	0.01118	-0.00069
	273.146	9.8539	0.59503	5.2e-4	3.7e-5	2.8e-3	2.8e-3	2.7e-4	9.4e-5	1.4e-3	1.4e-3	4.8e-4	4.8e-4	0.60925	0.01118	-0.00068
	273.146	9.8539	0.59501	9.4e-4	1.6e-4	2.5e-3	2.5e-3	1.7e-4	3.6e-5	1.4e-3	1.4e-3	4.8e-4	4.8e-4	0.60925	0.01118	-0.00068
V47	273.146	10.8864	0.60682	6.3e-4	6.5e-5	2.8e-3	2.8e-3	2.8e-4	4.5e-5	2.7e-3	2.7e-3	4.8e-4	4.8e-4	0.61856	0.01222	0.02203
	273.147	10.8864	0.60684	5.5e-4	4.8e-5	2.5e-3	2.5e-3	1.9e-4	2.6e-5	2.7e-3	2.7e-3	4.8e-4	4.8e-4	0.61857	0.01222	0.02203
	273.147	10.8865	0.60686	1.1e-3	3.4e-4	2.4e-3	2.4e-3	3.4e-4	6.8e-5	2.7e-3	2.7e-3	4.8e-4	4.8e-4	0.61857	0.01222	0.02203
	273.146	10.8865	0.60683	8.5e-4	1.4e-4	3.0e-3	3.0e-3	2.2e-4	4.1e-5	2.7e-3	2.7e-3	4.8e-4	4.8e-4	0.61856	0.01222	0.02203
	273.146	10.8865	0.60685	8.8e-4	2.8e-4	2.8e-3	2.8e-3	2.7e-4	5.6e-5	2.7e-3	2.7e-3	4.8e-4	4.8e-4	0.61856	0.01222	0.02203
V48	273.146	11.3312	0.62771	6.2e-4	1.0e-4	2.6e-3	2.6e-3	2.5e-4	3.6e-5	2.7e-3	2.7e-3	4.8e-4	5.3e-4^{+}	0.63335	0.01451	0.08798^{+}
	273.147	11.3313	0.62763	5.5e-4	7.3e-5	2.4e-3	2.4e-3	2.9e-4	4.6e-5	2.7e-3	2.7e-3	4.8e-4	5.3e-4^{+}	0.63336	0.01451	0.08799^{+}
	273.146	11.3312	0.62768	6.8e-4	2.0e-4	2.3e-3	2.3e-3	2.9e-4	4.1e-5	2.7e-3	2.7e-3	4.8e-4	5.3e-4^{+}	0.63335	0.01451	0.08798^{+}
	273.146	11.3312	0.62760	5.3e-4	6.0e-5	2.3e-3	2.3e-3	2.7e-4	4.5e-5	2.7e-3	2.7e-3	4.8e-4	5.3e-4^{+}	0.63335	0.01451	0.08798^{+}
	273.146	11.3313	0.62757	5.6e-4	3.7e-5	2.5e-3	2.5e-3	2.8e-4	5.1e-5	2.7e-3	2.7e-3	4.8e-4	5.3e-4^{+}	0.63335	0.01451	0.08799^{+}
V49*	273.145	11.5578	0.66099	8.3e-4	1.2e-4	2.1e-3	2.1e-3	1.8e-4	4.5e-5	2.7e-3	2.7e-3	4.8e-4	1.1e-3^{+}	0.64900	0.01974	0.36702^{+}
	273.145	11.5579	0.66096	7.4e-4	7.1e-5	3.0e-3	3.0e-3	1.7e-4	2.4e-5	2.7e-3	2.7e-3	4.8e-4	1.1e-3^{+}	0.64901	0.01974	0.36757^{+}
	273.145	11.5578	0.66093	6.3e-4	9.9e-5	2.8e-3	2.8e-3	1.3e-4	1.9e-5	2.7e-3	2.7e-3	4.8e-4	1.1e-3^{+}	0.64900	0.01973	0.36684^{+}
V50*	273.146	11.5780	0.67303	6.5e-4	1.6e-4	2.5e-3	2.5e-3	2.3e-4	5.3e-5	2.7e-3	2.7e-3	4.8e-4	3.0e-3^{+}	0.65120	0.02098	1.12607^{+}
	273.146	11.5780	0.67294	6.9e-4	1.2e-4	2.1e-3	2.1e-3	2.0e-4	2.8e-5	2.7e-3	2.7e-3	4.8e-4	3.0e-3^{+}	0.65119	0.02098	1.12668^{+}
	273.145	11.5780	0.67271	6.1e-4	9.1e-5	2.4e-3	2.4e-3	2.4e-4	3.8e-5	2.7e-3	2.7e-3	4.8e-4	3.1e-3^{+}	0.65119	0.02098	1.13799^{+}
	273.146	11.5780	0.67255	4.5e-4	6.2e-5	2.4e-3	2.4e-3	2.2e-4	4.6e-5	2.7e-3	2.7e-3	4.8e-4	3.1e-3^{+}	0.65119	0.02098	1.12707^{+}
	273.145	11.5780	0.67255	1.0e-3	1.0e-4	2.7e-3	2.7e-3	1.9e-4	3.7e-5	2.7e-3	2.7e-3	4.8e-4	3.1e-3^{+}	0.65119	0.02098	1.13580^{+}
P5	288.139	5.0859	0.99999	6.9e-4	2.8e-4	1.8e-3	1.8e-3	5.7e-5	2.9e-6	1.1e-3	1.1e-3					
V52	288.138	5.6498	0.94180	8.1e-4	1.6e-4	1.6e-3	1.6e-3	6.9e-5	3.0e-6	1.1e-3	1.1e-3	4.8e-4	4.9e-4	0.94518	0.01309	-0.08892
	288.135	5.6498	0.94168	1.1e-3	3.1e-4	1.5e-3	1.5e-3	6.5e-5	3.1e-6	1.1e-3	1.1e-3	4.8e-4	4.9e-4	0.94514	0.01309	-0.08891
	288.139	5.6498	0.94167	2.0e-3	4.5e-4	1.7e-3	1.8e-3	8.5e-5	7.4e-6	1.1e-3	1.1e-3	4.8e-4	4.9e-4	0.94519	0.01309	-0.08892
	288.140	5.6498	0.94166	1.6e-3	3.1e-4	1.7e-3	1.8e-3	7.3e-5	6.9e-6	1.1e-3	1.1e-3	4.8e-4	4.9e-4	0.94519	0.01309	-0.08892
	288.136	5.6498	0.94163	6.0e-4	1.1e-4	1.7e-3	1.7e-3	7.1e-5	6.0e-6	1.1e-3	1.1e-3	4.8e-4	4.9e-4	0.94515	0.01309	-0.08892
	288.135	5.6498	0.94163	6.6e-4	1.2e-4	1.7e-3	1.7e-3	6.6e-5	5.9e-6	1.1e-3	1.1e-3	4.8e-4	4.9e-4	0.94513	0.01309	-0.08891

V53	288.143	7.0494	0.84287	3.7e-4	5.0e-5	1.8e-3	1.8e-3	1.1e-4	7.3e-6	1.1e-3	1.1e-3	4.8e-4	4.8e-4	0.84963	0.01209	-0.05068
	288.142	7.0493	0.84275	3.7e-4	3.7e-5	1.8e-3	1.8e-3	8.7e-5	1.3e-5	1.1e-3	1.1e-3	4.8e-4	4.8e-4	0.84963	0.01209	-0.05068
	288.142	7.0493	0.84271	3.9e-4	6.9e-5	1.9e-3	1.9e-3	9.2e-5	5.9e-6	1.1e-3	1.1e-3	4.8e-4	4.8e-4	0.84963	0.01209	-0.05068
	288.142	7.0493	0.84268	4.0e-4	4.2e-5	1.8e-3	1.8e-3	1.3e-4	7.2e-6	1.1e-3	1.1e-3	4.8e-4	4.8e-4	0.84963	0.01209	-0.05068
	288.142	7.0493	0.84267	3.4e-4	5.5e-5	1.9e-3	1.9e-3	1.0e-4	8.6e-6	1.1e-3	1.1e-3	4.8e-4	4.8e-4	0.84963	0.01209	-0.05068
V54	288.134	8.4289	0.79087	6.2e-4	6.3e-5	1.6e-3	1.6e-3	1.6e-4	1.0e-5	1.2e-3	1.2e-3	4.8e-4	4.8e-4	0.79910	0.01177	-0.02272
	288.142	8.4288	0.79084	4.1e-4	2.4e-5	1.9e-3	1.9e-3	4.7e-4	4.4e-5	1.2e-3	1.2e-3	4.8e-4	4.8e-4	0.79920	0.01177	-0.02272
	288.142	8.4289	0.79082	2.8e-4	4.2e-5	1.9e-3	1.9e-3	1.7e-4	8.7e-6	1.2e-3	1.2e-3	4.8e-4	4.8e-4	0.79920	0.01177	-0.02272
	288.142	8.4289	0.79081	4.2e-4	4.5e-5	1.9e-3	1.9e-3	1.4e-4	1.8e-5	1.2e-3	1.2e-3	4.8e-4	4.8e-4	0.79920	0.01177	-0.02272
	288.142	8.4289	0.79075	2.6e-4	4.1e-5	1.9e-3	1.9e-3	1.1e-4	1.3e-5	1.2e-3	1.2e-3	4.8e-4	4.8e-4	0.79920	0.01177	-0.02272
	288.142	8.4289	0.79072	3.0e-4	3.4e-5	1.8e-3	1.8e-3	1.3e-4	6.5e-6	1.2e-3	1.2e-3	4.8e-4	4.8e-4	0.79920	0.01177	-0.02272
V55	288.136	8.8666	0.78344	4.5e-4	5.0e-5	1.7e-3	1.7e-3	1.7e-4	1.3e-5	1.3e-3	1.3e-3	4.8e-4	4.8e-4	0.79131	0.01201	-0.01263
	288.138	8.8666	0.78345	6.2e-4	2.5e-4	1.8e-3	1.8e-3	1.5e-4	1.2e-5	1.3e-3	1.3e-3	4.8e-4	4.8e-4	0.79134	0.01201	-0.01262
	288.138	8.8667	0.78344	1.1e-3	4.2e-4	1.8e-3	1.8e-3	1.9e-4	1.7e-5	1.3e-3	1.3e-3	4.8e-4	4.8e-4	0.79133	0.01201	-0.01263
	288.138	8.8666	0.78345	9.5e-4	2.3e-4	1.8e-3	1.8e-3	1.6e-4	2.4e-5	1.3e-3	1.3e-3	4.8e-4	4.8e-4	0.79133	0.01201	-0.01260
	288.136	8.8665	0.78344	9.7e-4	3.0e-4	1.7e-3	1.7e-3	1.2e-4	6.9e-6	1.3e-3	1.3e-3	4.8e-4	4.8e-4	0.79131	0.01201	-0.01261
V56	288.138	9.2573	0.78233	1.1e-3	4.1e-4	1.8e-3	1.8e-3	1.3e-4	3.3e-6	1.3e-3	1.3e-3	4.8e-4	4.8e-4	0.78869	0.01271	0.00527
	288.139	9.2574	0.78233	6.4e-4	2.1e-4	1.7e-3	1.7e-3	1.3e-4	6.4e-6	1.3e-3	1.3e-3	4.8e-4	4.8e-4	0.78871	0.01272	0.00012
	288.139	9.2573	0.78234	7.7e-4	1.7e-4	1.7e-3	1.7e-3	1.5e-4	1.6e-5	1.3e-3	1.3e-3	4.8e-4	4.8e-4	0.78870	0.01271	0.00308
V57	288.136	9.5784	0.78942	5.6e-4	7.2e-5	1.8e-3	1.8e-3	1.5e-4	1.2e-5	1.4e-3	1.4e-3	4.8e-4	4.9e-4^{+}	0.79157	0.01465	0.05484^{+}
	288.137	9.5783	0.78943	9.8e-4	3.4e-4	1.7e-3	1.7e-3	1.5e-4	7.1e-6	1.4e-3	1.4e-3	4.8e-4	4.9e-4^{+}	0.79158	0.01465	0.05484^{+}
	288.138	9.5783	0.78942	1.5e-3	3.2e-4	1.6e-3	1.7e-3	1.3e-4	1.4e-5	1.4e-3	1.4e-3	4.8e-4	4.9e-4^{+}	0.79159	0.01465	0.05483^{+}
	288.139	9.5784	0.78942	1.2e-3	2.8e-4	1.7e-3	1.7e-3	1.3e-4	1.5e-5	1.4e-3	1.4e-3	4.8e-4	4.9e-4^{+}	0.79161	0.01465	0.05485^{+}
	288.137	9.5784	0.78942	5.5e-4	4.6e-5	1.7e-3	1.7e-3	1.5e-4	1.2e-5	1.4e-3	1.4e-3	4.8e-4	4.9e-4^{+}	0.79159	0.01465	0.05484^{+}
V58	288.141	9.7065	0.79946	3.7e-4	3.9e-5	1.8e-3	1.8e-3	1.7e-4	1.1e-5	1.4e-3	1.4e-3	4.8e-4	5.1e-4^{+}	0.79558	0.01713	0.12831^{+}
	288.141	9.7065	0.79944	4.0e-4	6.1e-5	1.7e-3	1.7e-3	1.1e-4	1.3e-5	1.4e-3	1.4e-3	4.8e-4	5.1e-4^{+}	0.79557	0.01713	0.12832^{+}
	288.141	9.7065	0.79943	3.2e-4	3.3e-5	1.6e-3	1.6e-3	1.4e-4	1.3e-5	1.4e-3	1.4e-3	4.8e-4	5.1e-4^{+}	0.79557	0.01713	0.12831^{+}
	288.141	9.7066	0.79942	4.2e-4	2.1e-5	1.7e-3	1.7e-3	1.7e-4	1.6e-5	1.4e-3	1.4e-3	4.8e-4	5.1e-4^{+}	0.79558	0.01713	0.12845^{+}
V59	288.139	9.7232	0.80208	2.3e-3	1.0e-3	1.9e-3	2.2e-3	2.2e-4	3.1e-5	1.4e-3	1.4e-3	4.8e-4	5.3e-4^{+}	0.79630	0.01771	0.16625^{+}
	288.141	9.7232	0.80210	2.2e-4	4.1e-5	1.8e-3	1.8e-3	1.9e-4	1.2e-5	1.4e-3	1.4e-3	4.8e-4	5.3e-4^{+}	0.79634	0.01772	0.16623^{+}
	288.141	9.7232	0.80207	2.3e-4	3.3e-5	1.8e-3	1.8e-3	1.8e-4	1.6e-5	1.4e-3	1.4e-3	4.8e-4	5.3e-4^{+}	0.79634	0.01772	0.16629^{+}
	288.141	9.7232	0.80206	2.3e-4	2.2e-5	1.8e-3	1.8e-3	1.4e-4	9.4e-6	1.4e-3	1.4e-3	4.8e-4	5.3e-4^{+}	0.79634	0.01772	0.16618^{+}
	288.142	9.7232	0.80205	2.2e-4	2.3e-5	1.9e-3	1.9e-3	1.6e-4	1.2e-5	1.4e-3	1.4e-3	4.8e-4	5.3e-4^{+}	0.79634	0.01772	0.16611^{+}
V60	288.142	9.7447	0.80691	2.2e-4	2.6e-5	1.9e-3	1.9e-3	1.4e-4	7.9e-6	1.4e-3	1.4e-3	4.8e-4	6.4e-4^{+}	0.79746	0.01869	0.30671^{+}
	288.142	9.7447	0.80684	4.2e-4	3.8e-5	1.8e-3	1.8e-3	1.2e-4	5.8e-6	1.4e-3	1.4e-3	4.8e-4	6.4e-4^{+}	0.79746	0.01869	0.30679^{+}
	288.142	9.7447	0.80662	3.1e-4	5.1e-5	1.9e-3	1.9e-3	1.1e-4	6.0e-6	1.4e-3	1.4e-3	4.8e-4	6.4e-4^{+}	0.79746	0.01869	0.30692^{+}
	288.142	9.7447	0.80660	3.1e-4	2.2e-5	1.8e-3	1.8e-3	1.2e-4	5.1e-6	1.4e-3	1.4e-3	4.8e-4	6.4e-4^{+}	0.79746	0.01869	0.30695^{+}
P6	298.137	6.4328	0.99999	7.5e-4	1.1e-4	3.0e-3	3.0e-3	9.4e-5	8.6e-6	1.1e-3	1.1e-3					
V61	298.141	7.1110	0.95630	4.3e-4	6.0e-5	3.3e-3	3.3e-3	8.6e-5	8.5e-6	1.1e-3	1.1e-3	4.8e-4	4.8e-4	0.95967	0.01018	-0.05191
	298.141	7.1110	0.95625	4.0e-4	3.3e-5	3.2e-3	3.2e-3	7.5e-5	4.3e-6	1.1e-3	1.1e-3	4.8e-4	4.8e-4	0.95967	0.01018	-0.05191
	298.141	7.1110	0.95622	3.6e-4	7.8e-5	3.1e-3	3.1e-3	9.9e-5	1.6e-5	1.1e-3	1.1e-3	4.8e-4	4.8e-4	0.95967	0.01018	-0.05191
	298.141	7.1110	0.95622	1.5e-4	7.1e-6	3.4e-3	3.4e-3	9.4e-5	1.2e-5	1.1e-3	1.1e-3	4.8e-4	4.8e-4	0.95967	0.01018	-0.05191
	298.141	7.1110	0.95623	3.2e-4	2.0e-5	3.2e-3	3.2e-3	1.0e-4	1.0e-5	1.1e-3	1.1e-3	4.8e-4	4.8e-4	0.95967	0.01018	-0.05191
	298.140	7.1110	0.95622	3.0e-4	3.1e-5	3.1e-3	3.1e-3	8.1e-5	6.1e-6	1.1e-3	1.1e-3	4.8e-4	4.8e-4	0.95967	0.01018	-0.05191
V62	298.134	7.4191	0.94072	5.1e-4	4.5e-5	3.1e-3	3.1e-3	9.6e-5	8.2e-6	1.1e-3	1.1e-3	4.8e-4	4.8e-4	0.94482	0.01024	-0.04399
	298.134	7.4191	0.94071	5.0e-4	5.5e-5	3.0e-3	3.0e-3	8.7e-5	8.6e-6	1.1e-3	1.1e-3	4.8e-4	4.8e-4	0.94482	0.01024	-0.04399
	298.134	7.4191	0.94071	5.5e-4	1.2e-4	3.1e-3	3.2e-3	1.0e-4	1.1e-5	1.1e-3	1.1e-3	4.8e-4	4.8e-4	0.94482	0.01024	-0.04399
	298.138	7.4191	0.94073	1.6e-3	5.0e-4	3.2e-3	3.3e-3	1.1e-4	1.2e-5	1.1e-3	1.1e-3	4.8e-4	4.8e-4	0.94486	0.01024	-0.04399
	298.137	7.4191	0.94073	6.5e-4	1.9e-4	3.2e-3	3.2e-3	1.1e-4	1.1e-5	1.1e-3	1.1e-3	4.8e-4	4.8e-4	0.94485	0.01024	-0.04399
	298.136	7.4191	0.94072	4.7e-4	3.6e-5	3.2e-3	3.2e-3	8.6e-5	5.6e-6	1.1e-3	1.1e-3	4.8e-4	4.8e-4	0.94484	0.01024	-0.04399
V63	298.134	7.8396	0.92471	7.6e-4	1.6e-4	3.0e-3	3.0e-3	1.1e-4	9.2e-6	1.1e-3	1.1e-3	4.8e-4	4.8e-4	0.92880	0.01057	-0.03163
	298.134	7.8394	0.92468	6.3e-4	1.7e-4	3.0e-3	3.0e-3	1.3e-4	1.7e-5	1.1e-3	1.1e-3	4.8e-4	4.8e-4	0.92881	0.01057	-0.03163
	298.139	7.8393	0.92465	2.5e-3	1.1e-3	3.1e-3	3.3e-3	1.3e-4	3.8e-5	1.1e-3	1.1e-3	4.8e-4	4.8e-4	0.92887	0.01057	-0.03163
	298.141	7.8392	0.92464	2.2e-3	8.8e-4	3.2e-3	3.3e-3	3.7e-4	1.5e-4	1.1e-3	1.1e-3	4.8e-4	4.8e-4	0.92889	0.01057	-0.03163

	298.141	7.8390	0.92465	2.5e-4	3.6e-5	3.1e-3	3.1e-3	1.4e-4	1.9e-5	1.1e-3	1.1e-3	4.8e-4	4.8e-4	0.92889	0.01057	-0.03164
	298.141	7.8387	0.92467	2.1e-4	3.6e-5	3.1e-3	3.1e-3	1.0e-4	1.1e-5	1.1e-3	1.1e-3	4.8e-4	4.8e-4	0.92890	0.01057	-0.03165
V64	298.140	8.0258	0.91981	2.5e-4	5.0e-5	3.3e-3	3.3e-3	1.1e-4	9.0e-6	1.1e-3	1.1e-3	4.8e-4	4.8e-4	0.92365	0.01097	-0.02411
	298.140	8.0258	0.91979	2.2e-4	2.3e-5	3.3e-3	3.3e-3	1.1e-4	6.3e-6	1.1e-3	1.1e-3	4.8e-4	4.8e-4	0.92365	0.01097	-0.02411
	298.140	8.0258	0.91977	2.4e-4	6.2e-5	3.4e-3	3.4e-3	1.0e-4	6.5e-6	1.1e-3	1.1e-3	4.8e-4	4.8e-4	0.92365	0.01097	-0.02411
	298.140	8.0258	0.91977	2.2e-4	2.2e-5	3.4e-3	3.4e-3	1.1e-4	5.3e-6	1.1e-3	1.1e-3	4.8e-4	4.8e-4	0.92365	0.01097	-0.02411
	298.140	8.0258	0.91976	3.0e-4	2.0e-5	3.3e-3	3.3e-3	1.1e-4	9.9e-6	1.1e-3	1.1e-3	4.8e-4	4.8e-4	0.92364	0.01097	-0.02411
V65	298.134	8.1339	0.91821	7.2e-4	1.1e-4	3.1e-3	3.1e-3	1.2e-4	1.4e-5	1.2e-3	1.2e-3	4.8e-4	4.8e-4	0.92128	0.01144	-0.01802
	298.136	8.1339	0.91818	1.3e-3	5.5e-4	2.9e-3	2.9e-3	1.3e-4	2.3e-5	1.2e-3	1.2e-3	4.8e-4	4.8e-4	0.92130	0.01144	-0.01801
	298.134	8.1339	0.91818	5.6e-4	8.4e-5	2.9e-3	2.9e-3	1.4e-4	1.4e-5	1.2e-3	1.2e-3	4.8e-4	4.8e-4	0.92128	0.01144	-0.01802
	298.134	8.1339	0.91816	8.3e-4	3.3e-4	3.1e-3	3.1e-3	1.3e-4	1.7e-5	1.2e-3	1.2e-3	4.8e-4	4.8e-4	0.92128	0.01144	-0.01802
	298.135	8.1339	0.91815	5.3e-4	1.1e-4	3.2e-3	3.2e-3	1.2e-4	1.0e-5	1.2e-3	1.2e-3	4.8e-4	4.8e-4	0.92129	0.01144	-0.01802
V66	298.134	8.2648	0.91898	9.6e-4	1.8e-4	3.2e-3	3.2e-3	1.2e-4	1.8e-5	1.2e-3	1.2e-3	4.8e-4	4.8e-4^{+}	0.91965	0.01276	0.03529^{+}
	298.136	8.2648	0.91898	5.7e-4	5.2e-5	3.2e-3	3.2e-3	1.3e-4	1.8e-5	1.2e-3	1.2e-3	4.8e-4	4.8e-4^{+}	0.91967	0.01276	0.03530^{+}
	298.137	8.2648	0.91898	5.6e-4	7.2e-5	3.0e-3	3.0e-3	1.0e-4	1.7e-5	1.2e-3	1.2e-3	4.8e-4	4.8e-4^{+}	0.91968	0.01276	0.03529^{+}
V67	298.136	8.3019	0.92107	3.8e-4	5.9e-5	3.2e-3	3.2e-3	1.1e-4	2.2e-5	1.2e-3	1.2e-3	4.8e-4	4.9e-4^{+}	0.91959	0.01358	0.09541^{+}
	298.137	8.3019	0.92108	5.5e-4	6.5e-5	3.2e-3	3.2e-3	1.6e-4	2.7e-5	1.2e-3	1.2e-3	4.8e-4	4.9e-4^{+}	0.91961	0.01359	0.09540^{+}
	298.138	8.3019	0.92110	1.2e-3	5.0e-4	3.1e-3	3.2e-3	1.8e-4	1.2e-5	1.2e-3	1.2e-3	4.8e-4	4.9e-4^{+}	0.91962	0.01359	0.09535^{+}
	298.136	8.3020	0.92109	1.3e-3	5.7e-4	3.2e-3	3.3e-3	1.2e-4	2.0e-5	1.2e-3	1.2e-3	4.8e-4	4.9e-4^{+}	0.91959	0.01358	0.09552^{+}
V68	298.135	8.3180	0.92391	6.3e-4	1.5e-4	3.1e-3	3.1e-3	1.0e-4	8.5e-6	1.2e-3	1.2e-3	4.8e-4	6.9e-4^{+}	0.91964	0.01410	0.41623^{+}
	298.134	8.3180	0.92389	6.2e-4	9.8e-5	3.0e-3	3.0e-3	9.5e-5	8.2e-6	1.2e-3	1.2e-3	4.8e-4	6.8e-4^{+}	0.91963	0.01410	0.41573^{+}
	298.134	8.3180	0.92391	6.1e-4	1.1e-4	3.0e-3	3.0e-3	1.2e-4	8.8e-6	1.2e-3	1.2e-3	4.8e-4	6.9e-4^{+}	0.91962	0.01410	0.41580^{+}
	298.134	8.3180	0.92389	7.6e-4	2.6e-4	3.0e-3	3.0e-3	1.0e-4	9.1e-6	1.2e-3	1.2e-3	4.8e-4	6.9e-4^{+}	0.91963	0.01410	0.41859^{+}
	298.138	8.3180	0.92389	2.7e-3	1.2e-3	3.2e-3	3.4e-3	1.2e-4	1.2e-5	1.2e-3	1.2e-3	4.8e-4	6.9e-4^{+}	0.91967	0.01412	0.41944^{+}
	298.140	8.3180	0.92384	2.5e-4	3.5e-5	3.3e-3	3.3e-3	1.1e-4	9.2e-6	1.2e-3	1.2e-3	4.8e-4	6.9e-4^{+}	0.91971	0.01413	0.41870^{+}

Table A.4
Composition data at supercritical states for the liquid and vapor Rolsi™ samplers for $CO_2 + O_2$ at mean temperature $\bar{T}$, mean pressure $\bar{p}$, and sample mole fraction z_{CO_2}.

	Data			Temperature				Pressure				Composition
ID	$\bar{T}$ (K)	$\bar{p}$ (MPa)	z_{CO_2} (-)	$s(T)$ (K)	$s(\bar{T})$ (K)	$\bar{u}(T)$ (K)	$u_c(\bar{T})$ (K)	$s(p)$ (MPa)	$s(\bar{p})$ (MPa)	$\bar{u}(p)$ (MPa)	$u_c(\bar{p})$ (MPa)	$u(z_{CO_2})$ (-)
L12	218.149	14.4390	0.39451	5.6e-4	7.1e-5	3.4e-3	3.4e-3	2.0e-4	9.7e-6	2.8e-3	2.8e-3	4.8e-4
	218.148	14.4390	0.39451	8.8e-4	1.0e-4	3.3e-3	3.3e-3	1.9e-4	1.4e-5	2.8e-3	2.8e-3	4.8e-4
	218.148	14.4390	0.39449	1.1e-3	1.6e-4	3.3e-3	3.3e-3	2.3e-4	1.7e-5	2.8e-3	2.8e-3	4.8e-4
	218.147	14.4390	0.39451	8.1e-4	1.3e-4	3.4e-3	3.4e-3	1.7e-4	1.5e-5	2.8e-3	2.8e-3	4.8e-4
	218.148	14.4390	0.39449	6.8e-4	9.7e-5	3.4e-3	3.5e-3	2.3e-4	3.2e-5	2.8e-3	2.8e-3	4.8e-4
V13	218.147	14.4390	0.39474	1.5e-3	2.9e-4	3.4e-3	3.4e-3	1.4e-4	1.3e-5	2.8e-3	2.8e-3	4.8e-4
	218.147	14.4390	0.39473	9.6e-4	1.1e-4	3.5e-3	3.5e-3	1.6e-4	8.7e-6	2.8e-3	2.8e-3	4.8e-4
	218.147	14.4390	0.39472	1.3e-3	1.3e-4	3.5e-3	3.5e-3	1.6e-4	1.9e-5	2.8e-3	2.8e-3	4.8e-4
	218.147	14.4390	0.39471	8.7e-4	8.9e-5	3.4e-3	3.4e-3	1.3e-4	9.4e-6	2.8e-3	2.8e-3	4.8e-4
	218.147	14.4390	0.39469	9.9e-4	1.7e-4	3.3e-3	3.3e-3	1.4e-4	8.8e-6	2.8e-3	2.8e-3	4.8e-4
L26	233.142	14.2617	0.44462	6.4e-4	1.7e-4	7.3e-3	7.3e-3	2.0e-4	9.3e-6	2.8e-3	2.8e-3	4.8e-4
	233.142	14.2617	0.44464	6.4e-4	9.2e-5	7.0e-3	7.0e-3	2.1e-4	1.4e-5	2.8e-3	2.8e-3	4.8e-4
	233.144	14.2617	0.44464	1.4e-3	5.3e-4	7.7e-3	7.7e-3	2.1e-4	2.1e-5	2.8e-3	2.8e-3	4.8e-4
	233.142	14.2617	0.44469	9.7e-4	3.3e-4	7.7e-3	7.7e-3	1.8e-4	1.5e-5	2.8e-3	2.8e-3	4.8e-4
	233.142	14.2618	0.44466	4.5e-4	6.9e-5	7.5e-3	7.5e-3	1.8e-4	1.2e-5	2.8e-3	2.8e-3	4.8e-4
	233.142	14.2617	0.44468	6.7e-4	8.1e-5	7.2e-3	7.2e-3	1.3e-4	9.4e-6	2.8e-3	2.8e-3	4.8e-4
V27	233.142	14.2618	0.44442	4.9e-4	7.1e-5	7.6e-3	7.6e-3	2.0e-4	2.3e-5	2.8e-3	2.8e-3	4.8e-4
	233.142	14.2617	0.44444	6.3e-4	5.8e-5	7.3e-3	7.3e-3	1.4e-4	9.6e-6	2.8e-3	2.8e-3	4.8e-4
	233.142	14.2618	0.44446	6.4e-4	1.4e-4	7.6e-3	7.6e-3	1.7e-4	1.1e-5	2.8e-3	2.8e-3	4.8e-4
	233.142	14.2617	0.44447	4.9e-4	5.1e-5	7.5e-3	7.5e-3	1.9e-4	1.3e-5	2.8e-3	2.8e-3	4.8e-4
	233.142	14.2617	0.44446	3.8e-4	3.2e-5	7.4e-3	7.4e-3	1.3e-4	1.7e-5	2.8e-3	2.8e-3	4.8e-4
L38	253.147	13.3559	0.55473	5.7e-4	6.2e-5	5.8e-3	5.8e-3	3.0e-4	4.6e-5	2.7e-3	2.7e-3	4.8e-4
	253.147	13.3560	0.55471	6.0e-4	8.6e-5	6.1e-3	6.1e-3	2.6e-4	6.9e-5	2.7e-3	2.7e-3	4.8e-4
	253.147	13.3561	0.55470	8.1e-4	2.2e-4	5.7e-3	5.7e-3	4.1e-4	8.9e-5	2.7e-3	2.7e-3	4.8e-4
	253.147	13.3560	0.55462	6.4e-4	1.2e-4	6.0e-3	6.0e-3	2.3e-4	3.1e-5	2.7e-3	2.7e-3	4.8e-4
	253.147	13.3560	0.55465	7.3e-4	1.4e-4	5.8e-3	5.8e-3	1.9e-4	2.1e-5	2.7e-3	2.7e-3	4.8e-4
V39	253.148	13.3561	0.55473	6.8e-4	7.1e-5	5.7e-3	5.7e-3	2.7e-4	5.6e-5	2.7e-3	2.7e-3	4.8e-4
	253.147	13.3559	0.55469	6.6e-4	1.1e-4	5.8e-3	5.8e-3	2.7e-4	4.7e-5	2.7e-3	2.7e-3	4.8e-4
	253.147	13.3564	0.55469	6.7e-4	1.9e-4	5.4e-3	5.4e-3	1.5e-4	3.6e-5	2.7e-3	2.7e-3	4.8e-4
L49	273.144	11.5979	0.68190	1.0e-3	2.1e-4	3.0e-3	3.0e-3	1.9e-4	6.7e-5	2.7e-3	2.7e-3	4.8e-4
	273.146	11.5975	0.68187	7.2e-4	1.2e-4	2.9e-3	2.9e-3	1.4e-4	2.5e-5	2.7e-3	2.7e-3	4.8e-4
	273.146	11.5975	0.68186	5.5e-4	7.4e-5	2.4e-3	2.4e-3	2.1e-4	3.6e-5	2.7e-3	2.7e-3	4.8e-4
	273.146	11.5974	0.68195	6.6e-4	9.8e-5	2.5e-3	2.5e-3	3.5e-4	6.9e-5	2.7e-3	2.7e-3	4.8e-4
	273.145	11.5975	0.68195	8.0e-4	1.3e-4	2.1e-3	2.2e-3	1.9e-4	3.0e-5	2.7e-3	2.7e-3	4.8e-4
V51	273.144	11.5974	0.68220	6.4e-4	6.0e-5	2.9e-3	2.9e-3	2.6e-4	3.9e-5	2.7e-3	2.7e-3	4.8e-4
	273.144	11.5975	0.68220	9.4e-4	6.6e-5	2.6e-3	2.6e-3	1.9e-4	3.7e-5	2.7e-3	2.7e-3	4.8e-4
	273.144	11.5975	0.68218	8.9e-4	1.9e-4	2.3e-3	2.3e-3	1.8e-4	4.0e-5	2.7e-3	2.7e-3	4.8e-4
	273.145	11.5975	0.68219	1.1e-3	2.8e-4	2.3e-3	2.3e-3	2.2e-4	3.9e-5	2.7e-3	2.7e-3	4.8e-4
	273.144	11.5975	0.68217	6.6e-4	4.0e-5	2.6e-3	2.6e-3	1.8e-4	4.8e-5	2.7e-3	2.7e-3	4.8e-4
	273.145	11.5975	0.68218	9.8e-4	1.1e-4	2.4e-3	2.5e-3	1.6e-4	5.2e-5	2.7e-3	2.7e-3	4.8e-4

[a] Samples taken using liquid sampler given with ID L, samples taken using vapor sampler given with ID V.

Appendix B. Additional plots

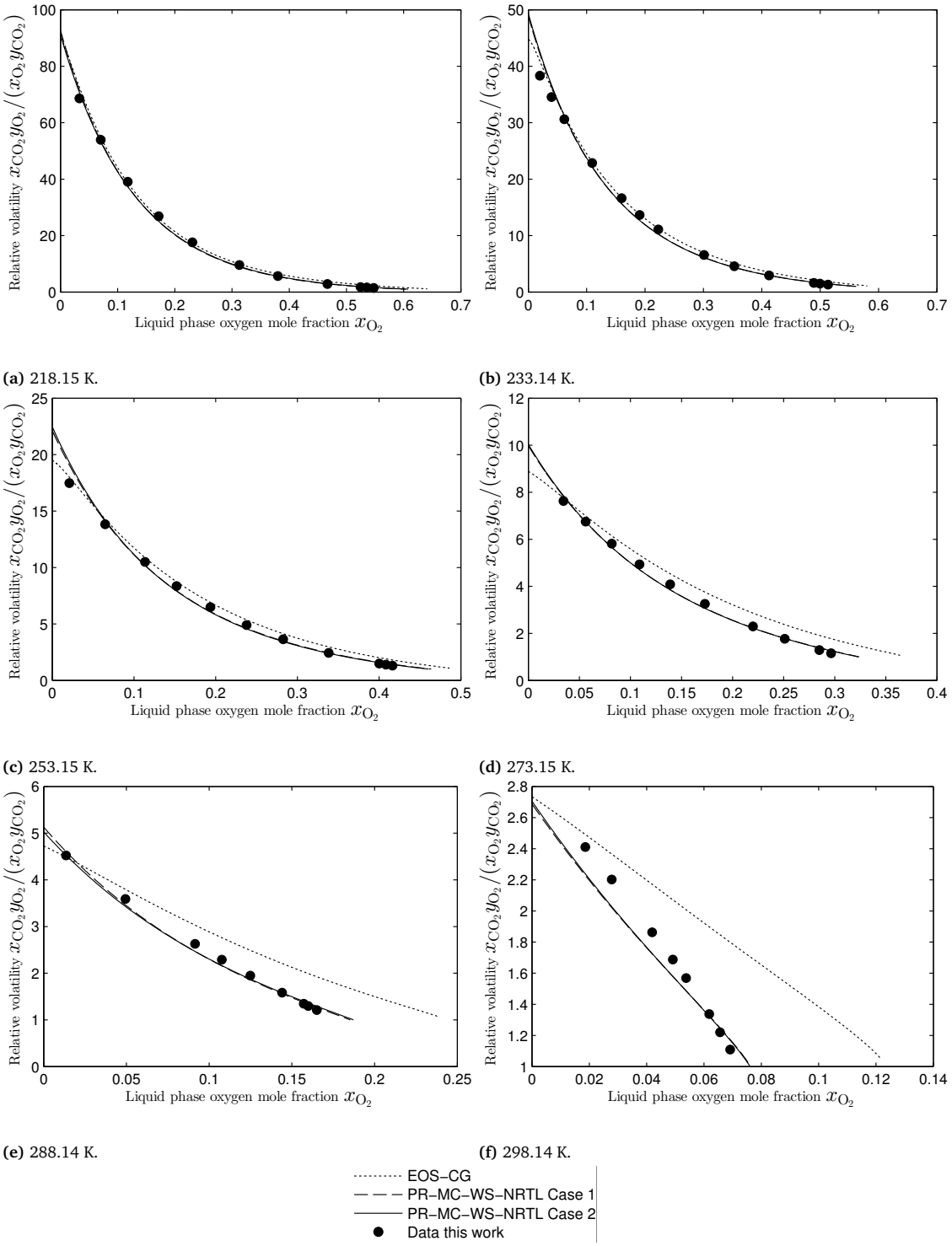

Fig. B.1. Measured relative volatilities compared with different models.

References

[1] S. F. Westman, H. G. J. Stang, S. W. Løvseth, A. Austegard, I. Snustad, S. Ø. Størset, I. S. Ertesvåg, Vapor-liquid equilibrium data for the carbon dioxide and nitrogen ($CO_2 + N_2$) system at the temperatures 223, 270, 298 and 303 K and pressures up to 18 MPa, Fluid Phase Equilib. 409 (2016) 207–241, URL http://dx.doi.org/10.1016/j.fluid.2015.09.034.

[2] S. T. Munkejord, M. Hammer, S. W. Løvseth, CO_2 transport: Data and models – a review, submitted.

[3] J. Gernert, R. Span, EOS-CG: A Helmholtz energy mixture model for humid gases and CCS mixtures, J. Chem. Thermodyn. 93 (2016) 274–293, URL http://dx.doi.org/10.1016/j.jct.2015.05.015.

[4] G. J. Gernert, A New Helmholtz Energy Model for Humid Gases and CCS Mixtures, PhD dissertation, Fakultät für Maschinenbau, Ruhr-Universität Bochum, Bochum, URL http://www-brs.ub.ruhr-uni-bochum.de/netahtml/HSS/Diss/GernertGeorgJohannes/diss.pdf, 2013.

[5] H. Li, J. P. Jakobsen, Ø. Wilhelmsen, J. Yan, PVTxy Properties of CO_2 Mixtures Relevant for CO_2 Capture, Transport and Storage: Review of Available Experimental Data and Theoretical Models, Appl. Energy 88 (11) (2011) 3567–3579, URL http://dx.doi.org/10.1016/j.apenergy.2011.03.052.

[6] R. Span, W. Wagner, A New Equation of State for Carbon Dioxide Covering the Fluid Region from the Triple-Point Temperature to 1100 K at Pressures up to 800 MPa, J. Phys. Chem. Ref. Data 25 (1996) 1509, URL http://dx.doi.org/10.1063/1.555991.

[7] S. W. Løvseth, G. Skaugen, H. G. J. Stang, J. P. Jakobsen, Ø. Wilhelmsen, R. Span, R. Wegge, CO_2Mix Project: Experimental Determination of Thermo-Physical Properties of CO_2-Rich Mixtures, Energy Procedia 37 (2013) 7841–7849, URL http://dx.doi.org/10.1016/j.egypro.2014.09.001.

[8] E. De Visser, C. Hendriks, M. Barrio, M. J. Mølnvik, G. de Koeijer, S. Liljemark, Y. Le Gallo, Dynamis CO_2 Quality Recommendations, Int. J. Greenhouse Gas Control 2 (4) (2008) 478–484, URL http://dx.doi.org/10.1016/j.ijggc.2008.04.006.

[9] H. G. J. Stang, S. W. Løvseth, S. Ø. Størset, B. Malvik, H. Rekstad, Accurate Measurements of CO_2 Rich Mixture Phase Equilibria Relevant for CCS Transport and Conditioning, Energy Procedia 37 (2013) 2897–2903, URL http://dx.doi.org/10.1016/j.egypro.2013.06.175.

[10] R. D. Chirico, T. W. de Loos, J. Gmehling, A. R. H. Goodwin, S. Gupta, W. M. Haynes, K. N. Marsh, V. Rives, J. D. Olson, C. Spencer, J. F. Brennecke, J. P. M. Trusler, Guidelines for Reporting of Phase Equilibrium Measurements (IUPAC Recommendations 2012), Pure Appl. Chem. 84 (8) (2012) 1785–1813, URL http://dx.doi.org/10.1351/PAC-REC-11-05-02.

[11] BIPM, IEC, IFCC, ILAC, IUPAC, IUPAP, ISO, OIML, Evaluation of Measurement Data - Guide for the Expression of Uncertainty in Measurement. JCGM 100: 2008, 2008.

[12] J. M. S. Fonseca, R. Dohrn, S. Peper, High-pressure fluid-phase equilibria: Experimental methods and systems investigated (2005–2008), Fluid Phase Equilib. 300 (1–2) (2011) 1–69, URL http://dx.doi.org/10.1016/j.fluid.2010.09.017.

[13] ARMINES, Patent n° FR 2 853 414, Procédé et dispositif pour prélever des micro-échantillons d'un fluide sous pression contenu dans un container, 2003.

[14] P. Guilbot, A. Valtz, H. Legendre, D. Richon, Rapid on-line sampler-injector: a reliable tool for HT-HP sampling and on-line GC analysis, Analusis 28 (5) (2000) 426–431, URL http://dx.doi.org/10.1051/analusis:2000128.

[15] S. F. Westman, H. G. J. Stang, S. Ø. Størset, H. Rekstad, A. Austegard, S. W. Løvseth, Accurate Phase Equilibrium Measurements of CO_2 Mixtures, Energy Procedia 51 (2014) 392–401, URL http://dx.doi.org/10.1016/j.egypro.2014.07.046.

[16] M. E. Wieser, T. B. Coplen, Atomic weights of the elements 2009 (IUPAC Technical Report), Pure Appl. Chem. 83 (2) (2010) 359–396, URL http://dx.doi.org/10.1351/PAC-REP-10-09-14.

[17] M. E. Wieser, N. Holden, T. B. Coplen, J. K. Böhlke, M. Berglund, W. A. Brand, P. De Bièvre, M. Gröning, R. D. Loss, J. Meija, T. Hirata, T. Prohaska, R. Schoenberg, G. O'Connor, T. Walczyk, S. Yoneda, X.-K. Zhu, Atomic weights of the elements 2011 (IUPAC Technical Report), Pure Appl. Chem. 85 (5) (2013) 1047–1078, URL http://dx.doi.org/10.1351/PAC-REP-13-03-02.

[18] G. H. Zenner, L. I. Dana, Liquid-vapor equilibrium compositions of carbon dioxide-oxygen-nitrogen mixtures, in: Chem. Eng. Prog., Symp. Ser., vol. 59, 36–41, 1963.

[19] A. Fredenslund, G. A. Sather, Gas-liquid equilibrium of the oxygen-carbon dioxide system, J. Chem. Eng. Data 15 (1) (1970) 17–22, URL http://dx.doi.org/10.1021/je60044a024.

[20] G. Kaminishi, T. Toriumi, Vapor-Liquid Phase Equilibrium in the CO_2-H_2, CO_2-N_2 and CO_2-O_2 Systems [in Japanese], Kogyo Kagaku Zasshi 69 (1966) 175–178, URL http://doi.org/10.1246/nikkashi1898.69.2_175.

[21] H. S. Booth, J. M. Carter, The Critical Constants of Carbon Dioxide-Oxygen Mixtures, J. Phys. Chem. 34 (12) (1930) 2801–2825, URL http://dx.doi.org/10.1021/j150318a013.

[22] N. K. Muirbrook, Experimental and Thermodynamic Study of the High-Pressure Vapor-Liquid Equilibria for the Nitrogen-Oxygen-Carbon Dioxide System, Ph.D. thesis, University of California, Berkeley, 1964.

[23] W. H. Keesom, Isothermals of mixtures of oxygen and carbon dioxide (with two plates), Commun. Phys. Lab. Univ. Leiden 88 (1903) 1–85.

[24] M. Ahmad, J. Gernert, E. Wilbers, Effect of impurities in captured CO_2 on liquid–vapor equilibrium, Fluid Phase Equilib. 363 (2014) 149–155, URL http://dx.doi.org/10.1016/j.fluid.2013.11.009.

[25] A. Fredenslund, J. Mollerup, O. Persson, Gas-liquid equilibrium of oxygen-carbon dioxide system, J. Chem. Eng. Data 17 (4) (1972) 440–443, URL http://dx.doi.org/10.1021/je60055a019.

[26] R. Engberg, D. Köpke, R. Eggers, Die Grenzflächenspannungen von CO_2–O_2–und Rauchgas-Mischungen, Chem. Ing. Tech. 81 (9) (2009) 1439–1443, URL http://dx.doi.org/10.1002/cite.200900052.

[27] M. S. Green, M. Vicentini-Missoni, J. M. H. Levelt Sengers, Scaling-Law Equation of State for Gases in the Critical Region, Phys. Rev. Lett. 18 (1967) 1113–1117, URL http://dx.doi.org/10.1103/PhysRevLett.18.1113.

[28] L. P. Kadanoff, W. Götze, D. Hamblen, R. Hecht, E. A. S. Lewis, V. V. Palciauskas, M. Rayl, J. Swift, D. Aspnes, J. Kane, Static Phenomena Near Critical Points: Theory and Experiment, Rev. Mod. Phys. 39 (1967) 395–431, URL http://dx.doi.org/10.1103/RevModPhys.39.395.

[29] M. E. Fisher, The theory of equilibrium critical phenomena, Rep. Prog. Phys. 30 (2) (1967) 615, URL http://dx.doi.org/10.1088/0034-4885/30/2/306.

[30] P. Ungerer, B. Tavitian, A. Boutin, Applications of Molecular Simulation in the Oil and Gas Industry. Monte Carlo Methods, chap. 2, Editions Technip, Paris, France, note: Equation 2.100 is lacking the critical composition term, 2005.

[31] V. Lachet, T. de Bruin, P. Ungerer, C. Coquelet, A. Valtz, V. Hasanov, F. Lockwood, D. Richon, Thermodynamic behavior of the CO_2+SO_2 mixture: Experimental and Monte Carlo simulation studies, Energy Procedia 1 (1) (2009) 1641 – 1647, URL http://dx.doi.org/10.1016/j.egypro.2009.01.215.

[32] J. Sengers, J. Levelt Sengers, A universal representation of the thermodynamic properties of fluids in the critical region, Int. J. Thermophys. 5 (2) (1984) 195–208, ISSN 0195-928X, URL http://dx.doi.org/10.1007/BF00505500.

[33] H. B. Callen, Thermodynamics and an Introduction to Thermostatistics, Wiley, 2 edn., ISBN 0471862568, 1985.

[34] O. Kunz, W. Wagner, The GERG-2008 Wide-Range Equation of State for Natural Gases and Other Mixtures: An Expansion of GERG-2004, J. Chem. Eng. Data 57 (11) (2012) 3032–3091, URL http://dx.doi.org/10.1021/je300655b.

[35] D.-Y. Peng, D. B. Robinson, A New Two-Constant Equation of State, Ind. Eng. Chem. Fundam. 15 (1) (1976) 59–64, URL http://dx.doi.org/10.1021/i160057a011.

[36] P. M. Mathias, T. W. Copeman, Extension of the Peng-Robinson equation of state to complex mixtures: Evaluation of the various forms of the local composition concept, Fluid Phase Equilib. 13 (1983) 91–108, URL http://dx.doi.org/10.1016/0378-3812(83)80084-3.

[37] D. S. H. Wong, S. I. Sandler, A Theoretically Correct Mixing Rule

for Cubic Equations of State, AIChE J. 38 (5) (1992) 671–680, URL http://dx.doi.org/10.1002/aic.690380505.

[38] H. Renon, J. M. Prausnitz, Local compositions in thermodynamic excess functions for liquid mixtures, AIChE J. 14 (1) (1968) 135–144, URL http://dx.doi.org/10.1002/aic.690140124.

[39] C. Coquelet, A. Valtz, F. Dieu, D. Richon, P. Arpentinier, F. Lockwood, Isothermal P, x, y data for the argon+carbon dioxide system at six temperatures from 233.32 to 299.21 K and pressures up to 14 MPa, Fluid Phase Equilib. 273 (1-2) (2008) 38–43, URL http://dx.doi.org/10.1016/j.fluid.2008.08.010.

[40] P. T. Boggs, R. H. Byrd, J. E. Rogers, R. B. Schnabel, User's Reference Guide for ODRPACK Version 2.01 Software for Weighted Orthogonal Distance Regression, URL http://docs.scipy.org/doc/external/odrpack_guide.pdf, 1992.

[41] X. Courtial, C.-B. Soo, C. Coquelet, P. Paricaud, D. Ramjugernath, D. Richon, Vapor–liquid equilibrium in the n-butane+methanol system, measurement and modeling from 323.2 to 443.2 K, Fluid Phase Equilib. 277 (2) (2009) 152–161, URL http://dx.doi.org/10.1016/j.fluid.2008.12.001.

[42] O. Chiavone-Filho, P. G. Amaral Filho, D. N. Silva, L. R. Terron, Alpha Function for a Series of Hydrocarbons to Peng-Robinson and van der Waals Equations of State, Ind. Eng. Chem. Res. 40 (26) (2001) 6240–6244, URL http://dx.doi.org/10.1021/ie001134o.

[43] R. Schmidt, W. Wagner, A new form of the equation of state for pure substances and its application to oxygen, Fluid Phase Equilib. 19 (3) (1985) 175–200, URL http://dx.doi.org/10.1016/0378-3812(85)87016-3.

[44] H. Preston-Thomas, The International Temperature Scale of 1990 (ITS-90), Metrologia 27 (1) (1990) 3–10, URL http://dx.doi.org/10.1088/0026-1394/27/1/002.